Performance Evaluation and Strengthening of Deficient Beam-Column Sub-assemblages under Cyclic Loading

Von der Fakultät für Bau- und Umweltingenieurwissenschaften der

Universität Stuttgart

zur Erlangung der Würde eines Doktors der Ingenieurwissenschaften (Dr.-Ing.) genehmigte Abhandlung

Vorgelegt von

Saptarshi Sasmal

aus Midnapore, West Bengal, Indien

Hauptberichter: Prof. Dr.-Ing. Balthasar Novák

Mitberichter: O.Univ.Prof. Dipl.-Ing. Dr.techn. Dr.phil. Konrad Bergmeister

Tag der mündlichen Prüfung: 16. Oktober 2009

Institut für Leichtbau Entwerfen und Konstruieren
2009

Gedruckt mit Unterstützung des Deutschen Akademischen Austauschdienstes

Acknowledgements

First of all, I would like to express my sincere gratitude to Prof. Dr.-Ing. Balthasar Novák, Professor of Institute for Lightweight Structures and Conceptual Design (ILEK), Universitaet Stuttgart. He has not only been my doctoral supervisor who provided me countless helpful suggestions, important advice and constant encouragement during developing my thesis, he guided me from the initial stage of application for scholarship, dealing in language school in a new atmosphere, to stay in Stuttgart. Without his constant support, it could have been impossible.

I wish to express my appreciation to Prof. Dr.-Ing. Werner Sobek, Director and Professor of Institute for Lightweight Structures and Conceptual Design (ILEK), Universitaet Stuttgart, for allowing me to avail all the facilities available at the institute.

Special thanks are due to CSIR, in general and, Dr. N. Lakshmanan (Former Director), Dr. Nagesh R. Iyer (Director) and Dr. K. Ramanjaneyulu (Deputy Director) of Structural Engineering Research Centre (SERC), CSIR, Chennai, India, in particular, for giving me the permission to carry out my doctoral work at Universitaet Stuttgart under study leave and to facilitate me in conducting the experimental works in heavy testing laboratory of SERC.

It is my pleasure to express my gratefulness to Dr. Ramanjaneyulu, V. Srinivas, all colleagues and students at SERC, India, on behalf of devoting their time and energy during the experimental studies and providing many valuable suggestions which indeed helped in executing the tests.

I wish to express my cordial appreciation to Deutscher Akademischer Austausch Dienst (DAAD) for awarding me the scholarship to develop my doctoral thesis at Universitaet Stuttgart. I must mention Ms. H. Bossmann, Ms. S. Kammüller and Ms. H. Islam for their patience in listening to all problems, kindness in helping to the maximum extent and promptness in dealing each of the matters with utmost care.

I would like to gratefully acknowledge the valuable assistance and help in both technical and personal aspects received from Dipl.-Ing. Constanze Röhm. Special gratitude goes to Dipl.-Bibl. Christian Assenbaum of ILEK who helped in finding out any odd book or journal and of course, with a charming face. I would like to appreciate the warmth that I had received from all ILEK colleagues and friends; in particular the help and assistance to any type of problem rendered by Ms. Ilse Guy, Ms. Manuela Brüggeboes, Dr.-Ing. Jochen Röhm, Dipl.-Ing. Björn Frettlöhr and Dipl.-Ing. Frank Reichert.

I would like to express my heartiest thanks to Prof. Novák, his wife Mrs. Christa Novák and their young delightful children for their kindness and affection, and for never letting me feel that I am away from my home. Countless weekends spent with them are indeed a treasure in memory.

Finally, I am forever indebted to my patents, brothers, uncle and aunt in Germany and other family members. Without my mother's single handed protection, endless patience and enthusiasm, and my wife Maitri's help, encouragement and enormous mental support, this study would not have been completed.

Above all, I bow down to the Almighty for giving me the opportunity to see the beautiful world.

Abstract

Evidence from the previous earthquakes has posed a serious question on the performance of reinforced concrete (RC) structures, both existing and newly built, under seismic loading. In the present study, exterior beam-column sub-assemblage which is proved to be one of the most critical components of an RC structure has been chosen for investigation. European Codes and Indian Standards of practice for seismic design have been considered for designing and detailing the sub-assemblages of a most regular and conventional RC structure. Different specimens represented the existing condition of buildings designed according to the available knowledge and prevailing guidelines at different times. The experimental investigations under repeated cyclic loading have shown that 'GLD' specimen can hardly withstand any reverse loading due to insufficient reinforcement, inadequate bonding and poor detailing. Among the 'NonDuctile' specimens, Indian Standard based specimen exhibited better performance (strength deterioration, stiffness degradation and energy dissipation) over the Eurocode based specimen, even though in both cases energy dissipation was mainly through the damage in joint region which is extremely unwanted. The strength hierarchy of all the specimens has been developed based on the results obtained from experimental and analytical studies for identification and quantification of required improvements of deficient sub-assemblages towards 'Ductile' ones.

After the experimental investigations, severely damaged specimens were further studied for adequate retrofitting to ensure their re-usability in post-earthquake scenario. An effective, simple and economical retrofitting scheme has been proposed here by judiciously using GFRP in members beyond the joint and steel plate in the joint region holding by through-through bolts. Surface treatment and epoxy injection were carried out to re-install concrete integrity and bond. From the experimental investigation, it has have noted that the retrofitted 'NonDuctile' and 'Ductile' specimens could be able to regain, if not better, their original seismic performance. Deformation capacity of the retrofitted 'NonDuctile' specimen was also considerably increased with respect to undamaged ones. Further, in both retrofitted specimens, strength deterioration with increase in displacement demand was extremely low. Thus, the retrofitting schemes as proposed in this study could effectively be implemented for damaged 'NonDuctile' or 'Ductile' sub-assemblages for their further usage.

Three different schemes have been proposed in this study for upgradation of poorly designed 'GLD' structures which are present in massive quantity throughout the world. The schemes have been developed by using hybrid FRP-steel plate system. Using the analytical formulation, a detailed study has been carried out on improvement of strength and ductility due to application of external reinforcement and confinement. CFRP fabric and CFRP laminate were used for flexural strengthening, GFRP wrap was used for confinement of beam and column sections and steel plate-bolt system was adopted for confinement and shear strength enhancement of the joint. From the cyclic load test as adopted for original 'GLD' specimen, it has been observed that the seismic performance of the upgraded specimens can be considerably improved by using these schemes. For example, double the energy dissipation was achieved at same drift ratio and final energy dissipation was 5 times more than that obtained from original 'GLD' specimen. Most importantly, the plastic hinge shifted in the beam away the joint and in last upgraded specimen where only D-region upgradation was carried out, it could even form a spread plastic hinge in the beam, which ensures large and consistent dissipation of energy with increase in drift demand.

Finally, non-linear Finite Element analysis using software ATENA has been carried out on 'GLD', 'NonDuctile' and upgraded specimens. Material and geometrical models have suitably been incorporated in the numerical analyses. The results obtained from numerical analyses are in good agreement with that from experimental investigations. A comparative study on energy dissipation obtained from both numerical and experimental studies has been carried out and correlated for practical use. Influence of axial load in column has also been explored. Further, a parametric study has also been conducted to investigate the effects of amount of bending FRP, number of wrapping layers, bond behaviour and role of individual upgradation components on the overall performance of the upgraded specimens which would offer the scope for any further modifications on the proposed schemes. The study as a whole would provide the promising aspects on strengthening of deficient structural components and encourage for further research.

Kurzdarstellung

In der vorliegenden Studie wurden außenliegende Balken-Stützen-Verbindungskomponenten (Rahmenknoten), welche eine der kritischsten Zonen in einem Stahlbetontragwerk darstellen, untersucht. Eurocodes (EC) und Indian Standards (IS) wurden zur Auslegung und Detaillierung eines Rahmenknotens eines regelmäßigen konventionellen Stahlbetontragwerks verwendet. Die verschiedenen Versuchskörper repräsentierten die bestehenden Zustände von Gebäuden, die nach unterschiedlichem Stand der Technik errichtet wurden. Die experimentellen Untersuchungen unter wiederholter zyklischer Belastung haben gezeigt, dass die nur für Schwerelasten bemessenen ‚GLD'-Versuchskörper aufgrund der ungenügenden Bewehrung und Verankerung sowie schlechter Detaillierung kaum einer zyklischen Belastung widerstehen können. Unter den ‚NonDuctile'-Versuchskörpern zeigte der nach IS ausgelegte Versuchskörper ein besseres Verhalten (bzgl. Traglast-, Steifigkeitsabnahme und Energiedissipation) als der nach EC ausgelegte Versuchskörper, wobei in beiden Fällen die Energiedissipation und Schädigung hauptsächlich im Knoten erfolgte, was höchst unerwünscht ist. Schließlich wurde die Widerstandshierarchie aller Versuchskörper basierend auf den Ergebnissen der experimentellen sowie analytischen Studien entwickelt, um die erforderlichen Maßnahmen an den unzulänglichen Versuchskörpern für ein besseres Verhalten unter Erdbeben zu identifizieren und zu quantifizieren.

Nach den Experimenten wurden die stark beschädigten Versuchskörper untersucht um eine passende Instandsetzungs-Lösung zu entwickeln, die die Weiternutzung nach einem Erdbeben ermöglichen sollte. Hierfür wurde eine effektive, einfache und ökonomische Lösung vorgeschlagen. In den Bereichen neben dem Knoten wird GFRP einsetzt und im Knoten eine Stahlplatte, die mit durch den Knoten gehenden Bolzen gehalten wird. Zuvor wurde die beschädigte Knotenoberfläche vorbereitet und die Risse mit Epoxy-Injektionen gefüllt um die Knotenintegrität und den Verbund wieder herzustellen. Bei den experimentellen Untersuchungen zeigte sich, dass die Instand gesetzten ‚NonDuctile' und ‚Ductile'-Versuchskörper ihr ursprüngliches seismisches Verhalten wieder gewonnen, wenn nicht sogar verbessert hatten. Die Deformationskapazität der Instand gesetzten ‚NonDuctile'-Versuchskörper wurde im Vergleich zu den Ausgangskörpern beträchtlich verbessert. Des Weiteren war die Traglastabnahme bei zunehmender Verschiebung in beiden wieder Instand gesetzten Versuchskörpern sehr gering. Daher können die hier vorgeschlagenen Instandsetzungs-Lösungen effektiv bei den Knoten beschädigter ‚NonDuctile' und ‚Ductile' Tragwerke angewendet werden um sie nach einem Erdbeben weiter zu verwenden.

Zur Verstärkung von ‚GLD'-Tragwerken, die in großer Zahl weltweit zu finden sind, wurden drei verschiedene Vorschläge gemacht. Hierbei kommt ein hybrides FRP-Stahlplatten-System zum Einsatz. Unter Verwendung einer analytischen Formulierung, wurde eine detaillierte Studie zur Verbesserung der Tragfähigkeit und Duktilität durch extern aufgebrachte Bewehrung und Umschnürung durchgeführt. CFRP-Gewebe und CFRP-Laminat wurden zur Erhöhung der Biegetragfähigkeit verwendet, zur Verbesserung der Umschnürungswirkung wurde GFRP um Balken- und Stützenbereiche gewickelt und das Stahlplatten-Bolzen-System wurde zur Steigerung der Umschnürung und Schubtragfähigkeit des Knotens angebracht. Der zyklische Belastungstest zeigte, dass das seismische Verhalten gegenüber dem unverstärkten ‚GLD'-Versuchskörper beträchtlich verbessert werden konnte. Zum Beispiel konnte beim maximalen Drift-Verhältnis des unverstärkten Versuchskörpers bereits die doppelte Energiedissipation erzielt werden und die gesamte dissipierte Energie bei Versuchende war fünf Mal so groß. Außerdem konnte das plastische Gelenk weg vom Knoten in den Balken geschoben werden und im letzten Versuchskörper, in dem nur der D-Bereich verstärkt wurde, entstand ein verteiltes plastisches Gelenk im Balken, welches große und gleichmäßige Energiedissipation mit zunehmendem Drift-Bedarf sicherstellt.

Zuletzt wurde eine nichtlineare Finite Elemente Analyse mit der Software ATENA an den ‚GLD', ‚NonDuctile' und verstärkten Versuchskörpern durchgeführt. Die Ergebnisse der numerischen Berechnungen stimmten gut mit den experimentellen Ergebnissen überein. Die erhaltene Energiedissipation aus den numerischen und den experimentellen Untersuchungen wurde verglichen und für die praktische Verwendung korreliert. Der Einfluss der Axiallast in der Stütze wurde ebenfalls untersucht. Des Weiteren wurde eine Parameterstudie durchgeführt um die

Vorschläge weiter zu verbessern. Hierbei wurden die Biegeverstärkung, die Umschnürung, das Verbundverhalten und die einzelnen Verstärkungs-Komponenten variiert, um deren Einfluss auf das Gesamtverhalten der verstärkten Versuchskörper auszuloten.

Content

List of Abbreviations

ACI	American Concrete Institute
CEB	Comite Euro-International du Beton
CFRP	Carbon fiber reinforced polymer
CSA	Canadian Standards Association
D distance	Distance equals to depth of the member
D-region	Disturbed region
DL	Dead load
'Ductile'	Designed based on earthquake loads and with full ductile detailing
FRP	Fiber reinforced polymers
GFRP	Glass fiber reinforced polymer
'GLD'	Gravity Load Designed sub-assemblage used in this study
IS	Indian Standard
LL	Live load
LVDT	Linear variable differential transducer
'NonDuctile'	Designed based on earthquake loads but without any ductile detailing
NZS	New Zealand Standard
RC	Reinforced concrete
SL	Seismic load
SP-1	'GLD' specimen based on Indian Standard
SP-2	'GLD' specimen based on Eurocode
SP-3	'NonDuctile' designed based on Indian Standard
SP-4	'NonDuctile' designed based on Eurocode
SP-5	'Ductile' designed based on Indian Standard
SP-6	'Ductile' designed based on Eurocode
SP-3R	Retrofitting of damaged specimen SP-3
SP-5R	Retrofitting of damaged specimen SP-5
SP1-U1	Upgradation of 'GLD' specimen SP-1 using CFRP fiber
SP1-U2	Upgradation of 'GLD' specimen SP-1 using CFRP laminate
SP1-U3	Upgradation (only in D-region) of 'GLD' specimen SP-1 using CFRP fiber
SP-1()	Intermediate upgradation on existing 'GLD' specimen
SP1-U2()	Parametric specimens derived from upgraded 'GLD' specimen SP1-U2
SP1-U3()	Parametric specimens derived from upgraded 'GLD' specimen SP1-U3

List of Notations

α_D	=	Angle of diagonal strut with respect to the horizontal axis
Δl	=	Applied displacement at the tip of the beam
ε_c	=	Strain corresponding to compressive strength of unconfined concrete
ε_c^{eq}	=	Equivalent uniaxial strain of concrete
ε_{cc}	=	Strain corresponding to compressive strength of confined concrete
ε_{cu}	=	Ultimate strain of confined concrete
ε_d , ε_r	=	Average principal strains in d- and r-directions, respectively
$\varepsilon_{f(b)}$	=	Strain in FRP at bottom of section
$\varepsilon_{f(t)}$	=	Strain in FRP at top of section
ε_{fu}	=	Strain in FRP corresponding to its failure strength
ε_{fud}	=	FRP tensile failure design strain
ε_h , ε_v	=	Average principal strains in horizontal- and vertical-directions, respectively
$\varepsilon_{\lim}$	=	Strain corresponding to maximum tensile strength of reinforcement
$\varepsilon_{s(1)} \cdots \varepsilon_{s(n)}$	=	Strain in different layers of reinforcement
ε_y	=	Strain corresponding to tensile yielding of reinforcement
γ	=	Shear deformation (angle)
ξ	=	Softening coefficient
ξ_{m-w}	=	Hydrostatic length of the stress vector in Haigh-Westergaard stress space
ξ_ε	=	Softening coefficient for strain
ξ_σ	=	Softening coefficient for stress
ξ_{stress}	=	Softening coefficient calculated from constitutive relation
ξ_{strain}	=	Softening coefficient calculated from strain compatibility
κ	=	Curvature
v_{jh}	=	Horizontal shear stress in joint
v_{jv}	=	Vertical shear stress in joint
$\varnothing$	=	Diameter of reinforcement bar
Φ_1 , Φ_2 ..	=	Strength reduction factor
ρ_{m-w}	=	Deviatoric length of the stress vector in Haigh-Westergaard stress space
ρ_x	=	Volumetric percentage of reinforcement in x-direction
σ_c^{ef}	=	Effective stress in concrete
σ_D	=	Maximum diagonal compressive stress
$\sigma_{f(b)}$	=	Stress in FRP at bottom of section
$\sigma_{f(t)}$	=	Stress in FRP at top of section
$\sigma_{s(1)} \cdots \sigma_{s(n)}$	=	Stress in different layers of reinforcement
θ_{m-w}	=	Angle of the stress vector in Haigh-Westergaard stress space
A_{strut}	=	Cross-sectional area of diagonal strut
b_{je}	=	Effective width of beam in joint zone
c_{ts}	=	Coefficient for tensile stiffening
E	=	Elastic modulus of reinforcement

E_c	=	Secant modulus of concrete
E_{ci}	=	Tangent modulus of concrete
E_d	=	Softening modulus of concrete
E_f	=	Elastic modulus of FRP
f_c	=	Compressive strength of concrete cylinder
f_{cm}	=	Compressive strength of concrete cylinder (mean value)
$f_c^{'}$	=	Specified compressive strength of concrete
$f_c^{'ef}$	=	Effective compressive strength of concrete
f_{cc}	=	Compressive strength of confined concrete
$f_{ct,fl}$	=	Bending flexural strength from prism test
f_{ctm}	=	Prism tensile strength
f_{c0}	=	Unconfined compressive strength
f_{fy}	=	Strength of FRP
f_h	=	Average axial stresses in the horizontal direction
f_j	=	Strength of confinement at joint
f_l	=	Effective lateral confining stress
$f_{\max}$	=	Ultimate strength of reinforcement
$f_{s,x}$	=	Stress in steel at a given strain of ε_x
$f_t^{'ef}$	=	Effective tensile strength of concrete
f_v	=	Average axial stresses in the vertical direction
f_y	=	Specified tensile yield strength of reinforcement
F_D	=	Compressive force carried by diagonal strut
F_H	=	Tensile force carried by horizontal ties in column
F_V	=	Tensile force carried by intermediate main reinforcement of column
F_{yh}	=	Tensile strength (at yielding) of horizontal ties
F_{yv}	=	Tensile strength (at yielding) of intermediate vertical column reinforcement
G_F	=	Fracture energy
G_{Fo}	=	Basic value of fracture energy dependent on particle size
h	=	Height of section
h_b	=	Height of beam
h_c	=	Width of column along the beam direction
k_e	=	Degree of confinement
l_b	=	Length of the beam from the column face
L_t	=	Characteristic length
P	=	Load applied at tip of the beam
p_c	=	Nominal principal compressive stress
p_t	=	Nominal principal tensile stress
R_D	=	Fraction of joint shear carried by diagonal strut
R_H	=	Fraction of joint shear carried by horizontal mechanism
R_V	=	Fraction of joint shear carried by vertical mechanism
S_e / a_g	=	Spectral acceleration

t_f	=	Thickness of FRP wrapping
$T(S)$	=	Time period
V_c	=	Shear resistance contribution from concrete
V_{Col}	=	Shear force in column beyond joint zone
$V_{C,beam-hinge}$	=	Amount of shear in column to produce hinge formation in beam
$V_{C,beam-shear}$	=	Amount of shear in column to produce shear failure in beam
$V_{C,col-hinge}$	=	Amount of shear in column to produce hinge formation in column
$V_{C,col-shear}$	=	Amount of shear in column to produce shear failure in column
$V_{C,jt-shear}$	=	Amount of shear in column to produce joint shear failure
V_f	=	Shear resistance contribution from FRP
V_{jh}	=	Horizontal shear force in joint
V_{jv}	=	Vertical shear force in joint
V_s	=	Shear resistance contribution from steel
$V_{str,h}$	=	Horizontal component of strength developed from diagonal strut
V_t	=	Total shear strength at a strengthened section
w	=	Crack opening
w_c	=	Crack opening at the complete release of stress
Z	=	Lever arm for resisting moment

1 Introduction

In various parts of the world, reinforced concrete (RC) structures even in seismic zones have been designed only for gravity load. Such structures though performing well under conventional gravity load case, could lead to a questionable structural performance under earthquake. In most cases, those structures are vulnerable to any moderate or major earthquake. Along with the seismic prone zones like Himalayan region in India, Iran, Turkey, New Zealand and fault region in US etc., devastations from earthquake have also been seen at the places believed to be seismically not-so-active (as shown in *Fig. 1.1*) and hence, the existing structures need immediate assessment to avoid a collapse which brings a huge loss of human lives and economy that the world has witnessed for several times. Moreover, for new structures, the specifications and detailing provisions, though available to a certain extent, have to be considered in such a way that the structure would be able to efficiently resist seismic actions. Generally, a three phase approach is followed to describe a structure under seismic loading, i.e. (i) the structure must have adequate lateral stiffness to control the inter-story drifts such that no damage would occur to non-structural elements during minor but frequently occurring earthquakes, (ii) during moderate earthquakes, some damage to non-structural elements is permitted, but the structural element must have adequate strength to remain elastic so that no damage would occur, and (iii) during rare and strong earthquakes, the structure must be ductile enough to prevent collapse by aiming for repairable damage which would ascertain economic feasibility.

Fig. 1.1 Earthquake damage of (left) RC building inter-story collapse in Bhuj, India (2001) [source: NICEE, IIT Kanpur], (right) in Schwäbische Alb (1978) [source: Erdbebensicher Bauen]

Hence, both for existing structures and newly designed structures, the structural mechanism has to be evolved in a way so that the seismic energy which is introduced into the structure must be dissipated within the structure. Energy dissipation takes place mainly through inelastic behaviour of the structural system since the structure must be damaged to dissipate energy. If seismic energy is dissipated at locations which make the structure unable to satisfy the equilibrium of forces, collapse is inevitable. As *Fig. 1.2* shows that, for avoiding any collapse in column or in joint, a commonly termed “strong column-weak beam” concept is generally followed over “strong beam-weak column”.

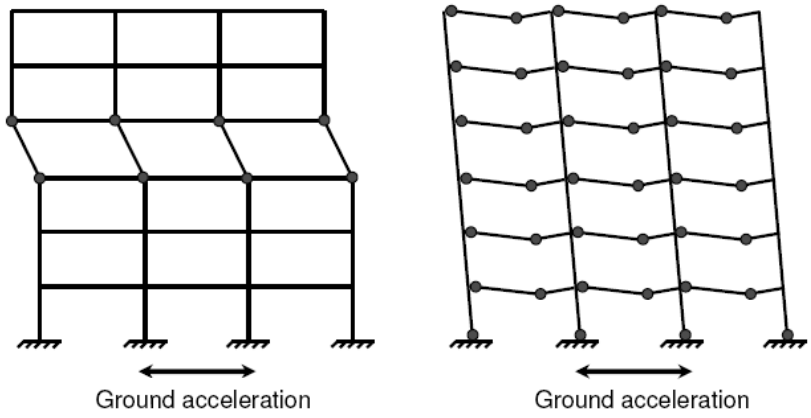

Fig. 1.2 Development of plastic hinge in -column and -beam, respectively

An earthquake resistant structure should dissipate seismic energy through damage in the structural system, but collapse should not occur. Further, damage should occur at preferable location which does not lead to collapse. Experience from previous earthquakes reveals that beam-column joints and column ends are wrong locations to dissipate seismic energy. Shear failures and anchorage failures of reinforcing bars are wrong types of damage which dissipate very little energy and lead to collapse. So, the force transfer mechanism in the critical zones (D-regions) is the single vital local parameter for seismic resistance capacity of a structure. But, still today, shear transfer mechanism and force flow in the critical zones under seismic loading are not clearly understood which has the reflection in different design approaches and detailing requirements stipulated by various national and international standards for a particular structural component under seismic loading. Further, under-designed structures, though commonly practiced throughout the world are vulnerable to even any moderate seismic event due to their lack in any consideration of either seismic forces or ductile design. Therefore, it demands for assessment of their seismic performances with respect to the modern codes of practice towards adequate and timely strengthening against any undesirable collapse. Nevertheless, there is no such information on comparative performance of existing structures designed based on prevailing practicing standards (codes of practice) in different stages of their development. Further, stipulated provisions for seismic

design of structures differ from one standard to another. These issues need to be looked into.

Just after any earthquake, there is a common concern on a critical issue, i.e., the possibility of effective and reasonable retrofit of damaged structures for post-earthquake usage. Seismic retrofit of reinforced concrete structures is aimed at strengthening its structures, in general, and components, in particular, to achieve more and consistent strength and/or ductility and energy dissipation. Depending on type of damage, location and usage of the structure, degree of retrofit can be determined. But, in most cases, after a strong earthquake if the degree of damage is severe then the structures are thought to be irreparable and are abandoned in spite of huge economic impact. In view of this, to ensure further usability, it is required to investigate the retrofit possibilities of severely damaged structural components which represent the existing structures designed based on old codal provisions or newly built structures based on modern codes of practice.

Further, a large number of the existing structures throughout the world were constructed before 1970s' when only gravity load was considered for design. Even, in substantial number of newly built structures hardly any ductile codal provision is followed but merely gravity load design (GLD) concept is still practiced. Experience from devastating earthquakes in last few decades has compelled to progressively revise the seismic zonation maps of different countries. The existing GLD structures in the zones with medium or high seismic probability can not simply be approved from its safety point of view. In the same time, though those are seriously vulnerable to seismic loading, replacement of the GLD structures with newly built ductile designed structures is neither socially feasible nor economically viable. Hence, it is indispensable to develop upgradation schemes for the GLD structures where the upgradation schemes must be structurally adequate, economically reasonable and technically practicable as well.

A number of research works have been performed towards performance evaluation of existing structures, repair or retrofitting of damaged structures and upgradation of poorly designed structures. It is opined that the reported research works are rather discrete. In the present study, it is attempted to present a systematic approach starting from evaluation of performance to development of upgradation schemes where the observations from the previous steps are effectively utilized in the next step of study. Secondly, studies on comparative performance of existing structures designed based on prevailing codes of practice of different countries in different stages of their development are rare. Finally, as discussed before, strengthening of deficient [either damaged or under-designed (undamaged)] structures/components need far more attention and an in-depth investigation with a quantified target and towards a more effective solution. For better and useful

discussion, relevant knowledge available-, scopes identified- and the motivation obtained- for present studies would be presented in the respective sections.

Objectives of the research work

By keeping in mind the issues discussed above, the objectives of this research work are framed as:

1. Evaluation of performance of beam-column sub-assemblages of existing structures designed based on prevailing practicing standards in different stages of their development

2. Development of suitable retrofitting strategies for damaged beam-column sub-assemblages to provide the adequate resistibility to the seismically affected structures for possible future earthquake

3. Development of suitable upgradation schemes for beam-column sub-assemblages of simple gravity load designed structures to improve the under-designed non-seismic structure towards the modern ductile structures

Outline of the thesis

This thesis deals with the performance, retrofitting and upgradation of beam-column sub-assemblages of the existing RC structures built at different times. The following is the chapter-wise outline of the present research work.

Chapter 2 presents a brief on the present research works conducted on performance of existing RC structures/components designed based on different codes of practice. General introduction to the load transfer mechanism in beam-column joint connections and the differences in response based on geometry are also discussed. Finally, the description on representative structure, the most crucial structural component, codes of practice to be considered and details of specimens used in the study are provided.

Chapter 3 deals with the casting procedure, material testing and the test set up employed in the experimental investigations. Results obtained and observations made from the experimental studies are presented. Further, the strength of the specimens corresponding to each failure mode (joint shear, beam/column flexure, beam/column shear) is analytically

determined, compared with the experimental results and used for identifying the strength hierarchy of the specimens.

Chapter 4 brings out the development and performance of retrofitting strategies proposed in this study. Before that, the existing procedures and trend of research in last few decades for structural strengthening is brought out, and the inadequately attended and better options are identified. Two retrofitting strategies for non-ductile and ductile structural components are discussed and the comparative performance (load-displacement hysteresis, stiffness degradation, strength deterioration, energy dissipation, etc.) of the retrofitted and undamaged specimens are evaluated from experimental investigation.

Chapter 5 describes the basic principles and target for upgradation of poorly designed structures. For the three upgradation schemes proposed in this research work, quantity and disposition of material required for each of the schemes are analytically evaluated. Influences of constant- and variable- confinement effect on strength of the sections are investigated. Installation procedure of upgradation schemes is described in step by step. Finally, to obtain the level of both qualitative and quantitative improvements by applying those upgradation schemes, the experimental results and the failure patterns are compared with all the undamaged specimens considered in this study.

Chapter 6 illustrates the non-linear Finite Element analysis (FEA) of the undamaged and upgraded specimens. First, the numerical models developed using ATENA are validated with the experimental results. The crucial issues like material models, support condition, types of elements, mesh distribution, analysis procedure are briefly described. Since, it is not possible to conduct all the studies using experimental means, further detailed parametric studies on amount and distribution of materials for upgradation are carried out which would provide a scope for optimisation as well.

Chapter 7 summarizes the conclusions derived from the entire study. Further, few identified issues are also recommended as the scopes for future research on the present topic.

2 Theoretical aspects and representative specimens

It is indeed a crucial but significant matter to choose the representative structure and the vital components for carrying out the investigation on performance evaluation of existing reinforced concrete (RC) structures under seismic loading. Before identifying the representative structure and its most important component which plays the great role in RC structures under seismic loading, an in-depth review of literature is carried out and a very brief of it is being presented below to identify the trend and focus of current research work on this particular topic.

2.1 A brief on state of the art

In last few decades, a number of research works have been carried out to understand the behaviour of existing buildings and possible scopes for improvements in structural design under seismic loading. The major concern is focussed for those structures which were typically built in seismic-prone countries before the introduction of adequate seismic design code provisions and the implementation of concepts of capacity design in the 1970s'. Beaufait and Williams (1968) presented a study on behaviour of reinforced concrete portal frames under sway loading to investigate the role of joint reinforcement steel on ultimate load capacity of the structure. Two types of sway loading (cyclic and uni-directional) were considered for a number of portal frames where the cyclic sway loading was used to represent the simplified seismic loading. Durrani and Wight (1985) and Ehsani and Wight (1985) discussed the seismic behaviour of interior and exterior beam-column joints, respectively, under seismic loading where the specimens were designed according to the recommendations of ACI-ASCE Committee 352 (1976). The findings were compared with the ductile beam-column joints of moment resisting frames to identify the role of joint hoop reinforcement. Ahmed and Shah (1985) discussed the behaviour of hoop confined concrete under high strain rates. Based on the results obtained from the study, empirical equations were proposed to predict the effect of strain rate on material property of concrete. It was observed that for both plain and hoop confined concrete there was an increase in elasticity, peak stress and peak strain, but it was difficult to obtain the post peak behaviour of plain concrete.

Aycardi et al. (1994) studied the performance of GLD sub-assemblages (according to ACI 318-89, 1989) under seismic loading. Parameters like axial load level, with- and without- lap splice were studied. It was also attempted to analytically model the seismic behaviour and to identify the parameters which play the key role under seismic loading. Bracci et al. (1995) conducted a series of tests to evaluate the seismic resistance of GLD structural frames (according to ACI 318-89). A 3-storied RC scaled model was experimented under various level of earthquake. Both global and local performance of the structure and its components were studied to determine the strength and deformation capacity under seismic loading. The major observation was that the GLD structures mainly suffered from strong beam-weak column behaviour with poor reinforcement detailing. El-Attar et al. (1997) brought out a study on behaviour of GLD RC buildings (according to ACI 318) under seismic loading. It was found that GLD RC buildings without walls would experience very large deformations associated with considerable stiffness degradation during a moderate earthquake.

Simulated seismic load tests on interior and exterior beam-column joints with substandard reinforcement details (pre-1970s') were described by Hakuto et al. (2000), by considering an existing RC building designed in late 1950s' (based on New Zealand code which does not conform to present NZS 3101:1995). It was pointed out that moment resisting frames with such detailing would show extremely poor performance under severe earthquake. A gravity load collapse mechanism of RC frames was investigated by Elwood and Moehle (2002) using a shake table to observe the process of dynamic shear and axial load failures. The RC frame was characterised by low ductile columns with a predominant shear failure mode which accelerated the lateral strength degradation procedure. It was concluded that axial stress on the column influences the behaviour of the column during shaking, particularly after shear failure. Dhakal et al. (2005) carried out an experimental study on dynamic response of GLD (according to British Standard BS8110-1985) RC connections. It was observed that, though the connection zones are most important parts in dissipating energy during earthquake, most of the GLD connections are weaker than the adjoining structure and failed in shear.

A comparative study on seismic behaviour of columns in ordinary and intermediate moment resisting frames (according to ACI 318-02) was carried out by Han and Jee (2005). It was pointed out that all the ordinary and intermediate moment resisting frames have strength greater than specified by ACI 318 and show a considerably high drift capacity. Seismic performance of scaled exterior beam-column joints designed according to modern building codes was investigated by Tsonos (2007). Scaled beam-column joints were designed according to Eurocode 2 (2005) & Eurocode 8 (2006); ACI 318-02 & ACI 352R-02 and new Greek Earthquake Resistant Code (1995) and tested under cyclic loading. It was observed that the joint designed according to ACI 352R-02 and one of the joints based on Eurocode 2

and Eurocode 8 performed satisfactorily under cyclic loading whereas the other joints could not meet the desired performance stipulated by Eurocode and Greek code.

The review shows that the seismic behaviour of existing RC structure and its components, particularly the beam-column joints, designed based on different codes of practice has attracted a considerable attention from the researchers. Since, most of the research works on seismic performance of RC structures had considered American standard (ACI-318), New Zealand Standard (NZS 3101) or British Standard (BS 8110) for designing the existing structure, in this study European Codes (Eurocode 2 and Eurocode 8) and Indian Standards for seismic design (IS 456-2000 and IS 13920-1993) have been considered for analysis, design and detailing of a conventional RC structure. It is worthy to state that both the codes have an extensive use in Europe and South Asia which are prominently seismic prone zones. Further, before rationally identifying the single most crucial component of a representative structure during seismic event, it is required to understand the behaviour, force transfer mechanism and failure modes of the critical components of RC structure.

2.2 Deficiencies of non-seismically designed structures and components

The present knowledge has confirmed the expected inherent weaknesses of the existing under-designed structures as observed in past earthquake events. Typical structural deficiencies of pre-1970s' buildings can be described (Schofield et al., 2006) as *i*) inadequate confining effects in the potential plastic regions, *ii*) insufficient transverse reinforcement in the beam-column joint regions, *iii*) insufficient amount of column longitudinal and transverse reinforcement, *iv*) inadequate anchorage detailing, for both longitudinal and transverse reinforcement, *v*) insufficient lap splices in column reinforcement just above the floor or at the foundation level, *vi*) insufficient shear reinforcement in wall systems when compared to the expected lateral demand, *vii*) inadequate design of the foundations to account for overturning moment caused by lateral loading, and *viii*) lower quality of materials (concrete and steel) when compared to current practice.

It has also been found that due to inadequate reinforcement detailing, absence of transverse reinforcement in the joint region, brittle failure mechanisms are expected either at local level (e.g. shear failure in the joints, columns or beams) or global level (e.g. soft storey mechanism).

2.2.1 Beam-column joint: the most critical structural component under seismic loading

A joint is defined as the portion of the column within the depth of the deepest beam that frames into the column. The functional requirement of a joint which is the zone of intersection of beams and columns is to enable the adjoining members (*Fig. 2.1*) to develop and sustain their ultimate capacity. The role of these joints becomes more critical under seismic loading.

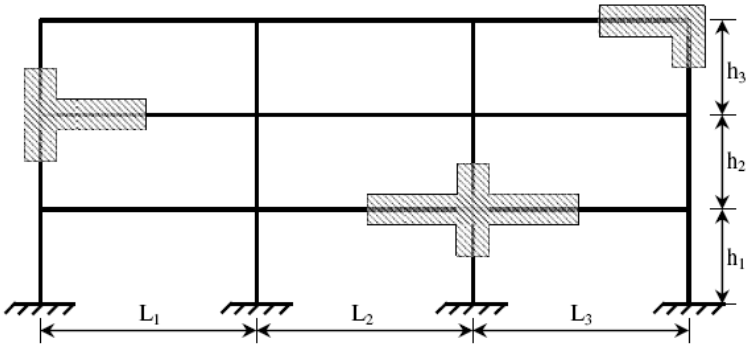

Fig. 2.1 Typical reinforced concrete frame with different beam-column joints

The severity of forces and demands on the performance of these joints necessitate a comprehensive understanding of their seismic behaviour. These forces develop complex mechanisms involving bond and shear within the joint. The pattern of forces acting on a joint depends upon the configuration of the joint and the types of load acting on it. The forces on an exterior and interior joint under seismic loading can be depicted as shown in *Fig. 2.2*. The tension and compression from the beam ends and axial loads from the columns can be transmitted directly through the joint. Due to seismic loading, the equilibrium forces from beams and columns develop diagonal tensile and compressive stresses within the joint (as shown in *Fig. 2.2*).

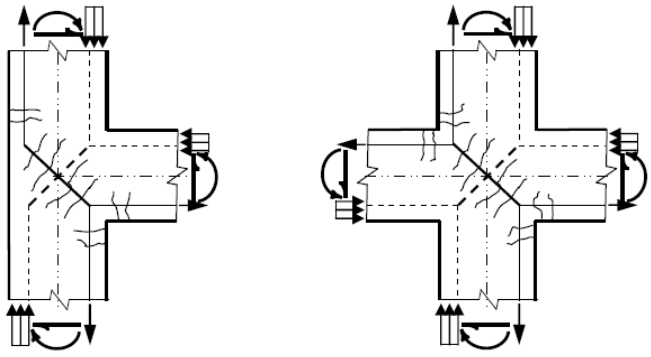

Fig. 2.2 Beam-column joints under seismic loading (only upward loading is shown)

Established research works and past evidences illustrated that the failure in an RC beam-column joint can arise in form of the following modes (Dutta and Mander 2001):

1. Shear or flexure-shear failure of the column outside potential plastic hinge zone
2. Failure of the connections by one of the following:
    - Bond failure of the lap-splice zone at the end of the columns
    - Anchorage-bond failure within the connection
    - Joint shear failure adjacent to the column
3. Premature concrete failure due to lack of confinement
4. Failure of the confined core concrete due to buckling of the longitudinal reinforcing bars
5. Fracture of the transverse hoop reinforcement (leading to failure modes 1–3)
6. Failure due to low cycle fatigue of the longitudinal reinforcement

2.3 Performance criteria

The joints should have adequate strength, stiffness and ductility to resist- and transfer- the internal forces induced by the framing members. The moment resisting frame is expected to obtain ductility and energy dissipation capacity from flexural yield mechanism at the plastic hinges. Beam-column joint behaviour is controlled by bond and shear failure mechanisms, which are weak sources for energy dissipation.

Under horizontal earthquake event, the moments and shear forces generated in the beams and columns of a building frame introduce internal stress resultants at the faces of joint core (as shown *Fig. 2.3*). The stress resultants cause both horizontal and vertical shear forces in the joint cores. Finally, internal diagonal tensile and compressive stresses would occur due to the development of joint core shear. If the diagonal stress is large enough, it would lead to diagonal cracking (in tension) or crushing (in compression) of the core concrete. Unless adequate shear resistance is provided in the joint core, failure of the joint core may eventually occur along the corner to corner diagonal plane.

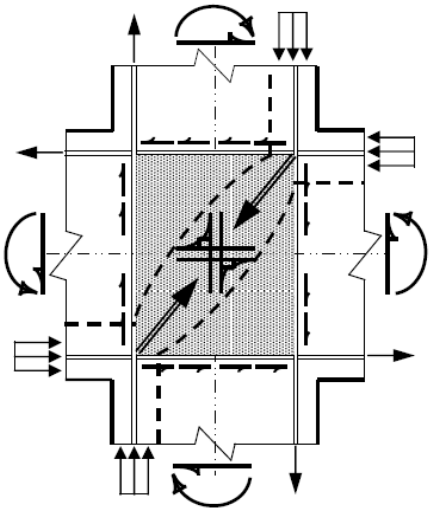

Fig. 2.3 Force transfer mechanism within a joint under seismic loading (only one direction is shown)

The performance criteria for joints under seismic actions are summarized as follows:

1. The joint should have *sufficient strength* to activate- and utilize- the maximum capacities in the adjoining flexural members.
2. The *degradation* of joints should be so limited such that the load carrying capacity of the columns is not affected in design level.
3. *Brittle mode* of failure (shear) should always be avoided and preferred to have a *ductile flexural mode* of failure in beams.
4. The joint deformation should not result in increased *storey drift*.

2.4 Joint shear strength

In general, the joint region can be idealized as a two dimensional structural plane subjected to internal forces from the beam and column acting on the joint face. The forces are primarily compressive, tensile and shear in nature. As mentioned before, the shear forces in the joint region develop diagonal compressive- and tensile- forces within the joint core, resulting in the formation of a diagonal failure plane. The essential components of the shear resisting mechanism are being discussed here, for better understanding, with respect to a general symmetric interior joint.

The resistance to shear forces in a joint core can be based on two widely accepted mechanisms. The *strut mechanism* (as shown in left of *Fig. 2.4*) transfers shear forces through a diagonal concrete strut. This strut sustains only compression and is assumed to be inclined at an angle close to that of the potential corner to corner failure plane. It is reported

that this type of mechanism is developed at the initial loading stage before significant flexural rotation which causes substantial reinforcement strain and full depth cracking. Due to the normal forces transmitted from the compression zone(s) of the adjoining members, shear forces are introduced. The diagonal compressive force is activated primarily by concrete compression forces at the two corners of the joint core and also by some bond forces transmitted from the beam and column reinforcements. At this stage, a minimum amount of joint hoop reinforcement would be effective for confinement purpose. The contribution of this mechanism sustaining a diagonal compression force is referred as the “shear carried by the concrete”.

The *truss mechanism* is activated in the later stage by following bar yielding and bond deterioration. This mechanism consists of the contribution to the shear resistance from the vertical and horizontal reinforcements inside the joint core. It is postulated to be a network of small compressive struts in the core concrete and tensile forces along the horizontal and vertical reinforcements (right of *Fig. 2.4*). These bond forces are idealised as uniformly distributed shear flow. If the joint core reinforcement is adequate, a diagonal compression field with a resultant diagonal force can still be sustained to transmit the bond forces despite of extensive cracking in the joint core. The truss mechanism generating this compression field involves the participation of horizontal reinforcement (in form of joint hoops), vertical reinforcement (in form of column intermediate bars), and numerous diagonal concrete struts. The contribution of this mechanism is referred as the “shear carried by the reinforcement”.

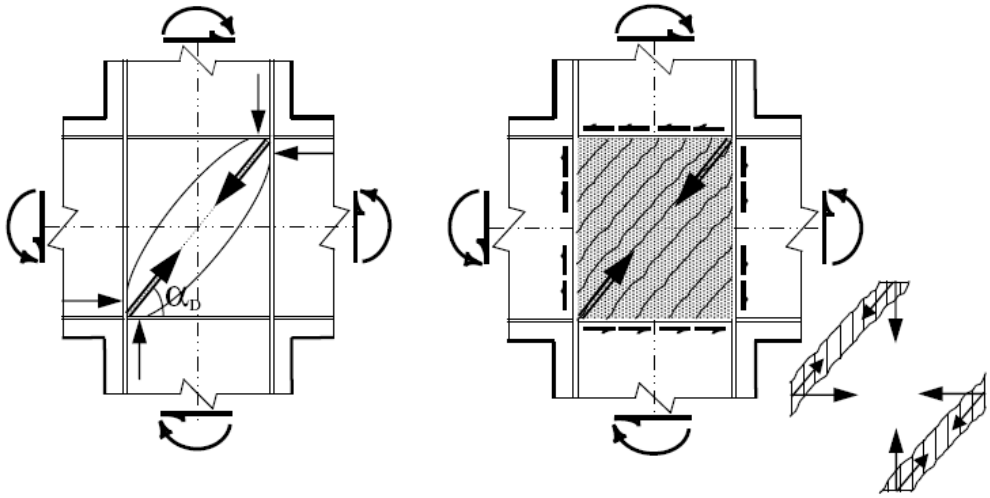

Fig. 2.4 Strut mechanism (left) and truss mechanism (right)

It is seen that the behaviour of beam-column joints under seismic load can be deduced from equilibrium principles relevant to diagonally cracked reinforced concrete elements. Consideration of shear deformation of joint core (*Fig. 2.5*) shows that shear stress applied to

the boundaries of a joint core can be transferred by means of diagonal compression field. In comparison to the tensile strains in the reinforcements, the concrete diagonal compressive strains are generally negligible. Hence, as shown in figure (*Fig. 2.5*), there is a tendency for the joint core to dilate as seismic actions continue. This implies that both vertical and horizontal reinforcements passing through the joint core would be stretched.

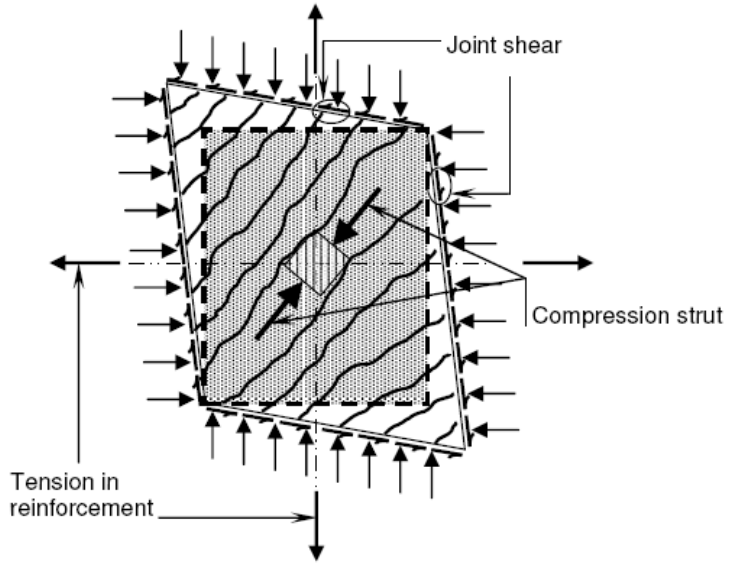

Fig. 2.5 Diagonal compression field induced by shear deformation

The behaviour of a typical interior beam-column joint of a frame under seismic load, as discussed above, can similarly be applied to an exterior joint. *Fig. 2.6* shows the features of an exterior beam-column joint where one beam frames into the column. The external forces acting on one face of the joint develop high shear stresses within the joint. The increase in shear stresses intensifies the diagonal stresses, causing diagonal cracks when tensile stresses exceed the tensile strength of concrete. Extensive cracking occurs within the joint under load reversals, affecting its strength and stiffness. In due course, the joint becomes flexible enough to undergo substantial shear deformation. Therefore, it is essential to thoroughly determine the shear force demand and the shear strength of the beam-column joints, in general, and exterior ones, in particular. Since, the codal guidelines aim at the beam hinging mechanism, joint shear strength only in the horizontal direction is focused in the further discussions.

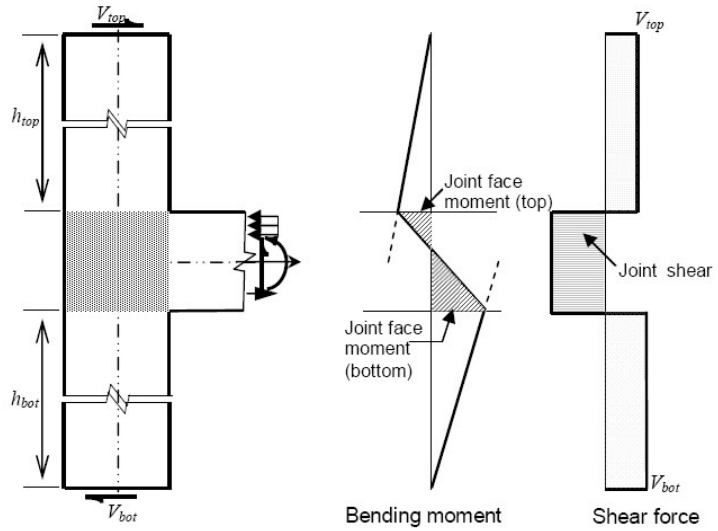

Fig. 2.6 Bending moment and horizontal shear force diagram in an exterior joint

The mechanisms of shear resistance of beam-column joint cores imply that the bond stresses developed in the longitudinal bars of beam(s) and column(s) play a very important role in the shear behaviour of joints. During a severe earthquake, modern building frames with ductile design are expected to develop plastic hinges at or near the ends of beams and a very high bond stress can occur which could lead to excessive slip or bond failure (*Fig. 2.7*) of the beam bars.

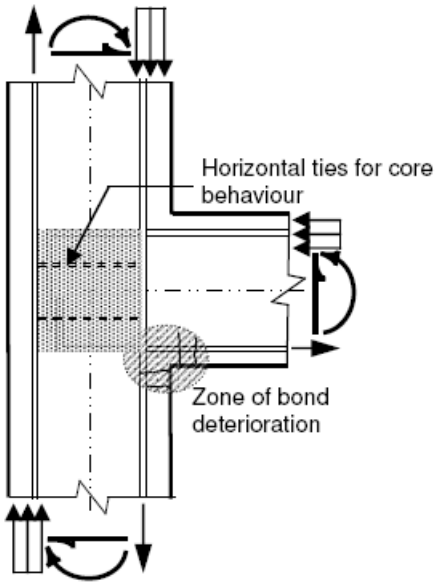

Fig. 2.7 Critical zone of exterior joint for bond deterioration under seismic loading

Different damage or failure modes, as discussed in section 2.2.1, are expected in beam-column joints depending on the type of joint (exterior or interior) and the adopted structural details i.e. presence of transverse reinforcement in the joint, use of plain round or deformed bars etc. The existing poorly designed frame structures are characterized, as pointed out

before, mostly by flexible columns, weak joints and strong beams, and non-ductile reinforcement detailing. Possible damage mechanisms of exterior beam-column joints with no transverse reinforcement in the joint region are shown in *Fig. 2.8* (Pampanin et al., 2003).

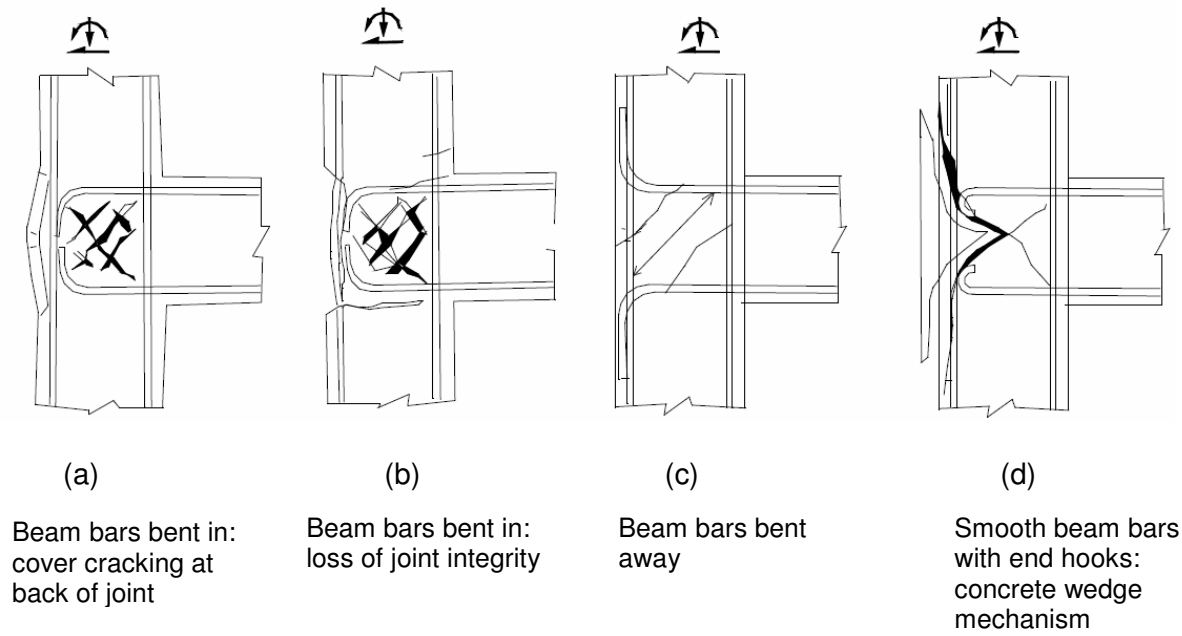

Fig. 2.8 Alternative damage mechanisms for exterior joints (Pampanin et al., 2003)

Each of the failure modes mentioned above can be avoided, or delayed with proper reinforcement detailing: (i) by providing sufficient anchorage to the longitudinal reinforcement, and (ii) sufficient transverse reinforcement. It is well examined that due to sudden discontinuity of the geometry, exterior joints are more vulnerable to seismic loading than the interior one because it demands to explore additional parameters such as bond-slip of reinforcement [Pampanin et al. (2003)]. Hence, in the present study, exterior beam-column joint has been chosen for investigating the performance under seismic type loading.

2.4.1 Principal stress levels in joints

In design of beam-column joints of building frames, it has been the practice to set shear stress limits based on the nominal shear stress calculated as

$$\nu_{jh} = \frac{V_{jh}}{b_{je} h_c} \text{ and } \nu_{jv} = \frac{V_{jv}}{b_{je} h_b} \qquad (2.1)$$

$$V_{jv} = \frac{V_{jh} \cdot h_b}{h_c} \qquad (2.2)$$

where, V_{jh} = $T_B - V_{Col}$ *(calculated from the moment at beam on joint face/lever arm as shown in Fig. 2.9)*

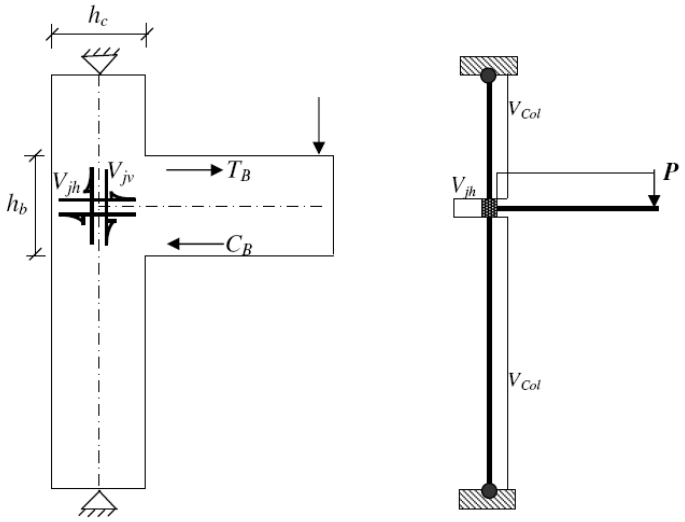

Fig. 2.9 Development of joint shear stress (cross section not in scale)

For typical knee and tee (exterior) joint conditions, limit shear stress is considered to be $1.0\sqrt{f_c'}$ MPa and $1.25\sqrt{f_c'}$ MPa, respectively. It can further be argued on these limits because these limits are primarily based on the performance of joints designed without specific consideration of force transfer mechanisms. Moreover, the well-designed (in accordance to modern seismic codes) joints have shown to sustain significantly higher shear stress levels without distress.

A simple Mohr's circle analysis for stresses shows that the nominal principal stresses in the joint region are given by

$$p_c, p_t = \frac{f_v + f_h}{2} \pm \sqrt{\left(\frac{f_v - f_h}{2}\right)^2 + v_j^2} \qquad (2.3)$$

where, v_j = *joint shear stress*

In an exterior beam-column joint, f_h is derived from the mean axial force at the centre of the joint. f_v is calculated from the column axial load including the seismic component. For *type 2* joints (as defined in ACI-ASCE 352), the concrete contribution is limited by the assumed occurrence of diagonal tension failure at $0.29\sqrt{f_c'}$ MPa which can be increased to 0.42 $\sqrt{f_c'}$ MPa for joints confined by transverse beams. According to Priestley (1997), joint failure due to diagonal tension takes place progressively and hence, is less brittle than diagonal compressive failure. The latter can thus be more critical in the case of joints with high shear stress level and high normal forces. The failure criterion based on compressive stress is suggested as

$$p_c = \frac{f_v + f_h}{2} + \sqrt{\left(\frac{f_v - f_h}{2}\right)^2 + v_j^2} < 0.5 f_c^{'} \qquad (2.4)$$

After deciding the codes of practice for analysis and design of RC structure for the present study, giving the brief on the force transfer mechanism-, failure pattern- and performance criteria- for beam-column joints and identifying the exterior beam-column joint as the crucial structural component, now the details on the specimens will be presented next.

2.5 Analysis and design of structural sub-assemblage

As mentioned before, European Codes (Eurocode 2 and Eurocode 8) and Indian Standards for seismic design (IS 456-2000 and IS 13920-1993) have been considered in this study for analysis, design and detailing the beam-column sub-assemblages (joints) of a most regular and conventional RC structure (shown in *Fig. 2.10*). Here, the term 'beam-column joint' is defined by an RC joint and adjacent beam(s) and column(s) with typical length, whereas 'beam-column sub-assemblage' represents a portion of RC structure around beam-column joint to characterise the true behaviour (force distribution) of the global structure. For obtaining the seismic forces developed at structural components, response spectrum analysis of the selected RC building was carried out where the spectrum was adopted from Eurocode 8 (shown in *Fig. 2.11*). The structure considered in this study was assumed to be in Class D (soft to firm cohesive soil), Importance factor =1.0 and situated in Zone 3 which is maximum assigned in Germany. In Eurocode 8, two types of spectrum are suggested. It is advised to use Type-2 for earthquakes that contribute most to the seismic hazard defined for the site for the purpose of probabilistic hazard assessment, otherwise Type-1 can be used. In the present study Type-1 spectra has been considered.

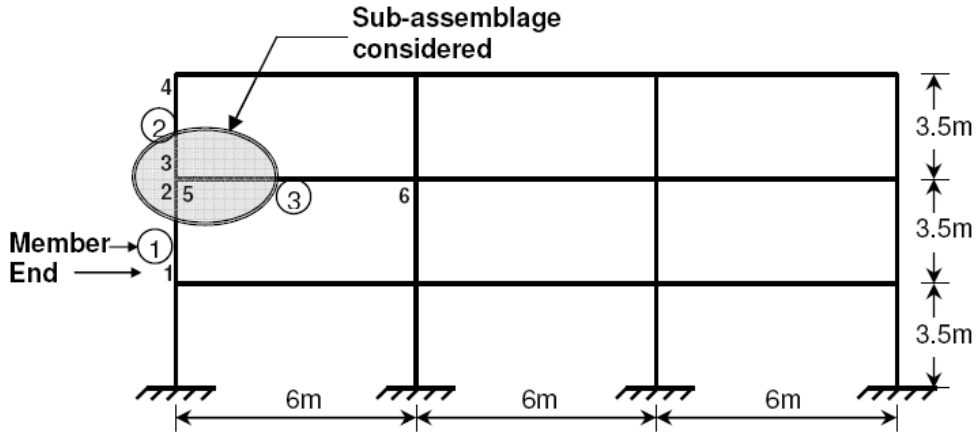

Fig. 2.10 General arrangement of the building frame considered in the present study (dimensions of beam and column are 300 x 400 and 300 x 300 respectively)

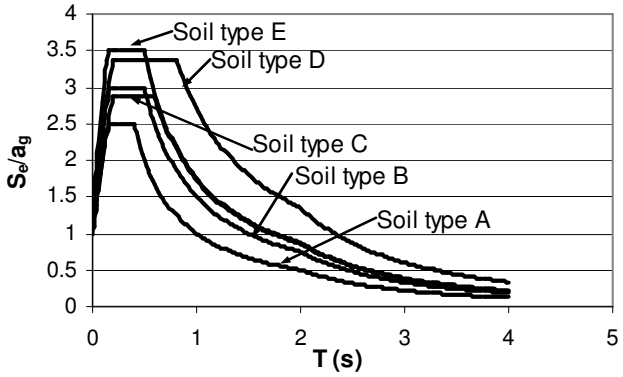

Fig. 2.11 Elastic Response Spectra for building class Type-1 (5% damping)

2.5.1 Result from response spectrum analysis

In response spectrum analysis, first the free vibrational analysis is carried out. Based on the fundamental time periods of the given structure, the correspoding spectral acceleration is adopted for calculating induced base shear due to seismic loading. Hence, individual mass in nodes needs to be assigned. Next, the induced base shear is distributed at different storey levels. Finally, the given structure with distributed loads is analysed to obtain the member forces due to seismic loading. For the particular frame considered in this study, frequencies corresponding to first and fifth fundamental mode were found to be 1.3 Hz and 17.1 Hz, respectively, and first three modes were considered in response spectrum analysis. Since the exterior beam-column joint has been identified as one of the most crucial structural component during earthquake, the analysis results from dead load (DL), live load (LL) and seismic load (SL) are presented only for the sub-assemblage considered in this study. The member numbers and the end node numbers are shown in *Fig. 2.10* which are referred in the results presented in *Table 2.1* to *Table 2.3*. The primary results (obtained from *Table 2.1*) were used for different load combinations as specified by Indian Standard and Eurocodes (*Table 2.2* and *Table 2.3* respectively). It is also to mention that the enhancements of shear corresponding to moment resistance capacity of the elements were also duly considered.

Table 2.1 Forces obtained from analysis (in kN, m unit)

Member and location		**DL(unfactored)**			**LL (unfactored)**			**SL (unfactored)**		
		Axial	**Shear**	**Bending**	**Axial**	**Shear**	**Bending**	**Axial**	**Shear**	**Bending**
1	**1**	-110.1	10.78	19.76	-66.6	7.61	13.95	60.8	60.52	95.12
	2	-102.2	10.78	-17.97	-66.6	7.61	-12.69	60.8	60.52	116.7
2	**3**	-53.8	13.79	21.37	-32.4	9.74	15.08	16	23.25	29.09
	4	-45.9	13.79	-26.91	-32.4	9.74	-18.99	16	23.25	52.60
3	**5**	3	48.4	-39.34	2.1	34.17	-27.77	8	44.71	143.91
	6	3	-53.6	-54.93	2.1	-37.83	-38.77	8	44.71	124.36
Axial force with (-) ve is compressive										

Table 2.2 Forces considered for design (in kN, m unit) according to Indian Standard

Member and location		1.5 DL +1.5 LL			1.5DL + 1.5 SL			1.2DL + 1.2 LL+1.2 SL		
		Axial	**Shear**	**Bending**	**Axial**	**Shear**	**Bending**	**Axial**	**Shear**	**Bending**
1	**1**	-265.05	27.59	50.57	-256.35	106.95	172.32	-285.0	94.69	154.59
	2	-253.2	27.59	45.99	-244.5	106.95	202.00	-275.52	94.69	176.83
2	**3**	-129.3	35.29	54.675	-104.7	55.56	75.69	-122.64	56.14	78.65
	4	-117.45	35.29	68.85	-92.85	55.56	119.27	-113.16	56.14	118.2
3	**5**	7.65	123.86	100.66	16.5	139.67	274.88	15.72	152.54	253.22
	6	7.65	137.15	140.55	16.5	147.47	268.94	15.72	163.37	261.67
Axial force with (-) ve is compressive										

Table 2.3 Forces considered for design (in kN, m unit) according to Eurocode

Member and location		1.35 DL + 1.5 LL			1.0 DL + 0.6 LL + 1.0 SL		
		Axial	**Shear**	**Bending**	**Axial**	**Shear**	**Bending**
1	**1**	-248.4	25.97	47.60	-210.86	75.87	123.25
	2	-237.8	25.97	-43.29	-202.96	75.87	142.28
2	**3**	-121.2	33.23	51.47	-89.24	42.88	59.51
	4	-110.6	33.23	-64.82	-81.34	42.88	90.90
3	**5**	7.2	116.59	-94.76	12.26	113.61	199.91
	6	7.2	-129.11	-132.31	12.26	121.01	202.55
Axial force with (-) ve is compressive							

The exterior joint (selected sub-assemblage) was then designed and detailed based on different types of existing design considerations as (i) only gravity load design (pre 1970s'), (ii) seismic design as per the codal provisions but without any special ductile detailing (post 1970s' but before ductile design concept), and (iii) seismic design as per the codal provisions with special ductile detailing specified by the corresponding codes of practice.

It is important to mention here that the threshold of 1970s' as a limit to define the earthquake risk of building can be technically argued upon since the post-1970s' RC buildings have not suddenly been improved to a great extent to fulfil adequate seismic performance. Moreover, until recently, the inadequate reinforcement, especially in joints, has been practiced and that causes the loss of cover concrete combined with buckling of the longitudinal bars due to inadequacy in confinement. But, it is true to state that after 1970s', an extensive modification on the design concept for RC structures under seismic loading has been taken place.

Structural sub-assemblages designed in this study, as mentioned above, represent the existing condition of buildings designed according to the available knowledge and prevailing guidelines at different times spanning from gravity load design concept to fully earthquake resistant design. For ready reference, a brief on the seismic criteria and detailing provisions from Eurocode (EC) and Indian Standards (IS) are given in *Appendix (C)*.

2.6 Details of the structural sub-assemblages

Total six numbers of specimens were designed and detailed based on Eurocode and Indian Standards for three different stages of codal evolution (described in *Table 2.4*). It is to mention that there is a provision in Eurocode to choose the level of ductility as medium or high. Since the high ductile detailing from Eurocode is comparable to ductile detailing of Indian Standard (SP-5), only one specimen using medium ductility provision from Eurocode (SP-6) has been considered in this study. Concrete and steel strength for the specimens were considered to be 30 MPa and 500 MPa respectively. It is understandable that the gravity load designed structures (representing pre-1970s') with so high strength of steel may not be feasible, but to bring uniformity among the test specimens, such strength was chosen and designed accordingly. All sub-assemblages had the same general and cross-sectional dimensions as: height of column is 3.80 m and length of beam is 1.70 m with cross-sections of column and beam were 300 mm x 300 mm and 300 mm x 400 mm, respectively. The geometry of the components (top and bottom portion of column and beam length from joint face) was chosen to match the bending moment distribution at the joint based on which it was designed for. Only Specimens 5 and 6 included seismic detailing. For the ductile specimens, beam and column stirrup spacings are presented in the table, first for joint and adjacent zones for the confinement (as stipulated by the codes) followed by the rest part of the member, respectively. Reinforcement details of the specimens are shown in *Fig. 2.12*. A detailed experimental study was carried out to investigate the seismic performance of the structural component which will be discussed in Chapter 3.

Table 2.4 Specimens details

Specimens	**Code of practice**	**Reinforcement details**			
		Beam main	Column main	Beam stirrup	Column stirrup
Specimen-1 (**SP-1**) GLD	IS 456-2000	(2+2*)-16∅ top (2+1*)-16∅ bot (* =extra reinf)	4-25∅	2^{L}-8∅ @130 c/c	2^{L}-8∅@300 c/c
Specimen-2 (**SP-2**) GLD	EC 2: 1-1:2004 EN 1990:2002	(2+2*)-16∅ top (2+1*)-16∅ bot (* =extra reinf)	8-16∅	2^{L}-8∅ @145 c/c	2^{L}-8∅@300 c/c
Specimen-3 (**SP-3**) GLD+Seismic Load	IS 456-2000	4-25∅ top 4-16∅+1-25∅ bot	12-25∅	2^{L}-8∅ @110 c/c	2^{L}-8∅@140 c/c
Specimen-4 (**SP-4**) GLD+Seismic Load	EC 2: 1-1:2004, EN 1990:2002 EC 8 (EN 1998-1:2004)	3-16∅+2-25∅ top 5-16∅ bot	8-25∅	2^{L}-8∅ @120 c/c	2^{L}-8∅@130 c/c
Specimen-5 (**SP-5**) GLD+Seismic Load +ductile detailing	IS 456-2000, IS 13920-1998	4-25∅ top 4-16∅+1-25∅ bot	12-25∅	2^{L}-10∅ @100 /120 c/c	2^{L}-10∅@75/150 c/c
Specimen-6 (**SP-6**) GLD+Seismic Load +ductile detailing (medium)	EC 2: 1-1:2004, EN 1990:2002 EC 8 (EN 1998-1:2004)	3-16∅ + 2-25∅ top 5-16∅ bot	8-25∅	2^{L}-10∅ @100/150 c/c	2^{L}-10∅ @120/200 c/c

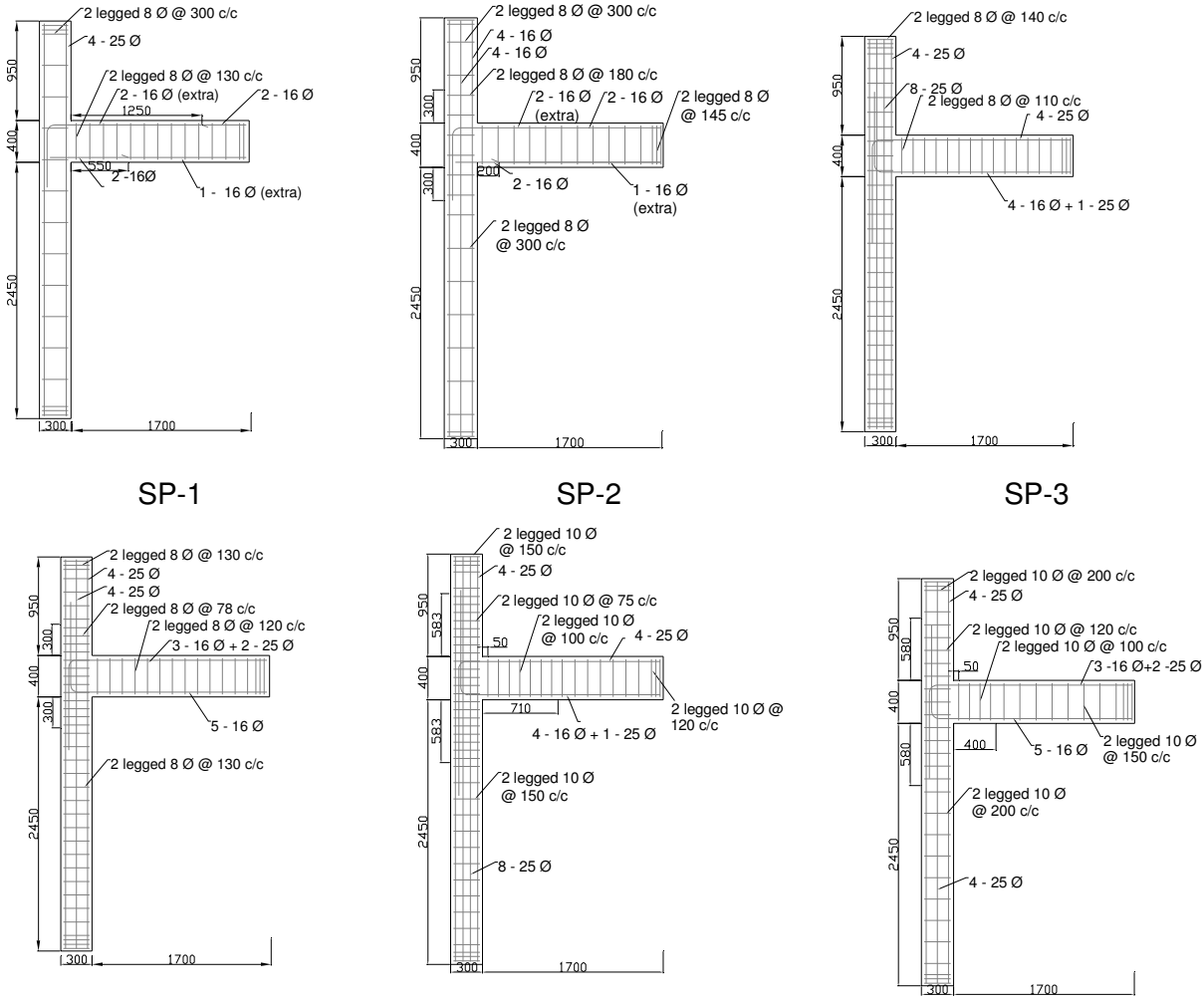

Fig. 2.12 Reinforcement details of the specimens considered in the present study

3 Evaluation of performance of sub-assemblages

Out of six specimens, as mentioned in preceeding chapter, it has been observed that the gravity load designed specimen based on Eurocode (SP-2) was quite similar to the specimen design based on Indian Standard (SP-1). Hence, only SP-1 (hereinafter called as 'GLD' specimen) was experimentally investigated along with the other two sets of specimens; SP-3 and SP-4 (hereinafter called as 'NonDuctile' specimen), and SP-5 and SP-6 (hereinafter called as 'Ductile' specimen) according to Indian Standard and Eurocode, respectively. Performance of the specimens has been experimentally and analytically evaluated and the obtained results would be used in further studies for determining the extent of retrofitting and level of upgradation of the specimens (presented in Chapter 4 and Chapter 5). Details of the experimental and analytical studies on the specimens representing the critical components of the existing structures are discussed below.

3.1 Casting of specimens

Experimental studies were carried out at Structural Engineering Research centre (SERC), Chennai, India. For better accuracy in geometry and superior surface finish, re-usable steel moulds were fabricated for casting the specimens. Reinforcement cage with instrumented strain gages and casting of the typical specimen is shown in *Fig. 3.1*.

Fig. 3.1 Instrumentation and casting of specimen (typical)

Material batching was carried out based on the mix design developed at SERC. Mixing of the material was done by a concrete mixer and a vibrator was used for compaction during concreting. Cover to reinforcement was assured by placing pre-cast cover blocks. During casting of each of the specimens, number of cubes (150x150x150 mm), cylinders (150x300 mm) and prisms (100x100x500 mm) were cast to obtain the material behaviour of concrete. Adequate curing was ensured for all the specimens and other items (cylinders, cubes and prisms) required for material testing.

3.1.1 Concrete properties

For getting the compressive strength of concrete, cubes were tested using UTM (Universal Testing Machine) and the tensile strength of concrete was obtained by 4-point bending test as shown in *Fig. 3.2*. Cylinders were tested in automated MTS system to get the cylinder compressive strength and entire envelop of the E-modulus of the specimens until failure (as shown in *Fig. 3.3*) which would be required for numerical investigations discussed in Chapter 6.

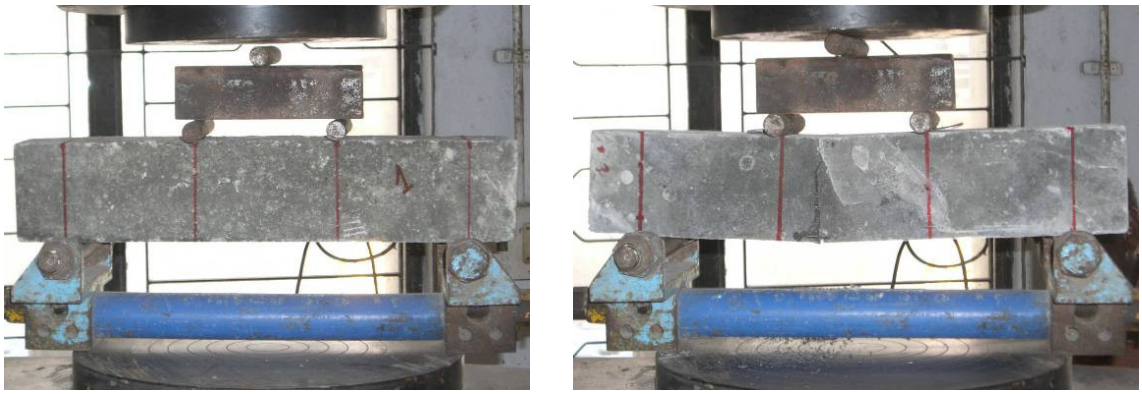

Fig. 3.2 4-point bending test of concrete prisms

Fig. 3.3 Test of concrete cylinders

Concrete material properties of 'GLD' and 'NonDuctile' specimens obtained from the tests are presented in *Table 3.1*.

Table 3.1 Concrete properties (average) obtained from the tests

	Cube compressive strength f_{cube} [MPa]	Prism tensile strength f_{ctm} [MPa]	E-modulus (MPa)
SP-1	37.16	4.28	22910
SP-3	35.00	4.08	23500
SP-4	36.17	4.18	22670

Here, prism tensile strength was calculated (as given in Eq. 3.1 based on CEB-FIP model code 90) from flexural strength which was directly obtained from the 4-point bending test.

$$f_{ctm} = f_{ct,fl} \cdot \frac{1.5 \cdot \left(\frac{h_b}{h_0}\right)^{0.7}}{1 + 1.5 \cdot \left(\frac{h_b}{h_0}\right)^{0.7}} \qquad (3.1)$$

h_b = *height of the prism section (in this case, 100 mm)*

h_0 =*100 mm*

3.2 Test set up and loading

The test specimens were instrumented with strain gages bonded on beam and column reinforcements (main bars, ties, stirrups) and LVDTs (linear variable displacement transducers), which were mounted on the joint surface for measuring shear deformation as well as attached to the beam and the column (as shown in Appendix *Fig. A1*).

The test set up was arranged on the test floor so that the beam-column sub-assemblage could be rest on the floor and the cyclic load was applied in the plane of the test floor. Vertical arrangement of the test set-up was avoided to make the test arrangement simplified and to apply a predefined axial load in column through a hydraulic jack resting on test floor. An axial load of 300 kN was applied to the column through the jack positioned between the column and one of the reaction block heads. The schematic diagram of the test set up is shown in *Fig. 3.4*.

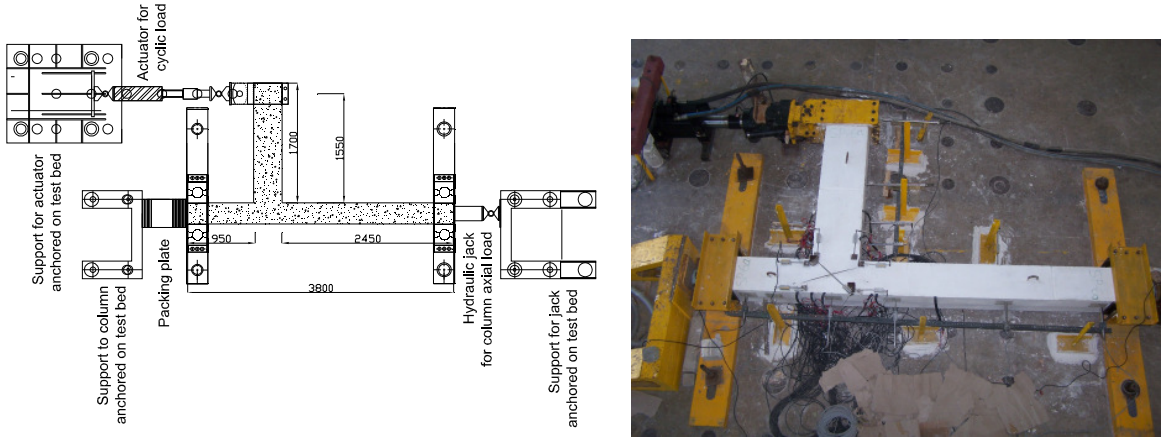

Fig. 3.4 (a) Schematic diagram of the test set up placed on test floor, (b) actual set up

The axial load was kept constant during the test. The lateral load was applied on the beam tip in displacement control mode according to the load history shown in *Fig. 3.5*. Reverse cyclic load was applied in terms of drift ratio (%) of the component where the drift is calculated as

$$\text{Drift ratio (\%)} = \frac{\Delta l}{l_b} \times 100$$

Where Δl and l_b are the applied displacement at the beam tip and the length of the beam from column face to the application point of the displacement.

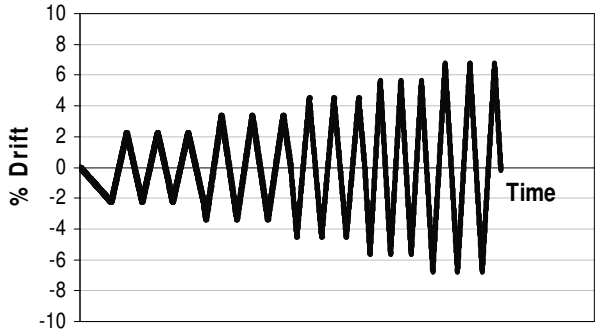

Fig. 3.5 Typical cyclic load history adopted in experiments

The amplitudes of the peaks in the displacement history were multiples of the yield displacement, whereas the yield displacement was defined as the tip displacement corresponding to yielding of the beam top reinforcement at the column face. From several alternative load histories, it is stated in FIB Bulletin 24 (2003) that the most severe strength degradation could be observed in specimens subjected to three systematic cycles at each drift level. Hence, in this study also, three complete cycles were repeated at each

displacement ductility level, finally to the maximum travel length of the actuator shaft, as applicable. The lateral displacement increments were applied in a quasi-static reverse cyclic manner. Although in the case of seismic action, the loading rates are higher than the rates corresponding to static conditions, it is advantageous that the quasi-static cyclic testing allows a careful monitoring of the specimen behaviour during the test and application of slow loading does not affect the material behaviour whereas high rate of loading may do.

3.3 Results and discussion

During the test of the specimens, it has been observed that the failure of the 'GLD' specimen (SP-1) was due to inadequacy in bond capacity of bottom main reinforcement in beam as there was no such detailing against reverse loading. Initially, under downward displacement, cracks started in the joint but, with increase in upward displacement, bond failure was found as the main mode of failure (as shown in *Fig. 3.6*). For the specimens designed for earthquake loading but without any ductile detailing ('NonDuctile' specimens SP-3 and SP-4), the behaviour was much improved in comparison to SP-1, but predominant shear failure of the joints and wedging out of concrete in joint occurred (as shown in *Fig. 3.7* and *Fig. 3.8*). The failure pattern of both the specimens (based on Indian Standard and Eurocode) was qualitatively same. Cover cracking at the back of the column and loosening of concrete integrity were also noted under higher level of loading. Though at initial stage of loading, bending cracks were observed in the beam and column outside the joint, no such contribution in dissipating energy was noticed in further steps. Hence, the major energy dissipation took place in the joint region only.

Fig. 3.6 Initial crack and final failure pattern of specimen SP-1

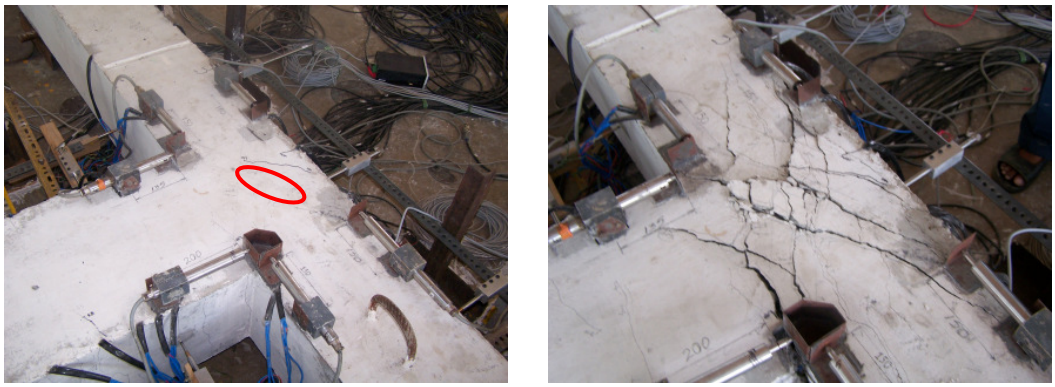

Fig. 3.7 Initial crack and final failure pattern of specimen SP-3

Fig. 3.8 Initial crack and final failure pattern of specimen SP-4

The primary objective of the study presented here is on evaluating the performance of sub-assemblages from existing under-designed structures (non-seismic 'NonDuctile'- and poorly designed 'GLD'- structures) and hence, discussion on experimental investigation is limited to the behaviour of 'GLD' and 'NonDuctile' specimens. Discussion on experimental investigation on- and behaviour of- 'Ductile' specimens (SP-5 and SP-6) can be found elsewhere [Novák et al. (2008)]. In the following sections and chapters, during discussion on the performance of the existing 'GLD' and 'NonDuctile' specimens and further retrofitting and upgradation, behaviour and results reported on 'Ductile' specimens are also duly referred for bringing out more insights, comparison and deficiencies.

3.3.1 General behaviour

As stated earlier, a number of strain gages were pasted on bending and shear reinforcement of beam and column. The previous research works emphasised that the role of the column ties is an important issue because the inadequate presence of column ties in joint would lead to a joint shear failure which is very common either in 'GLD' or 'NonDuctile' structures. In view of this, strain developed in the column ties along the height of the column has been

studied for all the specimens. Since it has been observed that the qualitative strain profiles for all the 'GLD' and 'NonDuctile' specimens were quite similar in nature, strain profile in column ties of only SP-4 is presented in *Fig. 3.9*. The figure clearly shows a very high shear demand in the joint region along the height of the column and it has also been noticed from the figure that a few of the strain gages inside the joint region did not function when a higher cyclic load was applied, possibly due to the development of very high strain. It underlines the inadequacy in joint shear reinforcement in 'NonDuctile' specimen which was obviously more deplorable in 'GLD' specimen since no such reinforcement was present there. Further, the strain distribution along the beam reinforcement has also been studied to investigate the development of strain in the reinforcement with the increase in displacement level and variation of strain along the length of the beam from the joint. Typical strain distributions at beam bottom and top reinforcements of SP-4 are shown in *Fig. 3.10* and *Fig. 3.11*, respectively. It reveals that under higher load (with applied displacement), strain would drastically reduce due to slip or loss of bond anchorage. Further, the strain gage near the joint face abruptly attracted very high strain which points out that the beam-column joint line could potentially be a line of failure unless the joint fails before that. Since the 'NonDuctile' specimens did not have any ductile detailing, there was no prospect to develop a plastic hinge in beam. Development of strain in beam top and bottom reinforcement was quite similar in other 'NonDuctile' specimen (SP-3). For 'GLD' specimen, though the beam top reinforcement bar performed well in initial displacement cycles, strain in beam bottom reinforcement did not fully develop because of high amount of slip in the bar due to lack in any anchorage mechanism.

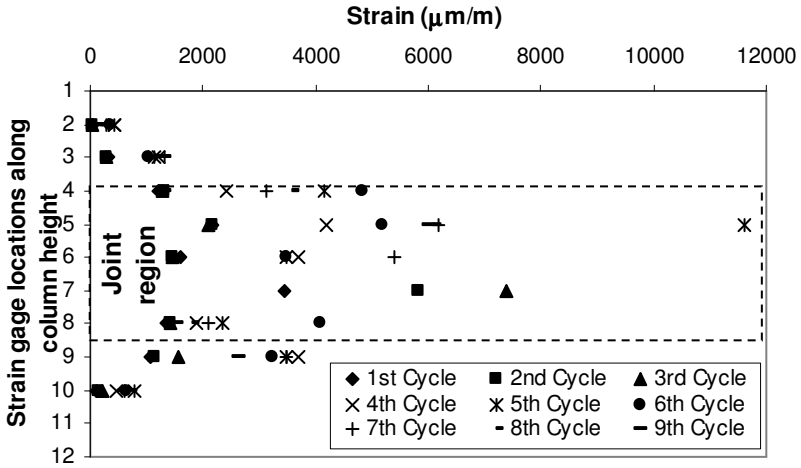

Fig. 3.9 Strain distribution in ties along the height of the column of SP-4

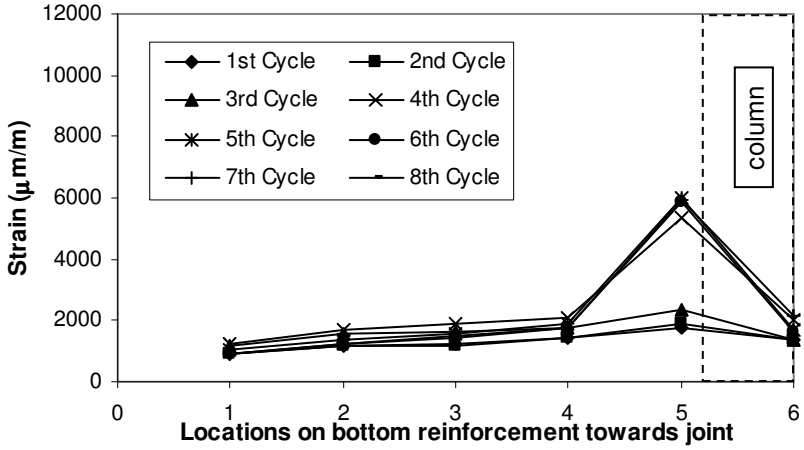

Fig. 3.10 Strain distribution in main reinforcement (bottom) of beam of SP-4

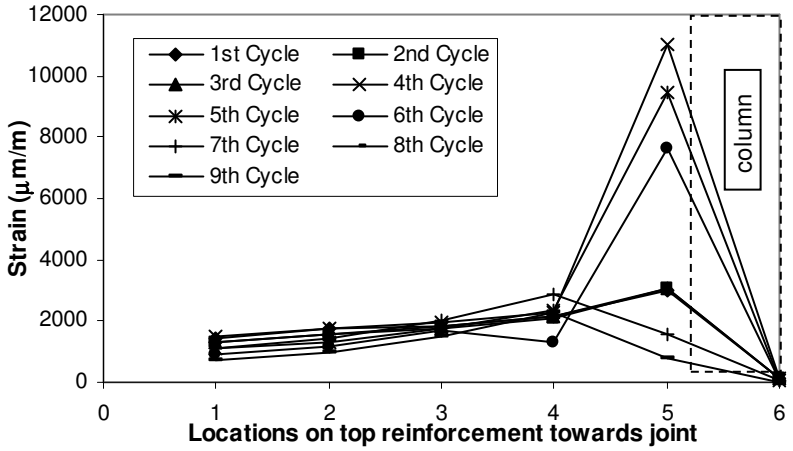

Fig. 3.11 Strain distribution in main reinforcement (top) of beam of SP-4

3.3.2 Shear deformation (angle)

Generally, codes of practice provide the procedure for designing the joints based on demand and supply in terms of shear stress and bond. But, this approach can be considered as weak since no importance on magnitude of deformation which requires for developing the limit state in the joint, is incorporated. Until now, relation between magnitude of joint distortion and the nominal strength of joint as a whole is not yet clear whereas the experimental results from previous researchers showed that the joint deformation can be served as an indicator of the performance of the joint as a whole [Pantazopoulou and Bonacci (1994)]. *Fig. 3.12* shows the guidelines of acceptable limits for existing structures (FEMA 273) where 'd' is the shear deformation angle at peak strength, 'e' is the shear deformation at collapse level and

'c' is residual shear strength. For RC structures, it is considered to have an 'e' value of 0.01 whereas 'd' value should not exceed 0.005 for non-conforming joints.

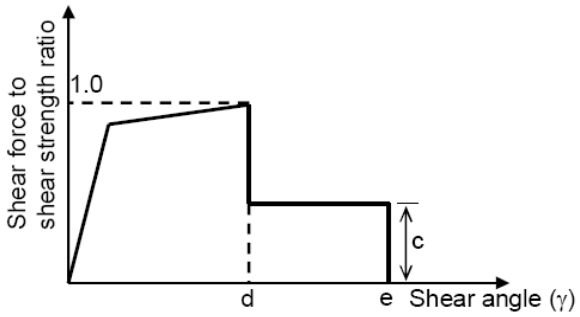

Fig. 3.12 Shear strength-shear angle model for RC joints

Since, joints regions in the RC structures are imposed to high shear, so the shear distortion behaviour of the specimens is important to investigate in this study. A schematic diagram of the undeformed and deformed shape of the joint is shown in *Fig. 3.13*. Though during experiment, orthogonality of the LVDTs for recording the deformation in the diagonal direction could be difficult to precisely maintain as theoretically required, but the orthogonality can be assumed for simplified mathematical evaluation in calculating shear distortion angle from the diagonal displacements.

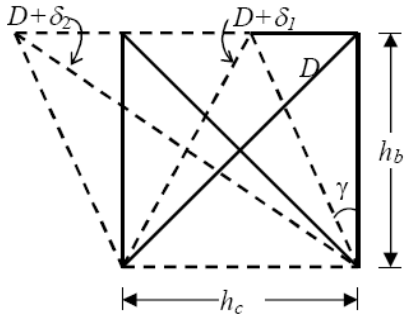

Fig. 3.13 Beam-column joint before and after shear deformation (idealized)

From the simple Pythagoras's theorem, it can be stated that (from *Fig. 3.13*)

$$(D+\delta_2)^2-(D+\delta_1)^2=(h_c+x)^2-(h_c-x)^2 \qquad (3.2)$$

x = *horizontal deformation of the joint*

And, finally, $\gamma=\dfrac{(2D+\delta_1+\delta_2)(\delta_2-\delta_1)}{4\cdot h_c\cdot h_b}$ *(3.3)*

γ = *shear deformation (angle)*

During the application of cyclic loading, measured shear distortion angle (through the deformation of diagonally placed LVDTs) for 'GLD' specimen (SP-1) and 'NonDuctile' specimen (SP-4) are shown in *Fig. 3.14* and *Fig. 3.15*, respectively. It is to mention here that

'NonDuctile' specimen SP-3 was tested first in this test series. So, the diagonal LVDTs were not placed on SP-3 to facilitate in observing the start of the cracks and their propagations without any hindrance. So the shear distortion diagram for SP-3 could not be investigated.

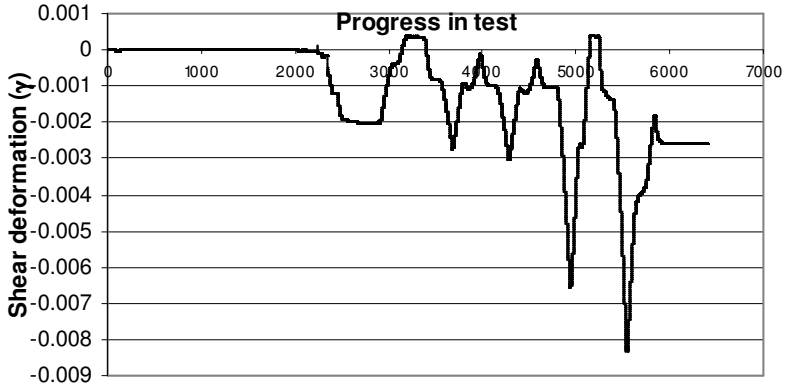

Fig. 3.14 Development of shear deformation with time in 'GLD' specimen SP-1

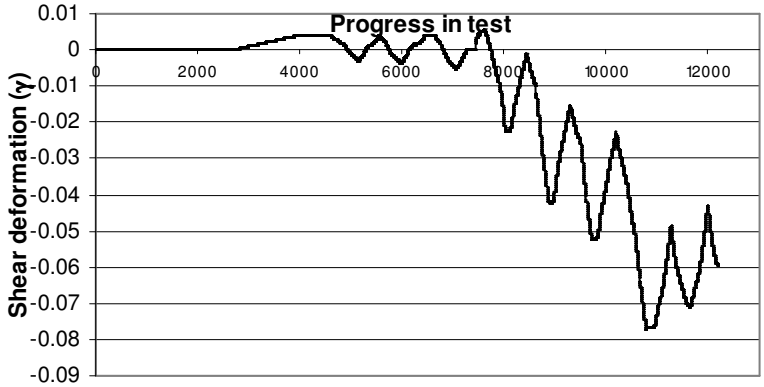

Fig. 3.15 Development of shear deformation with time in 'NonDuctile' specimen SP-4

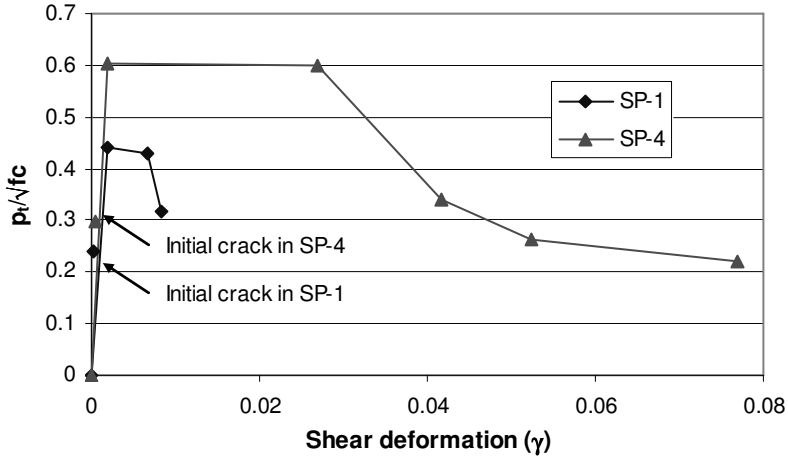

Fig. 3.16 Shear deformation vs principal tensile stress in the joint of the specimens

Current code provisions tend to limit the nominal shear stress in the joint expressed as function of concrete tensile strength ($k.\sqrt{f_c^{'}}$) which can also be seen from *Fig. 3.16*. It is shown that shear strength of beam-column joint can be related to its tensile strength (where k is an empirical constant). It has been found that the initial crack formed in the specimens at very early stage of shear deformation and it was, in comparison to 'GLD' specimen, slightly improved in 'Nonductile' specimen. Due to poor anchorage in the beam reinforcement of 'GLD' specimen SP-1, applied load on tip of the beam was not properly transferred through the joint which led to a wide crack at the beam-column joint line as can be seen in *Fig. 3.6*. Hence with displacement, the calculated shear deformation angle seems to be lower in comparison with 'NonDuctile' specimen. But, instead of better response, low shear angle with beam tip displacement (as shown in *Fig. 3.14*) was rather caused due to poor load transfer from beam to column through joint. Further, in 'NonDuctile' specimen SP-4, shear deformation was considerably high and with last displacement cycle (drift ratio ≈6.5) it has been found to be around 0.078 and generally restricted magnitude of shear angle as 0.01 (FEMA 273) reached at a drift ratio as low as 2.2. Hence, from shear deformation criteria, the under-designed specimens are found to be alarming.

3.3.3 Behaviour at milestone events

Structural behaviour parameters like shear stress and principal stresses in joint, which are important for evaluating the performance of joint region have also been studied with the development of different milestone events like first crack, yielding of reinforcement and maximum strain level in reinforcements and those are presented in *Table 3.2* to *Table 3.4* for SP-1, SP-3 and SP-4, respectively.

Table 3.2 Behaviour parameters for SP-1 during milestone events

Events in specimen	Strain (μm/m)	Drift ratio	Load (kN)	Shear stress (v_j) MPa	Principal stress (p_c) MPa	Principal stress (p_t) MPa	Shear deformation (γ)
First crack	-	-0.9	-56	-2.61	4.77	1.43	0.00014
Yielding of top beam bar	-	-1.4	-82.5	-3.85	5.86	2.53	0.0015
Maximum strain in top beam bar	5438	-3.2	-85	-3.97	5.97	2.64	0.0058
Yielding of bottom beam bar	-	-	-	-	-	-	-
Maximum strain in bot beam bar	1791	1.9	56	2.61	4.77	1.43	0.00037
Yielding of column bar	-	-	-	-	-	-	-
Maximum strain in column bar	903	-3.2	-68	-3.17	5.25	1.92	0.008
Maximum displacement (down)	-	-3.2	-68	-3.17	5.25	1.92	0.008
Maximum displacement (up)	-	3.2	39.2	1.83	4.14	0.81	0.0004

Table 3.3 Behaviour parameters for SP-3 during milestone events

Events in specimen	Strain (μm/m)	Drift ratio	Load (kN)	Shear stress (v_j) MPa	Principal stress (p_c) MPa	Principal stress (p_t) MPa	Shear deformation (γ)
First crack	-	-0.6	-58	-2.71	4.85	1.51	NA
Yielding of top beam bar	-	-4.1	-89.7	-4.19	6.17	2.84	NA
Maximum strain in top beam bar	6400	-7.7	-53.1	-2.48	4.65	1.32	NA
Yielding of bottom beam bar	-	3.7	83.74	3.91	5.92	2.58	NA
Maximum strain in bot beam bar	5087	4.3	83.98	3.92	5.93	2.59	NA
Yielding of column bar	-	6.1	101.4	4.73	6.68	3.35	NA
Maximum strain in column bar	2596	6.4	103.5	4.83	6.78	3.44	NA
Maximum displacement (down)	-	-6.5	-102.2	-4.77	6.72	3.39	NA
Maximum displacement (up)	-	6.5	61.95	2.89	5.00	1.67	NA

Table 3.4 Behaviour parameters for SP-4 during milestone events

Events in specimen	Strain (μm/m)	Drift ratio	Load (kN)	Shear stress (v_j) MPa	Principal stress (p_c) MPa	Principal stress (p_t) MPa	Shear deformation (γ)
First crack	-	-0.8	-64.8	-3.02	5.12	1.79	0.00038
Yielding of top beam bar	-	-1.9	-129.2	-6.03	7.92	4.59	0.0032
Maximum strain in top beam bar	11382	-4.8	-135.6	-6.33	8.21	4.88	0.077
Yielding of bottom beam bar	-	2.1	71.2	3.32	5.38	2.05	0.0667
Maximum strain in bot beam bar	6092	4.7	69.07	3.22	5.30	1.96	0.051
Yielding of column bar	-	-4.6	-134.7	-6.29	8.17	4.84	0.077
Maximum strain in column bar	5734	-6.8	-106.6	-4.97	6.91	3.58	0.0246
Maximum displacement (down)	-	-6.8	-106.6	-4.97	6.91	3.58	0.0246
Maximum displacement (up)	-	6.8	62.79	2.93	5.04	1.70	0.07527

From the tables presented above, few important points can be discussed on the behaviour of the specimens. Those are, (*i*) reinforcement in 'GLD' specimen was not properly utilised as the reinforcement at beam bottom had not even yielded and strain in column reinforcement was very low, (*ii*) yielding of beam reinforcement in both the 'NonDuctile' specimens was observed whereas the final maximum strain in bottom reinforcement was not as high as in top bars, (*iii*) in both the 'NonDuctile' specimens column reinforcements were yielded but at a very high drift ratio, (*iv*) maximum strain in column reinforcement of SP-4 was much higher that that observed in SP-3 (just at yielding limit) which showed a better protection of column of SP-3 from formation of plastic hinge in column, (*v*) maximum shear stress induced to joint of 'NonDuctile' specimens varied between $1.0\sqrt{f_c^{'}}$ MPa and $1.25\sqrt{f_c^{'}}$ MPa as expected for non-conforming exterior joints (section 2.4.1) but did not hold good for 'GLD' specimen, (*vi*) For 'NonDuctile' specimens, principal compressive stress in joint to produce extensive damage was found to be much lower than $0.5 f_c^{'}$ which is thought to be a limit for diagonal compressive stress to produce damage, (*vii*) maximum principal tensile stress developed in joints of 'NonDuctile' specimens was between $0.3\sqrt{f_c^{'}}$ MPa to $0.9\sqrt{f_c^{'}}$ MPa which was more

than that values ($0.29\sqrt{f_c'}$ MPa to $0.42\sqrt{f_c'}$) suggested by Priestley (1997), (*viii*) both the principal stresses developed in the joint of 'GLD' specimen were much lesser than that expected for non-conforming joints which again shows an improper load transfer mechanism in 'GLD' specimen, and (*ix*) shear deformation of the joint before the yielding of beam reinforcements (either top or bottom) was considerably high in comparison with stipulated value (0.01) for non-conforming exterior joints and higher shear deformation could impose additional shear drift in global structure.

3.3.4 Stiffness, strength and energy dissipation

The most important parameter for seismic performance of structural D-regions can be described by load-displacement hysteresis during the cyclic loading which can indicate the ductility capacity and energy dissipation efficiency of the component. It is well proven that the beam-column joint of reinforced concrete structure is the single crucial component in dissipating seismic energy during earthquake. In view of this, load-displacement hysteresis diagrams for each specimen (SP-1, SP-3 and SP-4) are presented in *Fig. 3.17*. The figures clearly present the extremely poor performance of the 'GLD' specimen. Further, the improvement in behaviour can be found as the design provisions are enhanced ('NonDuctile' specimens). It is important to mention here that, though SP-3 and SP-4 showed an improved performance in comparison to SP-1, energy dissipation capacity had not been increased to the desired extent for seismic design due to its lacking in ductile detailing. For all the under-designed specimens (SP-1, SP-3 and SP-4), a weak joint or inadequate anchorage caused the final failure. The load-displacement envelops of the specimens show (in *Fig. 3.18*) that SP-3 performed better than SP-4 under positive (upward) displacement cycles whereas under downward displacement cycles, the difference was negligible. It is also clear that the load-displacement envelops from 'NonDuctile' specimens are very close to the 'Ductile' ones (results obtained from Novák et al., 2008) and that signifies that the strength of the 'NonDuctile' specimens was not much different from the 'Ductile' specimens.

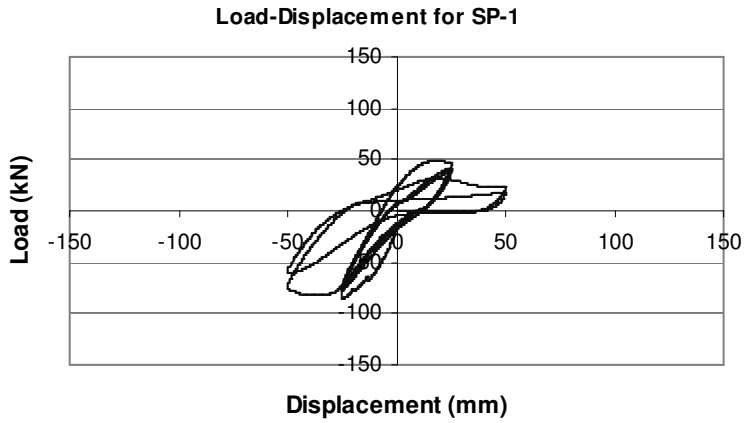

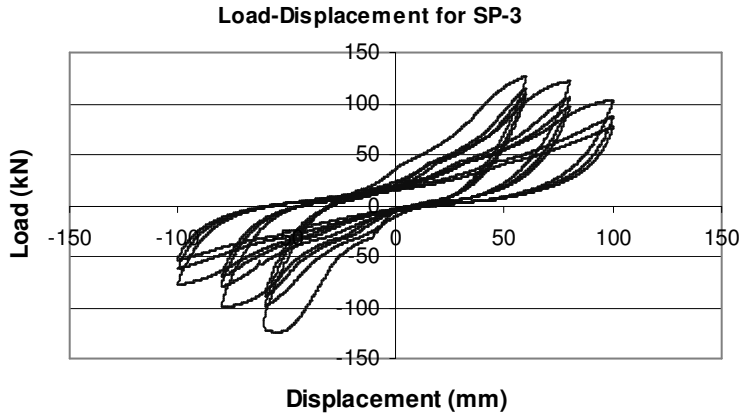

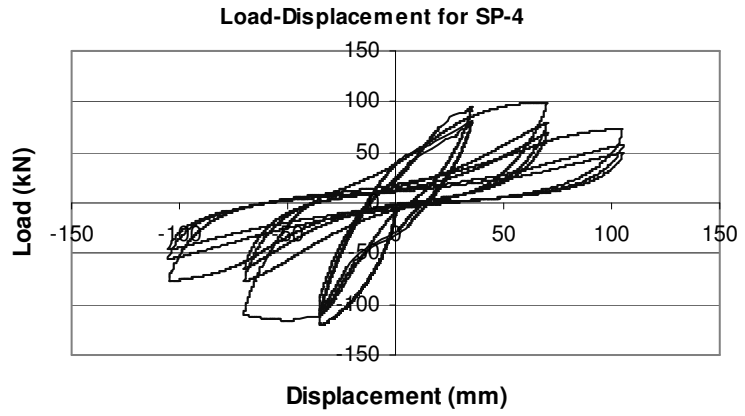

Fig. 3.17 Load-displacement hysteresis of the specimens (SP-1, SP-3 and SP-4 respectively)

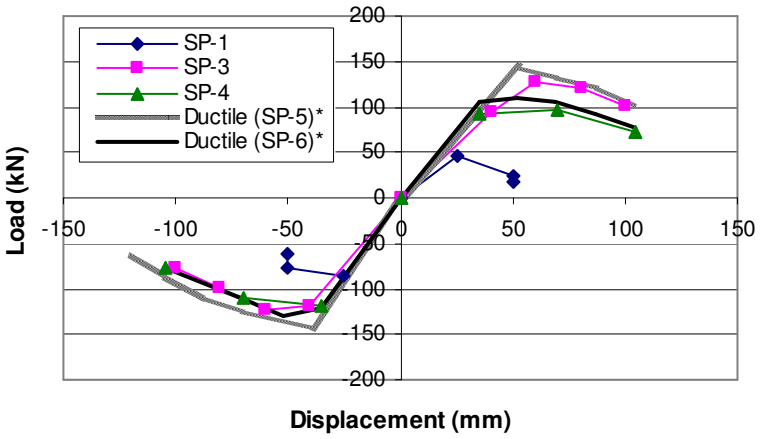

Fig. 3.18 Load-displacement envelop of the specimens

For seismic design, stiffness degradation and strength deterioration are two very significant indicators for comparative performance studies. For the specimens considered in this study, stiffness degradation and strength deterioration are shown in *Fig. 3.19* and *Fig. 3.20*, respectively. Here, it is worth mentioning that for all the specimens, rate of stiffness degradation and strength deterioration in first cycle under a given drift ratio was maximum and it reduced gradually in further cycles under that particular drift ratio. Similar to load-displacement envelop, it is clear that reduction in stiffness and strength for 'GLD' specimen was very drastic. For example, 82% and 64% of stiffness degradation and 65% and 30% of strength deterioration have been observed (*Fig. 3.19* and *Fig. 3.20*) at drift ratio of ±3 only. Since, the top reinforcement in the beam of SP-1 went far beyond yielding under negative displacement (downward), strength deterioration with increase in displacement was not as severe as the other behaviour parameters. In the 'NonDuctile' specimens also it has been observed that the reduction in stiffness and strength were significantly high. Under maximum positive displacement (drift ratio ≈6.5), 38% deterioration in strength and 63% degradation in stiffness were noted in SP-3 whereas for SP-4, these were 50% and 82% respectively. Similarly, under maximum negative displacement (drift ratio ≈6.5), 56% deterioration in strength and 77% degradation in stiffness were observed in SP-3 whereas these were 61% and 87% respectively, for SP-4. Therefore, though strength and stiffness reductions among the 'NonDuctile' specimens were not quite different under negative displacement cycles, SP-3 showed a better behaviour under positive displacement. Hence, a superior behaviour (load-displacement envelop, stiffness degradation and strength deterioration) has been identified in 'NonDuctile' specimen designed based on Indian Standard (SP-3) in comparison with the 'NonDuctile' specimen designed based on Eurocode (SP-4).

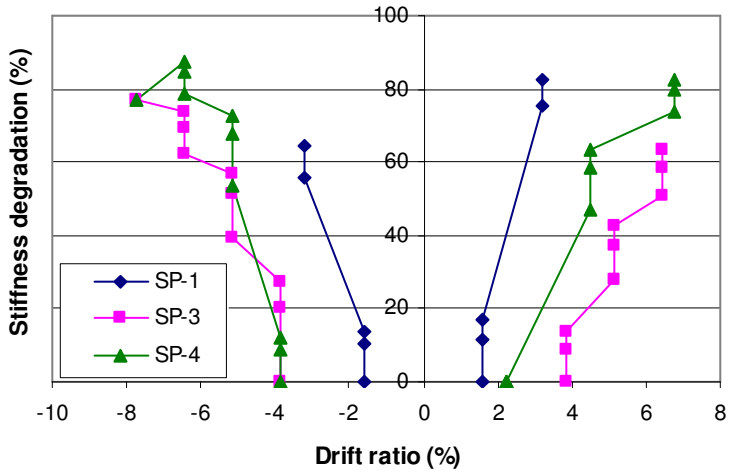

Fig. 3.19 Comparison of stiffness degradation of the specimens

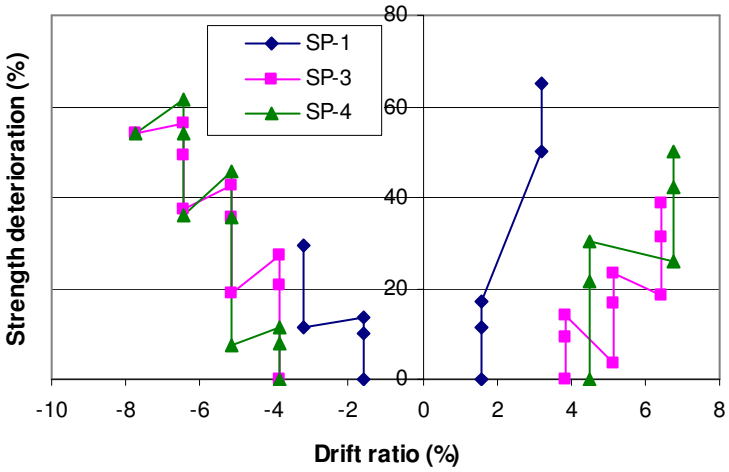

Fig. 3.20 Comparison of strength deterioration of the specimens

The cumulative energy dissipation capacity with respect to the drift ratio of all the specimens considered in this study is presented in *Fig. 3.21* which broadly reflects the comparative seismic performance of the specimens. The figure clearly depicts the improvement of the specimens designed according to the advancement of the codes of practice. The 'GLD' specimen could hardly dissipate seismic energy. Among the seismically analysed specimens without ductile detailing, the specimen designed according to Indian Standard (SP-3) showed a better performance (with a 33% more energy dissipation capacity) over the Eurocode (SP-4) due to higher percentage of reinforcement in both beam and column in specimen (SP-3). But, it is to underline that the 'NonDuctile' specimen SP-3 though showed good energy dissipation, but, it was 35% less than the specimen with ductile detailing (Novák et al. 2008).

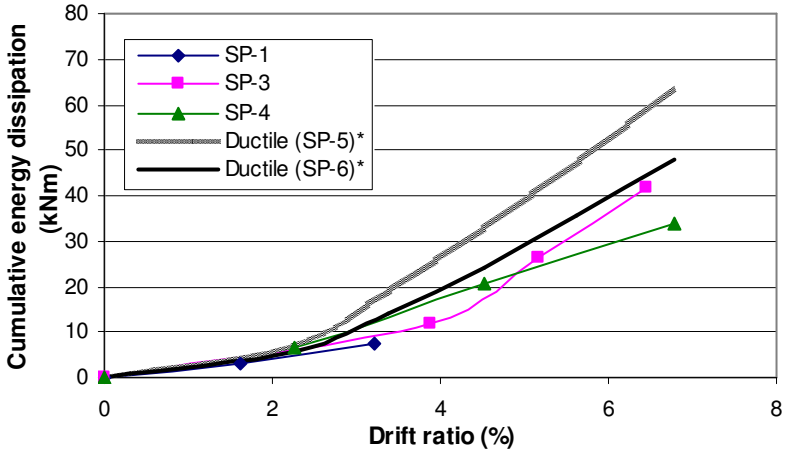

Fig. 3.21 Cumulative energy dissipation capabilities of the specimens

3.4 Summary on experimental results

To summarize the results obtained from experiments, two widely used structural design guidelines (Eurocode and Indian Standard) have been considered to evaluate the seismic performance of the structural D-region with different stages of codal evolution (GLD and seismic design without ductile detailing). The central objective of the study is to evaluate the performance of the under-designed existing structures designed according to the prevailing guidelines. It is observed that the 'GLD' specimen exhibited an extremely low energy dissipation capacity in comparison to the 'NonDuctile' one. The specimens of second level ('NonDuctile' specimens), though provided almost same deformability, the specimen designed according to Indian Standard (SP-3) showed better performance over the Eurocode (SP-4) due to higher percentage of reinforcement in both beam and column in specimen (SP-3). Still the energy dissipations were 35% and 23% less than the same group of specimens (Indian Standard and Eurocode, respectively) with ductile detailing (results obtained from Novák et al., 2008). Stiffness degradation and strength deterioration of the specimens were severe, though comparatively better response was obtained from Indian Standard based 'NonDuctile' specimen. The present study emphasises the fact that the existing reinforced concrete structures which were either 'GLD' or 'NonDuctile', require immediate and adequate improvements to avoid any catastrophic failure. The 'GLD' structures need a thorough upgradation since the seismic behaviour parameters like occurrence of damage, shear deformation, strength deterioration, stiffness degradation and cumulative energy dissipation were extremely vulnerable. Among the 'NonDuctile' specimens, though Indian Standard based specimen provided a better performance over the Eurocode ones, but the main targets of ductile detailing, i.e., column stirrups to provide adequate confinement to joint

concrete, low shear deformation, consistent and large energy dissipation, location of damage beyond the column and joint zones by forming plastic hinge, were totally absent.

3.5 Analytical evaluation of strength of components

Along with the experimental investigations, analytical studies have also been carried out to evaluate the strength of different components, i.e., beam, column and joint separately which would be required to identify the condition of the existing structures/components. Though the primary objective of the study is to evaluate the performance of the under-designed structural components ('GLD' and 'NonDuctile'), it is essential to analytically investigate all the specimens i.e. 'GLD', 'NonDuctile' and 'Ductile' specimens, since the further objective of the present study is to develop strategies for retrofitting of damaged 'NonDuctile' and 'Ductile' specimens, and to develop schemes for upgradation of poorly designed 'GLD' specimens towards a ductile ones. Hence, to evaluate the level and extent of required strengthening, behaviour of the specimens represent the modern codal requirement ('Ductile') needs to be evaluated as well. Procedure adopted in this study and obtained results are briefly discussed below.

3.5.1 Material model

In analytical formulation, first it has been attempted to evaluate the shear strength of the joints of any RC beam-column sub-assemblage. For this, a suitable concrete model is required which can capture the significant effects of concrete constitutive laws. A detailed softening material behaviour of concrete was considered in this study. The basic concrete stress-strain behaviour was assumed as a second order parabolic behaviour of concrete proposed by Hognestad (1951) since the softening behaviour can easily be incorporated in this constitutive model. The concrete model was proposed as

$$f_c = f_c^{'}\left[2\left(\frac{\varepsilon}{\varepsilon_c}\right)-\left(\frac{\varepsilon}{\varepsilon_c}\right)^2\right] \qquad (3.4)$$

The softening behaviour of the concrete material model and further assumptions used in this study are described here.

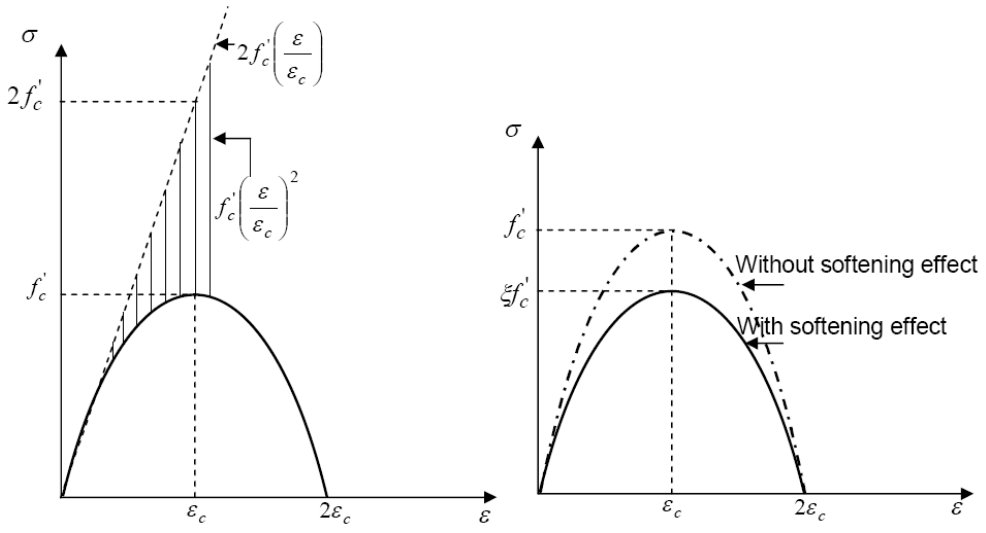

(a) (b)

Fig. 3.22 Stress-strain behaviour of concrete under compression (Hognestad, 1951)

The Eq. 3.4 is graphically plotted in *Fig. 3.22*(a) and the initial slope of the curve in *Fig. 3.22*(a) is $E_c = 2f_c'\varepsilon_c$. This can be called as non-softened stress-strain behaviour of concrete. It is to mention that in the actual stress-strain curve of concrete, the stress can not become zero when the strain reaches to $2\varepsilon_c$. So it is the fact that the last 1/8th part of the curve is not valid as proposed in Eq. 3.4. The applicability of the Eq. 3.4 can be assumed to be valid up to $1.75\varepsilon_c$ (or a strain of 0.0035).

When the peak stress is softened linearly by a softening coefficient ξ, which varies from zero to unity, then the softened peak stress σ_p is

$$\sigma_p = \xi f_c' \qquad (3.5)$$

and the stress-softened curve becomes

$$\sigma_p = \xi f_c'\left[2\left(\frac{\varepsilon}{\varepsilon_c}\right) - \left(\frac{\varepsilon}{\varepsilon_c}\right)^2\right] \qquad (3.6)$$

This equation is plotted as the solid curve as shown in *Fig. 3.22*(b). The initial slope of the curve is $E_c = 2\xi f_c' / \varepsilon_c$.

3.5.2 Softening in both stress and strain

When both the stress and strain at the peak point of the stress-strain curve are softened, then two softened coefficients (defined as ξ_σ and ξ_ε for stress and strain respectively) are adopted.

$$\sigma_p = \xi_\sigma f_c^{'} \text{ and } \varepsilon_p = \xi_\varepsilon \varepsilon_c \qquad (3.7)$$

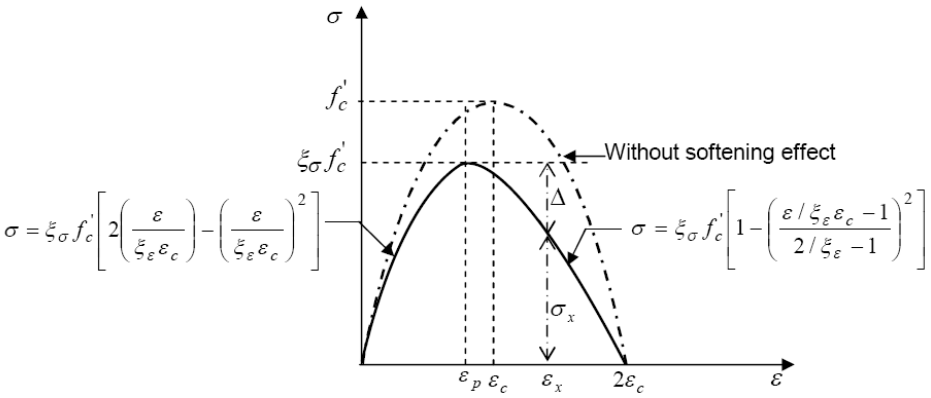

Fig. 3.23 Stress and strain softening in concrete model

As shown in the above *Fig. 3.23*, the complete stress-strain curve is expressed [Hsu (1993)] by two different equations to express the behaviour in the ascending and descending branch of softened concrete model.

The descending part of the curve, as shown in *Fig. 3.23*, is also assumed to be parabolic curve from the peak point to the point of $2\varepsilon_c$. The degradation of the stress from the peak (σ_p) can be measured as the vertical distance from the parabolic curve to the peak stress level (designated as Δ) located at a horizontal distance $\varepsilon_x - \varepsilon_p$. The ratio of Δ/σ_P can be obtained from parabolic shape

$$\frac{\Delta}{\sigma_P} = \left(\frac{\varepsilon - \varepsilon_p}{2\varepsilon_c - \varepsilon_p}\right)^2 \qquad (3.8)$$

Then the stress σ_x at the location of ε_x can be finally deduced as

$$\sigma_x = \xi_\sigma f_c^{'}\left[1 - \left(\frac{\varepsilon/\xi_\varepsilon \varepsilon_c - 1}{2/\xi_\varepsilon - 1}\right)^2\right] \qquad (3.9)$$

If the two softening coefficients are close, it is assumed a proportional softening of stress and strain ($\xi_\sigma = \xi_\varepsilon = \xi$), then the simplified curve (*Fig. 3.24*) is

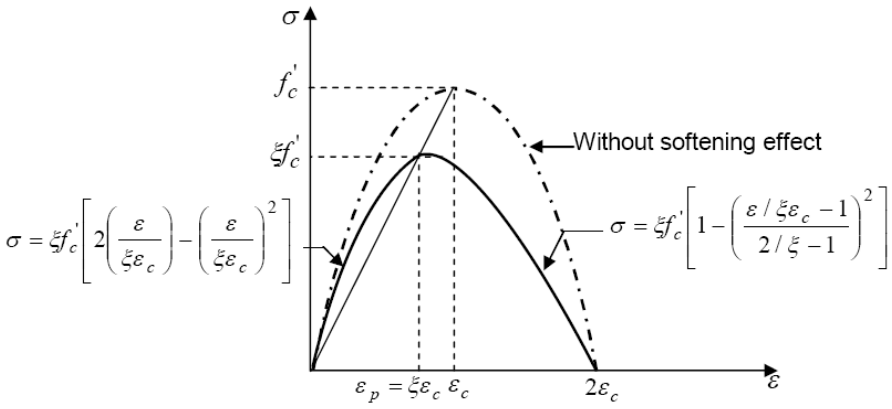

Fig. 3.24 Proportional softening of stress and strain

In the present analytical formulation for calculating shear strength of joint in beam-column sub-assemblages, a concrete model with an equal softening coefficient for ascending and descending branches of the material behaviour was considered.

3.5.3 Algorithm of the computer program used in this study

In the present study, shear strength of existing reinforced concrete joint was assessed by incorporating a soften concrete model as described above. The basic formulation on soften strut and tie model used for predicting the shear strength can be found elsewhere [Hwang and Lee (1999)]. In this model, any RC joint would resist the external force using three mechanisms, i.e. (i) diagonal mechanism (by concrete strut), (ii) horizontal mechanism (by joint reinforcement stirrups as ties), and (iii) vertical mechanism (by column intermediate reinforcement as ties) as shown in *Fig. 3.25*.

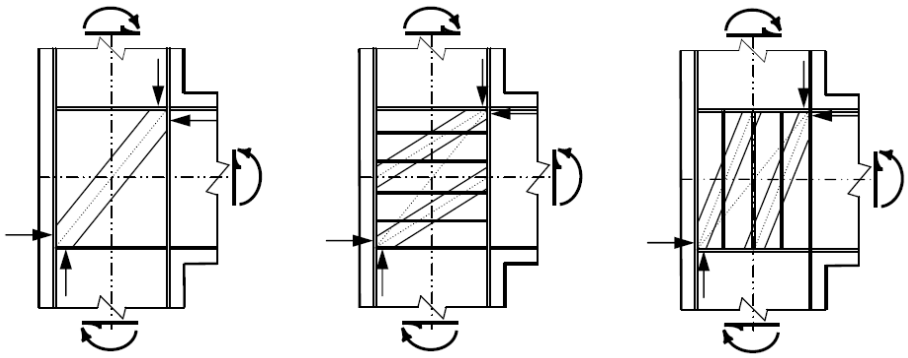

Fig. 3.25 Joint shear resisting mechanism: (a) diagonal mechanism, (b) horizontal mechanism, and (c) vertical mechanism

The flow chart of the computer program developed in this study for assessing the shear strength of the joint in beam-column sub-assemblages is shown in the Appendix *Fig. A2*. It can be observed from the flowchart that the assumption of proportional softening of stress

and strain (as discussed in section 3.5.2) was a vital pivoting parameter in convergence of iterative shear strength. In the joint, increase in compressive strength of concrete due to presence of stirrup confinement, if any, as suggested in CEB/FIP Model Code 90 (given in Eq. 3.10) was incorporated in the formulation.

$$k_e = \left(1 - \frac{s_h}{2b_c}\right)\left(1 - \frac{s_h}{2h_c}\right)\left(1 - \frac{\sum b_i^2}{6b_c h_c}\right)^2 \qquad (3.10)$$

b_c and h_c = *width and depth of the column at joint*

s_h = *stirrup spacing*

b_i = *spacing of the longitudinal reinforcement*

3.5.4 Variation of shear strength (horizontal) with different reinforcement

Using the computer program developed in this study, a parametric study has been carried out to bring out the role of stirrup reinforcement in the joint and axial load in the column in changing the shear strength of joint. As the horizontal shear strength is more important than vertical shear strength in the joint (to develop beam hinge), only the results for horizontal shear strength is presented here. A joint with geometry as used for the experimental studies was considered with different amount of vertical and horizontal reinforcement. It is noted from the study that presence of horizontal reinforcement plays more significant role than vertical reinforcement in improving the horizontal shear strength in the joint. A typical result using a particular amount of vertical reinforcement and axial load (300 kN), is shown in *Fig. 3.26* where amount of horizontal reinforcement is a parameter.

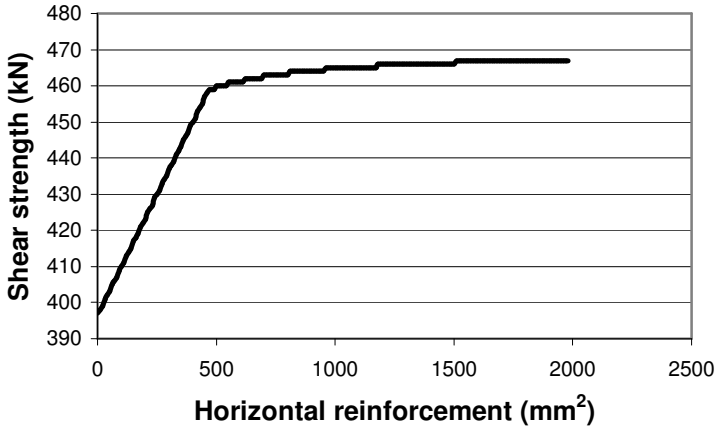

Fig. 3.26 Shear strength of an RC joint with different amount of horizontal reinforcement

From the *Fig. 3.26*, it is to cite that the first branch of the curve is the zone of pre-yielding of the horizontal reinforcement which is followed by the crushing of concrete in the second part of the curve. Hence, after a certain amount of horizontal and vertical reinforcement, increase in shear strength would not be so prominent because concrete crushing in the diagonal direction would be the primary failure mode. This behaviour obtained from the present analytical study, supports the fact that (Priestley et al. 1996) "if the nominal principal compression stresses exceed the crushing strength of the concrete, special joint reinforcement is unlikely to be particularly effective. In this context, it should be noted that crushing must be expected at a nominal compressive stress significantly less than $f_c^{'}$, since the average stress will be less than the maximum and compression strength is reduced by transverse strain in the joint region (modified compression field theory)".

3.5.5 Evaluation of joint strength of the specimens obtained from analytical study

Horizontal shear strength of the specimens was obtained from the analytical study based on the algorithm of the computer program given in *Fig. A2* (Appendix). Since the size of diagonal strut in the joint is a function of axial load in the column (Paulay and Priestley, 1992), applied axial load (up to a certain extent) would have a prominent influence on the joint shear strength. It is to mention that an approximate axial load of 300 kN was applied in the column during the experiments. With the chosen geometrical, material and reinforcement details, shear strength of the specimens in horizontal direction is presented in *Table 3.5*. Joint shear strength of the specimens was studied with- and without- axial load.

Table 3.5 Shear strength (in kN) of the joints obtained from the analytical study

Specimen	Without axial load	With axial load of 300 kN	Remarks
SP-1	244	338	strength from diagonal strut (no reinforcement in joint)
SP-2	289	397	strength from diagonal strut and yielding of vertical reinforcement (no horizontal reinforcement)
SP-3	330	439	strength from diagonal strut and yielding of horizontal reinforcement (vertical reinforcement unyielding)
SP-4	329	438	strength from diagonal strut and yielding of horizontal reinforcement (vertical reinforcement unyielding)
SP-5	339	465	strength from diagonal strut (horizontal and vertical reinforcement unyielding)
SP-6	337	461	strength from diagonal strut (horizontal and vertical reinforcement unyielding)

3.6 Strength of the specimens from different failure modes

It is evident that the failure of the beam-column sub-assemblages can be either (ignoring mixed mode of failure) from (i) moment hinge in column, (ii) moment hinge in beam, (iii) joint shear, (iv) shear in column, or (v) shear in beam. Each of the failure modes should be investigated before determining the final strength of the specimens. This is also required to obtain the strength hierarchy of the components of the specimen to map the possible global behaviour of the structure.

3.6.1 Strength from moment resistance capacity of beam and column

In the previous section, shear strength of the joints was calculated which would be used for determining the strength of the specimen if joint shear is the crucial parameter. Similarly, in this section moment capacities of the specimens (both beam and column) have been evaluated to calculate respective strength of the specimen. For moment-curvature and axial load-moment interaction analysis, a computer program was developed where the non-linear portion of steel was modelled as

$$f_{s,x} = f_y \left[1.20 - 0.20 \left(\frac{\varepsilon_{\lim} - \varepsilon_x}{\varepsilon_{\lim} - \varepsilon_y} \right)^2 \right] \qquad (3.11)$$

and concrete model was adopted as proposed by Mander et al. (1988). A detailed discussion on this concrete model, and its usability and uniqueness will be presented later. The main reinforcement detailings of 'NonDuctile' and 'Ductile' specimens using a particular code of practice (SP-3 and SP-5; or SP-4 and SP-6) were identical. So, the moment-curvature analysis and the axial force-moment interaction were carried out for specimens SP-1, SP-3, and SP-4. With the adopted material models, the moment-curvatures and the axial force-moment interactions for the specimens, as mentioned above, were calculated and the behaviour of the specimens is shown in *Fig. 3.27* and *Fig. 3.28*.

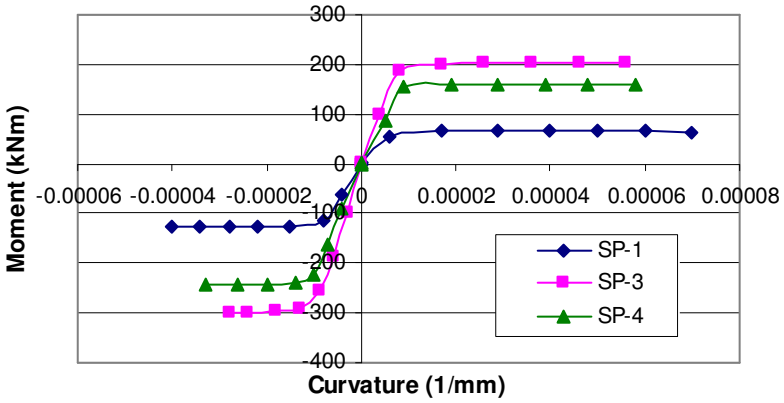

Fig. 3.27 Comparison of beam moment-curvature of the specimens

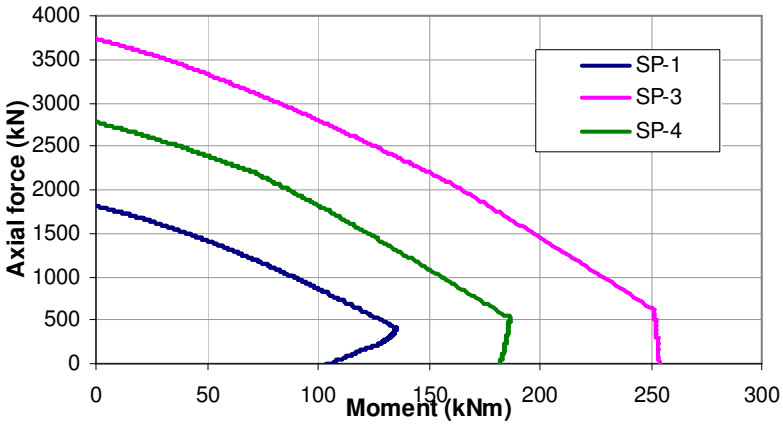

Fig. 3.28 Axial force-moment interaction diagrams for the specimens (column section)

It is important to mention here that the moment resistance of the column is shown for one section of the column of a particular beam-column sub-assemblage. To check the moment resistance capacity of the column with respect to beam (M_R) of the total specimen (sub-assemblage), moment resistance capacity has to be calculated by considering the column from both sides of the joint to arrive at the total moment capacity of the column at the joint. From a strong column-weak beam concept, the capacity of column with respect to beam has to be more than unity in any case. Moreover, different codes have specified the desired factor for moment resisting capacity of column to beam. In general, this provision is crucial for interior beam-column joints where the summation of moment resisting capacity of both side beams should be less (with a certain magnitude) than that from both parts of column. So, for exterior beam-column joint it is not playing so vital role since beam from only one side is connected to the joint. But, the calculation of moment resistance capacity of the components would be useful to determine the strength of different parts of the beam-column sub-assemblages around the joint. This would also help to identify the predominant mode (beam, column or joint) of failure by reaching the maximum strength. Maximum beam tip load corresponding to the bending strength of the components is presented in *Table 3.6*. It is to

note that the 'GLD' specimen based on Eurocode (SP-2) was not experimentally investigated as it has been found that the specimen was quite similar to that of Indian Standard based designed ones (SP-1). But for comparison of the results of different specimens obtained from analytical studies, the results of SP-2 have also been included.

Table 3.6 Calculation of beam tip load from moment resistance capacity

	Maximum moment capacity of beam (kNm)		Load at beam tip corresponding to beam moment capacity (kN)		Maximum moment capacity of column (kNm)	Load at beam tip corresponding to column moment capacity (kN)
	(+)ve	(-)ve	(+)ve	(-)ve		
SP-1	64.78	125.67	42.47	82.4	103.83	94.29
SP-2[$]	64.78	125.67	42.47	82.4	68.79	62.48
SP-3	202.8	300.39	132.98	196.9	254.39	230.7
SP-4	158.2	243.19	103.7	159.5	184.17	167.27
SP-5*	202.8	300.39	132.98	196.9	254.39	230.7
SP-6*	158.2	243.19	103.7	159.5	184.17	167.27
* These specimens were designed as per ductile provisions and hence, have not been discussed before. The results tabulated here would be required for development of upgradation schemes as discussed in Chapter 5.						
$ Not studied experimentally						

3.6.2 Strength from shear resistance capacity of joint

When shear failure of joint is the crucial mode of failure in beam-column sub-assemblages, the available strength of the specimens can be calculated from the evaluated joint shear strength.

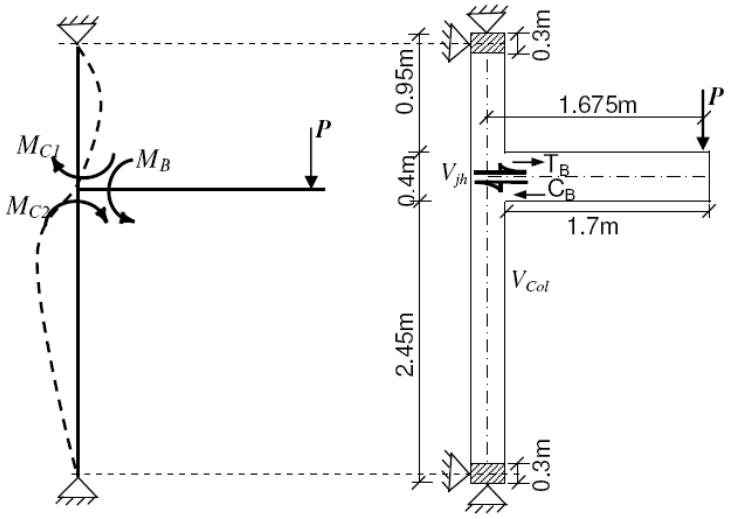

Fig. 3.29 Free body diagram to evaluate the joint shear force

From the equilibrium conditions (as shown in *Fig. 3.29*), developed shear in the joint can be calculated. If the applied force in the beam tip = P

From moment equilibrium (about bottom column hinge):

V_{Col} = 0.479P, M_{C1} = 0.383P and M_{C2}=1.1P *(3.12)*

Joint shear (V_{jh}) = M_B/Z - V_{Col} = *4.19P* *(3.13)*

Hence, from the known joint shear strength (horizontal), strength of the beam-column sub-assemblage, in terms of beam tip load, can be determined in case the joint shear failure is the critical parameter. For all the specimens, evaluated strength of the specimens (in terms of beam tip load) corresponding to the joint shear strength (as given in *Table 3.5*) is presented in *Table 3.7*.

3.6.3 Strength from shear resistance capacity of beam and column

For the specimens (SP-1 to SP-6) with given geometry and reinforcement details, it has been aimed to calculate the available shear strength at different sections of column and beam components in beam-column sub-assemblage. For 'GLD' and 'NonDuctile' specimens, initial design for shear was carried out based on the section force from the analysis. But, for 'Ductile' specimens, different codes of practice stipulate further guidelines for additional reinforcement in improving ductility which would, of course, improve the shear strength as well. So, design shear force and the available shear strength of the specimens need to be investigated. Unlike design for moment, design approach for shear is considerably different for different codes of practice as shear design contains two parts; namely, shear contribution from concrete and shear contribution from steel. Further, Eurocode 2 provides flexibility to the user in assuming the strut angle (between 18-60 degree) depending on concrete strength and ratio between shear load to shear contribution from concrete. Hence, for a given geometry and reinforcement details, calculated shear strength of a particular section would change with the magnitude of considered strut angle. In view of this, a comparative study was carried out in evaluating shear strength of beam and column of the specimens using different codes of practice [ACI 318-02, CSA-1994, NZS-3101, IS-456-2000 and Eurocode 2].

Contribution of concrete to shear strength for beams and columns of the specimens calculated from different codes is shown in *Fig. 3.30* and *Fig. 3.31* respectively.

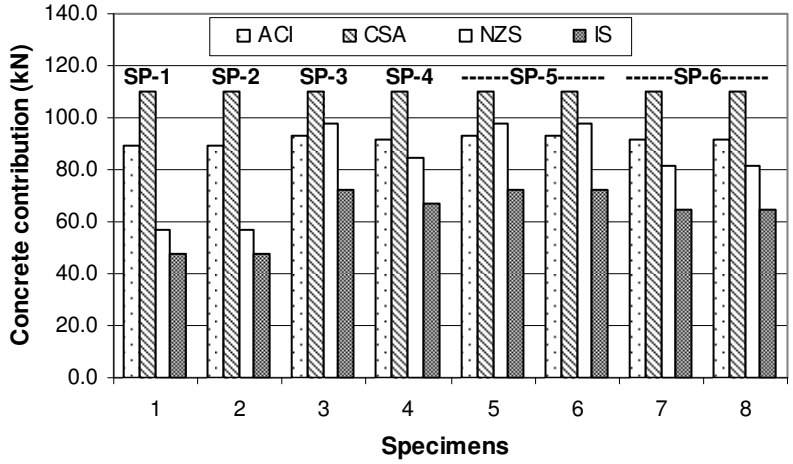

Fig. 3.30 Concrete contribution to shear in beam of the specimens (SP-1 to SP-6)

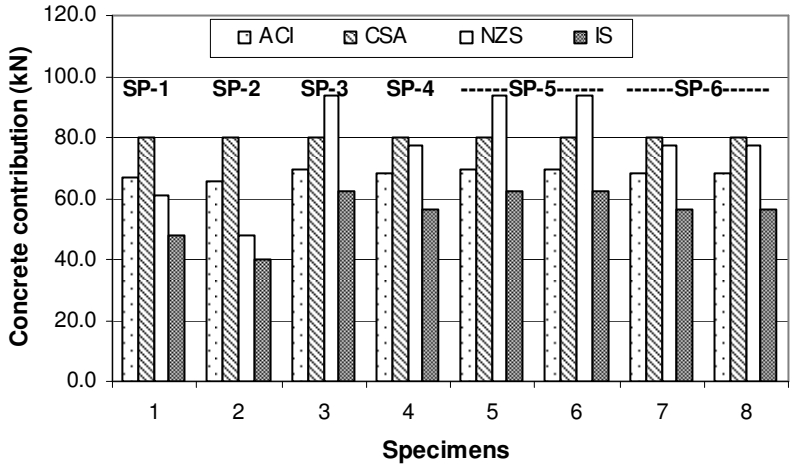

Fig. 3.31 Concrete contribution to shear in column of the specimens (SP-1 to SP-6)

Here, digits (from 1-4) in horizontal axis represent the specimen number from SP-1 to SP-4, respectively. Digits 5 and 6 correspond to the sections with non-ductile and ductile detailing, respectively, of the specimen SP-5. Similarly, digits 7 and 8 are for SP-6 and for sections with non-ductile and ductile detailing, respectively. It is observed that NZS-3101 provides higher shear strength when the longitudinal reinforcement (for bending) in the particular section is considerably high (SP-3 and SP-5). Otherwise, Canadian code (CSA 1994) gives the highest shear strength for a given geometry. On the other hand, IS-456-2000 is consistently conservative in calculating the shear strength from concrete.

Since, the steel contribution to shear strength is quite straight forward and has uniformity among the codes, those results are not presented separately. Total shear strength at sections of beam and column taking the contribution from both concrete and steel for different specimens are shown in *Fig. 3.32* and *Fig. 3.33*. It is interesting to note that though

there are significant differences among the codes in calculating the concrete contribution to shear, but the total shear strength at a section of a particular specimen calculated from different codes of practice is not so different. Further, shear strengths of beam and columns for 'GLD' and 'NonDuctile' specimens (SP-1 and SP-2; and SP-3 and SP-4) were quite uniform. *Fig. 3.32* shows that shear strength at the ductile zone of beam of 'Ductile' specimens (SP-5 and SP-6) was almost similar whereas shear strength at non-ductile zone of beam of SP-5 was little higher than SP-6. But, column shear strength in ductile zone of Indian Standard designed 'Ductile' specimen (SP-5) was much higher than Eurocode based designed 'Ductile' specimen SP-6 (as shown in *Fig. 3.33*) while shear strength in non-ductile zone of column of SP-5 was little higher than SP-6.

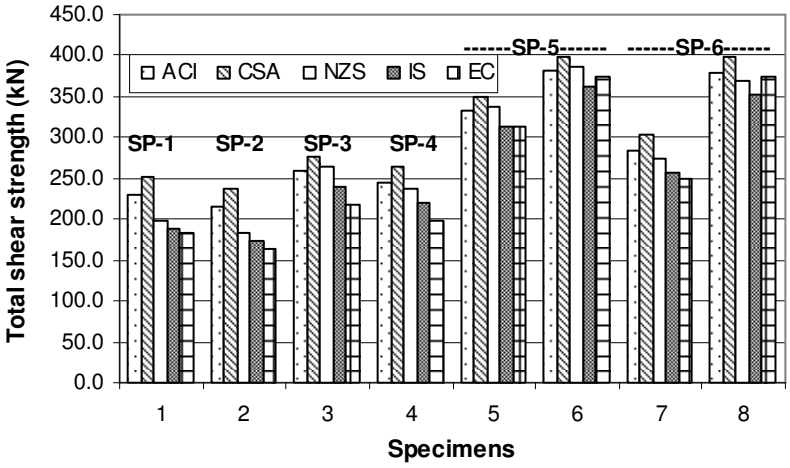

Fig. 3.32 Total shear strength of beams of the specimens (SP-1 to SP-6)

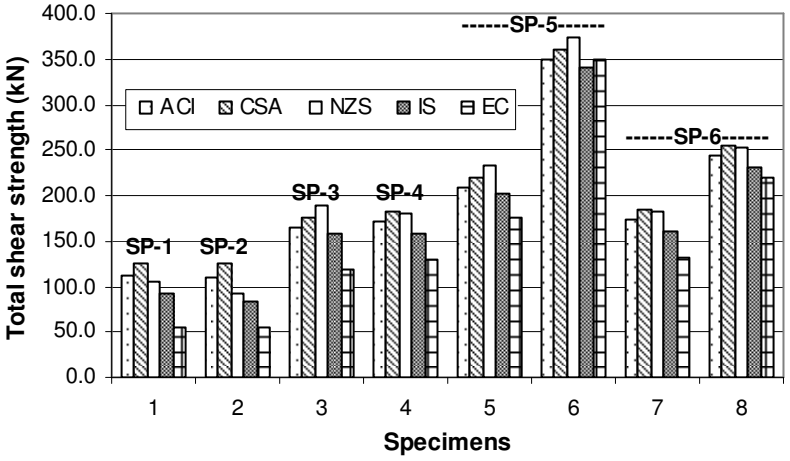

Fig. 3.33 Total shear strength of columns of the specimens (SP-1 to SP-6)

3.6.4 Comparison of strength calculated from different failure criteria and experimental results

Comparison of maximum beam tip load (strength of specimen) as obtained from the moment resistance capacity, joint shear strength and member shear strength, as discussed in the preceeding sections, is presented in *Table 3.7*. Member shear strength of ductile zone has not been considered since with a uniform shear demand in column, non-ductile zones would always be critical. Shear strengths of beam and column of the specimens were calculated as average of values obtained from different codes of practice.

Table 3.7 Strength (in kN) calculation from different failure criteria

	Strength of specimens evaluated using							
	Analytical studies						Experimental studies (positive load denotes upward direction)	
	From moment resistance capacity (positive moment denotes tension in beam bottom reinforcement)			From Joint shear strength[§] [*Table 3.5*]	From shear strength of beam and column[$]			
	Beam		Column		Beam	Column	(+)ve	(-)ve
	(+)ve	(-)ve						
SP-1	42.47	82.4	94.29	80.67	210.44	204.6	47.03	86.38
SP-2	42.47	82.4	62.48	94.75	194.96	195.5	Not available	
SP-3	132.98	196.9	230.7	104.77	251.59	336.9	123.64	126.91
SP-4	103.7	159.5	167.27	104.53	232.85	343.2	99.57	119.70
SP-5	132.98	196.9	230.7	110.98	329.25	434.4	141.99*	142.19*
SP-6	103.7	159.5	167.27	110.02	273.30	347.9	110.45*	126.47*

* Obtained from Novák et al. (2008)
[$] Shear strength of non-ductile zones has been considered
[§] Joint shear capacity calculated with 300 kN axial load in column

It is evident from *Table 3.7* that the strength of beam-column sub-assemblages obtained from the experimental investigations can be closely inter-related with the results obtained from the analytical studies towards identifying the mode of failure of the specimens. It can be noted that in most of the cases, the maximum beam tip load (strength of the specimens) corresponding to the shear strength of the joint obtained from the analytical study is very close to that obtained from the experiments and is followed by the strength corresponding to moment capacity of beam. Further, though for all the specimens, shear strength of the columns is less than that of beams (as shown in *Fig. 3.30* to *Fig. 3.33*), but the beam tip load corresponding to column shear strength is more than that for beam shear strength, owing to its geometry. Hence, strength of the specimens would not be guided by shear failure of beam and column (as presented in *Table 3.7*). These observations of possible specimen strength from different failure criteria and the strength hierarchy of the specimens would be used in further studies for developing retrofitting strategies for damaged specimens and upgradation schemes for poorly designed 'GLD' specimens.

4 Development of strategies for retrofitting of damaged specimens

Seismic retrofit of reinforced concrete structures is aimed at strengthening its structures and members to achieve more strength and/or ductility and energy dissipation. The final objective could be obtained by adopting the local strengthening of members in order to achieve a global ductile behaviour. In case of beam-column joints, moving the location of failure from the column to the joint can improve the global behaviour of the frame. It would reduce the displacement demand on the column. However, the shear failure of the joint is brittle and does not provide sufficient warning. Its influence on global performance needs to be evaluated to understand how much contribution it could provide in terms of energy dissipation of the entire frame. In order to further improve along the hierarchy of strength, the joint should also be strengthened. Strengthening of both column and joint could allow moving from the previous intermediate level of the hierarchy of strength (i.e., shear failure of the joint) to its upper bound (i.e., failure of the beams). That is the most widely accepted concept of seismic strengthening where strong column-weak beam and high shear-low flexural capacity based failure mode would be achieved to attain the best results from seismic strengthening.

4.1 Seismic strengthening criteria

Two categories can be defined for strengthening: structural *system*-level and *member*-level. Improvement of structural systems by adding structural walls, damping devices, base isolators, steel braces, or steel shear plates, has an impact on the global structural response to earthquakes (*Fig. 4.1*), whereas, improvement in member-level approach, such as concrete, steel jacketing or fiber composite is used to improve the performance of individual deficient elements/components such as columns, beams, and walls or their combinations (*Fig. 4.2*). In member-level approach, the objective is to increase the deformation capacity of deficient components so that the global structure responds at the design level and the component would be below their specified limit state (Moehle 2000).

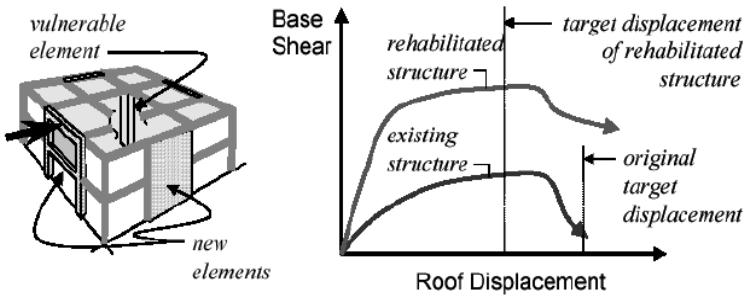

Fig. 4.1 Global modification of the structural system (Moehle, 2000)

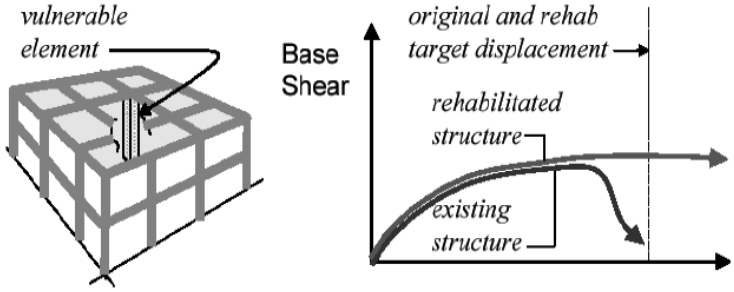

Fig. 4.2 Local modification of the structural components (Moehle, 2000)

In terms of the behaviour of the under-designed frames, the lower bound pertains to the column failure. Strengthening of columns, by providing them with higher strength using confinement and/or more flexural reinforcement, could move the failure to occur in the joint. Calvi et al. (2002) underlined that the global behaviour of the frame could be boosted by shifting the failure from the column to the joint region of beam-column sub-assemblage and further the joint should be attempted for strengthening next. That means, the critical failure mode shifts from shear failure of the joint to the beam failure. It will be further tried to form a flexural failure in the beam over a shear failure. Formation of plastic hinges at a safe distance in beam would mean that a ductile and very effective energy dissipating mechanism can be achieved, maintaining the integrity of the global structure.

Strengthening of RC beam-column joints is a challenging task that poses major practical difficulties. A variety of techniques have also been applied to joints. Over the years, different methods and techniques have been proposed to strengthen existing and damaged structures by providing external confining stresses. The concept of jacketing using traditional materials has been investigated to provide such forces where externally applied jackets are used as the reinforcement to contain and confine the concrete. Section enlargement is one of the methods used in strengthening concrete members. Enlargement is the placement of RC jacket around the existing structural member to achieve the desired section properties and performance. Steel jacketing has been proven to be an effective technique to enhance the

seismic performance of old structures. This type of jacket provides a passive type of confinement that is activated after concrete starts to dilate and expands laterally in the compression zone as a function of high axial compression strains. More recently, a new technique for strengthening structural elements has been emerged. The technique involves the use of fiber reinforced polymers (FRP) as externally bonded reinforcement in critical regions of RC elements. FRPs have become perhaps the most attractive material to be used in strengthening of structures/components, due to its unique mechanical properties.

4.2 State of the art on strengthening of RC structures

Before pursuing any attempt in developing retrofitting strategies for already damaged specimens and upgradation schemes for 'GLD' specimens, it is aimed to study the existing strengthening techniques that are reported by the researchers since last few decades. In the present study, the term 'strengthening' encompasses all the efforts that target towards improvement in performance of structure or its members, where the efforts may either be repair, retrofitting, rehabilitation or upgradation. Entire strengthening techniques reported in literature can be divided into four groups; by (i) concrete jacketing, (ii) steel jacketing, (iii) FRP jacketing, and (iv) other techniques beyond jacketing. From an exhaustive review of literature on strengthening of RC structures, only selective, relevant and important research works in each type of strengthening techniques are reported here.

4.2.1 Concrete jacketing

The effectiveness of three different strengthening techniques to encase the column with, (i) rectangular or circular steel sections, (ii) steel straps, (iii) welded wire fabric, in enhancing the lateral load response of identical RC short columns in seismic regions was studied by Bett et al. (1988). It was found that the columns strengthened by jacketing, both with- and without-supplementary cross ties, were much stiffer and laterally stronger than the original unstrengthened one. A rehabilitation scheme for reinforced concrete frame connection by using concrete jacketing was proposed by Alcocer and Jirsa (1993). Rodriguez and Park (1994) performed seismic load tests on RC columns strengthened by reinforced concrete jacketing. Two arrangements of transverse reinforcement in the jacket were investigated. It was observed that the jacketed columns behaved in a ductile manner with higher strength and lower rate of strength degradation. A repair technique was designed by Stoppenhagen et al. (1995) to strengthen and repair reinforced concrete frames with heavily damaged columns. The columns were repaired and strengthened by completely encasing the damaged columns using concrete jacketing. McLean and Marsh (1999) described an

experimental study by investigating retrofitting measures for improving the seismic performance of the foundations of existing bridges. An added reinforced concrete overlay provided an effective retrofit for the as-built footings.

A waffle-flat-plate RC structure retrofitted by concrete jacketing with prior epoxy injection subjected to cyclic loading simulating a severe earthquake was tested by Rodriguez and Santiago (1998). Takiguchi and Abdullah (2001) discussed the results of a research program on the strengthening, by using circular ferro-cement jackets, of square RC columns that are susceptible to shear failure. A research was conducted by Shama et al. (2002) to investigate the seismic performance of steel pile-to-pile cap connections representative of construction practice in the eastern US. Performance of specimens retrofitted in accordance with the theoretical model was investigated in this study. Retrofit was done by increasing embedment length with an additional concrete jacket. Since, the main reinforcement of lap-spliced columns just above the joint region, discontinuous bottom beam reinforcement, and little or no joint transverse reinforcement are the most critical details of interior beam-column joints in old buildings, Shannag et al. (2002) and Shannag and Alhassan (2005) tested the interior beam-column joints representing these critical reinforcement details under cyclic load. It was observed that these specimens behaved weakly and attained low load carrying capacity, small energy dissipation, and failed in diagonal shear in the joint region. After testing, the specimens were repaired using high performance fiber reinforced concrete (HPFRC) jacket, all around the joint in column regions, and re-tested up to failure. Higher load levels were attained, more ductile behaviour was achieved, substantial energy dissipation was observed, and slower stiffness degradation was also noted. Dogan and Krstulovic-Opara (2003) presented a seismic retrofit technique using two types of HPFRCs: slurry-infiltrated fiber concrete (SIFCON) and slurry-infiltrated mat concrete (SIMCON). Use of continuous SIMCON jackets increased the column flexural capacity, shifted plastic hinges from column to beam and increased the stiffness, strength, and energy dissipation capacity of the tested specimen. Retrofit of the discontinuous beam bottom reinforcement with SIFCON and external reinforcement improved the anchorage of discontinuous bars and provided continuity of the bottom reinforcement.

Hamilton et al. (2004) investigated the lateral performance and suitability of shotcrete as a means to retrofit bridge columns for improvement of flexural ductility and shear strength. As the performance of the frames relied on adequate confinement of the joints, Bligh et al. (2005) used concrete jackets as a rehabilitation scheme to simulate the confinement that would be provided by framing members on all four sides of the joint. Due to the concrete jacketing, the clear span of beams and columns were reduced which led to increase in shear demand in beam and column. Hence, the shear strength of the retrofitted structural

components was re-checked. An experimental study was performed by Júlio et al. (2005) to analyze the influence of the interface treatment on the structural behaviour of columns strengthened by RC jacketing. Harajli (2007) presented the results of experimental investigation for evaluating the cyclic response of already damaged concrete members repaired by concrete confinement and casting new concrete. Three types of concrete confinement were investigated, namely, (i) internal confinement by steel ties or (ii) wire mesh reinforcement, and (iii) external confinement by FRP laminates. It was found that repairing the bond-damaged zone through concrete confinement led to substantial regain of flexural stiffness, strength and energy absorption and dissipation capacity. For illustration, few reported schemes as discussed above for strengthening using concrete jacketing are shown in *Appendix (A1)*.

4.2.2 Steel jacketing

Migliacci et al. (1983) reported on the behaviour of exterior frame connections jacketed by a steel skeleton made of steel angles and straps. To improve the confinement of the beams and columns, the straps were prestressed by preheating. They concluded that steel jacketing enhanced the strength and energy dissipation capacity, however prestressing by preheating should not be relied upon while it is difficult to control in the field. Corazao and Durrani (1989) proposed strengthening of beam-column joints using concrete jacketing and external steel encasement. Specimens strengthened by reinforced concrete and steel encasement showed increase in strength, stiffness and ductility and exhibited desirable failure mechanism. Strengthening by reinforced concrete jacketing requires more labour than other strengthening techniques. The placement of continuous ties around the column in the joint region can be difficult. Another complication in case of strengthening by external steel reinforcement is that the transfer of stress at the connection region is not properly understood either. An interior beam-column joint was rehabilitated and tested [Estrada JI. (1990)] using steel plates anchored to the beam bottom face at each side of the joint and connected together using threaded steel rods driven through the column. The idea was to replace the inadequately anchored steel bars with equivalent steel plates. Steel plate jacketing was used to enhance the joint shear strength. Test results showed that joint jacketing was ineffective in improving the joint shear strength due to slippage of the steel plates. The specimen reached a drift of 4% without significant deterioration in strength.

Chai et al. (1991) reported the results of investigation on retrofitted circular columns by encasing the plastic hinge regions with a bonded steel jacket to enhance flexural strength, ductility and shear strength. It was shown that steel jacketing resulted in column ductility as high as those available from confined columns designed according to current codes, and

exhibited bond failures in lap splices of longitudinal reinforcement in plastic hinge region. Steel jacketing increased the column stiffness by about 10 to 15 percent. Beres et al. (1992) investigated the behaviour of two rehabilitation schemes. The first scheme was intended for interior joints in which the retrofit was designed to prevent the pull out of discontinuous bottom beam reinforcement. This was achieved by bolting steel channel sections into the bottom surfaces of beams on each side of the joint. The second scheme was intended for exterior joints in which the retrofit was designed to reduce vertical cracks propagating in the column lap splice zone above the joint. Mechanical attachment of steel plates placed around the deficient member has been developed to repair many structures [Karbhari (1993)]. The use of such technique to provide lateral confinement to the concrete in compression was studied extensively [Fuelong (1967); Knowles and Park (1969)], and showed to increase the compressive load carrying capacity and ductility of the concrete columns. Hoffschild et al. (1993) proposed a method of retrofit which consisted of encasing the RC joint with a circular grouted steel jacket. The casing caused an increase in moment capacity of the section which forced most of the specimens to fail outside the jacket.

Adin et al. (1993) proposed an epoxy based repair scheme for RC beam-column joints under cyclic loading. Subsequently, thin steel plate envelopes were applied, sealed and epoxy injected. Two types of steel plates represented two and three dimensional joint repair. Priestley et al. (1994a,b) investigated the behaviour of a column strengthened by a rectangular flat steel jacket. In their investigation, the columns behaved poorly under cyclic lateral load as a result of the outward bulging. It was noted that jacketed columns performed extremely well and stable hysteresis loops were achieved at displacement ductility level of 8. Biddah et al. (1997) and Ghobarah et al. (1997) proposed a seismic upgradation technique for existing RC frame connections using corrugated steel jacketing. Aboutaha et al. (1999a) proposed rehabilitation schemes for shear critical concrete columns by using rectangular steel jackets to evaluate the effectiveness of thin rectangular steel jackets for seismic retrofit of large rectangular RC columns with inadequate shear strength. Aboutaha et al. (1999b) presented an experimental investigation of seismic repair of lap splice failures in damaged concrete columns using steel jackets with adhesive anchor bolts or through rods. Zhang et al. (2001) presented the results of a study on the behaviour and strength of two-way square RC slabs bonded with a steel plate. Cheng et al. (2004) developed a repair technique for hollow-bridge columns with fractured and buckled longitudinal reinforcement. To restore the column's flexural strength, the fractured longitudinal bars were replaced with dog-bone shaped bars. In addition, a steel jacket was placed in the plastic hinge region in order to enhance the deformation capacity of the repaired columns. Test results showed that the damaged columns could be repaired very fast, regaining almost 90% strength of the original column and a comparable degree of restoration of ultimate displacement to the original

columns could be achieved. However, the regain of stiffness and ductility of the original column were not so satisfactory. For illustration, few such schemes on steel jacketing are shown in *Appendix (A2)*.

4.2.3 Fiber Reinforced Plastics (FRP)

Compared to concrete or steel jacketing techniques, application of FRP to the deficient structures is new. But, since last 15-20 years, a number of research works have been carried out to evaluate the performance and limitations of FRP on strengthening of RC members. Several experimental investigations have been reported on the behaviour of concrete beams strengthened for flexure using externally bonded FRP plates, sheets, or fabrics. Saadatmanesh and Ehsani (1991) examined the behaviour of concrete beams strengthened for flexure using glass fiber-reinforced polymer (GFRP) plates. Ritchie et al. (1991) tested RC beams strengthened for flexure using GFRP, carbon fiber-reinforced polymer (CFRP), and laminates. Triantafillou and Plevris (1992) studied the behaviour of RC beams strengthened for flexure using CFRP sheets. Beams with deficient shear strength were damaged to predetermined level (the appearance of first shear crack) and then repaired by Fiber Glass Plate Bonding (FGPB) techniques [Al-Sulaimani et al. (1994)] with different shear repair schemes to upgrade the shear capacity of the specimen beams. Nanni and Norris (1995) generated experimental data to evaluate the behaviour of concrete members laterally confined with FRP composites. Two different types of FRP confinement (braided aramid FRP tape and pre-formed glass-aramid shells) were investigated. It was found that flexural strength and ductility were enhanced by the use of FRP jackets. Improvements were found to be dependent on jacketing method, shape of member cross-section, level of the axial load, and failure mode. Norris et al. (1997) investigated the behaviour of concrete beams strengthened using CFRP uni-directional sheets and CFRP woven fabrics. In all of these investigations, the strengthened beams showed higher ultimate loads compared to the existing ones. Saadatmanesh (1997) strengthened concrete and masonry structures using FRP for extending service life. Three types of FRP as composite plates, strap and epoxy bonded composite fabrics were used.

According to studies conducted by Chajes et al. (1998), the failure modes from FRP retrofitted structure were identified as (i) flexural failure due to either compressive failure of the concrete or tensile failure of the FRP, usually accompanied by yielding of the longitudinal steel bars; (ii) shear failure if the FRP application shifts the critical condition of the element to shear capacity; and (iii) failure of the bond connection between the plate or fabric and the cover concrete or failure of the bond between the cover concrete and the internal steel

reinforcement. FRP-strengthened RC joints were studied by Pantelides et al. (1997, 1999) to strengthen RC bridge bents with CFRP sheets in the cap beam-column joints under quasi-static lateral load. It was concluded that the composite wrap increased the shear capacity of the joints by almost 35%. Mirmiran et al. (1998) discussed how FRP materials significantly enhanced the strength, ductility and durability of concrete columns. A comprehensive state-of-the-art review of the different composite repair systems was presented by Mosallam (1998) and Marsh (1998).

Geng et al. (1998) and Mosallam (1999) used composite overlays to strengthen simple models of beam-column joints and recorded increases in the strength, stiffness, and ductility of the specimens. Castellani et al. (1999) performed full-scale seismic testing of a scaled two-storied, two-bay RC building at the European Laboratory for Structural Assessment (ELSA, Ispra). The damaged building (cracking and slippage of beam reinforcements) was repaired, strengthened with CFRP in the joints, and re-tested. It was suggested that the composite materials prove to be the good candidates for strengthening of joints if the proper detailing is implemented. Tsonos and Stylianidis (1999) performed a simulated seismic load test of an exterior joint model strengthened with FRP. Considerable increase in the strength, energy dissipation and stiffness characteristics compared to the control (unstrengthened) specimen were recorded. Gergely et al. (2000) tested a series of scaled exterior beam-column joints strengthened with CFRP sheets. Main variables in this investigation were the concrete surface preparation and the fiber orientation. It was concluded that FRP composites can provide a viable solution in improving the shear capacity of exterior RC joints. Mosallam (2000) introduced an innovative technique using polymer composites for repair and retrofit of RC moment frame connections. Epoxy injection as well as carbon-epoxy and E-glass-epoxy quasi-isotropic laminates were used for retrofitting the specimens. Test results indicated that the use of composite would considerably increase the stiffness, strength, and ductility of these connections.

Parra-Montesinos and Wight (2001) repaired hybrid RC column-to-steel beam connections, severely damaged during earthquake, by wrapping the column regions just above and below the steel beam with carbon fiber sheets. El-Amoury and Ghobarah (2002) used GFRP sheets to upgrade the shear strength of the beam-column joints and to reduce the potential for bond-slip of the bottom bars of the beam. An innovative, uniaxial ductile FRP fabric was developed and manufactured by Grace et al. (2002) for strengthening RC beams. The fabric was a hybrid of two types of carbon fibers and one type of glass fiber, and designed to provide a pseudo-ductile behaviour with a low yield-equivalent strain value in tension. The fabric was designed so that it would have the potential to yield simultaneously with the steel reinforcement of strengthened beams.

Antonopoulos and Triantafillou (2003) reported the findings from experimental investigation of FRP-strengthened RC beam-column joints. The issues like effectiveness of strips (laminates) versus sheets (fabrics), number of strips or number of sheet layers, mechanical anchorages, type of fibers (carbon versus glass), level of axial load in the column, damage in the joint prior to strengthening, and effect of transverse beam were discussed. Experimental results on the effects of cyclic loading on slip at the FRP-concrete interface, crack opening, and strain profiles along the bonded FRP joint were presented by Bizindavyi et al. (2003). D'Ayala et al. (2003) brought out the effectiveness of FRP strengthening of beam-column joints typical for building construction in Europe before the introduction of seismic codes. In view of this, suitability of CFRP wrapping of the beam-column joints was explored as a technique for strengthening. Iacobucci et al. (2003) investigated the prospect of strengthening of deficient- and repaired damaged square columns with CFRP jackets.

Shin and Lee (2003) examined the effect of sustaining loads on the flexural behaviour of strengthened RC beams with CFRP laminates. Aidoo et al. (2004) described the fatigue behaviour of CFRP strengthened RC bridge girders. It was demonstrated that the matrix composition has a greater effect on fatigue performance than the type of fiber used. Pseudo-dynamic testing of bridge columns was performed by Chang et al. (2004), in order to investigate the seismic responses of as-built and repaired RC bridge columns under near-fault ground motions. The damaged bridge column was repaired with CFRP sheets. Harajli and Rteil (2004) presented the results of an experimental investigation undertaken to evaluate the seismic performance of gravity load designed RC columns and retrofitted with externally bonded CFRP flexible sheets. Prota et al. (2004) provided upgradation schemes for under-designed reinforced concrete beam-column joints using combined use of FRP laminates and bars.

Pulido et al. (2004a,b) tested two-column bents retrofitted using CFRP fibers before testing. The CFRP retrofit efficiently modified the failure mode and enhanced the overall performance, lateral load-carrying capacity, and displacement ductility. The study reported by Sause et al. (2004) investigated the use of CFRP composite jackets as a method of retrofitting existing non-ductile RC building columns. A thorough review on beam-column joint rehabilitation techniques was presented by Said and Nehdi (2004a,b). The response of a full scale frame repaired using CFRP laminates was investigated by Balsamo (2005). Cheng et al. (2005) investigated the seismic performance of as-built, strengthened, and repaired hollow bridge columns with insufficient shear strength where strengthening was carried out using CFRP jackets and dog-bone-shaped bars and then re-tested. Ludovico et al. (2005) investigated the flexural behaviour of full-scale damaged prestressed concrete (PC) bridge girders upgraded with externally bonded CFRP laminates. Stark et al. (2005) presented the

results of an experimental program on seismic strengthening of slab-column connections upgraded by externally installed CFRP stirrups.

Full-scale experimental investigation of repair of RC bridge using CFRP was reported by Aidoo (2006). Corte et al. (2006) discussed the results of an experimental investigation on the use of composite materials for controlling the type of plastic collapse mechanism of a full scale structure. The structure was repaired and strengthened by externally bonded CFRP to change the plastic collapse mechanism from a column-sway to a beam-sway type. Harries et al. (2006) investigated the use of CFRP jackets as a seismic retrofit measure for deficient lap splices in structural components designed as compression only members. The residual performance of FRP-retrofitted RC columns following a limited seismic damage was explored by Shan et al. (2006). Yalcin et al. (2008) described a retrofitting proposal for RC columns using CFRP sheets to improve their strength and ductility capacities where the plain rebars were initially used in the columns. Ghosh and Sheikh (2007) directed toward the evaluation of the effectiveness of CFRP jackets in strengthening and repair of columns with poor lap splices and inadequate transverse confinement reinforcement in the potential plastic hinge regions near beam-column joints under simulated earthquake loading. Mosallam and Banerjee (2007) presented the results of an experimental investigation on shear strength enhancement of RC beams by externally reinforced FRP composites. Three composite systems (i) carbon/epoxy wet layup, (ii) E-glass/epoxy wet layup and (iii) carbon/epoxy pre-cured strips were used for retrofit and repair evaluation. A comparative study on the experimental results with published analytical models was also conducted in order to evaluate the different analytical models and to identify the influencing factors on the shear behaviour of FRP strengthened reinforced concrete beams. Few strengthening schemes using FRP jacketing as discussed above are shown in *Appendix (A3)*.

4.2.4 Other techniques for retrofitting beyond jacketing

A cost effective and efficient technique for strengthening RC columns was described by Frangou et al. (1995) by involving post-tensioned metal strips around RC columns. The experimental work supported the idea of such strengthening to increase member strength and ductility to higher levels than those possible by conventional retrofitting techniques. Experimental and theoretical studies on seismic retrofit of RC circular columns with poor lap-splice details using prefabricated composite jacketing was conducted by Xiao and Ma (1997). The retrofitted columns showed significant improvement in seismic performance. A seismic retrofit of hinged and fixed RC bridge columns with short bar anchorage in footings was suggested by Darwish et al. (1999). Tsonos (1999) conducted a series of tests to determine the effectiveness of the United Nations Industrial Development Organization (UNIDO)

manual guidelines for the repair and strengthening of beam-column joints damaged by severe earthquakes. Current techniques based on externally bonded steel plates and FRP laminates which possess the problem of mismatch of their tensile strength and stiffness with that of the concrete structure being retrofitted, were eliminated by Alaee and Karihaloo (2003) by using high-performance fiber-reinforced concrete mixes called as CARDIFRC. Bracci et al. (1995) analysed partially prestressed concrete- and two masonry- retrofit alternatives to improve the local and global response of the frame structures designed only for gravity loads and constructed in low-to-moderate seismic zones. Lowes and Moehle (1999) evaluated beam-column joints in older RC bridge structures with non-prestressed and prestressed retrofitting. Pampanin et al. (2006) proposed a non-invasive seismic retrofit solution for existing under-designed RC frame structures. A diagonal metallic haunch system was devised at the beam-column connections to protect the joint panel zone from extensive damage and brittle shear mechanism. Palermo et al. (2006) provided a hybrid solution by exploring the self-centring properties using unbonded post-tensioned tendons/cables with axial load, and energy dissipation capacity provided by mild steel. The main advantages of the proposed hybrid solution were noted as the lack of damage in the structural elements, self-centring properties by the unbonded post-tensioned tendons, and the high levels of ductility with a very stable hysteresis behaviour. As example, few schemes for strengthening of structural components using concepts beyond jacketing are shown in *Appendix (A4)*.

From the review of literature on strengthening of RC structures and components for seismic loading, as briefly presented above, it has been identified that concrete as a retrofitting material has been used for a long time. But, the construction difficulties, time requirement, need for invasion have enforced the researchers to find out any other substitute materials. Externally bonded steel plates are widely used due to (i) being quick, (ii) causing minimal site disruption, and (iii) producing only minimal change in section size. On the other hand, (i) occurrence of undesirable shear failures, (ii) difficulty in handling heavy steel plates, (iii) corrosion of the steel, and (iv) need for uncontrolled site welding have limited its acceptability.

FRP material would appear to offer an ideal alternative to steel plates, as it has (i) high strength to weight ratio, (ii) high stiffness to weight ratio, (iii) quite inert chemical property, offering significant potential for lightweight, cost effective and durable retrofit, (iv) non-yielding elastic property up to failure (confining pressure increases continuously with increase in concrete dilation as damage builds up and is therefore much more effective than conventional stirrups), and (v) unique ability to decouple between strength and stiffness. But, retrofitting using FRP is also vulnerable due to (i) undesirable brittle failures due to a large mismatch in the tensile strength and stiffness with that of concrete (the linear-elastic

behaviour up to failure of the fibers and the orthotropic behaviour of the laminates), (ii) vulnerable to delamination and (iii) prone to rupture at corner due to stress concentration.

Hence, it is evident that each of the materials so far used for strengthening, is surrounded by its own constraints. So, it is aimed at exploring the advantages and restricting the limitations, to the possible extent, of available materials to develop strategy/scheme which can be cost effective, constructible, comparatively fast with minimum invasion and most importantly, should be effective by ensuring protective strength hierarchy towards a safe performance under seismic loading.

In the present study, it has been attempted to carry out the investigations on two aspects.

(1) In *pre-earthquake scenario*: Development of suitable upgradation schemes for poorly designed gravity load structures which exist in huge number through out the world. After recent devastating earthquakes and their further consequences, concerns about earthquake are more serious and demanding. So, an attempt has been paid to develop suitable upgradation schemes which would be adequate and efficient as well. Development and performance of the upgradation scheme(s) are discussed in Chapter 5.

(2) In *post-earthquake scenario*: Development of suitable strategies for already damaged structural components so that those can further be used even if there is a possibility for earthquake in future. This is of great importance as in most of the cases after earthquake, it is not clear to abandon a structure or to retrofit. If the structure has to be retrofitted, then the further question is imposed as how much retrofitting is sufficient for re-using a damaged structure without compromising its safety. In the present study, the term ‘strategy’ stands for the entire steps of retrofitting of damaged specimens, i.e., from removal of damaged parts, cleaning, injection of chemical for internal integrity of concrete, filling the external cracks and wide damages, surface preparation, application of suitable material (FRP/steel/concrete) for restoration of structural behaviour parameters etc. Since, the previous research works pointed out the significant role of each of the steps (mentioned above) on final performance of retrofitted specimens, a carefully organised strategy is required to achieve the goal. Development and performance of the retrofitting strategies are discussed in the following sections.

4.3 Material models used for analysis towards strengthening of members

For evaluating the strengthening (both retrofitting and upgradation) schemes, the material models used for evaluating shear strength of joints of the specimens, as presented in Chapter 3, needs to be re-checked when the material model for concrete is concerned. For evaluating the joint shear strength it is important to incorporate the softening law in the constitutive model and post peak behaviour of concrete is not imperative. But for analytical formulation to strengthen the RC members, a material model is needed which is able to correctly represent its behaviour throughout its strain history. Further, strengthening would change the degree of confinement of the member which leads to a considerable change in behaviour of concrete. So, a few widely used material models for concrete have been discussed in search of obtaining the required ones which would be capable for both.

As presented in Chapter 3, the second order parabolic behaviour of concrete proposed by Hognestad (1951) as

$$f_c = f_c^{'}\left[2\left(\frac{\varepsilon}{\varepsilon_c}\right)-\left(\frac{\varepsilon}{\varepsilon_c}\right)^2\right] \qquad (4.1)$$

was used during evaluating the shear strength of joints of the specimens. This proposed curve was obtained by using an experimental ε_c for each individual specimen instead of a fixed value of 0.002. The proposed equation is a good prediction for the ascending branch but limited to the concrete compressive strength to 60 MPa. As it is clearly shown that the concrete stress becomes zero when the strain reaches a value of $2\varepsilon_c$, the proposed equation does not represent the residual stress in the post peak region.

The model used by Carreira and Chu (1985) is a generalised form of serpentine curve as

$$f_c = f_c^{'}\left[\frac{\beta\left(\frac{\varepsilon}{\varepsilon_c}\right)}{\beta-1+\left(\frac{\varepsilon}{\varepsilon_c}\right)^{\beta}}\right] \qquad (4.2)$$

Where β is a material parameter dependent on the shape of the stress-strain curve, and is determined as $\beta = \dfrac{1}{1-\left(f_c^{'}/\varepsilon_c \cdot E_{it}\right)}$ where E_{it} is calculated from empirical equation using maximum stress ($f_c^{'}$) and corresponding strain (ε_c). Popovics (1973) first proposed the

equation that was later used by Carreira and Chu (1985) as given in Eq. 4.2, but with $\beta = 0.058 f_c^{'} + 1.0$

Mander et al. (1988) proposed the concrete stress-strain behaviour as follows:

$$f_c = \frac{f_{cc} \cdot x \cdot r}{r - 1 + x^r} \tag{4.3}$$

$$f_{cc} = f_{c0}\left(2.254\sqrt{1 + \frac{7.94 f_l}{f_{c0}}} - \frac{2 f_l}{f_{c0}} - 1.254 \right) \tag{4.4}$$

where f_l is the effective lateral confining stress and a reduced (based on shape of the section) value from the total confining pressure.

$$f_{l,total} = \frac{2 \cdot f_y \cdot A_{sp}}{l \cdot s} \text{ (for section with steel stirrups)} \tag{4.5}$$

Where A_{sp} is area of stirrup, l and s are the effective dimension of the section and spacing of stirrups, respectively.

Total confining pressure in x-direction was proposed as

$$f_{l,total,x} = \frac{1}{2} \cdot \rho_x \cdot f_{fy} \text{ (for section with FRP)} \tag{4.6}$$

Similarly it can be calculated for y direction as well.

Based on the shape of the section, effective confining stress was presented as

$$f_l = k_e \cdot f_{l,total} \tag{4.7}$$

Typical values of k_e for rectangular and circular sections were suggested to be taken as 0.75 and 0.9 respectively (Priestley et al. 1996).

In Eq. 4.3, $x = \frac{\varepsilon_c}{\varepsilon_{cc}}$ *(4.8)*

$$\varepsilon_{cc} = 0.002\left[1 + 5\left(\frac{f_{cc}}{f_{c0}} - 1 \right) \right] \tag{4.9}$$

$$r = \frac{E_c}{E_c - E_{\sec}} \text{ where } E_c = 5000\sqrt{f_c^{'}} \text{ and } E_{\sec} = \frac{f_{cc}}{\varepsilon_{cc}} \tag{4.10}$$

Ultimate strain of concrete confined by FRP is limited to

$$\varepsilon_{cu} = 0.004 + \frac{1.4 \rho_f \cdot f_{fy} \cdot \varepsilon_{fu}}{f_{cc}} \tag{4.11}$$

Hoshikuma (1997) derived a model by considering all boundary conditions which a parabolic model can not satisfy. A polynomial was proposed as

$$f_c = C_1\varepsilon_c^n + C_2\varepsilon_c + C_3 \qquad (4.12)$$

Where the constants (C_1, C_2, C_3, C_4 and n) were determined by satisfying the boundary conditions and the final form was proposed as

$$f_c = E_c\varepsilon\left[1-\frac{1}{n}\left(\frac{\varepsilon}{\varepsilon_c}\right)^{n-1}\right] \qquad (4.13)$$

Where n is a coefficient described as

$$n = \frac{E_c\varepsilon_c}{E_c\varepsilon_c - f_c^{'}} \qquad (4.14)$$

The descending branch of the stress-strain curve was idealised by a straight line as

$$f_c = f_c^{'} - E_{des}(\varepsilon - \varepsilon_c) \qquad (4.15)$$

Where E_{des} is the deterioration rate obtained from the regression analysis of the test data.

CEB (1990) suggests two equations to describe the stress-strain behaviour of two ranges of concrete strains as

The ascending branch of the stress-strain diagram ($|\varepsilon| < |\varepsilon_{c,\lim}|$) is described as

$$f_c = f_c^{'}\frac{\frac{E_{ci}}{E_{c1}}\frac{\varepsilon}{\varepsilon_{c1}} - \left(\frac{\varepsilon}{\varepsilon_{c1}}\right)^2}{1+\left(\frac{E_{ci}}{E_{c1}}-2\right)\cdot\left(\frac{\varepsilon}{\varepsilon_{c1}}\right)} \qquad (4.16)$$

where, E_{c1} is the secant modulus corresponding to strain of ε_{c1}, and ε_{c1} is taken as 0.0022.

The descending branch of the stress-strain diagram ($|\varepsilon| > |\varepsilon_{c,\lim}|$) is described as

$$f_c = f_c^{'}\left[\left(\frac{1}{\varepsilon_{c,\lim}/\varepsilon_{c1}}\eta - \frac{2}{(\varepsilon_{c,\lim}/\varepsilon_{c1})^2}\right)\cdot\left(\frac{\varepsilon}{\varepsilon_{c1}}\right)^2 + \left(\frac{4}{\varepsilon_{c,\lim}/\varepsilon_{c1}} - \eta\right)\cdot\left(\frac{\varepsilon}{\varepsilon_{c1}}\right)\right]^{-1} \qquad (4.17)$$

$$\text{where } \eta = \frac{4\left[\left(\frac{\varepsilon_{c,\lim}}{\varepsilon_{c1}}\right)^2\left(\frac{E_{ci}}{E_{c1}}-2\right)+2\cdot\left(\frac{\varepsilon_{c,\lim}}{\varepsilon_{c1}}\right)-\frac{E_{ci}}{E_{c1}}\right]}{\left[\left(\frac{\varepsilon_{c,\lim}}{\varepsilon_{c1}}\right)\cdot\left(\frac{E_{ci}}{E_{c1}}-2\right)+1\right]^2} \qquad (4.18)$$

The limiting strain ($\varepsilon_{c,\lim}$) is the concrete strain when concrete stress is equal to $0.5f_c^{'}$ in the descending part of the stress-strain curve, as

$$\varepsilon_{c,\lim} = \varepsilon_{c1}\left[\frac{1}{2}\left(\frac{1}{2}\frac{E_{ci}}{E_{c1}}+1\right)+\sqrt{\frac{1}{4}\left(\frac{1}{2}\frac{E_{ci}}{E_{c1}}+1\right)^2-\frac{1}{2}}\right] \qquad (4.19)$$

The stress-strain models described above are shown in *Fig. 4.3* and *Fig. 4.4*. The first one (*Fig. 4.3*) is shown mainly for ascending part of stress-strain curve of concrete and the later (*Fig. 4.4*) is shown to get the comparative behaviour of concrete for entire zone as proposed by different researchers. It is clear from the diagrams that the ascending branch of the concrete models proposed by different researchers (and code of practice) are well in agreement but a considerable amount of disparity does exist in the descending part of the concrete models.

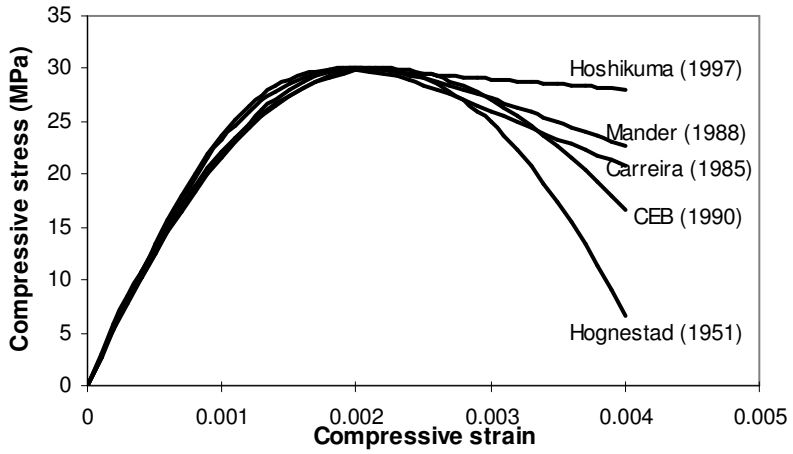

Fig. 4.3 Concrete stress-strain behaviour at small strain range

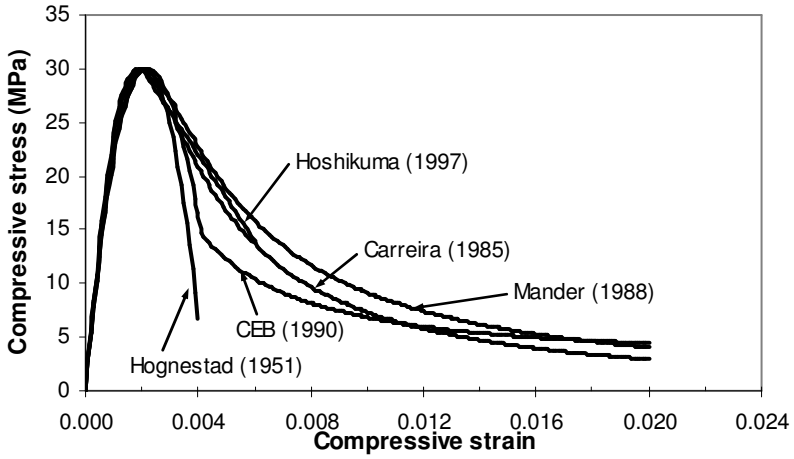

Fig. 4.4 Concrete stress-strain behaviour for entire strain range

From the above study on proposed stress-strain behaviour of concrete which is an ever challenging and contentious issue, it is clearly shown that the most appreciated models that have been studied here are of same nature when strain in concrete is limited to ε_c (ascending part of the model). But, at larger strain (descending part of model), the proposed models behave differently and magnify their limitations. For instance, in need of concrete model which can perform well in large strain, Hognestad (1951) and Hoshikuma (1997) can not be used as they had explicitly mentioned about their limited experimental studies. The concrete model proposed by Mander (1988) has been observed to be quite consistent and robust even for large strain cases. In Mander's (1988) model only one single formulation is capable in reflecting the concrete behaviour both for ascending and descending parts which is unique from the other models. Further, both for confined and unconfined concrete, the same model can be used since the confinement effect was incorporated in the constitutive model in a general form. As the aim of the study has been the assessment of the existing structure and finally to provide the suitable retrofitting measure for damaged components and upgradation schemes for aseismically analysed and/or poorly designed components, additional confinement to the concrete would be useful for enhancing strength and ductility. Hence, the unified material model proposed by Mander (1988) was considered for the present study.

For analytical study, the steel and FRP material models were used as shown in *Fig. 4.5* and *Fig. 4.6* respectively. Non-linear portion of steel was modelled as described in Eq. 3.11.

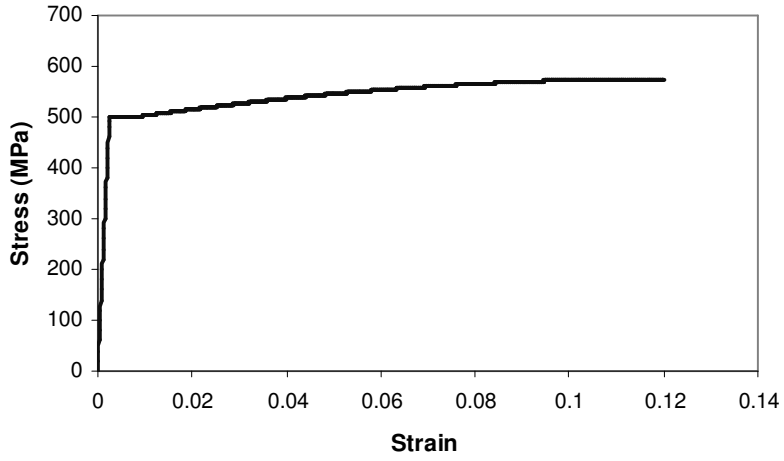

Fig. 4.5 Material model for steel considered in this study

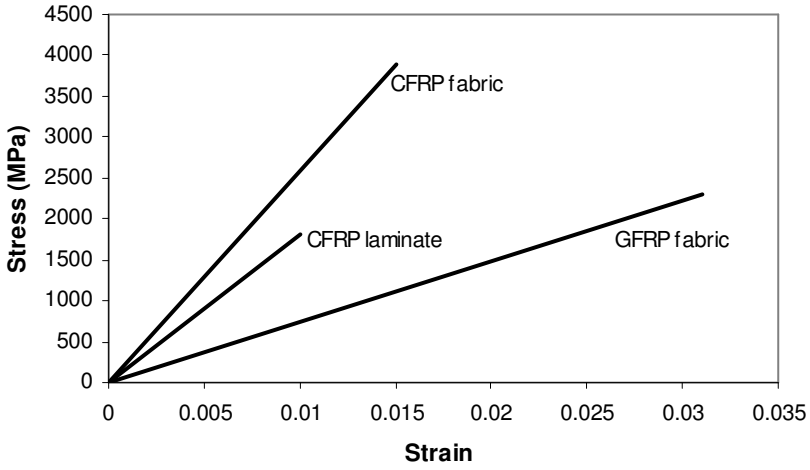

Fig. 4.6 Material model for FRP (available from vendor)

4.4 Fiber section analysis of existing and strengthened sections

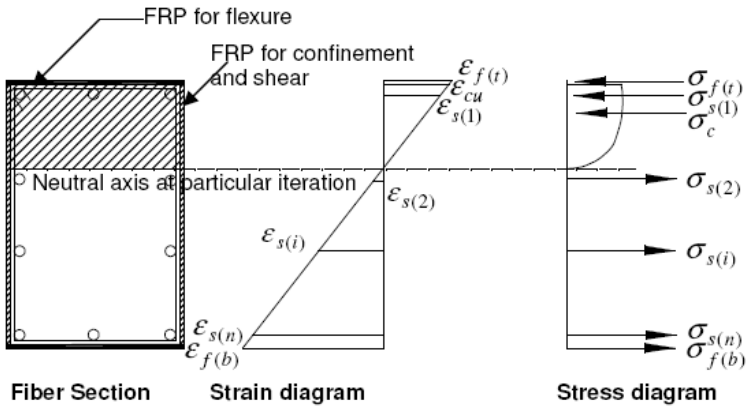

Fig. 4.7 FRP strengthened section and stress strain diagrams

A fiber section analysis (as shown in *Fig. 4.7*) was carried out to develop the axial load-moment (P-M) interaction and moment-curvature (M-κ) diagram for strengthened sections. In the figure, suffix '*t*' and '*b*' stand for the fiber at top and bottom respectively, '*c*' is for concrete, '*s*' is for reinforcing steel and '*f*' is for FRP. In this study '*n*' number of reinforcement layers was considered for developing both (P-M) interaction and (M-κ) diagram. For unconfined concrete maximum concrete strain was limited to 0.35% and for confined concrete the stress-strain relationship was calculated based on degree of confinement as described in Eqs. 4.3-4.11. An analytical model and the computer program have been developed to calculate the (P-M) and (M-κ) diagrams for confined and unconfined concrete with different level of strengthening (GFRP, CFRP, number of layer etc.) to reach the target strength. The material models of concrete, FRP and steel as shown in *Fig. 4.4*, *Fig. 4.5* and *Fig. 4.6* were used in the computer program.

It is clear from the reported studies (described in the section 4.2.3) that a proper confinement can considerably improve the concrete behaviour itself and hence, the structural behaviour can also be improved by providing adequate confinement. Using the computer program, a thorough study was carried out to evaluate the effect of strength and ductility of the member sections with different degrees of confinement. For illustration, *Fig. 4.8* shows the axial force (P)-moment (M) interaction behaviour of the concrete column of SP-3 (which is also same for SP-5) with different degrees of confinement. It is clear from the figure that with increase in confinement, both axial load and moment carrying capacities of the section increase considerably. It is needed to mention that to calculate the maximum strain and strength of confined concrete, Mander's (1988) proposal was followed and the confinement by GFRP with rupture strain of 3.1% and tensile strength of 2300 MPa were considered here for showing the effect of confinement (*Fig. 4.8*). To note, 0.1% volumetric confinement (ρ) is equal to 1 layer of GFRP around that particular section.

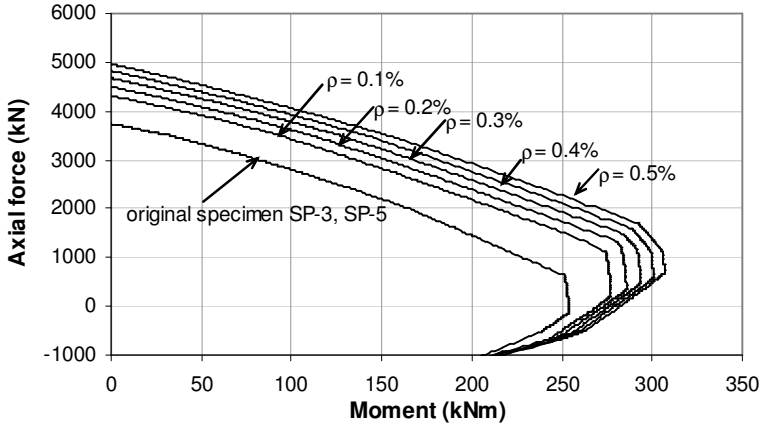

Fig. 4.8 P-M interaction of SP-3/SP-5 with different degrees of confinements

It can be also shown that M-κ relationships are similarly improved by providing confinement. In this Chapter, the main objective is kept to retrofit the damaged reinforced concrete specimens as 'NonDuctile' SP-3 and 'Ductile' SP-5. From the experimental investigation, it was found that the main reinforcement bars in beam and column had not failed but were in yielding zone. So, a proper confinement and an adequate continuity from column to beam would be required to regain its performance of the damaged retrofitted specimens, if simultaneously, the repair work is successfully carried out. Hence, the basic idea of retrofitting was controlled by joint strengthening and confinement.

4.5 Proposed retrofitting strategy for already damaged specimen SP-3

In the present study, retrofitting strategy was developed and the performance of the proposed retrofitting strategy has been compared with the results obtained from the original undamaged specimens. Towards this, damaged specimens SP-3 ('NonDuctile') and SP-5 ('Ductile') were chosen for implementing the retrofitting strategies. In the first step, damaged 'NonDuctile' specimen SP-3 was retrofitted (called as SP-3R) as shown in Appendix *Fig. A3*. It was intended that after the first test of retrofitted specimen, second retrofitting strategy for SP-5 would be developed by incorporating any possible and required improvement that would be observed during the experimental investigation of SP-3R.

4.5.1 Description of retrofitted specimen SP-3R

As can be seen from *Fig. A3* (in Appendix), a combined approach was adopted for the retrofitting scheme by judiciously using both steel plate and FRP. From the reported research works, it is clear that the FRP is extremely good for confinement and strength enhancement, but it is difficult to be placed at beam-column joint. On the other hand, steel plate jacketing though has been researched extremely, but limited to its application due to the reasons mentioned in section 4.2.4 along with its unsatisfactory performance in bonding with concrete. In this study, steel plate was restricted to the joint region only and was placed using 5 numbers of through-through bolts. FRP applications are mainly limited due to their exorbitant cost implications. It is found from the in-depth review of literature that due to superior material behaviour of CFRP, most of the research works have been carried out using CFRP instead of GFRP. But, the cost of CFRP fabric is much higher than GFRP. So, in this study only GFRP was thoughtfully attempted to be used by maintaining desired performance and by keeping the economic constraints in feasible range.

First, damaged concrete was removed from all parts of the specimen and the surface was cleaned using a blower to avoid dust on the surface. At pre-decided locations, holes were drilled in the joint region for placing the bolts (as shown in *Fig. 4.9*). Then the internal cracks were grouted with Sikadur 53UF^{TM} by pressure injection. An epoxy based mortar (Sikadur 41^{TM}) was used for filling the cavities and doing the patch work. Where the damage was large, extra concrete was placed after adding a suitable chemical (Sikadur 32LP^{TM}) for attaining the adequate bond between old and new concrete.

Fig. 4.9 Removal of damaged concrete and drilling for through bolts in SP-3R

From the results obtained from the cyclic test of SP-3, it was observed that some of the stirrups in column and beam failed and maximum strain level in main reinforcement bars of column and beam though exceeded yielding but well below the ultimate level. Thus, the main reinforcing bars could be assumed to take further loading.

To provide continuity after damage and to arrest the deviating force during displacement cycles, FRP in form of “L” needs to be placed in both top and bottom surfaces of the beam near the joint. Hence, 4 layers of composite GFRP were placed in “L” shape locations. First, epoxy (Sikadur 330^{TM}) was applied on the dust free, repaired concrete surface before placement of any GFRP fabrics. Afterward, each layer of GFRP was paced with consecutive application of epoxy layer. A special rolling device was used to properly impregnate epoxy in each layer of GFRP. As it is always a problematic issue for FRP anchorage, in addition to adequate length, GFRP wrap was provided in both beam and column to provide additional anchorage to the “L” shape GFRP and offer adequate confinement to damaged concrete. 4 layers of GFRP were provided as wrapping. Numbers of layers of wrapping were calculated to attain the peak confined strain of concrete as proposed by Priestley et al. (1996). Since a prolonged and deep crack was observed in the damaged specimen, 3 numbers of laminates were provided at the back the column to arrest the previous cracks from further propagation. After finishing all FRP applications, the 3-parts steel plate with 4 mm thickness was placed to the joint faces using 5 numbers of through-through bolts which ensured the confinement to

the damaged joint. Thickness of the plate was determined from bearing criteria of the bolts. To obtain a good contact with concrete surface which is essential for confinement, an epoxy based thixotropic adhesive (Sikadur 31PBA^{TM}) was applied between concrete and steel plate. The bolts were tightened using hand torque. After applying all the retrofitting components, final retrofitted scheme ready for testing is shown in *Fig. 4.10*.

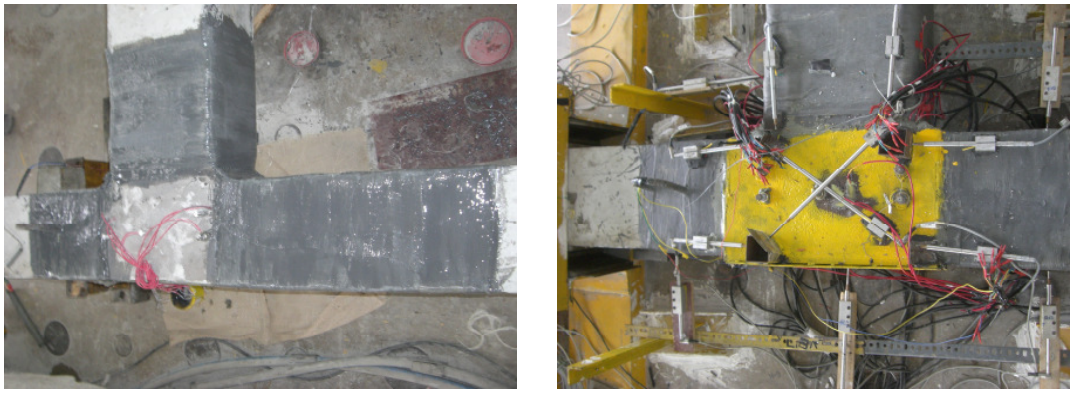

Fig. 4.10 Application of FRP on repaired surface and steel plate on joint of SP-3R

After the cyclic test of SP-3, it was doubtful on functionality of the existing strain gages due to severe damage in pre-retrofitted specimen and the application of FRP wrapping and steel plate had made it difficult to collect the existing strain gages for further use. Hence, a new instrumentation scheme was developed where the LVDTs were placed along the both sides of the beam length and column height to evaluate the displacement profile. Additionally, new strain gages were pasted on the steel plate (in three directions), both sides of each of the five bolts and on FRP placed on beam top and bottom. The retrofitted specimen was tested under cyclic loading as used for undamaged specimen (shown in *Fig. 3.5*).

4.5.2 Results and discussion

During the test of the specimen (SP-3R), it was observed that the initial crack developed at the beam-column junction line where a big crack prevailed before retrofitting. Due to the practical difficulty during retrofitting, a length of around 30-50 mm in beam from the joint face was left without any additional material (steel plate or FRP) during retrofitting (as shown in left of *Fig. 4.11*). With the increment in displacement of both positive and negative cycles, the crack became wider. But, it was interesting to note that the “L” shape FRP though started lifted up from the corner but did not rupture at this level which ensured the efficiency of 4 layers of GFRP in resisting the deviation force. After the usual displacement cycles, finally, a large displacement of 175 mm was imposed on the specimen and then the FRP wrapping in both column and beam failed by rupture (as shown in *Fig. 4.11*).

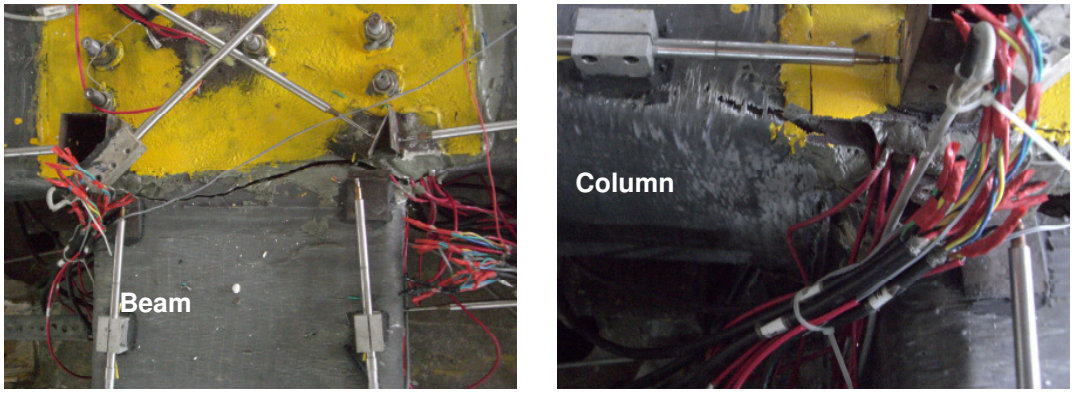

Fig. 4.11 Initial crack during the test (left) and final FRP rupture in SP-3R (right)

The load-displacement hysteresis loops for both SP-3 and SP-3R are shown in *Fig. 4.12* for better comparison and to identify the level of retrofitting. It is clear from the figure that the positive strength (upward loading) of the retrofitted specimen was though monotonically increasing, but could not gain its undamaged strength whereas the negative strength was fully restored. It is worth-mentioning that the most important parameters like stiffness degradation, strength deterioration and energy dissipation (both individual cycle and cumulative) showed a better response from the retrofitted specimen in comparison with the original one, as can be seen from *Fig. 4.13* to *Fig. 4.16*, respectively.

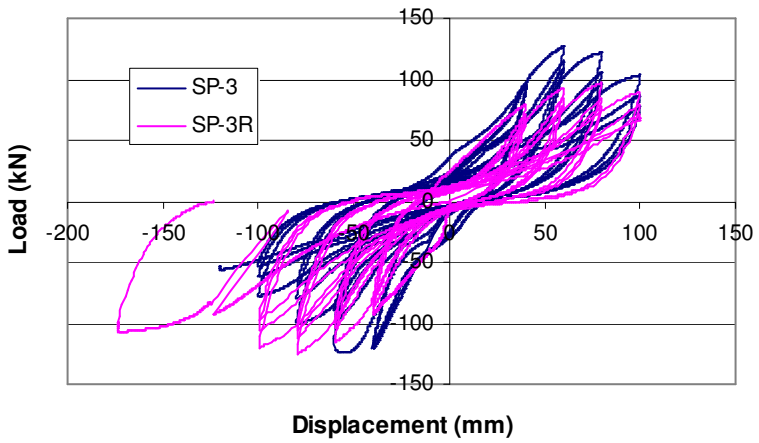

Fig. 4.12 Load-displacement hysteresis of SP-3 and SP-3R

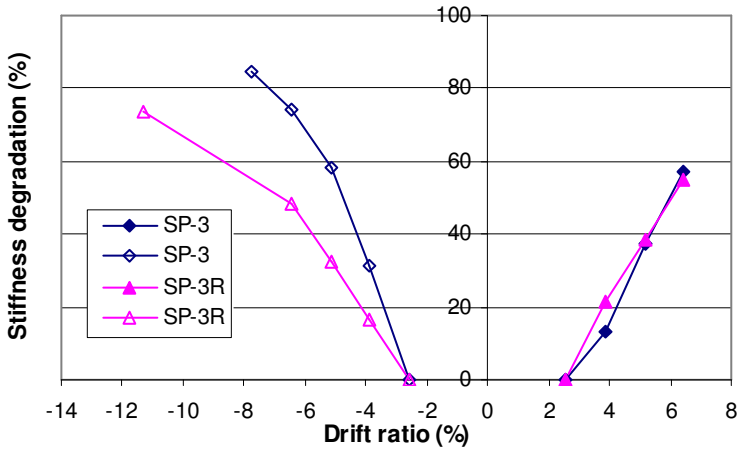

Fig. 4.13 Comparison of stiffness degradation of SP-3 and SP-3R

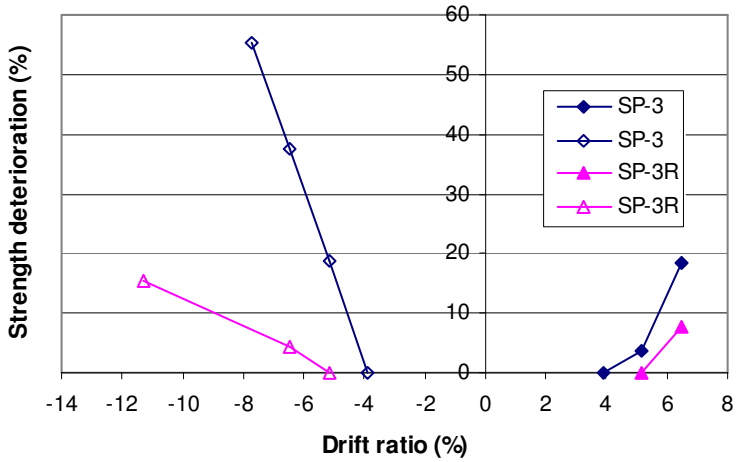

Fig. 4.14 Comparison of strength deterioration of SP-3 and SP-3R

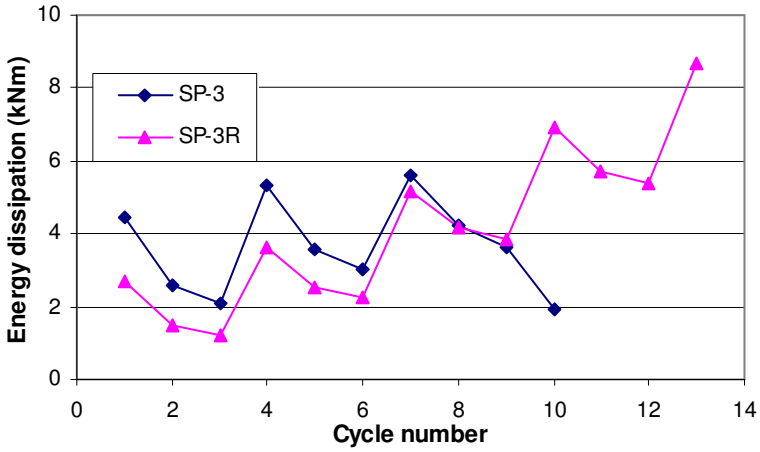

Fig. 4.15 Comparison of per cycle energy dissipation in SP-3 and SP-3R

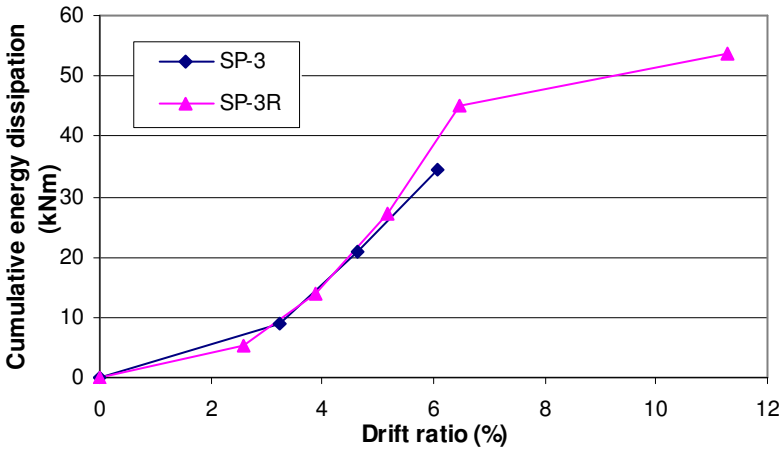

Fig. 4.16 Comparison of cumulative energy dissipation in SP-3 and SP-3R

From *Fig. 4.12* to *Fig. 4.16*, it is evident that the retrofitted specimen (SP-3R) was not only able to regain its original characteristics; it showed a better behaviour as well. Since the original damaged specimen was a 'NonDuctile' one, it was desired to improve the behaviour (in terms of energy dissipation, stiffness degradation etc.). For example, stiffness degradations in both original and retrofitted specimens were observed to be same at maximum positive displacement, but at maximum negative displacement those were 85% and 74% in original and retrofitted specimen, respectively (*Fig. 4.13*). Regarding strength deterioration, in original specimen it was observed to be 18% and 55% at maximum positive and negative displacement level, respectively. However, at maximum positive and negative displacement levels, those were noted as 8% and 15% in retrofitted specimen (*Fig. 4.14*). Reduction in strength deterioration or stiffness degradation has a prominent and significant effect on its seismic performance. Per cycle energy dissipation of retrofitted specimen was much superior than that obtained from original specimen since in retrofitted specimen a monotonically improving and consistent nature could be found whereas in original specimen it started with a better quantity but failed to sustain it (*Fig. 4.15*) and this phenomenon was same in terms of cumulative energy dissipation also. Original specimen was restricted to a drift ratio of ≈ 6.5 and was not imposed to a very large displacement demand (drift ratio of 11 to 12) at final stage but the retrofitted specimen was. Hence, for comparison, at the same drift ratio before the final large displacement, cumulative energy dissipation obtained from the retrofitted specimen was almost 25% more than that produced by the original specimen (*Fig. 4.16*).

It is important to investigate the behaviour of the retrofitting components such as steel plate, FRP and additional bolts to hold the steel plate because it would show the role of the

components and can be used for further improvement (if any). The behaviour of those retrofitting components is shown in *Fig. 4.17* to *Fig. 4.19*.

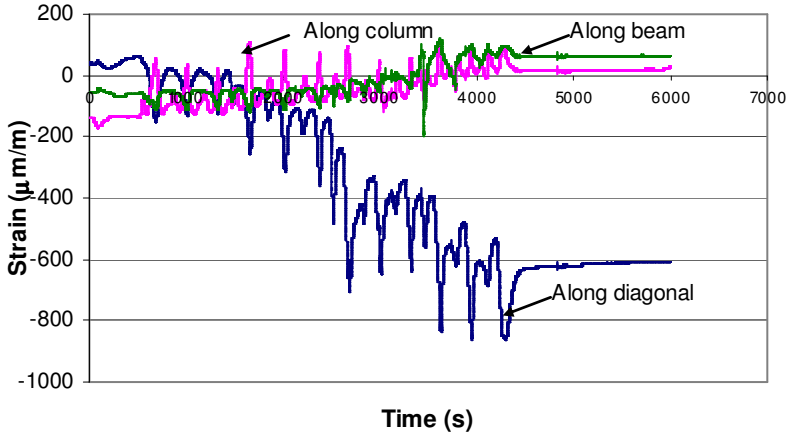

Fig. 4.17 Development of strain in steel plate (top side) during cyclic loading

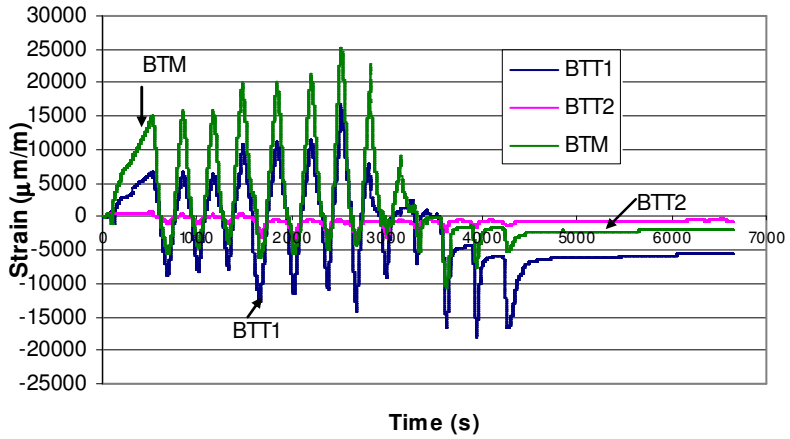

Fig. 4.18 Development of strain in FRP on top face of beam during cyclic loading

(BTT1 : joint line edge, BTT2 : away from joint line, BTM: mid of joint line)

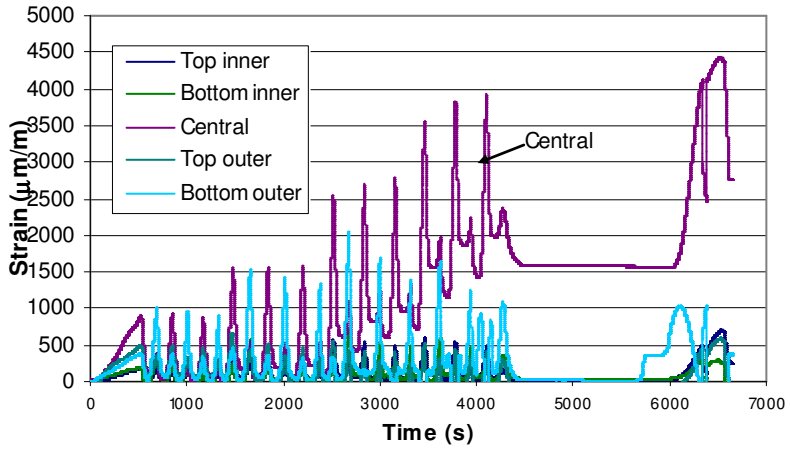

Fig. 4.19 Development of strain in bolts for steel plate during cyclic loading

It has been observed (*Fig. 4.17*) that the diagonal strain (stress) in steel plate was much more than the orthogonal direction as it is the principal force transferring path through diagonal strut. For further optimisation and to reduce material usage, actual strength and limiting strain of GFRP used for the study can be checked from *Fig. 4.18*. To the author's knowledge, use of bolts in this type of operation and its behaviour are not reported in literature. So, the study on actual developed strain along the bolt axis at different locations is very interesting and shows (*Fig. 4.19*) that the bolts along the diagonal struts are to resist an immense amount of axial strain and thus, designing the adequate size and judicious disposition of bolts for design of retrofitting schemes are important issues.

4.6 Proposed retrofitting strategy for already damaged specimen SP-5

Obtaining the insights from the investigations on SP-3R, a retrofitting strategy with minor modification from one that was adopted for SP-3R, has been proposed for damaged 'Ductile' specimen SP-5. The basic retrofitting materials were same. But, in the joint region, another 2 layers of GFRP were placed in "U" form to obtain the continuation between column and beam. The retrofitting scheme with all the details can be seen in Appendix *Fig. A4*.

4.6.1 Description of retrofitted specimen SP-5R

Both steel plate and FRP were used for the retrofitting scheme as shown in *Fig. A4* (in Appendix). Similar to SP-3R, steel plate was restricted to the joint region only and placed using 5 numbers of through-through bolts. Though initially, it was planned to place the through-through bolts at 4 corners and at the middle, but due to presence of heavy reinforcement from beam and column, corner 2 bolts were shifted to the middle. It was found from the experimental results of SP-3R that proper application of GFRP could provide a considerable improvement in performance of damaged structures. Hence, in this case (SP-5R) also GFRP was used for confinement and arresting the deviation force.

Fig. 4.20 Damaged specimen SP-5 (Novák et al. 2008)

Damage pattern of 'Ductile' specimen SP-5 is shown in *Fig. 4.20*. First, the damaged concrete was removed from all parts of the specimen and surface was hand cleaned to avoid dust on the surface. The procedure for repair and surface treatment were identical as that were followed for SP-3R. Since the original specimen SP-5 had undergone a very high drift level (≈ 13%), proper repair was very significant. A typical injection process and the routing inside damaged concrete are shown in *Fig. 4.21*.

Fig. 4.21 Crack filling operation using epoxy injection for damaged SP-5

The chemicals used for grouting, filling cavities and for FRP impregnation were same as that have been described for SP-3R. From the results obtained from the cyclic test of SP-5, it was reported that the main reinforcement bars of column and beam were yielding and none of them failed. Thus, similar to SP-3, main reinforcing bars were assumed to take further loading.

Before applying FRP in form of "L", 2 layers of "U" shaped GFRP were placed horizontally around the joint region. This would provide the connectivity between column and beam which was absent in SP-3R. Further, "L" shaped GFRP was placed in both top and bottom surface of the beam near the joint. Here, it is to mention that the length of "L" shaped GFRP along the beam was provided up to 300 mm from the joint whereas in SP-3R it was 400 mm. Further, the number of layers of GFRP wrapping in beam zone of SP-5R was reduced to 3 layers instead of 4 layers that were adopted in SP-3R. Reason for reduction in both length of "L" GFRP and number of layers of wrapping was the observations from the failure pattern of SP-3R where initial failure started at beam-column joint corner and with further displacement demand, rupture propagated towards the column (*Fig. 4.11*). To avoid this type of behaviour and to ensure the failure of FRP in beam before any damage in column or joint, amount of GFRP both in "L" shape and in wrap were reduced. Unlike in SP-3R, no laminate was provided on the back side of the column since it was observed to be not so effective. After finishing all FRP applications, the steel plate with 4 mm thick was placed on the joint faces using 5 numbers of through-through bolts. Further to provide a good contact and smooth

medium for placement of plate, an epoxy based thixotropic adhesive (Sikadur 31PBA^{TM}) was applied between "U" wrap in the joint and steel plate. The bolts were tightened using hand torque. During application of FRP in different stages and final retrofitted scheme ready for testing are shown in *Fig. 4.22*.

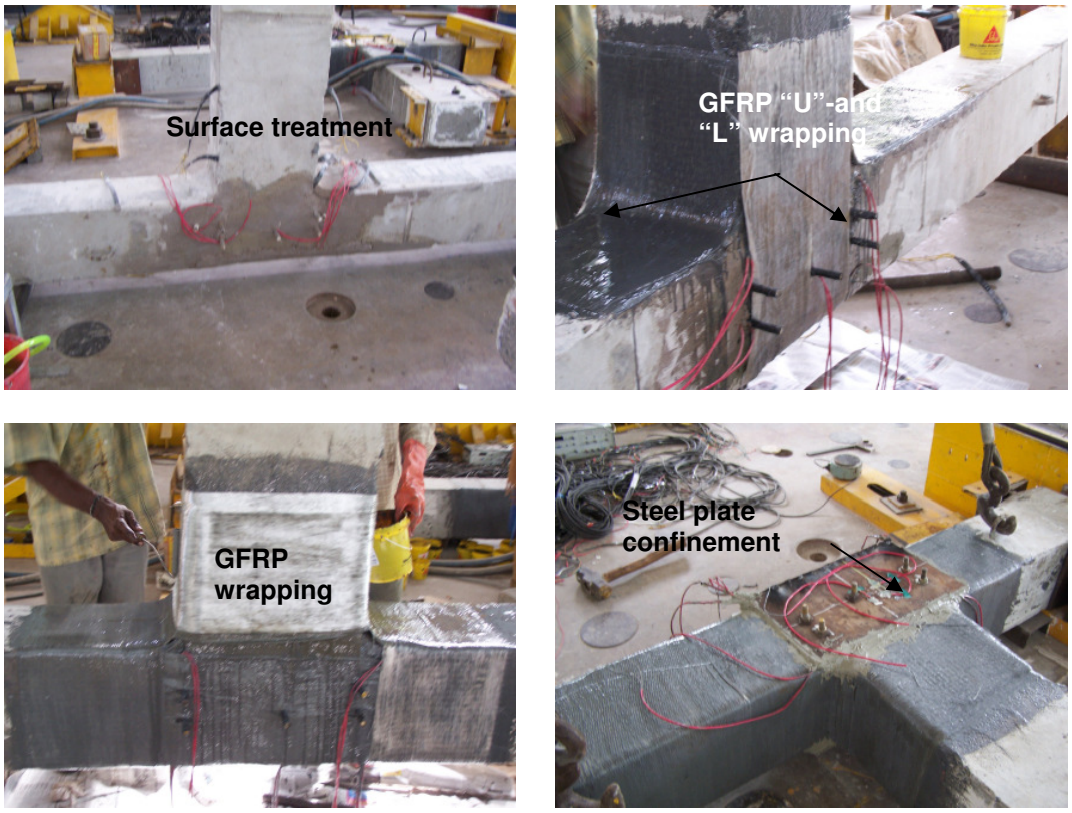

Fig. 4.22 Final surface treatment, application of FRP and steel plate used in SP-5R

Since the original SP-5 was finally imposed to a very high displacement demand, most of the important strain gages were damaged. Further, similar to SP-3R, LVDTs were placed along the both sides of the beam and column and new strain gages were pasted on the steel plate (in three directions), on bolts and on GFRP placed on beam top and bottom. The retrofitted specimen was tested under cyclic loading as used for previous undamaged ones (shown in *Fig. 3.5*).

4.6.2 Results and discussion

With the increment of displacement in both positive and negative cycles, it was found that no crack occurred near the joint region as was observed in SP-3R. Therefore, the effectiveness of "U" wrapping around the joint can be assured. But, it was interesting to note that the wrapping GFRP on beam started peeling off from concrete under the higher level of displacement. After the usual displacement cycles, finally, a large displacement of 184 mm was imposed on the specimen and then the FRP wrapping failed in rupture (as shown in *Fig.*

4.23). Due to lesser number of wrapping and shorter length of GFRP in beam, total damage (rupture, delamination and lifting) occurred in FRP in beam zone only and no rupture of FRP in column was found.

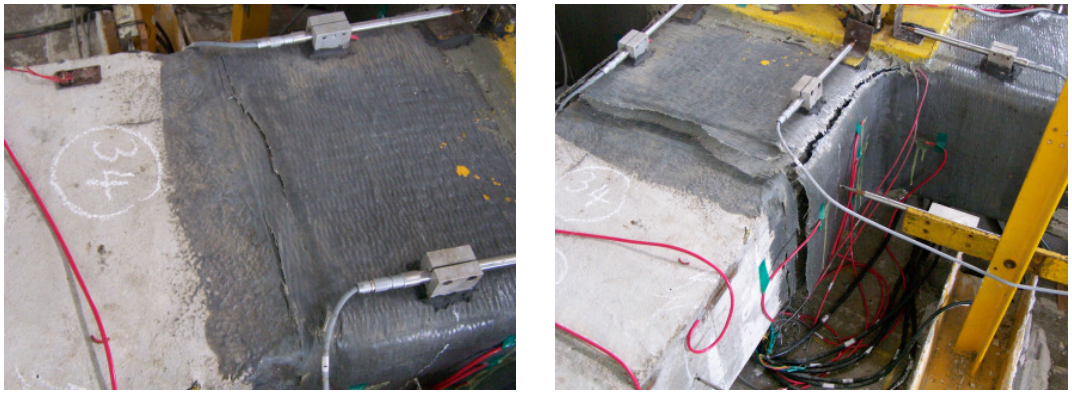

Fig. 4.23 Initial crack during the test (left) and final FRP rupture in SP-5R (right)

The load-displacement hysteresis for both SP-5 and SP-5R are shown in *Fig. 4.24* [details on original SP-5 and its behaviour can be found in Novák et al. (2008)]. It is clear from the figure that the positive strength (upward loading) of the retrofitted specimen could not be gained fully but the negative strength was almost same as the undamaged one. These were similar to that observed from SP-3R. It was also observed from *Fig. 4.24* that strength under both the positive and negative displacement cycles was consistently increasing. It is worth-mentioning that the parameters like stiffness degradation, strength deterioration and energy dissipation (both individual cycle and cumulative) also showed a better response from the retrofitted specimen as can be seen from *Fig. 4.25* to *Fig. 4.28* respectively.

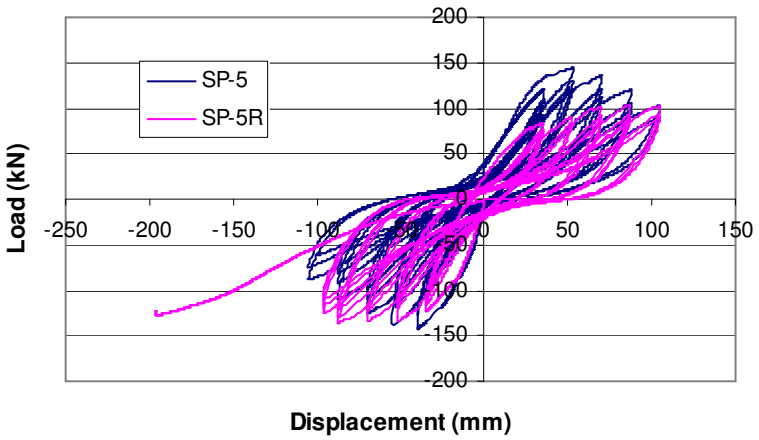

Fig. 4.24 Load-displacement hysteresis of SP-5 and SP-5R

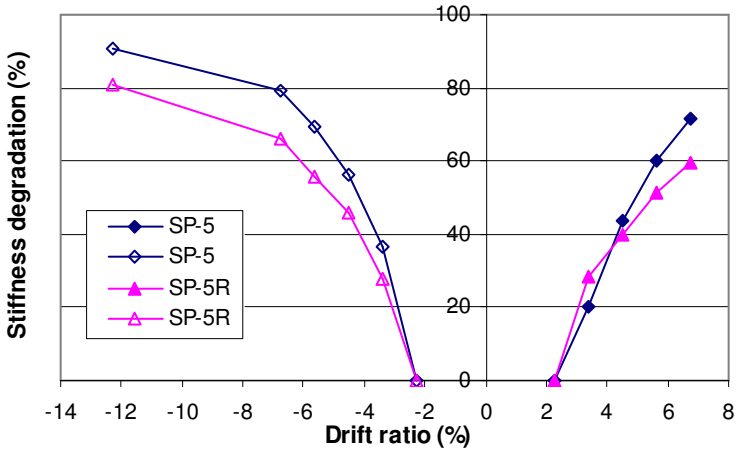

Fig. 4.25 Comparison of stiffness degradation of SP-5 and SP-5R

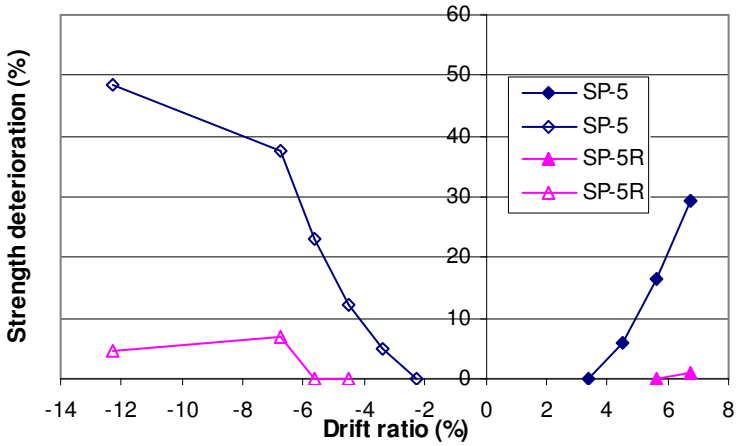

Fig. 4.26 Comparison of strength deterioration of SP-5 and SP-5R

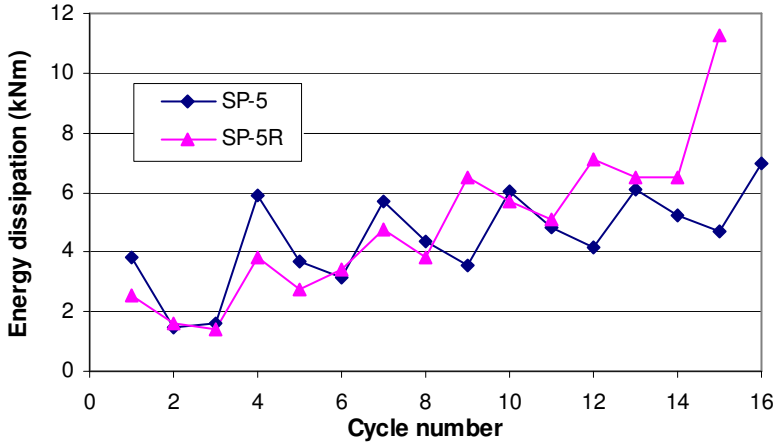

Fig. 4.27 Comparison of per cycle energy dissipation in SP-5 and SP-5R

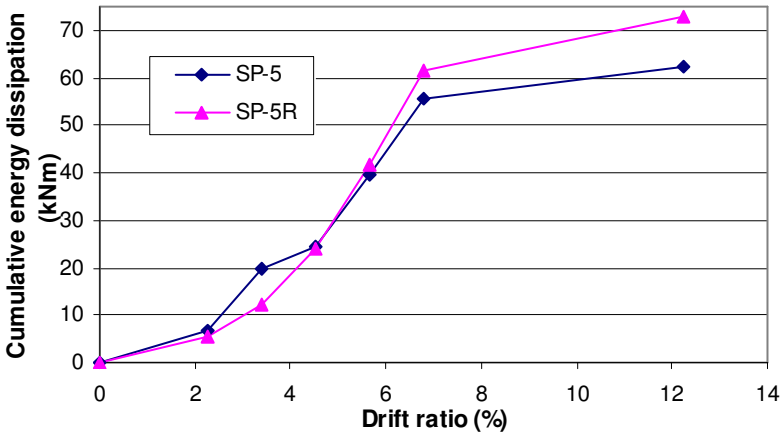

Fig. 4.28 Comparison of cumulative energy dissipation in SP-5 and SP-5R

The retrofitted specimen (SP-5R) was able to regain its original characteristics as can be seen from the above figures. Since the original damaged specimen was a 'Ductile' one, it was not ideally required to further improve the behaviour. Still, the stiffness degradation and strength deterioration were considerably slower than the original 'Ductile' specimen. Thus, it ensured a superior performance of the retrofitted specimen than the undamaged 'Ductile' specimen. For illustration, under maximum positive displacement, strength deterioration in original specimen was observed to be 30% whereas in retrofitted specimen it was totally absent (*Fig. 4.26*). Similarly, under maximum negative displacement, final strength deterioration in original specimen was 48% whereas in retrofitted specimen it was as small as 7% (*Fig. 4.26*). In SP-5, stiffness degradations were observed to be 72% and 91% at maximum positive and negative displacement levels, respectively. However, at same positive and negative displacement levels, those were noted as 60% and 81% in retrofitted specimen SP-5R (*Fig. 4.25*). An impressive behaviour was also found in retrofitted specimen when energy dissipation in each cycle was studied. Though in initial cycles, retrofitted specimen lagged behind the original specimen, it was consistently improving and after few cycles it exceeded the original specimen. This behaviour was kept unaltered till end (*Fig. 4.27*). Cumulative energy dissipations in both original and retrofitted specimens though were almost identical but at final displacement, the retrofitted specimen showed approx.15% more dissipation of cumulative energy (*Fig. 4.28*).

The behaviour of the retrofitting components such as steel plate, FRP and additional bolts to hold the steel plate are shown in *Fig. 4.29* to *Fig. 4.31* respectively.

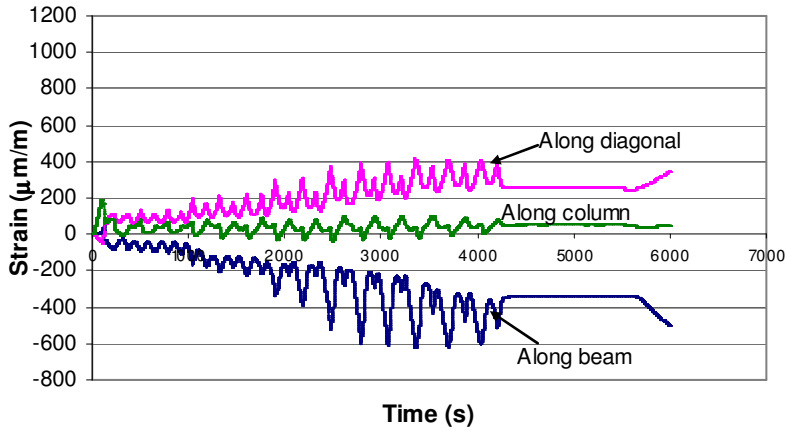

Fig. 4.29 Development of strain in steel plate (top side) during cyclic loading

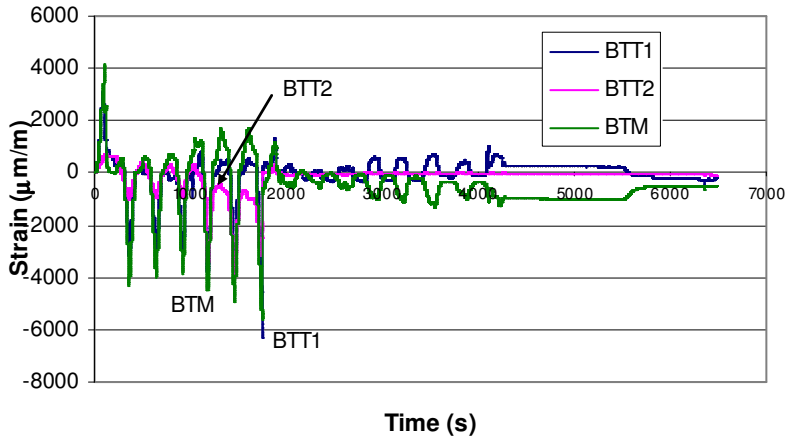

Fig. 4.30 Development of strain in FRP on top face of beam during cyclic loading

(BTT1 : joint line edge, BTT2 : away from joint line, BTM: mid of joint line)

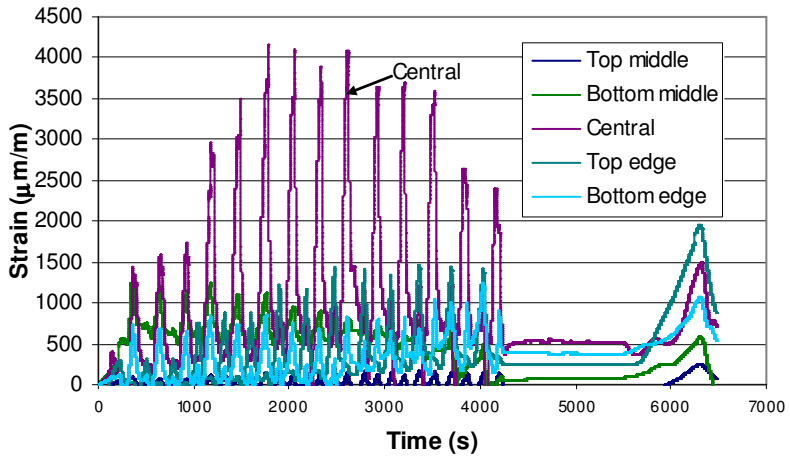

Fig. 4.31 Development of strain in bolts for steel plate during cyclic loading

It is observed (*Fig. 4.29*) that the strain in steel plate along the beam direction is much more than the orthogonal direction. *Fig. 4.30* shows that the strain in middle of wrapping was much higher than that at edges. After few cycles, FRP started delaminating from the face of the concrete and the induced strain reduced drastically. Similar to SP-3R, effectiveness of the bolts were directly related to their disposition (as can be seen from *Fig. 4.31*) and the bolt in the middle suffered from maximum strain (axial) since it had to carry a very high load from the compressive diagonal strut in joint.

4.7 Summary on retrofitting strategies

It can be summarized that both the retrofitting strategies were effective and able to restore the seismic performance to the original level, if not better. Towards this, initially a proper repair strategy is a must for proceeding further on retrofitting. Hence, the surface preparation, removal of loose concrete, filling of cavities and most importantly, appropriate injection of epoxy need to be carried out carefully. Further, GFRP in deviation lines and as wrapping, and steel plate in joint zone could be the good distribution of materials for retrofitting. It has also been found that the bolts, specially the central one, yielded in both cases (*Fig. 4.19* and *Fig. 4.31*). Hence, a high strength bolt may be a better option for adopting in the joint zone, provided it is available and economically viable. In both the studies, SP-3R and SP-5R, it has been noted that (*Fig. 4.17* and *Fig. 4.29*) stresses produced in steel plate were not very high. Nevertheless, reduction in steel plate thickness is not being suggested because beside the confinement issues, high axial stress in bolt has to be transferred through bearing stress on the plate, and lifting up of the plate corners could take plate during tightening of bolts if the plate is too thin. Difference in distribution of stress in top steel plate among the specimens (SP-3R and SP-5R) was noticed due to variation in compaction level of epoxy that was filled between steel plate and FRP/concrete in the joint zone. It was observed during execution of retrofitting work that providing the thixotropic epoxy between “U” shaped FRP or concrete surface and steel plate, particularly for uniform contact, was quite difficult since it was tried to use the partly pre-welded plate on joint face to reduce on-site welding works adjacent to FRP. Due to lower amount and shorter length of wrapping in beam of SP-5R, FRP failure in form of rupture (along with delamination) was found in beam portion of SP-5R (as can be seen from *Fig. 4.23*) which limited the FRP to develop its full strength (*Fig. 4.30*). But, in SP-3R, FRP wrap strain was up to 2.5% (*Fig. 4.18*) which is just below the failure strain of 3.1% provided by the manufacturer. Hence, it can be stated that a 4-layers of wrapping up to a distance D (i.e. 400 mm) from the joint face is advisable for retrofitting. Column and joint retrofitting of both the specimens were seen to be performing well without any failure or damage which is desired for any seismic design of RC structural components.

5 Development of schemes for upgradation of 'GLD' specimens

It is of great importance to upgrade the poorly designed 'GLD' structures since the inferior performance of those structures has been witnessed from the previous earthquakes. Further, the experimental results obtained from the present study also showed a drastic strength degradation and negligible energy dissipation capacity of the specimen SP-1 which represented the 'GLD' structures. It is well-understood that any upgradation work would involve various technical issues like existing condition of structure, seismic probability- and intensity- in the locality, importance of the structure, etc. Further, non-technical aspects like social-economic condition, invasiveness and feasibility issues would also play important roles. Hence, it is neither required nor practical to always upgrade the 'GLD' structure to a fully 'Ductile' one, but must be targeted to obtain a favourable and optimum performance.

5.1 Objectives and targets of the upgradation

In this study, the upgradation of the 'GLD' specimen SP-1 was intended to obtain the target performance as that could be expected from 'Ductile' specimen. Depending on the issues mentioned above, the objective has been to upgrade the specimen from 'GLD' level to the feasible 'Ductile' level. *Table 3.7* provides the strength hierarchy of the specimens corresponding to existing structures. The ideal strength hierarchy should be as

$$V_{C,beam-hinge} \leq \Phi_1 V_{C,beam-shear} \leq \Phi_2 V_{C,jt-shear} \leq \Phi_3 V_{C,col-hinge} \leq \Phi_4 V_{C,col-shear} \qquad (5.1)$$

But, it is evident from the results as presented in *Table 3.7* that the perfect strength hierarchy even for 'Ductile' specimen could not be achieved since the maximum beam tip load corresponding to joint shear should be greater than that obtained from beam hinge. Studies on the performance of 'Ductile' specimens reported that though the behaviour of 'Ductile' specimens were much improved than under-designed ones, those were unable to show a desirable behaviour like producing final failure by beam hinging, minimum damage in joint etc. under seismic loading. Hence, during developing the upgradation schemes, along with improving the 'GLD' specimens it would also be required to take into account the observed shortcomings of 'Ductile' specimens.

For generality, sectional strength of the components of all the specimens (used in the study on performance of existing structures as described in Chapter 3) is given in *Table 5.1* which would provide the existing and target strength of the specimens.

Table 5.1 Sectional strength from different failure criteria of the specimens considered for studies on performance of existing structures

	Bending capacity (kNm)			Member shear capacity* (kN)				Joint shear capacity§ (kN)
				Non-ductile zone		Ductile zone		
	Beam (+)ve	(-)ve	Column	Beam	Column	Beam	Column	
SP-1	64.78	125.67	103.83	210.44	97.91	-	-	338
SP-2	64.78	125.67	68.79	194.96	93.56	-	-	397
SP-3	202.81	300.39	254.39	251.58	161.27	-	-	439
SP-4	158.22	243.19	184.17	232.95	164.27	-	-	438
SP-5	202.81	300.39	254.39	329.25	207.88	380.16	354.67	465
SP-6	158.22	243.19	184.17	273.30	166.48	375.11	239.87	461
* Shear capacity calculated as average from all codes considered in this study § Joint shear capacity calculated with 300kN axial load in column								

5.2 Basic principles for FRP applications

Similar to retrofitting strategies described in Chapter 4, for upgradation also Fiber Reinforced Plastic (FRP) was used for strengthening the beam and column components with steel plate confinement on the joint. The analytical modelling is related to the different failure modes that may occur. Design was aimed to exclude the brittle failure mode. For the same reason, it should be guaranteed that the internal steel is sufficiently yielding, so that the strengthened member will fail in a ductile manner, despite the brittle nature of concrete crushing, FRP rupture and bond failure. Hence, the governing failure mode of a flexural member is either steel yielding/concrete crushing (before FRP rupture or debonding) corresponding to zone B in *Fig. 5.1*, or steel yielding/FRP failure (either FRP rupture or bond failure) corresponding to zone A in *Fig. 5.1* as described in FIB Bulletin14 (2001).

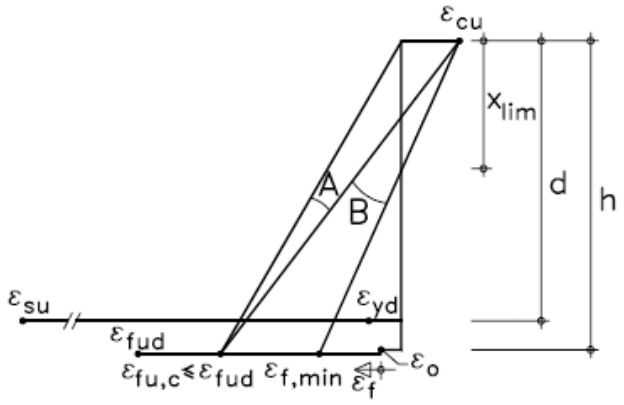

Fig. 5.1 Strain distribution in the critical section of strengthened flexural members [FIB Bulletin14 (2001)]

In *Fig. 5.1*, ε_0 is the initial strain at the extreme tensile fiber before strengthening, $\varepsilon_{f,\min}$ is the minimum allowable FRP strain at ultimate and $\varepsilon_{fu,c}$ is the FRP strain in the critical section at ultimate. In case of FRP fracture, $\varepsilon_{fu,c}$ equals the design value of the ultimate FRP strain ε_{fud}. Optimum design will correspond to simultaneous concrete crushing (ε_{cu} = 0.0035) and FRP tensile failure (ε_{fud}).

So, the failure modes for flexural strengthening would be

- *Steel yielding followed by concrete crushing*

  The flexural strength may be reached with yielding of the tensile steel reinforcement followed by crushing of the concrete in the compression zone, whereas the FRP is intact.

- *Steel yielding followed by FRP fracture*

  For relatively low ratios of both steel and FRP, flexural failure may occur by yielding of the tensile reinforcement followed by tensile fracture of the FRP.

- *Concrete crushing*

  For relatively high reinforcement ratios, failure of the RC element may be caused by compressive crushing of the concrete before the steel yields and the mode of failure is brittle. In this case, the main function of FRP is to provide the confinement to concrete which would definitely change the compressive capacity of concrete.

In the present study, 'GLD' specimen required adequate flexural and shear strengthening (seen from *Table 5.1*) to match with the 'Ductile' specimen. Since the shear strengthening of members would be carried out using required amount of FRP applied in form of wrapping around the section, it would add a degree of confinement to the concrete section. Hence, the concrete constitutive model (both maximum stress and ultimate strain) would further be changed. So, the design of upgradation was initiated by shear strengthening which helped in evaluating the modified concrete material properties by a detailed study of confinement effects. These modified properties of concrete were then used in analytical studies on flexural strengthening of the 'GLD' specimen for an effective use of material.

5.3 Shear strengthening of beam and column of SP-1

Total shear strength of any section is

$$V_t = V_c + V_s + V_f \qquad (5.2)$$

As recommended by Priestley et al. (1996)

$$V_f = 2t_f \cdot f_f \cdot h \cdot \cot\theta \quad (\theta \text{ is between } 35^0 \text{ to } 45^0), \qquad (5.3)$$

where, f_f = *stress in FRP corresponding to strain = 0.004*

t_f = *thickness of FRP wrapping*

As recommended by FIB Bulletin 14 (2001)

$$V_f = 0.9 \cdot \varepsilon_{fd} \cdot E_f \cdot \rho_f \cdot b_w \cdot h(\cot\theta + \cot\alpha)\sin\alpha \qquad (5.4)$$

where, ε_{fd} = *design value of effective FRP strain*

b_w = *minimum width of cross section*

ρ_f = *FRP reinforcement ratio equal to* $\dfrac{2t_f \sin\alpha}{b_w}$

θ = *angle of diagonal crack with respect to the member axis (=45^0)*

α = *angle between principal fiber orientation and longitudinal axis of member*

Hence, thickness of FRP required

$$t_f = \frac{1}{2} \cdot \frac{V_f}{0.9 \cdot \varepsilon_{fd} \cdot E_f \cdot d(\cot\theta + \cot\alpha)\sin^2\alpha} \qquad (5.5)$$

Amount of additional FRP wrapping (GFRP) required for shear resistance is presented in *Table 5.2* where the available strength was taken from SP-1 and the target shear strengths were considered for SP-5 (ductile), SP-5 (non-ductile) and SP-3.

Table 5.2 Calculation of additional shear strengthening (in mm) of SP-1

	SP-5 (ductile)	SP-5 (non-ductile)	SP-3	SP-5 (ductile)	SP-5 (non-ductile)	SP-3
	Shear strengthening of beam			**Shear strengthening of column**		
Target strength (kN)	380.16	329.25	251.58	354.67	207.88	161.27
Available strength of SP-1 (kN)	210.44	210.44	210.44	97.91	97.91	97.91
Required strength from FRP (kN)	169.72	118.81	41.14	256.76	109.97	63.36
Thickness of FRP [Priestley et al. (1996)]	0.86	0.61	0.21	1.31	0.56	0.32
Thickness of FRP [FIB 14 (2001)] with strain =0.005	0.74	0.51	0.18	1.11	0.48	0.27
Thickness of FRP [FIB 14 (2001)] with strain =0.02	0.18	0.13	0.04	0.28	0.19	0.07

Using GFRP with dry fiber thickness of 0.17 mm, 4 layers of GFRP on beam and columns were provided for shear strengthening. Here, target of strengthening was considered as the shear strength of non-ductile zone of 'Ductile' specimen. It is to mention that the FRP wrappings corresponding to additional reinforcement in ductile zone (special ductile detailing beyond shear requirement) need not to be considered because application of continuous FRP wrapping for enhancement of shear strength would automatically improve the ductility of the section. But, the degree and adequacy of improvement in ductility require to be checked properly.

5.4 Enhancement of ductility due to shear strengthening

Due to FRP wrapping in the beam and the column section, behaviour of concrete is improved because strength, ultimate strain and the corresponding stress of confined concrete would be positively changed. As stated earlier in Chapter 4, strength of confined concrete can be calculated using the model proposed by Mander et al. (1988). Using this model, strength of confined concrete can be computed based on the confining stress exerted from confining pressure. But, the most concerning issue is that a constant value of confining pressure was considered in this model throughout the loading history. This assumption is well justified in case of confinement using steel transverse reinforcement where a prolonged yielding zone of steel provides a constant confining pressure. But, in case of FRP confinement, confining pressure increases continuously until failure. Hence, a variable confining pressure model proposed by Spoelstra and Monti (1999) as 'modified Mander's model' has been considered in this study for calculating the stress state of concrete.

Starting from the Mander's model (described in Chapter 4, but salient points are re-iterated here for ready reference), confining pressure (f_l) was proposed as

$$f_l = \frac{1}{2} \cdot k_e \cdot \rho_f \cdot f_f \qquad (5.6)$$

Concrete strength at a given level of confinement (f_{cc}) is

$$f_{cc} = f_{c0}\left(2.254\sqrt{1+\frac{7.94 f_l}{f_{c0}}} - \frac{2 f_l}{f_{c0}} - 1.254\right) \qquad (5.7)$$

And finally, stress in concrete at a given concrete strain (ε_c) is

$$f_c = \frac{f_{cc} \cdot x \cdot r}{r - 1 + x^r} \qquad (5.8)$$

x and r = *are with their usual meaning as described in Mander's model (Eqs. 4.8 to 4.11)*

A variable lateral strain (ε_l) depending on concrete strain (ε_c) was proposed by Spoelstra and Monti (1999) as

$$\varepsilon_l = \frac{E_c \varepsilon_c - f_c}{2\beta \cdot f_c} \qquad (5.9)$$

$$\beta = \frac{5700}{\sqrt{f_{c0}}} - 500 \qquad (5.10)$$

where, E_c = $5700\sqrt{f_{c0}}$

The evaluation of lateral strain (ε_l) determines the corresponding level of confinement pressure (f_l) as

$$f_l = \frac{1}{2} \cdot k_e \cdot \rho_f \cdot f_f = \frac{1}{2} \cdot k_e \cdot \rho_f \cdot \left(E_f \cdot \varepsilon_f\right) \qquad (5.11)$$

where, ε_f = *strain in FRP (= lateral strain* ε_l *)*

Hence, at a particular level of strain in concrete (ε), to get the correct magnitude of confinement pressure (f_l) obtained from Eqs. (5.6) to (5.11), an iterative procedure has to be involved. Flow-chart of the computer program as suggested by Spoelstra and Monti (1999) is shown in *Fig. 5.2*. Here, the ultimate strain (ε_{cu}) and corresponding stress in concrete (f_{cu}) can be evaluated as given in Eqs. 5.12 and 5.13, respectively.

Ultimate strain (ε_{cu}) and ultimate stress (f_{cu}) were proposed as

$$\varepsilon_{cu} = \varepsilon_{cc}\left[\frac{E_{\sec}(E_c - E_{cu})}{E_{cu}(E_c - E_{\sec})}\right]^{1-E_{cu}/E_c} \qquad (5.12)$$

where, $E_{\sec}$ = $f_{cc} / \varepsilon_{cc}$

$$E_{cu} = (5700\sqrt{f_{c0}})/(1 + 2\beta \cdot \varepsilon_{fu}) \qquad (5.13)$$

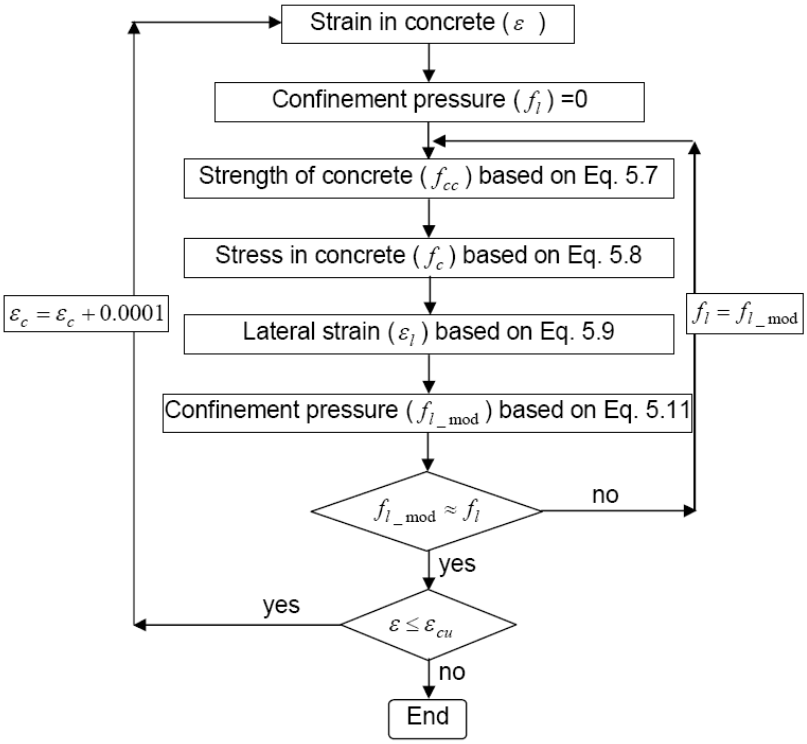

Fig. 5.2 Calculation of confinement pressure at a particular concrete strain

To illustrate this interactive phenomenon, development of confinement pressure (f_l) and simultaneous enhancement of concrete strength in the beam of SP-1 with 4 layers of GFRP (E modulus= 70000 MPa and tensile strength of 2300 MPa) wrapping with dry fiber thickness of 0.17 mm each, can be seen from *Fig. 5.3* and *Fig. 5.4,* respectively. From *Fig. 5.3*, behaviour of concrete and confinement must be noted. Here, concrete stress (f_c) represents the stress at a particular level of strain in concrete for a certain amount of confinement developed at that strain level. But, the strength of concrete (f_{cc}) at different levels of confinement pressure is shown in *Fig. 5.4*. Therefore, *Fig. 5.3* does not represent the strength of concrete, but the stress at a particular strain level. As an illustrative example, from *Fig. 5.3*, confinement strain (ε_l) of 0.03 generates a confinement stress (f_l) = 6.19 MPa. With a confinement stress of 6.19 MPa, concrete gets a stress (f_c) of 49.5 MPa at that given confinement strain level as can be seen from *Fig. 5.3*. Nevertheless, with the same level of confinement stress of 6.19 MPa, concrete has a peak stress (strength) of 59.85 MPa (as seen from *Fig. 5.4*) but at a strain level (ε_{cc}) of 0.012 which needs to be understood.

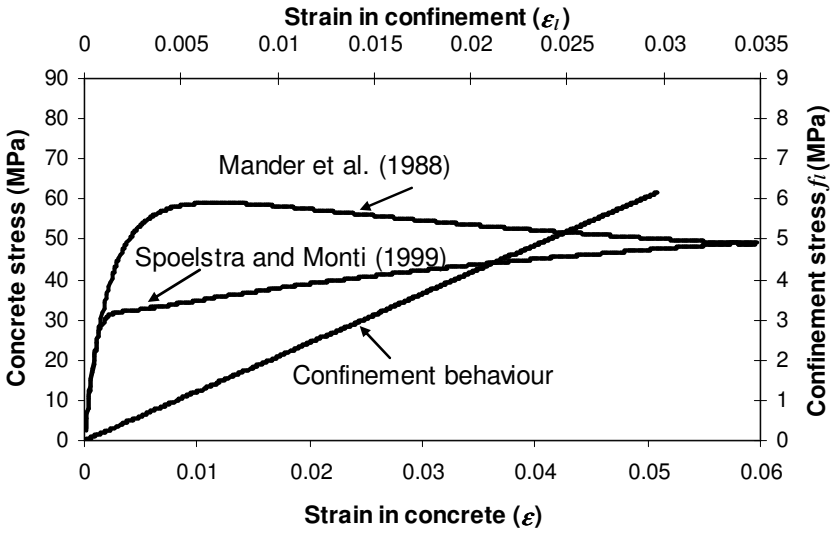

Fig. 5.3 Behaviour of concrete and confinement during monotonic increase in strain

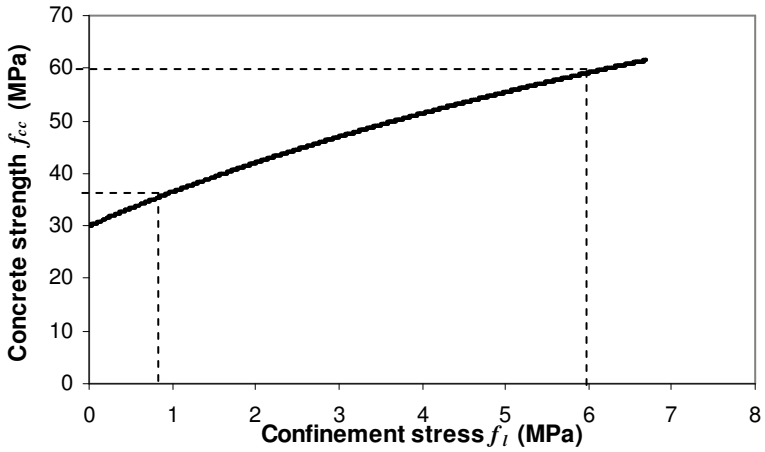

Fig. 5.4 Concrete strength (f_{cc}) at different level of confinement stress

Fig. 5.5 shows the concrete stress-strain behaviour with different levels of confinement pressure obtained from Mander's model. If the concrete strength (f_{cc}) obtained at different confinement pressure (as shown in *Fig. 5.4*) and the corresponding concrete strain (ε_{cc}) are also plotted in the same figure with Mander's model (as shown in *Fig. 5.5*), it is worth–mentioning that the results obtained from Spoelstra and Monti (1999) characterise a set of curves obtained from Mander's model with different levels of confinement.

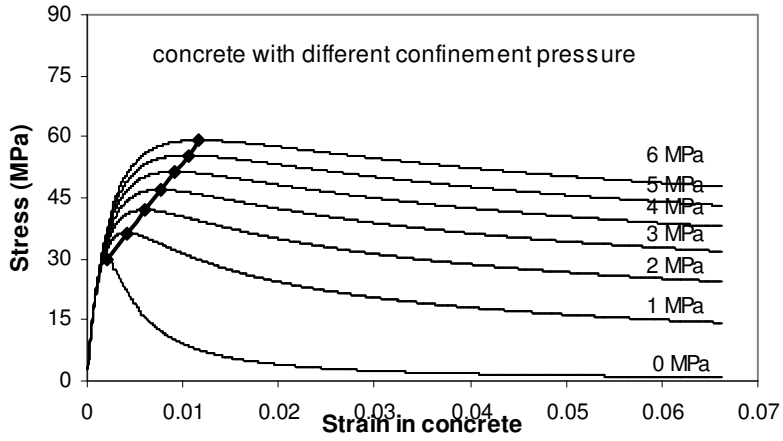

Fig. 5.5 Concrete strength (f_{cc}) obtained from Mander's- and Spoelstra's- model at different level of confinement stress

In the present study, based on Spoelstra and Monti's model, behaviour of confined concrete (from 4 layers of fully effective GFRP wrapping) in beam would lead to the maximum confinement pressure (f_l) = 6.68 MPa corresponding to lateral strain (ε_l) of 0.031 (maximum allowable strain in FRP as well). Similarly, the parameters for column of the specimens can also be evaluated.

For flexural strengthening, requirement of FRP was then calculated from analytical formulation using concrete model with- and without- confinement effect which provided the lower and upper bound requirement of strengthening, respectively. Moment resistance capacity for reinforced concrete sections (beam and column) was determined from moment-curvature behaviour (as discussed in Section 3). Further, for column, beside the moment-curvature behaviour, axial force-moment interaction behaviour also needs to be checked because presence of axial force leads to a higher moment resistance capacity, but at the same time, it reduces the ductility of the section.

5.5 Flexural upgradation of beam and column of 'GLD' specimen

It is clear from the previous study that the upgradation for shear would have an impact on enhancement in confinement of reinforced concrete section and degree of confinement would considerably influence the moment-curvature behaviour of the particular section. Therefore, a better design for shear resistance could simultaneously enhance the flexural capacity as well. This type of inter-related effects can only be expected in case of FRP based upgradation and certainly, with a proper level of execution. For flexural upgradation of the poorly designed specimen SP-1, different degrees of upgradation were studied to cater the

target strength. It has been aimed to use three different upgradation schemes using different materials, different structural arrangements and different extents of upgradation. Since, material properties, composite performance, feasibility of execution and economical issues are very different, therefore study on each upgradation scheme would enlighten the usefulness of the materials, effectiveness of structural arrangements and the overall performance of the upgradation as a whole. Material properties of the different FRP material used for analytical studies are shown in *Table 5.3*.

Table 5.3 Material properties of FRPs used in the present study

FRP material	Tensile E-Modulus (N/mm^2)	Tensile strength (N/mm^2)	Strain at break of fibers (%)
CFRP Laminate (CarboDur)	165000	1800	1.0
CFRP fabric (300C)	230000	3900	1.5
GFRP fabric (430G)	70000	2300	3.1

5.5.1 Flexural upgradation using CFRP fabric

For the first upgradation scheme, CFRP fabric (available from Sika Pvt Ltd, India) was used for the specimen. In moment-curvature analysis, material properties (as shown in *Table 5.3*) were used for three different cases, i.e., (i) without confinement effect, (ii) with confinement effect proposed by Mander et al. and (iii) with confinement effect proposed by Spoelstra and Monti. Different degrees of upgradation with enhancement of flexural capacity of beam (positive, negative) and column section of the 'GLD' specimen are shown in *Fig. 5.6* to *Fig. 5.8* respectively. For analytical evaluation of bending resistance capacity of a confined section at the moment critical zones, confinement using 4 layers of GFRP was assumed which would be provided to ensure the integrity of concrete and to secure the activation of the aggregate interlock mechanism. The moment-curvature analysis was performed until either of three conditions satisfies, i.e., (i) rupture of FRP (ii) crushing of concrete, and (iii) simultaneously both. Since, FRP does not have any plastic material property, reinforcing steel was aimed to be in yielding zone to avoid any brittle failure.

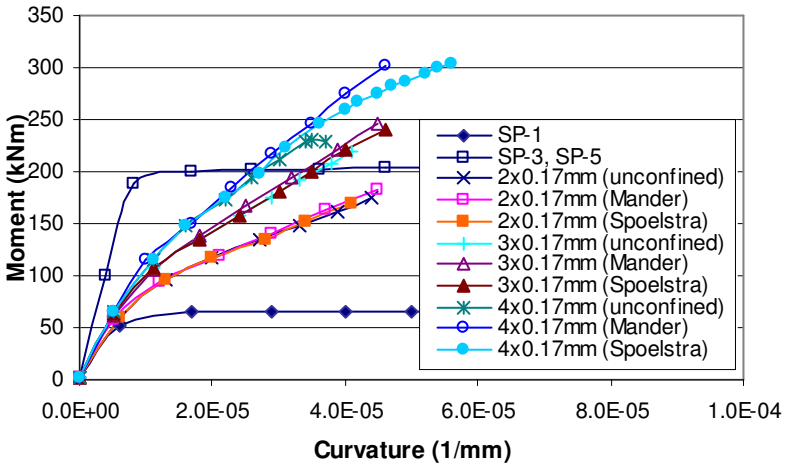

Fig. 5.6 Levels of flexural upgradation (positive) of beam using CFRP fabric

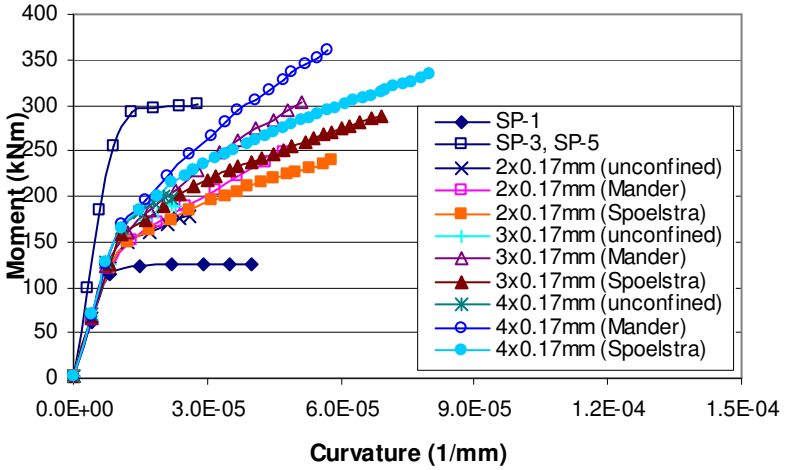

Fig. 5.7 Levels of flexural upgradation (negative) of beam using CFRP fabric

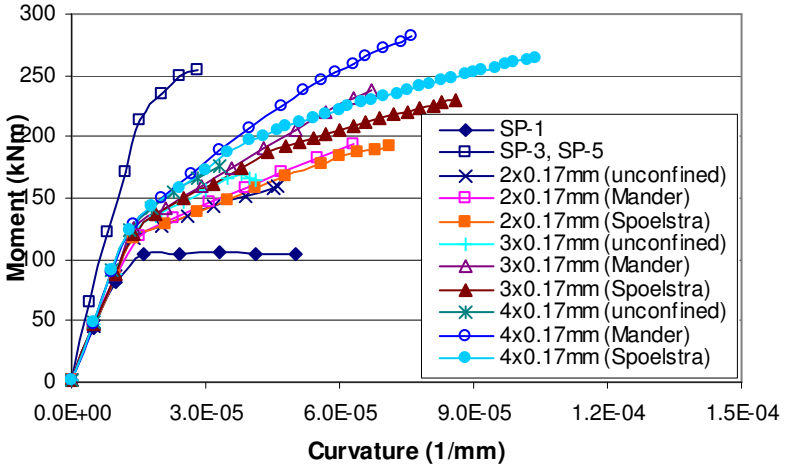

Fig. 5.8 Levels of flexural upgradation of column using CFRP fabric

It is important to note from the figures that in most of the cases, Mander's model shows a higher flexural capacity than that obtained from Spoelstra's model due to its limitations in

assumptions (constant confinement pressure throughout the loading history). But, the influence of the limitation reduces with the decrease in reinforcement in the section. Considering the target flexural strength as presented in *Table 5.1*, it was proposed to use 3 layers of CFRP fabric at bottom of beam and 4 layers of CFRP fabric at top of beam. For application of FRP in beam flexural strengthening, total width of the section, i.e., 300 mm was considered since it is a usual tailored fabric dimension. Similarly, 4 layers of CFRP fabric were proposed on both column faces. A continuity of CFRP was essential in the deviation zone of the column face. Therefore, for beam bottom also 4 layers of CFRP fabric were adopted to avoid the need for further anchorage of additional layer of CFRP. In both beam and column faces, amount of CFRP fabric was systematically reduced (curtailed) based on respective flexural demand. It is essential to specify that the reduction in strength and elastic modulus of composite FRP with the increase in number of layers was not considered in the analytical study and CFRP composite-concrete interface was assumed to be perfectly connected.

5.5.2 Flexural upgradation using CFRP laminate

In the next upgradation scheme, CFRP in laminate (obtained from the same company as CFRP fabric) form was used for 'GLD' specimen. Different degrees of upgradation with enhancement of flexural capacity of beam (positive, negative) and column section of the 'GLD' specimen are shown in *Fig. 5.9* to *Fig. 5.11,* respectively. Similar to the first scheme, for analytical evaluation of bending resistance capacity of a confined section, confinement using 4 layers of GFRP was assumed. Instead of column face, CFRP laminate in column was aimed to be provided on the sides to secure the continuity over the joint.

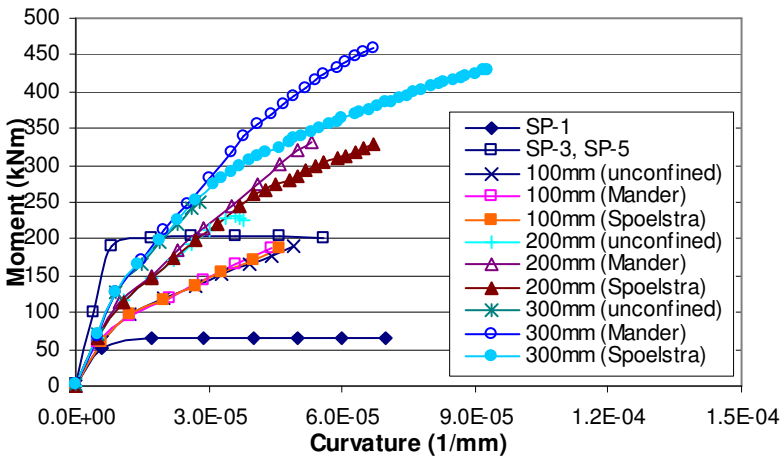

Fig. 5.9 Levels of flexural upgradation (positive) of beam using CFRP laminate

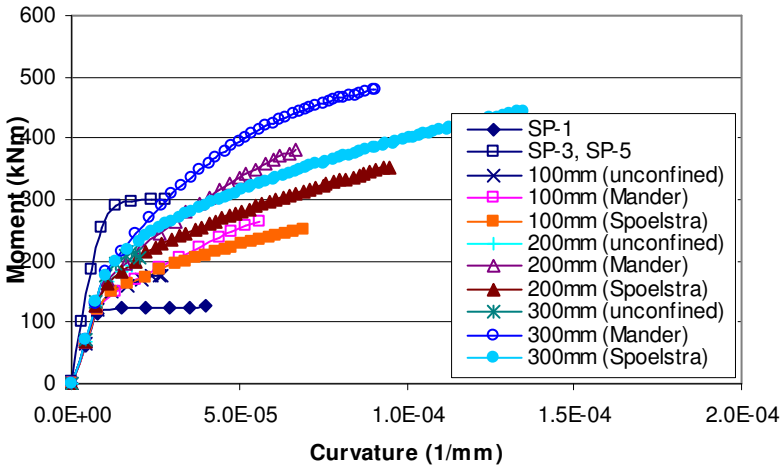

Fig. 5.10 Levels of flexural upgradation (negative) of beam using CFRP laminate

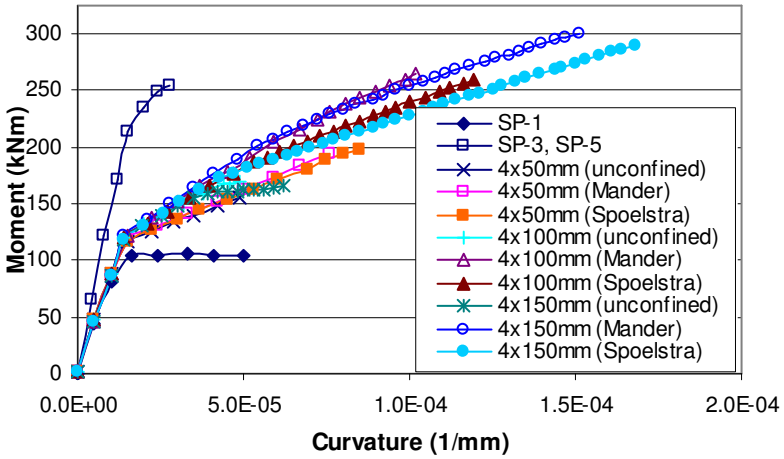

Fig. 5.11 Levels of flexural upgradation of column using CFRP laminate

The study brings out (as shown in *Fig. 5.9* to *Fig. 5.11*) that consideration of confinement effect due to wrapping has a considerable influence in determining flexural capacity of any reinforced concrete section. Similar to the previous case (enhancement of flexural capacity using CFRP fabric), it is to note that due to its limitations in assumptions (constant confinement pressure), Mander's model would show a higher flexural capacity than that obtained from Spoelstra's model. Considering the target flexural strength as presented in *Table 5.1*, it was proposed to use 150 mm wide CFRP laminate at both top and bottom of beam. Similarly, 4x100 mm CFRP laminates were proposed to be used on column side faces as longitudinal reinforcement. Intentionally, negative moment resistance capacity of beam of the upgraded specimen was kept little below the target strength since it was reported that top beam reinforcement of 'Ductile' specimen SP-5 was in early stage of yielding (as discussed in Chapter 4). In both beam and column faces, amount of laminate was systematically

curtailed based on respective flexural demand. In the analytical formulation, laminates were assumed to be attached on the concrete faces by using epoxy adhesive without any slip.

5.6 Joint upgradation

Similar to the retrofitting strategies (SP-3R and SP-5R), joint region was confined using 4 mm thick steel plate (as shown in *Fig. 5.12*). Three parts of steel plate were welded at site (one side before installation and the other after installation) and placed on the location using epoxy and further, through-through bolts were placed in the joint to provide mechanical confinement to the plate and to resist it from uplifting.

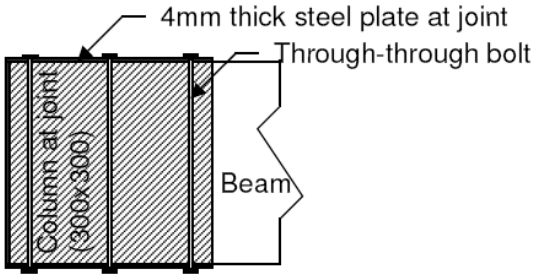

Fig. 5.12 Joint upgradation using steel plate

From this joint upgradation, percentage area of confinement due to application of steel plate (ρ_j) was 0.04. Using the strength of confinement (f_j) = 250 MPa, maximum confinement pressure (f_l) was evaluated as 3.75 MPa. Since the confinement of joint was provided by steel plate, Mander's assumption of constant confinement pressure would hold good. Therefore, compressive strength of confined concrete (f_{cc}) was evaluated to be 50.33 MPa under confinement.

From the computer program developed for calculating joint shear strength (discussed in Chapter 3), maximum horizontal shear strength of the joint with above mentioned confinement was calculated to be 432 kN which was little below the target shear strength of 'Ductile' specimen (SP-5) as 465 kN. However, the analytically calculated shear strength (= 432 kN) presented here was for the steel confined joint without any stirrup as it was the case of any upgraded joint of 'GLD' specimen. Due to the presence of steel plate with holding bolts, it would, of course, act as additional shear reinforcement in joint as well. In that case, it was found that the calculated shear strength of the steel confined concrete was well above the target shear strength of 465 kN.

5.7 Development of the upgradation schemes

Based on the above study, three different upgradation schemes were developed using FRP composites and steel plate. As mentioned before, first two schemes were flexurally upgraded by CFRP fabric and laminate, respectively, whereas GFRP was uniformly used for wrapping in both the upgradation schemes. In the third upgradation specimen, it has been aimed to upgrade only the D-region, leaving aside the need for strengthening beyond D region. Similar to first scheme, in third upgradation scheme also CFRP fabric was used for flexural strengthening and GFRP/CFRP fabric was applied for wrapping. It is to note that for all three upgradation specimens, joint strengthening was qualitatively similar except the position of bolts which depended on the location of reinforcement, layout of FRP and other site-based difficulties. Each of the upgradation schemes and preparation of the upgraded specimens are described below.

5.7.1 Upgraded specimen SP1-U1

The upgradation scheme was developed by providing CFRP fabric as reinforcement for flexural strengthening of beam and column. Due to its flexibility, CFRP fabric is the most convenient material for beam-column joint region. The target flexural strengths of beam and column were determined as described in the preceeding section. Schematic diagrams of each step of upgradation are enclosed in Appendix (*Fig. A5-1* to *Fig. A5-5*). Newly cast 'GLD' specimen (more than 28 days old) called as SP1-U1 was placed in the experimental laboratory. Before any application of FRP, sharp edges of each member were rounded off (15 mm radius) where it was proposed to be wrapped. Each face of beam and column of specimen SP1-U1 was cleaned from any dirt particle or dust. Then, flexural upgradation of both beam and column was carried out as shown in *Fig. 5.13*.

Fig. 5.13 Application of CFRP fabric on beam- and column- faces with different numbers of layers along the length of the members

After application of the flexural reinforcement in SP1-U1, it was kept for required curing time before further application of FRPs. To provide continuity between column and beam through the joint, 2 layers of "U" shaped GFRP were provided in the joint region with a 400 mm extension along the beam (as shown in *Fig. 5.14*).

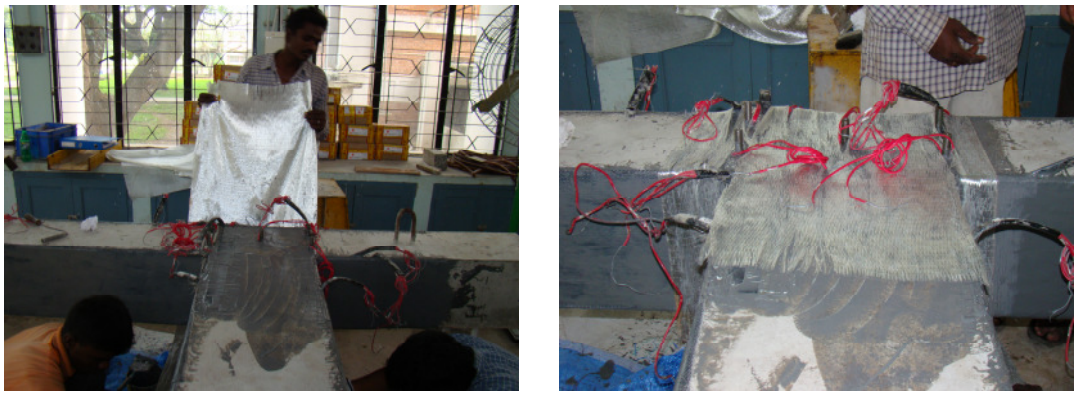

Fig. 5.14 Application of "U" shaped GFRP fabric for column to beam continuity

It is to state that shear strengthening is required to upgrade the poorly designed specimen from GLD stage to ductile stage when the available shear strength of 'Ductile' specimen needs to be reflected in 'GLD' specimen. On the other hand, the available shear strength of 'GLD' specimen SP-1 was sufficient to reach the flexural strength of beam of the upgraded specimen if the codal requirements for reinforcement in ductile zone are ignored. Nevertheless, for ensuring ductile behaviour and anchoring the flexural material, 4 layers of GFRP wrapping were provided in both beam and column but restricted to the D-region. To facilitate the transfer of tensile forces from FRP to member [Ritchie et al. (1991)], discrete wrapping (2 layers of GFRP) was provided at the location of curtailment of FRP as flexural reinforcement. *Fig. 5.15* shows the execution of the GFRP wrapping in column and beam respectively.

Fig. 5.15 Application of GFRP wrapping on column and beam respectively

In the last step, steel plate was placed in the joint region with 5 numbers of through-through bolts. It is to note that before application of FRP material, 5 numbers of through-through drillings (with a drill shaft diameter of 20 mm) were made in the predetermined locations in the joint face. Due to extreme heat and drill profile, considerable amount of dust firmly stuck to the surface of the holes which could not be removed by blower. So, water pressure was injected through the holes to make them entirely dust free which was very much essential for good contact between bolt and concrete through the filling adhesive material. Then, 16 mm diameter steel rods were placed in the holes (as shown in *Fig. 5.16*) with certain projections on both sides to tighten the rods with bolts.

Fig. 5.16 Placement of the bolts for steel plate confinement

3-parts steel plate with pre-punched holes in side plates was placed and the final welding in one side was carried out at site. *Fig. 5.17* shows that, before placement of the steel plates, Sika PBA31^{TM} epoxy was applied on the joint faces over the "U" shaped GFRP for acting as a medium for steel-concrete bonding and provided a smooth bearing surface for the steel plate towards effective confinement.

Fig. 5.17 Placement of the steel plate with through-through bolts

Final upgraded 'GLD' specimen SP1-U1 was kept in air for 3 days for gaining its strength and then placed in the test bed for cyclic load test as shown in *Fig. 5.18*.

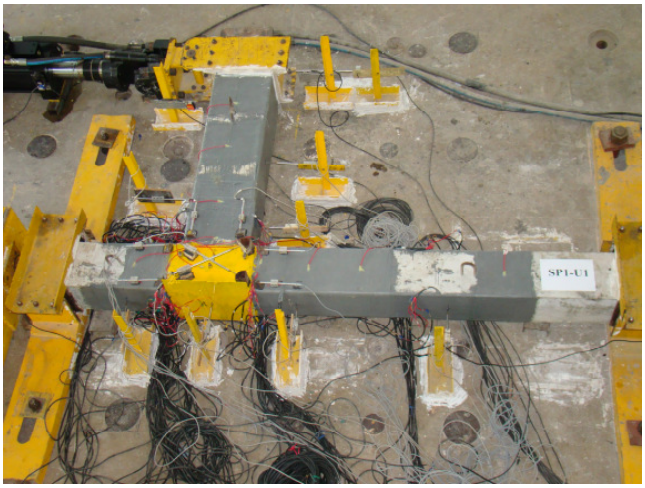

Fig. 5.18 Upgraded specimen SP1-U1 ready for test

5.7.2 Upgraded specimen SP1-U2

The upgradation scheme was developed by providing additional FRP reinforcement for flexural strengthening of beam and column using CFRP laminates. Similar to SP1-U1, this upgradation scheme was also aimed at full upgradation. But, instead of CFRP fabric, in this case CFRP laminate was used for flexural strengthening. CFRP laminate is easy to install and truly represents the reinforcement in any reinforced concrete structure. It is also seen that a large number of reported literature dealt with CFRP laminate for strengthening continuous, under-designed or distressed RC members, in general and without any D-region, in particular. During installation, it was quite challenging to provide CFRP laminate in both beam and column of the specimens because a continuation of reinforcement at the deviation point (beam meets the column) is essential for both beam and column individually. These features made the scheme tricky during execution.

The newly cast 'GLD' specimen for installing second upgradation scheme was called as SP1-U2. Similar to SP1-U1, before any application of FRP, proper surface preparation was carried out. It was proposed to provide continuous CFRP laminate in both sides of column over the joint face whereas laminates would be inserted inside the joint to provide adequate anchorage for beam top and bottom laminates. For inserting the CFRP laminate into the joint, two slots were made on top and bottom of the beam where the width of the slots was depending on the clear concrete area inside the joint without any presence of reinforcement. After scrutinizing the reinforcement locations in the cast specimen, it was decided to make a 150 mm wide slot on top of the beam and a 100 mm wide slot on bottom of the beam which were started from back side of the joint and were driven through the joint. For this operation, a special concrete cutting machine with a high speed, flat and adequately long (400 mm)

blade was engaged. It is noteworthy to state here that the machine was managed and operated by a single but skilled person. Since, the practical application of upgradation would obviously be at site and in some height from ground, the aspects of workability and application methods were checked and confirmed from the vendor. Due to high speed and friction between concrete and blade, any possibility of ignition or damage of blade was excluded by continuous supply of cold water along the blade and inside the slot. Since, any misalignment in drilling could damage the reinforcement bars, utmost care was taken in positioning, placement of the machine and verticality during operation.

Starting of slot from back side of the column, reaching of the cutting blade to the opposite side of the column which was just on the face of the beam, the complete slot on beam top and final positions of both the slots are shown in *Fig. 5.19*. It can be observed from the figures that the positioning and the operation were quite accurate so that the tip of the machine blade penetrated the column without any damage of reinforcement and could reach the other end by touching the beam surface. Since, the slots were through the column, depth and thickness of the slots were 300 mm and 5-7 mm, respectively, which were sufficient to insert the CFRP laminates with required epoxy.

Fig. 5.19 Different steps of concrete cutting operation for providing slots on beam top and bottom

Schematic diagrams of each step of upgradation are enclosed in Appendix (*Fig. A6-1* to *Fig. A6-5*). Beam flexural upgradation was carried out by using different lengths of CFRP

laminates depending on the flexural demand. To shift the plastic hinge to a pre-defined location (400 mm from the joint face), one of the top beam laminates was intentionally curtailed at 400 mm from the column face. Before placement of the laminates through the slots, these were properly instrumented. Upgradation of the beam for flexure is shown in *Fig. 5.20*. It was calculated (described in previous section) that 3 numbers of 50 mm wide laminates were required for beam bottom whereas the available slot width at beam bottom was 100 mm. So, the third laminate was placed above another two laminates, as can be seen in *Fig. 5.20*.

Fig. 5.20 Placement of laminates on beam top and bottom respectively

Since, the laminates in beam were inserted inside the joint, column laminates were provided on the side face of the column. Though the application of the laminates on side face of the column is not as effective as on the bending face, but was provided to accommodate both beam and column strengthening using laminates. In analytical formulation, the placement of laminates was properly taken care of in evaluating the amount the laminate required for columns. Flexural upgradation of column is shown in *Fig. 5.21*.

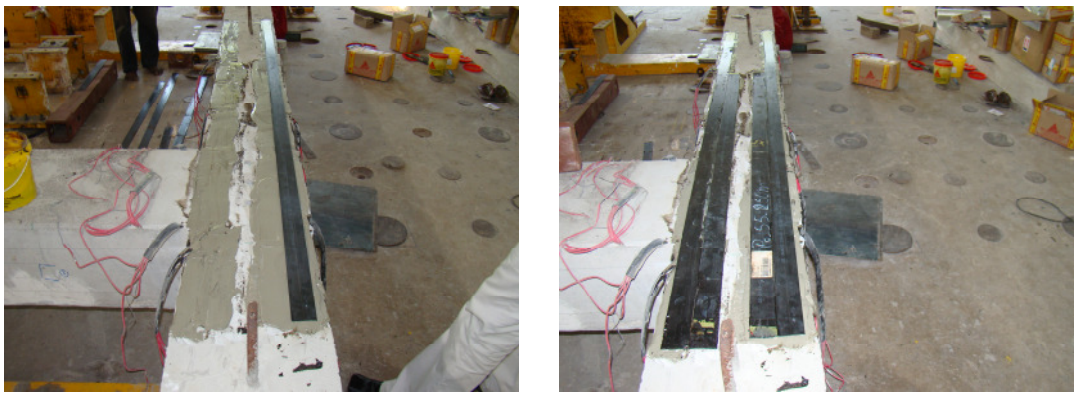

Fig. 5.21 Flexural strengthening of the column using CFRP laminate

After application of the flexural reinforcement in SP1-U2, it was kept for required curing time before further application of FRPs. Similar to SP1-U1, to provide continuity between column

and beam through the joint, 2 layers of "U" shaped GFRP were provided in the joint region with 400 mm extension in the beam. In the further step, 4 layers of GFRP wrapping were provided in both beam and column but restricted to the D-region. To provide additional anchorage to flexural FRP, discrete wrapping (2 layers of GFRP) was provided at the location of curtailment of flexural reinforcement.

Steel plate was provided in the joint region with 3 numbers of through-through bolts. Here, due to the presence of the laminates on both faces of column, 5 numbers of bolts could not be accommodated. Only at the centre line of the column in the joint zone, 3 numbers of bolts were provided. Similar to SP-1U1, 3-parts steel plate with holes in pre-assigned locations was placed on joint. *Fig. 5.22* shows the bolts locations and the placement of the plate for joint confinement.

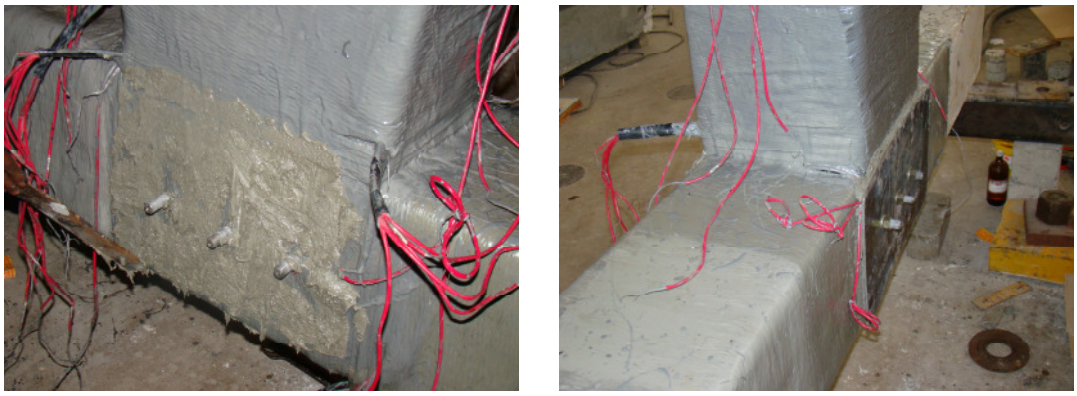

Fig. 5.22 Placement of the steel plate with through-through bolts

Final upgraded 'GLD' specimen SP1-U2 was kept in air for few days for gaining its strength and then placed in the test bed for cyclic load test as shown in *Fig. 5.23*.

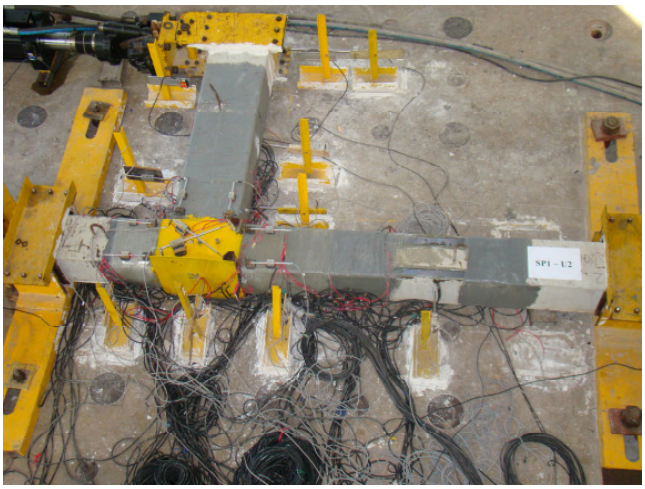

Fig. 5.23 Upgraded specimen SP1-U2 ready for test

5.7.3 Upgraded specimen SP1-U3

The last upgradation scheme was developed for D-region adjacent to the joint only. In earlier two cases (SP1-U1 and SP1-U2), it was assumed that the beam and the column would be upgraded to the full extent so that the weak zone should be located somewhere near the D-region. With steel plate confined joint, failure could occur at the joint line on the beam face. Further, in SP1-U2, a pre-defined weak zone was incorporated in the beam to shift the plastic hinge from the column face towards the beam. Now, in SP1-U3, the upgradation was concentrated only in the D-region. Similar to upgradation scheme SP1-U1, the main disturbed zone was upgraded using CFRP fabric for flexural strengthening. Schematic diagrams of each step of upgradation are enclosed in Appendix (*Fig. A7-1* to *Fig. A7-5*). *Fig. 5.24* shows the flexural strengthening of beam and column of the specimen SP1-U3.

Fig. 5.24 Flexural upgradation of SP1-U3

Since the beam bottom reinforcement of 'GLD' specimen does not have any anchorage inside the joint, 2 numbers of laminates (with a length of 400 mm away from the joint and along the beam) were provided on each side face of the beam to act as an external anchor device. For better placement and effective action, a groove of 5-7 mm depth was made prior to placement of the laminate. External groove and placement of laminate as external anchor device are shown in *Fig. 5.25*.

Fig. 5.25 Short laminate on side of beam bottom reinforcement

Similar to the other two upgradation schemes, to provide continuity between column and beam through the joint, 2 layers of "U" shaped GFRP were provided in the joint region with a 400 mm extension in the beam. It was observed during the experiment of retrofitted specimen SP-5R that due to a short length wrapping, the GFRP wrapping material in beam zone lifted up and failed which was not seen in SP-3R (with comparatively longer wrapping with more layers). Since, in SP1-U3 also, a concentrated upgradation was proposed, a mixed mode of wrapping was adopted by using both CFRP and GFRP fabrics. As seen in *Fig. 5.26*, first 300 mm in both beam and column were confined with 2 layers of CFRP fabric and rest of the D-region was wrapped with 2 layers of GFRP. Due to comparatively higher cost of CFRP fabric than GFRP, the mixed mode of wrapping would optimise the use of carbon fibers for concrete confinement.

Fig. 5.26 Wrapping works on beam and column (using CFRP near joint and GFRP away from the joint)

Finally, the steel plate with 5 numbers of through-through bolts was provided in the joint region. Unlike the other two upgradation schemes, 3-parts steel plate with pre-located holes was placed on three free faces of the joint and welded at site because pre-welding before installation supposed to create practical difficulty. *Fig. 5.27* shows the bolt locations and the placement of the individual side plates with tightening of bolts for joint confinement which were similar to SP1-U1.

Fig. 5.27 Placement of the steel plate with through-through bolts

Final upgraded 'GLD' specimen SP1-U3 is shown in *Fig. 5.28*. Similar to other upgraded specimens, it was kept in air for few days before placing in test bed.

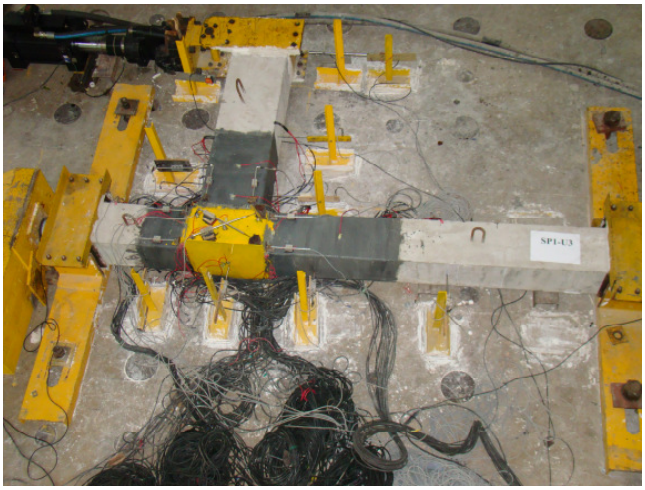

Fig. 5.28 Upgraded specimen SP1-U3 ready for test

Here, it is to point out that flexural strengthening using GFRP fabric was not adopted in any of the upgradation schemes, because it has been found from analytical studies (results are not presented) that in comparison to CFRP fabric, the required numbers of layers of GFRP fabric for flexural strengthening of 'GLD' specimens was quite high. Moreover, as the requirement of total quantity of wrapping material was more than the material required for flexure, cost implication due to CFRP instead of GFRP for flexural strengthening has not been given over importance. SP1-U1 and SP1-U2 would show the efficacy in using CFRP in fabric and laminate forms, respectively. Both the upgradation schemes targeted at almost same degree of upgradation. CFRP fabric is preferred at beam-column joints due to its flexibility in deviation zones, whereas CFRP laminate has a proven performance for flexural strengthening, thus makes the issue contradicting but challenging. SP1-U1 and SP1-U2 would also be studied for development of location of damage since the first upgradation (SP1-U1) was fully upgraded while the second upgradation (SP1-U2) was with an aim to shift the damage location to a safe distance in the beam from the joint face. SP1-U1 and SP1-U3 would be compared for response of fully and partly upgraded specimens. The primary idea was that in some seismic zones and structures with lesser importance, a scheme with partly upgradation may be satisfactory for adequate seismic performance because any upgradation scheme is closely related to feasibility, practical application and economic implications. Hence, these three upgradation schemes would provide the insight of upgradation of poorly designed 'GLD' specimens.

A step by step method for upgradation of deficient beam-column sub-assemblages, starting from the evaluated forces from seismic analysis of the global structure to final strengthening of a particular sub-assemblage using either laminate or fiber CFRP, is described in *Appendix (B)*.

5.8 Experimental investigations on upgraded specimens

All three upgraded specimens (SP1-U1, SP1-U2 and SP1-U3) were tested under identical cyclic load. Cyclic load history was used as same as that adopted for previous test of 'GLD' specimen SP-1. At each level of displacement, three repeated cycles were used. The displacement levels for 'GLD' specimen were ±25 mm and ±50 mm (as discussed in Chapter 3) while for upgradation schemes, two more displacement levels, i.e., ±75 mm and ±100 mm were considered where maximum displacement of 100 mm corresponds to a drift ratio ≈ 6.5. An axial load of 300 kN was applied through a hydraulic jack. In both top and bottom end of column, load cells were placed for measuring the applied load and reaction equilibrium. Before casting the specimens, strain gages were pasted on the reinforcements. Further, few more strain gages were placed on different locations of FRPs. LDVTs were placed on beam-column face adjacent to the joint region and along the column and beam length.

5.8.1 Development of cracks and damage pattern in upgraded specimens

During increase in displacement at beam tip, different patterns and locations of damage in the specimens were found. In SP1-U1, initial crack was found to be at beam-column joint line and it was consistent throughout the test and the final crack occurred also at the same location. Initial crack was found at 25 mm displacement whereas the final failure occurred at a displacement level of 100 mm (as shown in *Fig. 5.29*) which was the maximum target displacement for the upgraded specimens. Even after final failure, it was noticed that there was no drop in axial force in column (checked from both end load cells) which indicates that the upgradation scheme could ensure the column integrity, and that the energy dissipated through the damage along the beam-column joint line as shown in *Fig. 5.29*. During the experiment, it was verified that no FRP in column was overly strained or ruptured. During higher displacement drift, a lift in steel plate at discontinuous corner edges had taken place. But due to presence of bolts, it could not advance further towards the joint core. It underlines the fact that chemical bonded steel plate, as has been tried by few researchers, is not adequate for upgradation of joint region, and a suitable mechanical anchorage is required for the steel plate to obtain the desirable performance.

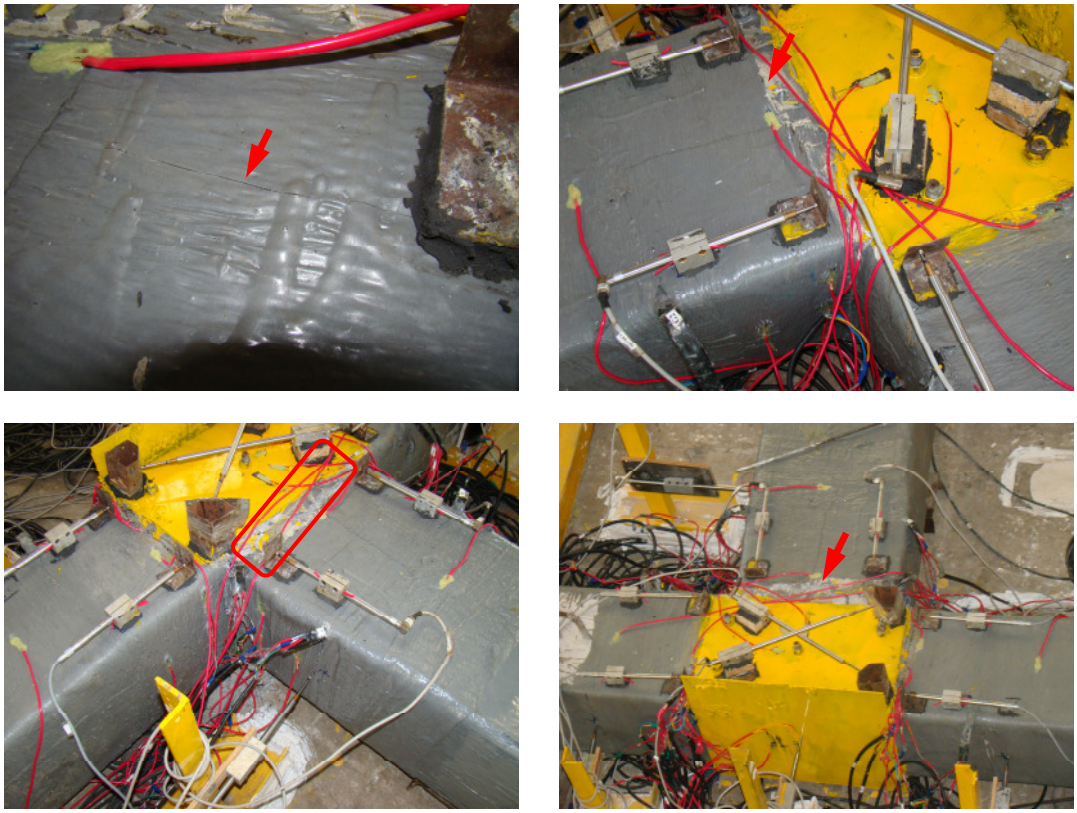

Fig. 5.29 Development of initial crack to final failure of SP1-U1 (left to right)

At the final stage of experiment (3rd cycle of 100 mm displacement), one of the beam bottom reinforcements in the joint line failed (broken) even though beam bottom reinforcement was prone to slip as no anchorage was present in the original 'GLD' specimen. It underlines that the axial force in the column along with the joint confinement using steel plate created 3-dimensional confinement in the joint region which was able to resist the straight reinforcement bars from slip. This phenomenon has a great significance as it can eliminate the poor response of 'GLD' specimens under reverse cyclic loading as it was found in SP-1.

In SP1-U2, initial crack was found (under 25 mm displacement) to be at beam-column joint line and the location of damage was shifted under higher displacement cycles. Under 50 mm displacement cycle, second line of crack was found at an approximate distance of 400 mm along the beam length and away from the joint face. With further loading, the first crack near the joint did not propagate any more and the second crack away from the joint played the main role for energy dissipation. From initiation of crack to final damage pattern at a displacement level of 100 mm is shown in *Fig. 5.30*.

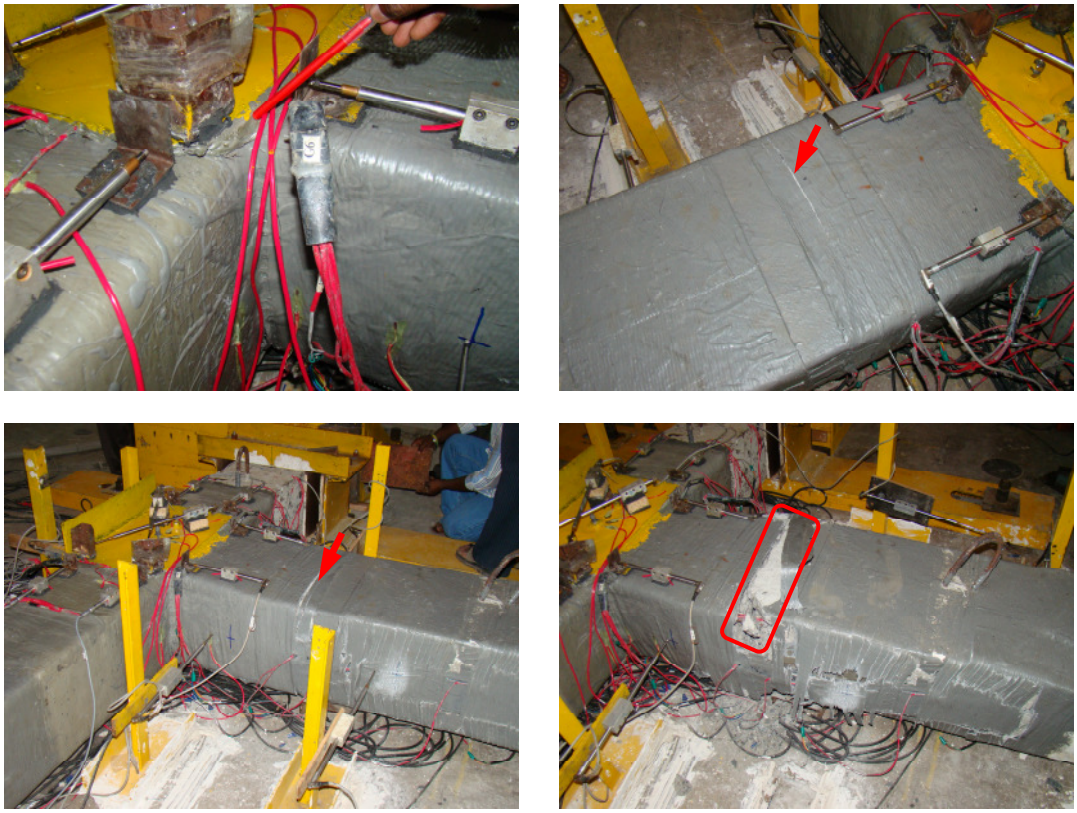

Fig. 5.30 Development of initial crack to final failure of SP1-U2 (left to right)

From the test, it was found that the joint and the column were without any damage even under a displacement level of 100 mm. Complete damage of the location at a distance of 400 mm from the joint would give the assurance of structural integrity, and a well established "strong column-weak beam" behaviour could be established even for 'GLD' specimens with this upgradation scheme.

Finally, SP1-U3 brought out a very interesting and promising behaviour. Initial crack was found (at 25 mm displacement) to be at an approximate distance of 400 mm along the beam length and away from the joint face. The same crack enlarged by dissipating energy under the higher displacement level (up to 75 mm). But, at the maximum level of displacement (100 mm), second line of crack was found at the beam-column joint line. It signifies that up to a displacement demand of 75 mm, energy dissipation mainly occurred at the location away from the joint. When bending CFRP near the deviation line started rupturing, second damage location was created near beam-column joint line. Hence, after the displacement cycle of 75 mm, the entire zone (from the joint face to a distance 400 mm along the beam length) was active in dissipating energy and formed a spread plastic hinge. Though the upgradation scheme SP1-U3 was a partial one, development of hinge at a distance of 400 mm from the joint face and further development of spread plastic hinge would definitely claim the ideal behaviour of reinforced concrete structures under seismic loading. With different

displacement cycles, development of different damage locations which acted as plastic hinge for energy dissipation are shown in *Fig. 5.31*.

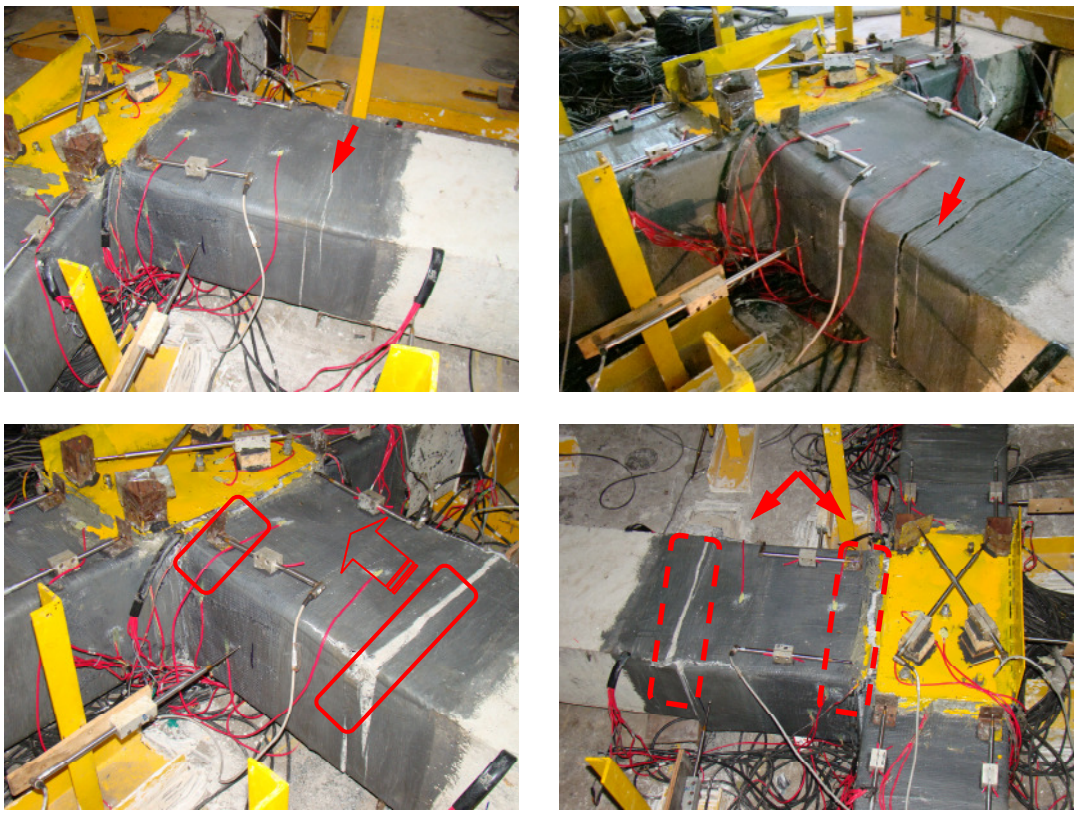

Fig. 5.31 Development of initial crack to final failure of SP1-U3 (left to right)

From the failure patterns of the specimens, it was found that none of the specimens failed due to joint damage (though could not be directly seen) or ineffective load transfer mechanism which were the main failure mode for 'GLD' specimen SP-1 and even for 'Ductile' specimen SP-5 and SP-6 (Novák et al. 2008).

5.8.2 Development of strain in beam and column reinforcements

Since the failure in SP1-U2 and SP1-U3 was observed at a distance D from the joint face which was one of the primary objectives, it is also important to investigate the real state of strain in reinforcement of beam and column of those specimens for further confirmation. Development of strain in top and bottom reinforcement of beam and column longitudinal reinforcement of SP1-U2 and SP1-U3 are shown in *Fig. 5.32* to *Fig. 5.37*, respectively. Since few of the strain gages were damaged during casting and another few seized to their workability during higher displacement cycles, strain devolvement along the beam and column reinforcement is shown with discrete points and even discontinuity where continuous data is not available.

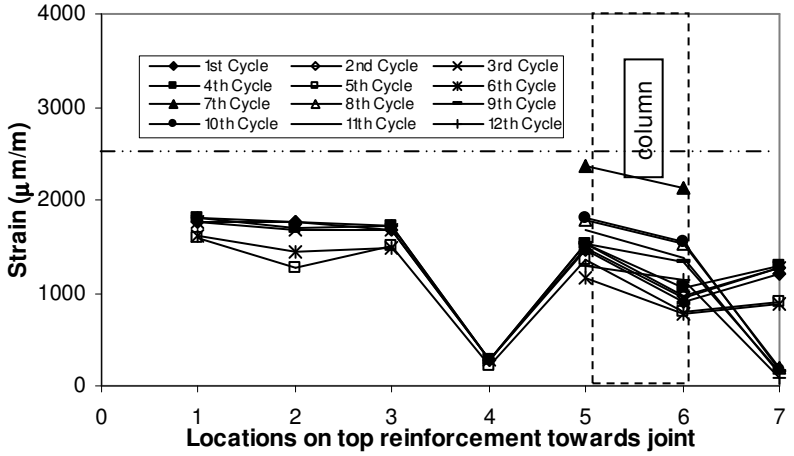

Fig. 5.32 Development of strain in top reinforcement of SP1-U2

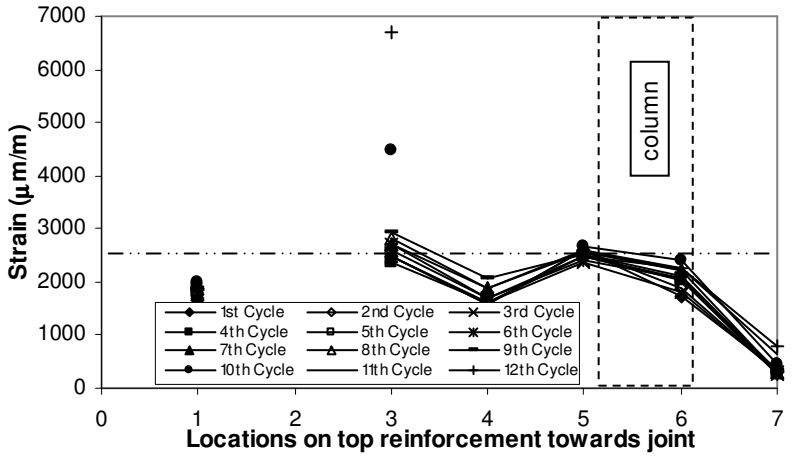

Fig. 5.33 Development of strain in top reinforcement of SP1-U3

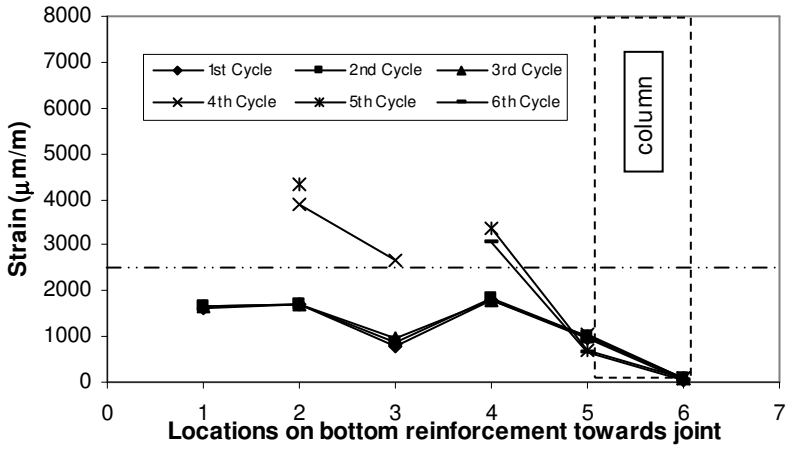

Fig. 5.34 Development of strain in bottom reinforcement of SP1-U2

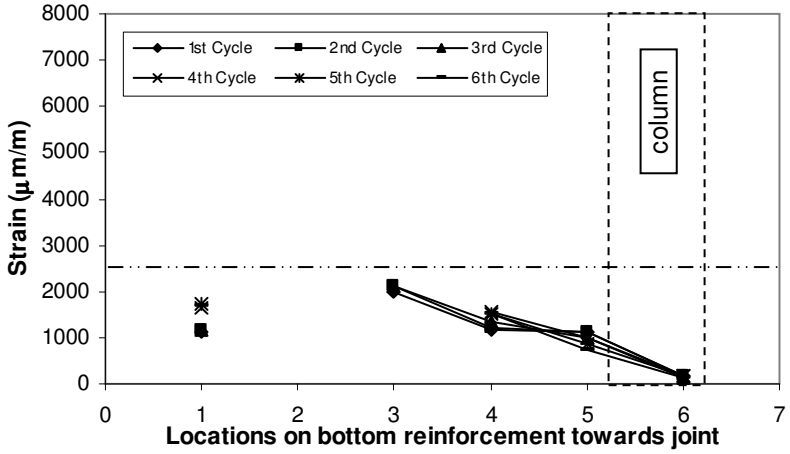

Fig. 5.35 Development of strain in bottom reinforcement of SP1-U3

Point 7 in horizontal axis of the figures (*Fig. 5.32* and *Fig. 5.33*) refers to the location at the middle of bent bar for anchorage of flexural reinforcement. It can be clearly observed that the developed strain in beam reinforcement (both in top and bottom) at a distance D from the joint face was very high with a sudden drop towards the joint. This led to the formation of plastic hinge at those locations. From *Fig. 5.34* and *Fig. 5.35* it can also be identified that unlike original 'GLD' specimen, the beam bottom reinforcements were significantly active in load transfer and in formation of plastic hinge. Hence, under reverse loading the problem of anchorage due to straight bottom reinforcement in original specimen could be efficiently handled. Top and bottom reinforcements in both the upgraded specimens (SP1-U2 and SP1-U3) were either yielded or near to yielding.

Strain in longitudinal reinforcement of column for SP1-U2 was much higher than that observed in SP1-U3 (as shown in *Fig. 5.36* and *Fig. 5.37*). Since the column of SP1-U2 was flexurally upgraded, contribution of column to total structural response was more than that was available from SP1-U3 where only the D-region was upgraded. It can also be noted that for both the specimens, location of development of maximum strain was little lower than the region where the lower part of the column meets the joint. Due to a high confinement for 300 mm from the joint face towards the lower part of the column, maximum rotation was shifted from the joint face.

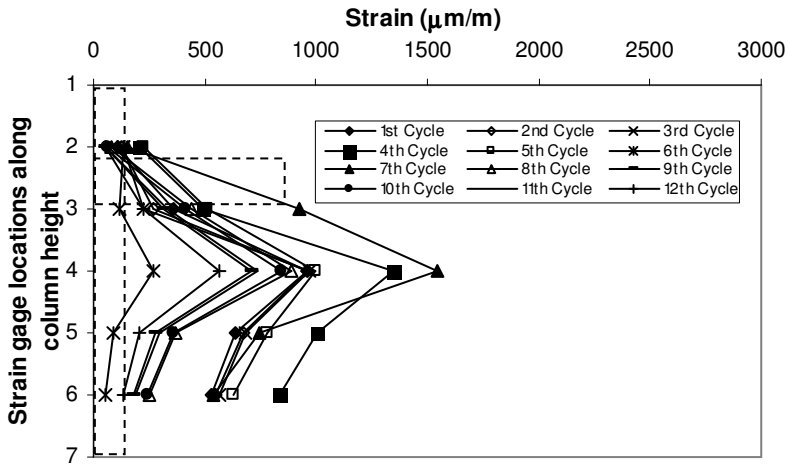

Fig. 5.36 Development of strain in column longitudinal reinforcement of SP1-U2

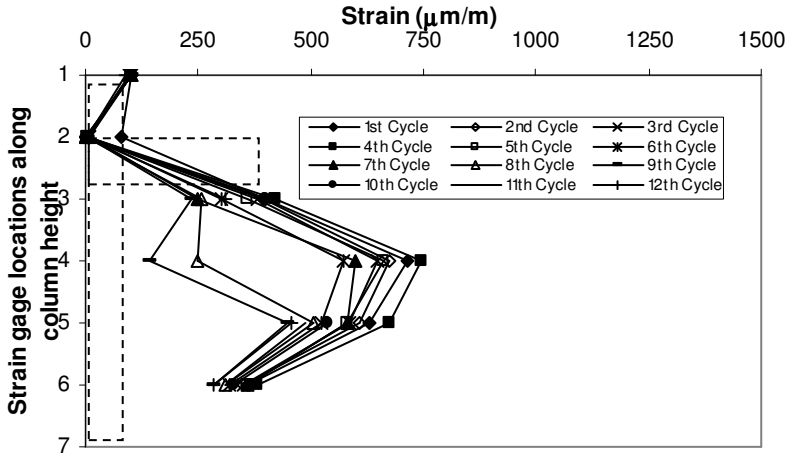

Fig. 5.37 Development of strain in column longitudinal reinforcement of SP1-U3

Development of strain in column stirrups near the joint of SP1-U2 and SP1-U3 are shown in *Fig. 5.38* and *Fig. 5.39*. For both the specimens, contribution of the stirrups was almost identical. Maximum strain was observed in the stirrup in lower part of the column and placed near to the joint. Among the upgraded specimens SP1-U2 and SP1-U3, the later showed larger strain in stirrups. Difference in maximum strain in stirrups of SP1-U2 and SP1-U3 is caused from the force transfer mechanism of the upgradation scheme since CFRP fiber for flexural strengthening of SP1-U3 was continuous from beam to column and was wrapped further whereas the laminates in SP1-U2 for flexural strengthening of column and beam were without any connectivity.

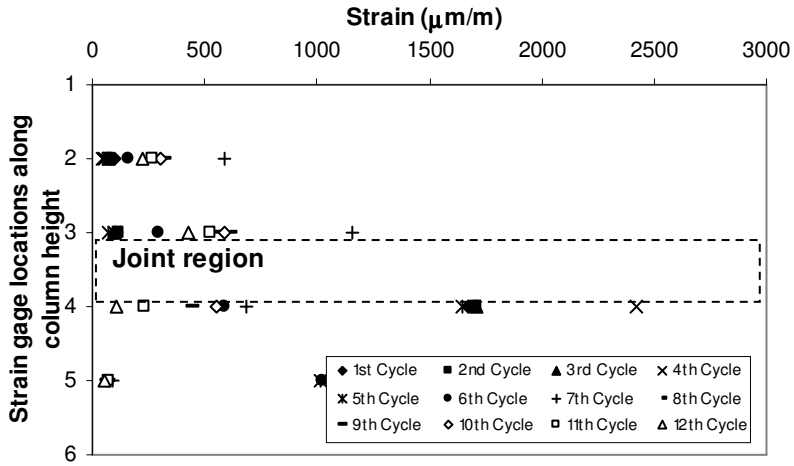

Fig. 5.38 Development of strain in column stirrups of SP1-U2

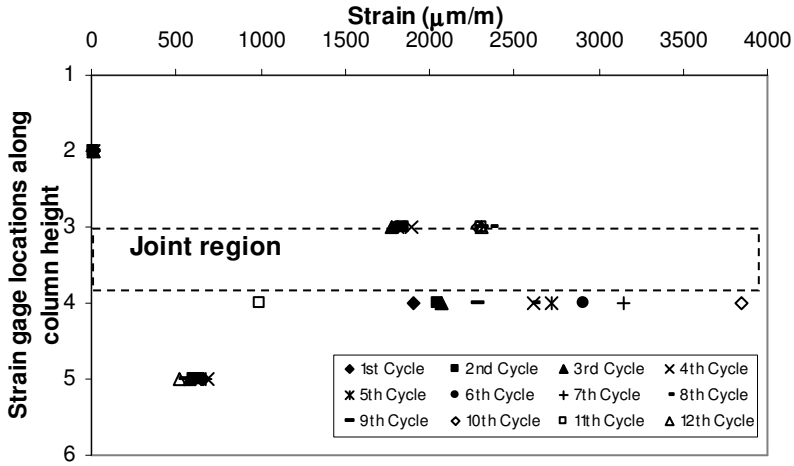

Fig. 5.39 Development of strain in column stirrups of SP1-U3

5.8.3 Development of member curvature near joint

During the loading history, curvature of each of the components joining at the joint would reflect the behaviour of the segments with respect to initiation of damage. To measure curvature, LDVTs were placed on both edges of beam and column face near the joint. During the entire load history, curvature of column (top and bottom) and beam for upgraded specimens SP1-U2 and SP1-U3 are presented in *Fig. 5.40* and *Fig. 5.41*, respectively. Though one of the specimens (SP1-U2) was fully upgraded and the other (SP1-U3) was just a D-region upgradation, envelop of curvature for the members were nearly similar. After first few initial cycles, in both the specimens, damage occurred and continuously propagated at a location away from the joint. Therefore, with the increase in displacement cycles, reduction in beam curvature (near joint) was noticed. Only at the last stage of loading, when cracks

formed at the joint face, then the beam curvature started increasing again. As mentioned before, six LVDTs (two in each member) were placed adjacent to the joint as shown in *Fig. A1* (in Appendix) for a measurable displacement distance of 150 mm (approximately). Hence the phenomenon only around the joint could directly be reflected.

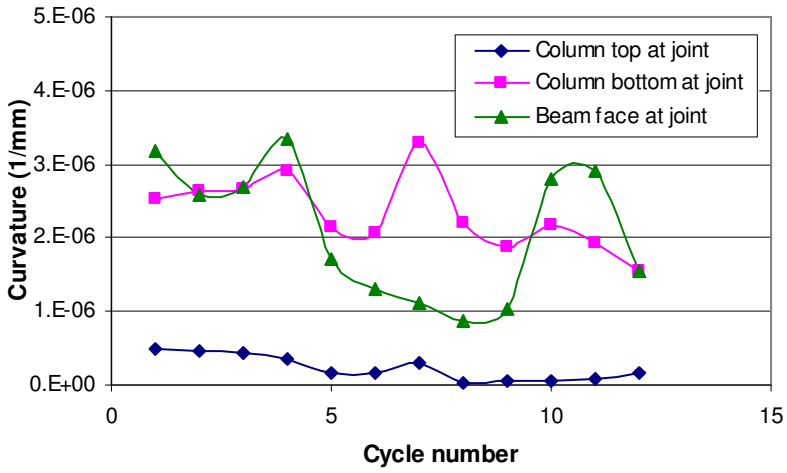

Fig. 5.40 Curvature of adjoining members in joint of SP1-U2

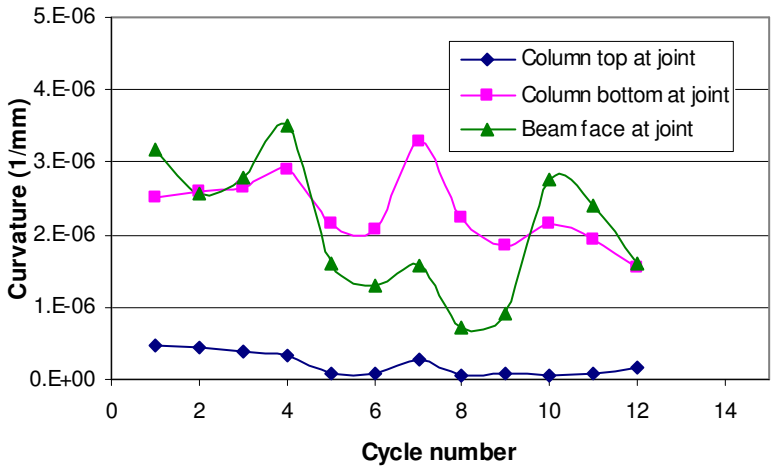

Fig. 5.41 Curvature of adjoining members in joint of SP1-U3

5.8.4 Seismic performance of upgraded specimens

Though the formation of promising damage patterns of SP1-U2 and SP1-U3 prompted to study their internal behaviours (state of reinforcement, curvature etc.), load-displacement hysteresis of all the upgraded specimens are presented in *Fig. 5.42* for a quantitative comparison and an exclusive discussion.

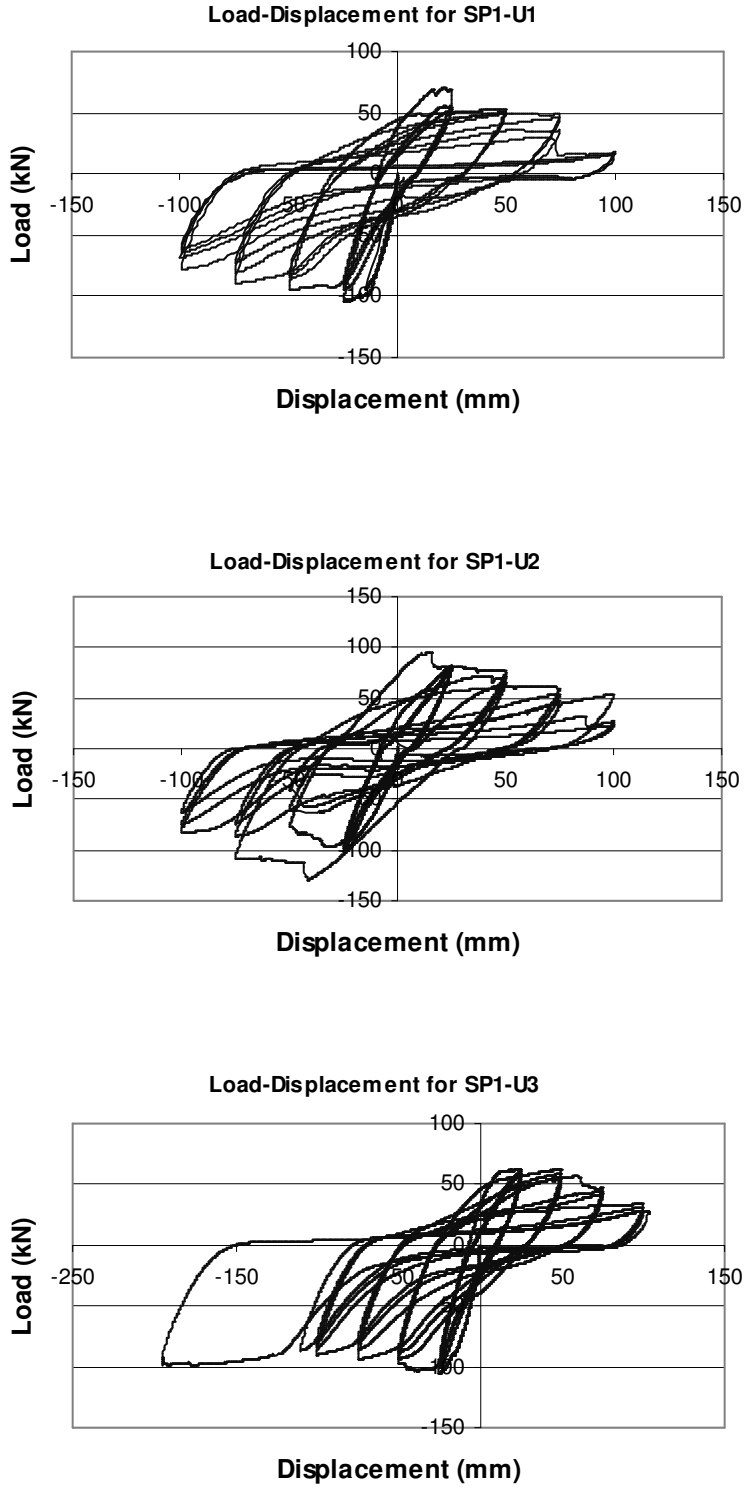

Fig. 5.42 Load-displacement hysteresis of upgraded specimens SP1-U1, SP1-U2 and SP1-U3 respectively

For comparison and better representation, all the hysteresis along with the original 'GLD' specimen SP-1 are shown in *Fig. 5.43*. It is clear from the figure that the responses of the upgraded specimens were way ahead of the 'GLD' specimen. But, it can be underlined that

SP1-U1 and SP1-U2 which were fully upgraded, could not achieve the target strength, explicitly during reverse loading. Since, the modern design practice suggests for capacity based design and ductility detailing for seismic loading, without a full strength upgradation of specimen, seismic performance criteria could be achieved. It is worth-mentioning that the most important parameters like stiffness degradation, strength deterioration and energy dissipation (both individual cycle and cumulative) have shown an impressive response in comparison with the original specimen as can be seen from *Fig. 5.44* to *Fig. 5.47*, respectively.

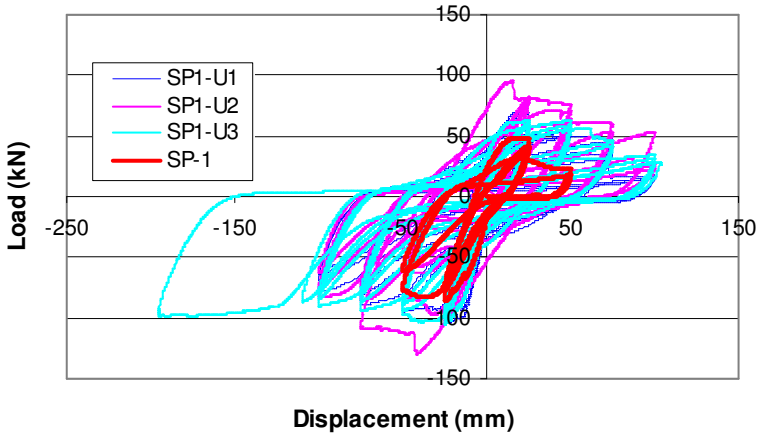

Fig. 5.43 Load-displacement hysteresis of 'GLD' and upgraded specimens

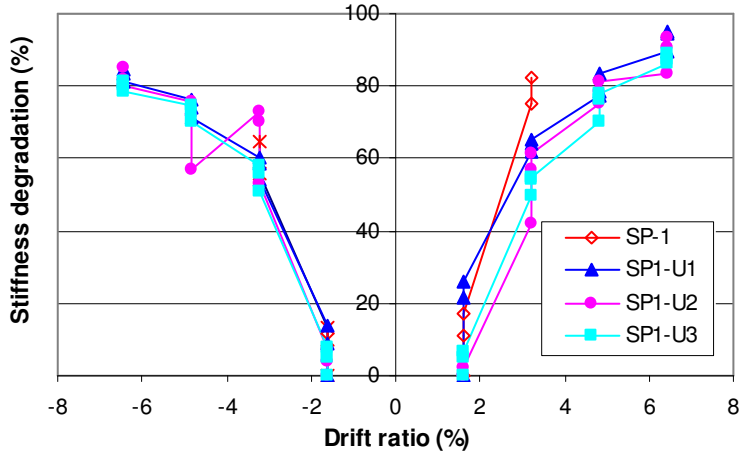

Fig. 5.44 Comparison of stiffness degradation of 'GLD' and upgraded specimens

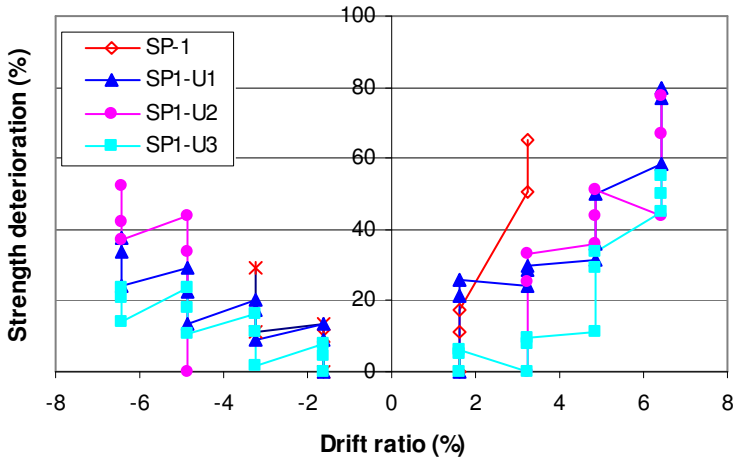

Fig. 5.45 Comparison of strength deterioration of 'GLD' and upgraded specimens

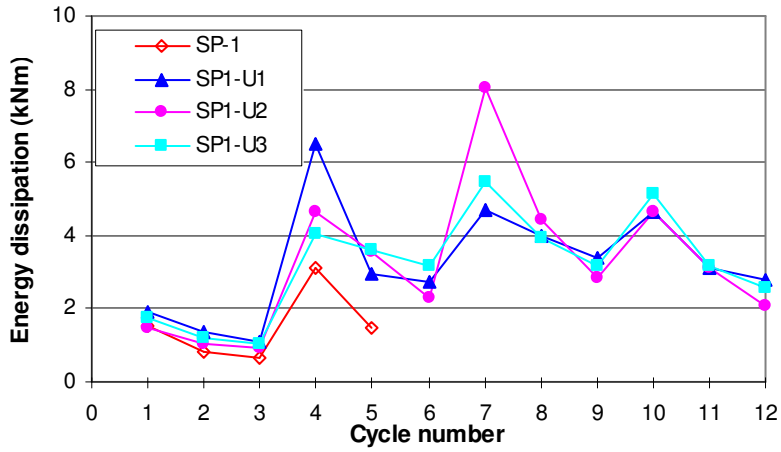

Fig. 5.46 Comparison of per cycle energy dissipation in 'GLD' and upgraded specimens

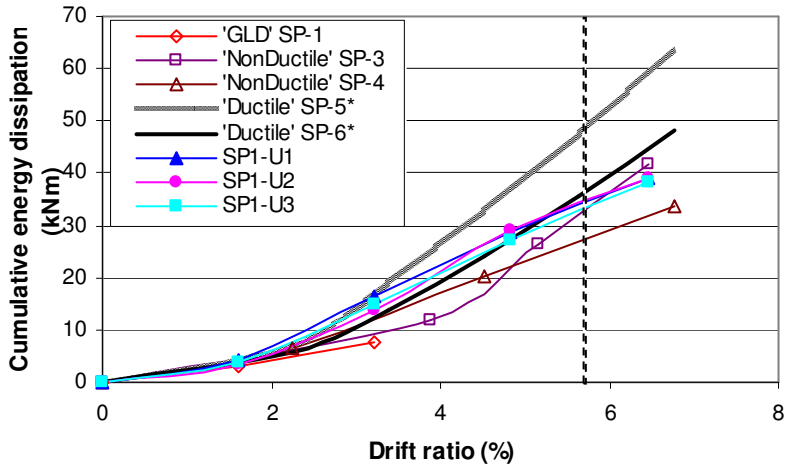

Fig. 5.47 Cumulative energy dissipation from upgraded- and all other- specimens corresponding to different stages of design of existing structures

The load-displacement hysteresis of the upgraded specimens showed a flat plateau during displacement cycles. It provided larger area under load-displacement curves and hence, the specimens were able to dissipate more energy. Additionally, a horizontal plateau also confirmed the formation of yielding of reinforcement in beam before any failure or rupture of FRP material which was also one of the most important aspects during design of upgradation schemes to avoid any unwanted brittle failure. Though the target displacement of 100 mm was adequate for seismic design of general structures, for academic interest, the last specimen (SP1-U3) was finally given to a maximum displacement of 200 mm and found that it could still be able to carry load, and the strength degradation was negligible.

From *Fig. 5.44* to *Fig. 5.47*, it is evident that the upgraded specimens (SP1-U1, SP1-U2 and SP1-U3) were able to provide a promising seismic performance. It is noticed that the stiffness degradation and strength deterioration were much slower and even with almost same stiffness degradation and strength deterioration, double the displacement demand could be achieved. Per cycle and cumulative energy dissipation were much higher than the original 'GLD' specimen. It is to mention that the first upgraded specimen (SP1-U1) dissipated maximum energy during 50 mm displacement cycle whereas the second upgraded specimen (SP1-U2) dissipated maximum energy during 75 mm displacement cycle. It is also to note that the third upgraded specimen (SP1-U3) provided almost uniform energy dissipation in 50 mm, 75 mm and 100 mm displacement (as evident from *Fig. 5.46* and *Table 5.4*). It signifies that the major damage occurred in SP1-U1 and SP1-U2 during 50 mm and 75 mm displacement cycle, respectively, since in further higher cycle(s), energy dissipation reduced. But, occurrence of damage in SP1-U3 was quite smooth, consistent and uniform.

Table 5.4 Quantification of cycle-wise and cumulative energy dissipation of specimens

	25 mm displacement (3 cycles)	50 mm displacement (3 cycles)	75 mm displacement (3 cycles)	100 mm displacement (3 cycles)	Cumulative energy
SP-1	2.9 (--)	4.6 (--)	Not available	Not available	7.5 (--)
SP1-U1	4.3 (48.3%)	12.2 (165.2%)	12.1 (-3.2%)	10.6 (-2.8%)	39.2 (422.7%)
SP1-U2	3.5 (20.6%)	10.5 (128.3%)	15.4 (23.2%)	9.8 (-10.1%)	39.2 (422.7%)
SP1-U3	4.0 (37.9%)	10.7 (132.6%)	12.5 (--)	10.9 (--)	38.1 (408%)
	Values in the parenthesis are percentage improvements with respect to SP-1		Values in the parenthesis are percentage improvements with respect to SP1-U3		

Cumulative energy dissipation at each displacement level was almost same for all the upgraded specimens (as shown in *Fig. 5.47* and last column of *Table 5.4*) which showed the

similar mode and magnitude of damages (irrespective of the location) in the upgraded specimens. At a displacement level of 50 mm and at final displacement level (100 mm), cumulative energy dissipation was approximately 2- and 5- times, respectively, higher than that obtained from the original 'GLD' specimen (SP-1) at its maximum displacement of 50 mm. For comparing the energy dissipation capacity with other specimens i.e. 'NonDuctile' specimens (SP-3 and SP-4) and 'Ductile' specimens (SP-5 and SP-6), it was found that the displacement cycles were different than that was adopted for original- and upgraded- 'GLD' specimens. Further, numbers of cycles to reach 100 mm (for upgraded 'GLD' specimens) and 105 mm for 'NonDuctile' and 'Ductile' specimens were not same. In view of this, a displacement level of 87 mm was chosen as reference and the energy dissipations from all the specimens were calculated at that displacement level. A linear interpolation of energy dissipation between two adjacent displacement levels was carried out for those specimens where 87 mm displacement cycle did not exist. From the study, it has been found that cumulative energy dissipations, at 87 mm displacement level, were almost identical for all upgraded 'GLD' specimens (SP1-U1, SP1-U2 and SP1-U3) and this was almost same as SP-3 and 20% more than that obtained from SP-4. Further, energy dissipations of upgraded specimens, at 87 mm displacement level, were 40% less than Indian Standard based 'Ductile' specimen SP-5 but almost similar to that obtained from Eurocode based 'Ductile' specimen SP-6.

5.9 Summary on upgradation schemes

The observations show that the entire strength upgradation could not be achieved for the poorly designed 'GLD' specimens, perhaps, due to the assumptions in analytical studies where concrete-FRP interface behaviour and bond-slip relations could not be accommodated and the reduction in strength in multi-layered composite was ignored. Hence, detailed 3-D non-linear numerical studies would be required to address those issues. Further, from the experimental investigations on upgradation schemes it can be summarized that the upgraded specimens showed better performance than all the original 'GLD' and 'NonDuctile' specimens and comparable to 'Ductile' specimen except SP-5 in terms of cumulative energy dissipation. It is worth mentioning that the formation of damage at a pre-defined location (away from the critical region) would be more beneficial in arriving at a better and safe seismic performance than the total energy dissipation. It was found from the experiments [described in Chapter 4 and referred in Novák et al. (2008)] that even for 'Ductile' specimens (SP-5 and SP-6), major damage occurred in joint region whereas the damage in upgraded specimens were out of- or away from- the joint. The third upgradation scheme (SP1-U3) though partly upgraded (only in D-region), still it could provide almost same energy

dissipation, and spread plastic hinge could be formed. Additionally, other seismic evaluation parameters like stiffness degradation and strength deterioration of the upgraded specimens were much slower than that observed from original 'GLD' specimen. Strain distribution in beam bottom reinforcement of upgraded specimens has shown a considerable reduction in the problem caused from inherent lack in anchorage of those reinforcements during reverse loading. Moreover, those effectively acted in transferring force from beam to column through joint and even yielded (or near yield) at high displacement level, as optimally desired. Thus, the study shows the promising aspects of the proposed upgradation schemes for practical applications in enormous number of existing 'GLD' structures throughout the world.

6 Non-linear Finite Element analysis

Mechanics of beam-column joint is quite complex and has not been fully explored either. The behaviour of beam-column joint with different variables can not be fully covered experimentally. Hence, beside the experimental investigations, a validated numerical model is required for further studies on behaviour of beam-column joints with different variables. Therefore, the aim has been to develop a fully validated, robust model that could be utilized as an investigative tool in conjunction with the experimental program. In the present study, a non-linear Finite Element (FE) program ATENA which is exclusively formulated for reinforced concrete structures has been used. The results obtained from the numerical studies were compared with that obtained from the experiments of existing and upgraded specimens. Then, the validated models have been employed for further studies on performance of existing and upgraded specimens.

6.1 Material properties

In any numerical investigation, it is utmost important to provide the material properties as realistic as possible. Like any other Finite Element analysis, in ATENA also certain assumptions and suitable theoretical simplifications are made. For understanding the assumptions in- and applicability of- ATENA for non-linear analysis of reinforced concrete structures/components, a highlight on necessary issues concerning the material models and their behaviour used in ATENA [ATENA Theory Manual, 2006] is presented in brief.

6.1.1 Concrete

Concrete model in ATENA is based on plane stress constitutive model. A smeared approach is used to model the crack properties so that the material properties defined for a material point are valid within a certain material volume. The concrete material model in ATENA has been included with the following effects of the concrete behaviour:

(i) Non-linear behaviour of concrete in compression including hardening and softening
(ii) Fracture of concrete in tension based on non-linear fracture mechanics
(iii) Biaxial strength failure criterion
(iv) Reduction of compressive strength after cracking

(v) Tension stiffening effect

(vi) Reduction in shear stiffness after cracking (variable shear retention)

(vii) Fixed and rotating crack model based on crack direction

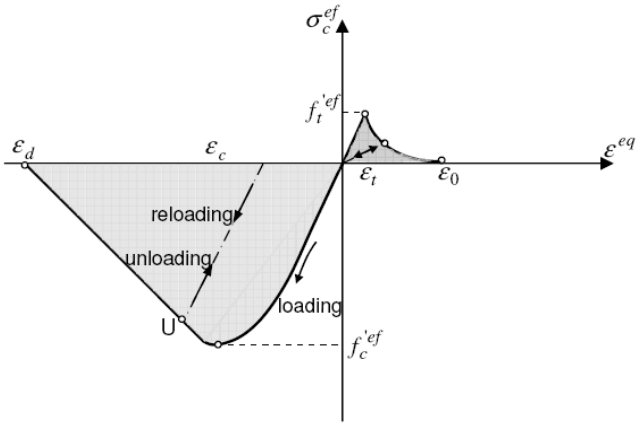

Fig. 6.1 Uniaxial constitutive law for concrete

The complete equivalent uniaxial stress-strain diagram for concrete is shown in *Fig. 6.1*. Generally, unloading is assumed to be a straight line and with subsequent reloading, linear unloading path is followed until the last loading point U is reached. After this point, the loading function is resumed (as shown in the above figure). A change from loading to unloading (and vice versa) is identified by change in sign of the increment of the strain. The relation between σ_c^{ef} and ε_c^{eq} is not unique and depending on the loading history. The equivalent uniaxial stress-strain has a relationship with the biaxial stress state since peak values of stress in compression ($f_c^{'ef}$) and tension ($f_t^{'ef}$) are also reflected in biaxial stress state.

The non-linear behaviour of concrete in the biaxial stress state is described by means of effective stress σ_c^{ef} , and the equivalent uniaxial strain ε_c^{eq} . Here, equivalent uniaxial strain is introduced in order to eliminate the Poisson's effect in the plane stress states, as

$$\varepsilon_c^{eq} = \frac{\sigma_{xi}}{E_{xi}} \qquad (6.1)$$

The equivalent uniaxial strain ε_c^{eq} can be considered as the strain that would be produced by the stress σ_{xi} in a uniaxial test with modulus E_{xi} associated with the direction i (as given in Eq. 6.1).

The behaviour of concrete in tension without cracks is assumed to be linear elastic. The modulus of concrete in tension E_{ci} is the initial elastic modulus of concrete in compression.

Two types of formulations are used for the crack opening: (i) a fictitious crack model which is based on a crack-opening law and fracture energy. Crack propagation in concrete can suitably be modelled using this formulation, and (ii) a stress-strain relation in a material point. In ATENA, a fictitious crack model based on a crack-opening law and fracture energy is used for tension after cracking. It is used in combination with the crack band. The exponential crack opening law is applied as shown in *Fig. 6.2*.

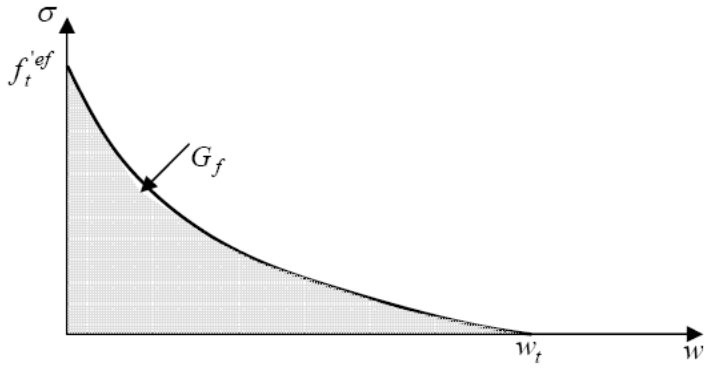

Fig. 6.2 Exponential crack opening law

In case of compression, the end point of the softening curve is defined by means of the plastic displacement w_d (*Fig. 6.3*). In this way, the softening displacement diagram indirectly reflects the energy required for generating a unit area of the failure plane. In ATENA, the descending branch of the compressive stress-strain behaviour of concrete is defined by $w_{d,max}$. It is the maximum possible post peak displacement of defined concrete. From the experiments of Van Mier (1986), the value of $w_{d,max}$ = 0.5 mm for normal concrete was proposed. But, this value leads to brittle failure of concrete in the corner of beam-column connections subjected to multi-axial compression. Further, it is shown from the experiments from Van Mier that concrete behaviour under multi-axial compression is much more ductile than in uniaxial tests. It is found from the present study on numerical analysis of exterior sub-assemblages that a value of 5 mm would provide an appreciable result. This value is used in the present study as default for the definition of the softening in compression. The softening law can be transformed from a fictitious failure plane of *Fig. 6.3* (left) to the stress-strain relation valid for the corresponding volume of continuous material as shown in right of *Fig. 6.3*. The stress-strain behaviour in *Fig. 6.3* demonstrates the compressive stress-strain relationship for concrete adopted in the software. For the ascending branch of concrete stress-strain behaviour, CEB-FIP (1990) recommendation and for descending part linear variation are adopted. The slope of softening law is defined by means of a softening modulus

E_d and it is defined by two strain limits, i.e., strain corresponding to compressive strength of concrete (ε_c) and a limiting compressive strain (ε_d). The later part of strain is calculated from plastic displacement (w_d) and band size during failure in compression (L_c).

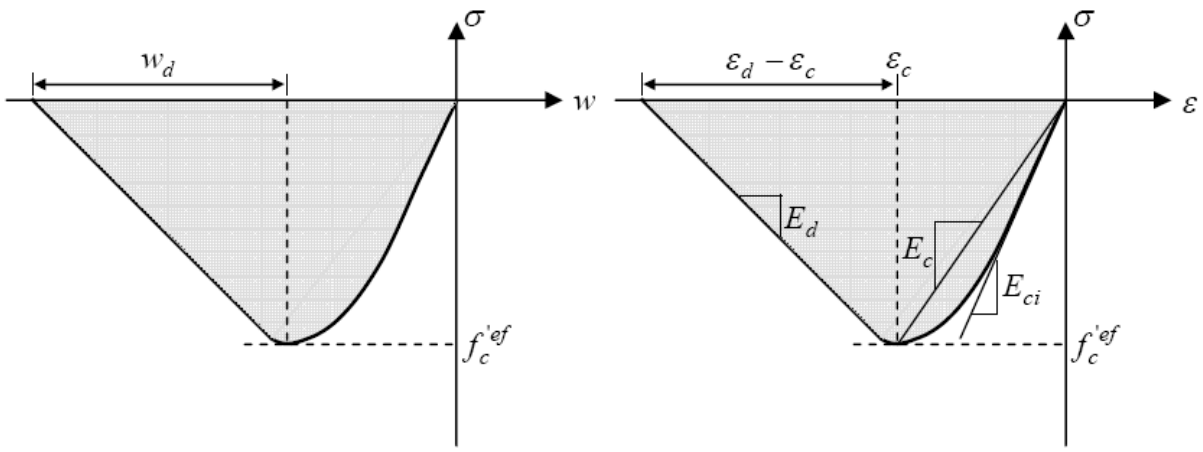

Fig. 6.3 Softening displacement and corresponding stress-strain diagram in compression

6.1.1.1 Fracturing model for concrete cracking

It is assumed that strains and stresses are converted into the material directions, which in case of rotated crack model correspond to the principal directions, and in case of fixed crack model, are given by the principal directions at the onset of cracking. In the present study, a fixed crack model is opted. If, σ'^{t}_{ij} identifies the trial stress and f'_{ij} is tensile strength in the material direction *i*, then

$$F_i^f = \sigma'^{t}_{ij} - f'_{ij} \leq 0 \qquad (6.2)$$

$$\sigma'^{t}_{ij} = \sigma'^{n-1}_{ij} + E_{ijkl}\Delta\varepsilon'_{kl} \qquad (6.3)$$

where F^f is Rankine's failure surface for fracture, $\Delta\varepsilon'^{f}_{kl}$ is fracturing strain increment for failure surface *k*. If Rankine's failure surface is not satisfied by trail stress (σ'^{t}_{ij}), then increment of fracture strain the direction *i*, can be calculated from

$$F_i^f = \sigma'^{t}_{ij} - f'_{ij} = \sigma'^{t}_{ij} - E_{iikl}\Delta\varepsilon'^{f}_{kl} - f'_{ij} = 0 \qquad (6.4)$$

The trial stress state is computed by the elastic predictor as given in Eq. 6.3. The crack opening *w* is computed from the summation of fracturing strain in direction *k* and the current increment of fracturing strain. Finally, the total sum of fracturing strain is multiplied by

characteristic length L_t. Bazant and Oh (1983) proposed the characteristic length as a crack band size. In ATENA, crack band size L_t is calculated as a size of the element projection in the crack direction (as shown in *Fig. 6.4*).

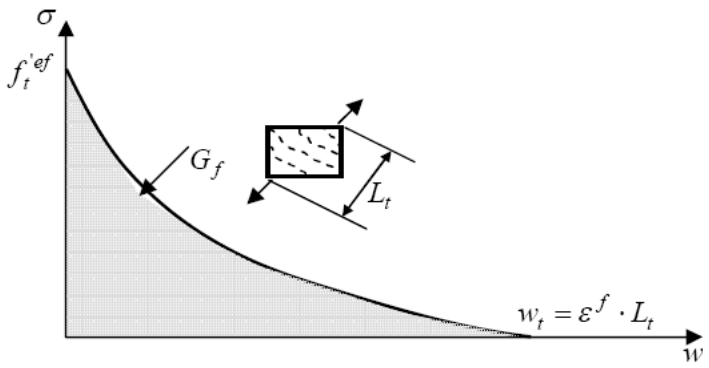

Fig. 6.4 Tensile softening and characteristic length

6.1.1.2 Plasticity model for concrete crushing

New stress state in the plasticity model is computed using the predictor-corrector formula (Eq. 6.5).

$$\sigma_{ij}^n = \sigma_{ij}^{n-1} + E_{ijkl}(\Delta\varepsilon_{kl} - \Delta\varepsilon_{kl}^p) = \sigma_{ij}^t - E_{ijkl}\Delta\varepsilon_{kl}^p = \sigma_{ij}^t - \sigma_{ij}^p \qquad (6.5)$$

$$F^p(\sigma_{ij}^t - \sigma_{ij}^p) = 0 \qquad (6.6)$$

$$\Delta\varepsilon_{ij}^p = \Delta\lambda \frac{\partial G^P(\sigma_{ij}^t)}{\partial \sigma_{ij}^t} \qquad (6.7)$$

where σ_{ij}^t and σ_{ij}^p are plastic predictor and corrector stresses, F^p is Menétry-Willam failure surface for plasticity, $\Delta\varepsilon_{ij}^p$ is plastic strain rate evaluated from the plasticity model, $\Delta\lambda$ is plastic multiplier and G^p represents the plastic potential function.

In the present plasticity model, Menétrey-Willam's three parameter failure surface as given in Eq. 6.8 is used in the ATENA material model

$$F^p(\xi_{m-w}, \rho_{m-w}, \theta_{m-w}) = \left[\sqrt{1.5}\,\frac{\rho_{m-w}}{f_c^{'}}\right]^2 + m(f_c', f_t', e)\left[\frac{\rho}{\sqrt{6}f_c'} r(\theta_{m-w}, e) + \frac{\xi_{m-w}}{\sqrt{3}f_c'}\right] - c = 0 \qquad (6.8)$$

where $r(\theta_{m-w}, e)$ is an elliptical function and e is the roundness of the failure surface (between 0.5 to 1 where 0.5 and 1 represent the failure surface with sharp corners and fully circular around the hydrostatic surface, respectively as shown in Fig. 6.5.

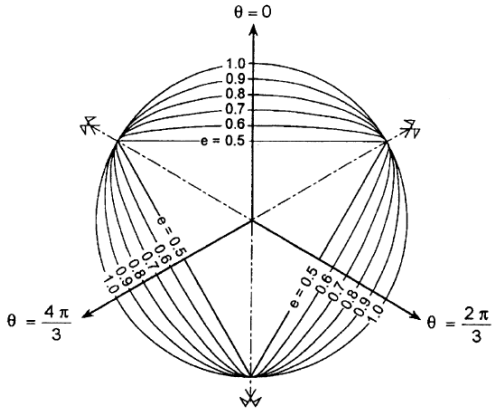

Fig. 6.5 Failure surfaces with different e

The position of failure surfaces can move depending on the value of strain hardening/softening parameter. The strain hardening is based on the equivalent plastic strain (ε_{eq}^{p}), which is calculated according to Eq. 6.9. For Menétrey-Willam surface, the hardening/softening is controlled by the parameter c (between 0 and 1) which evolves during the yielding/crushing process as expressed in Eq. 6.10.

$$\Delta\varepsilon_{eq}^{p} = \min\left(\Delta\varepsilon_{ij}^{p}\right) \tag{6.9}$$

$$c = \left(\frac{f_c'(\varepsilon_{eq}^{p})}{f_c'}\right)^2 \tag{6.10}$$

$$\sigma = f_{co} + (f_c' - f_{co})\sqrt{1-\left(\frac{\varepsilon_c - \varepsilon_c^{p}}{\varepsilon_c}\right)} \tag{6.11}$$

Where, $f_c'(\varepsilon_{eq}^{p})$ is hardening/softening law, which is based on the uniaxial compressive test (shown in *Fig. 6.6*). Elliptical ascending part of *Fig. 6.6* is developed based on Eq. 6.11.

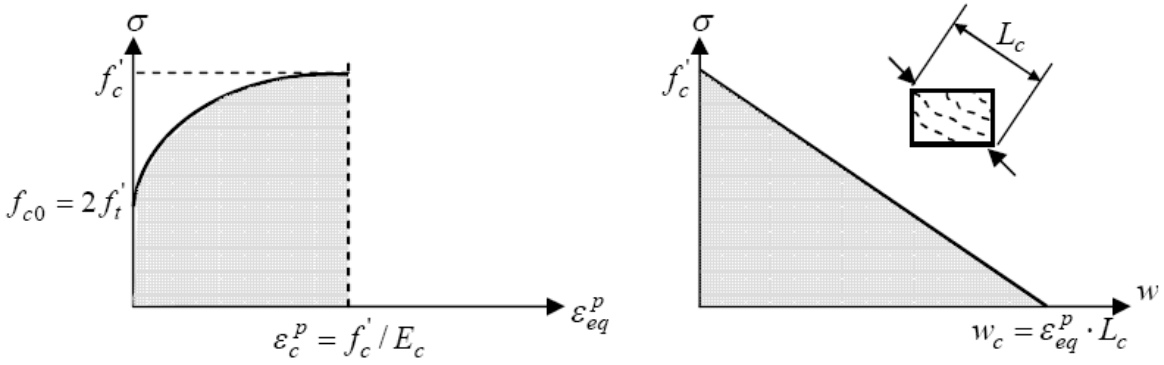

Fig. 6.6 Compressive hardening/softening

6.1.1.3 Tension stiffening

In concrete elements, cracks cannot fully develop through the concrete section in case reinforcement is present, and further concrete contributes to the steel stiffness. This behaviour called as tension stiffening is incorporated in concrete model "*CC3DNonLinCementitious2*" of ATENA by specifying a tension stiffening factor. This factor c_{ts} represents the relative limiting value of tensile strength in the tension stiffening diagram (*Fig. 6.7*). The tensile stress cannot drop below $c_{ts}\ f_t'^{ef}$ and the factor (c_{ts}) is recommended to a default value of 0.4 by CEB-FIP Model Code 1990.

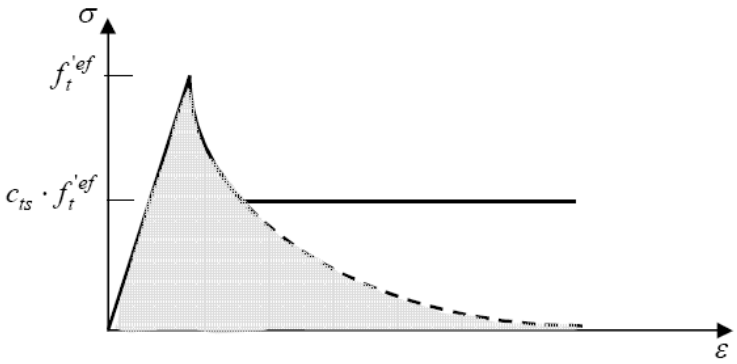

Fig. 6.7 Tension stiffening

6.1.1.4 Fracture energy

Fig. 6.4 has represented the basic definition of fracture energy. In ATENA concrete material model *"CC3DNonLinCimentitious2"* the same profile of fracture energy is used. There are different proposals in calculating the fracture energy of concrete. Eq. 6.12 presents the fracture energy proposed in CEB-FIP Model Code 90. It is mainly dependent on cylinder compressive strength and maximum particle size. However, it is mentioned that actual value may differ by almost 30% from the value obtained using Eq. 6.12. In this equation (Eq. 6.12) the empirical value of f_{cmo} is considered to be 10 MPa.

$$G_F = G_{F0}\left(\frac{f_{cm}}{f_{cm0}}\right)^{0.7} \qquad (6.12)$$

Remmel (1994) presented another approach in calculating fracture energy as given in Eq. 6.13 where compressive strength of concrete and particle size were the parameters. Here the empirical factor was taken as 65 for particle size of 16 mm. Results obtained from a series of tests were compared with the equation proposed (Eq. 6.13) by him and the equation proposed in CEB-FIP Model Code 90. It was pointed out that there was a good agreement among the results with Eq. 6.13 whereas Eq. 6.12 provides almost 25% lesser value than that obtained from the tests.

$$G_F = 65 \cdot \ln\left(1 + \frac{f_c}{10}\right) \text{ [N/m]} \qquad (6.13)$$

Vos (1983) also proposed an equation for calculating fracture energy as given in Eq. 6.14. Here, fracture energy was dependent on tensile strength of concrete. It was also observed that the values for fracture energy obtained from the equation proposed by Vos (Eq. 6.14) were considerably smaller than that obtained from Remmel (Eq. 6.13) or CEB-FIP Model Code 90 (Eq. 6.12).

$$G_F = 25 \cdot f_t'^{ef} \text{ [N/m]} \qquad (6.14)$$

In the present numerical study, fracture energy for concrete was initially calculated as proposed by Remmel and then further fine-tuned with the experimental response of the specimens.

6.1.2 Reinforcement

In FE model, the reinforcements (both longitudinal and transverse) were modelled as discrete reinforcing bars in form of truss elements. All sizes of reinforcement bars that were used in the experiments were tested for their stress-strain behaviour. Based on the behaviour found from material test, reinforcement bars in the numerical models were assumed to follow the bilinear law, i.e. elastic-plastic behaviour with strain hardening. It is also important to note that the behaviour of different diameters of reinforcements showed a variation in stress-strain relations though the elastic part was quite similar. Hence, in the numerical models post-yield behaviours for reinforcement bars with different diameters were incorporated accordingly.

In ATENA, Bauschinger's effect for reinforcement under cyclic loading is incorporated by using Menegotto-Pinto model (1973).

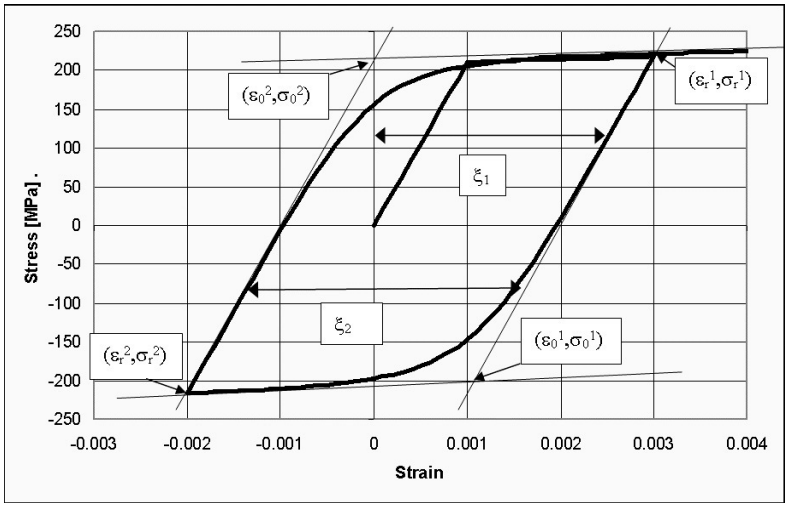

Fig. 6.8 Cycling reinforcement model based on Menegotto and Pinto (1973)

The stress-strain relationship is

$$\sigma^* = b\varepsilon^* + \frac{(1-b)\varepsilon^*}{\left(1+\varepsilon^{*R}\right)^{\frac{1}{R}}} \qquad (6.15)$$

where $\varepsilon^* = \dfrac{\varepsilon - \varepsilon_r}{\varepsilon_0 - \varepsilon_r}$ and $\sigma^* = \dfrac{\sigma - \sigma_r}{\sigma_0 - \sigma_r}$

A curved transition from a straight line asymptote with slope E_0 to another asymptote with slope E_1 can be seen from *Fig. 6.8*. In the figure, σ_0 and ε_0 are stress and strain at the point where two asymptotes meet, and σ_r and ε_r are stress and strain at the point where the last strain reversal with equal stress takes place. After each strain reversal, stress-strain sets (σ_0 and ε_0) and (σ_r and ε_r) are updated. R is a parameter which influences the shape of the transition curve and allows a good representation of the Bauschinger's effect. Further, strain hardening ratio (b) is calculated as ratio between slope E_1 and E_0.

6.1.3 Reinforcement bond model

Bond-slip relationship for reinforcement bars was chosen as proposed by CEB-FIB model code 1990. Bond-slip relation proposed in CEB-FIB model code 1990 is shown in *Fig. 6.9*. Concrete was considered to be without any confinement and the quality of construction was assumed to be poor. Bond strength at different level of slips can be calculated from Eqs. 6.16 to 6.19 whereas different levels of slip based on bond condition and degree of confinement in concrete are given in *Table 6.1*.

$$\tau = \tau_{\max}\left(\frac{s}{s_1}\right)^{\alpha} \qquad 0 \le s \le s_1 \qquad (6.16)$$

$$\tau = \tau_{\max} \qquad s_1 \le s \le s_2 \qquad (6.17)$$

$$\tau = \tau_{\max} - (\tau_{\max} - \tau_f)\left(\frac{s - s_2}{s_3 - s_2}\right) \qquad s_2 \le s \le s_3 \qquad (6.18)$$

$$\tau = \tau_f \qquad s_3 < s \qquad (6.19)$$

Table 6.1 Parameters for bond-slip relationship for ribbed bars (as proposed by CEB-FIB model code 1990)

	Unconfined concrete		Confined concrete	
	Good bond	Not good bond	Good bond	Not good bond
s_1	0.6 mm	0.6 mm	1.0 mm	
s_2	0.6 mm	0.6 mm	3.0 mm	
s_3	1.0 mm	2.5 mm	Rib spacing	
α	0.4		0.4	
$\tau_{\max}$	$2.0\sqrt{f_c}$	$1.0\sqrt{f_c}$	$2.5\sqrt{f_c}$	$1.25\sqrt{f_c}$
τ_f	0.15 $\tau_{\max}$		0.4 $\tau_{\max}$	

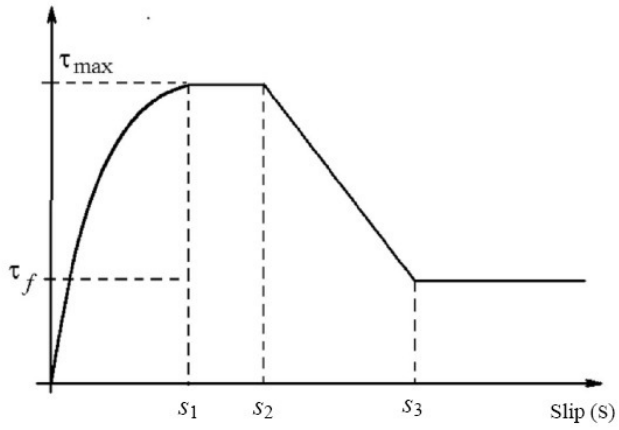

Fig. 6.9 Bond-slip relationship proposed by CEB-FIP model code 1990

6.1.4 Support plates

For modelling the specimens under testing condition, steel plates were modelled as "*3D elastic Isotropic"* which requires only elastic modulus of mild steel.

6.1.5 Spring materials

During experiments, specimens were provided with column top and bottom hinges using steel plates and rollers as shown in *Fig. 6.10*. These steel plates with rollers were inserted in between specimen and steel channels. It is obvious that during loading in beam tip, there was a movement at column top and bottom depending on the stiffness of the steel channel

which held the specimen and the hinging arrangement. To simulate this behaviour, springs were modelled at outer and inner sides of top and bottom ends of the column which would provide a certain degree of movement at the support locations. It is also to mention that the springs in the numerical models were effective in compression only.

Fig. 6.10 Support arrangements during testing

6.2 Geometric modelling

In this section, modelling details of the specimens ('GLD' and 'NonDuctile') using ATENA is discussed. Different micro-elements were created for different parts of the specimens based on D-region and B-regions. Geometries of the models corresponding to under-designed specimens SP-1, SP-3 and SP-4 were identical (except reinforcement details) and macro-elements of the typical numerical model of the specimens are shown in *Fig. 6.11*. Since the distribution of bending and shear (or tie) reinforcements of beam and column was different in the specimens, it was important to model those details accurately. Reinforcement models of the under-designed specimens are shown in *Fig. 6.12*.

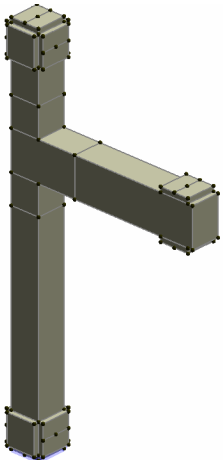

Fig. 6.11 Macro-elements of the numerical model

Here, reinforcements were modelled as discrete truss elements inside concrete. Curvature of beam bending reinforcement inside joint was modelled as truss members in polygons. It is significant to mention here that since the reinforcements were truss elements, effect of anchorage could not be simulated by mere modelling of the bent of reinforcement in one-dimensional form. Hence, another strut with same element property was provided at the bent corner of reinforcement which would make the reinforcement a two-dimensional truss. For each of the bending reinforcements, bond-slip relationship was incorporated as specified by CEB-FIP Model Code (as discussed in section 6.1.3) whereas the stirrups for beam and column were assumed to be perfectly bonded.

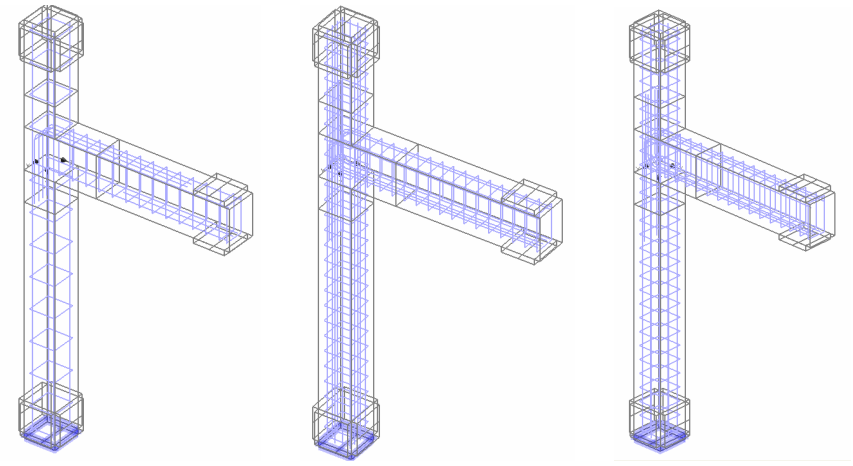

Fig. 6.12 Modelling of reinforcement for SP-1, SP-3 and SP-4, respectively

Concrete parts of the models were modelled using quadratic “Brick”- and steel plates were modelled using “Tetrahedral”- solid elements. Since, these numerical models were computational intensive due to cyclic loading, two different sizes of FE mesh were used. In the joint zone, three adjacent macro-elements were meshed with 50 mm size and the rest part of the model was meshed with 100 mm. Generated finite element mesh of the typical numerical model for the specimens is shown in *Fig. 6.13*:

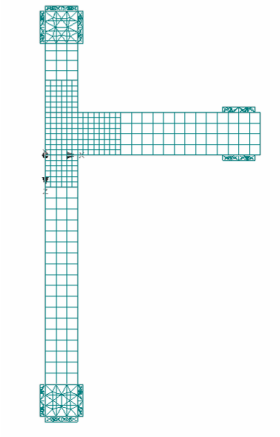

Fig. 6.13 Finite Element mesh for the numerical model

As discussed in section 6.1.5, 4 numbers of springs were added to the model at both face of column top and bottom. Stiffness of the top and the bottom springs were different to simulate the global behaviour of the test set-up as it was observed that the displacements at support due to positive (upward) loading were different from the negative loading. Numerical model with support condition is shown in *Fig. 6.14*.

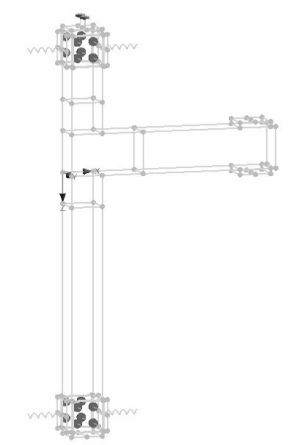

Fig. 6.14 Support conditions of the numerical model

At first, total column axial load of 300 kN was gradually applied in the numerical models in few steps and subsequently, the displacement cycles were applied at beam tip. Axial loading phase of the simulated model was solved by arc-length method and then the solver was changed to Newton-Raphson method during displacement cycles for better numerical efficiency. In each load step, a maximum of 40 iterations were specified.

6.3 Comparison of results from FE analysis and test

SP-1, SP-3 and SP-4 were numerically simulated, analysed and compared with the test results. For better numerical accuracy, displacements were incorporated in small steps. Initially, a convergence study was carried out with different displacement steps and finally, a displacement increment of 1 mm in each step was chosen by considering the accuracy of results and total number of steps required to simulate experimental investigations of the specimens under cyclic loading history. It was observed from the test results that the repetition of cycles in each displacement level would reduce its maximum load carrying capacity and stiffness under same drift demand. A study was further carried out to investigate the difference in results obtained from numerical analysis where with- and without- repetition of cycles in each displacement level was considered. *Fig. 6.15* shows a representative result from numerical analysis where repetitive and non-repetitive cyclic loading were considered. It is clear from the figure that using the repetitive cycle the obtained

strength and stiffness in subsequent cycles are lower than that obtained from non-repetitive cyclic loading, as found in experiment as well. Decrease in strength in next drift ratio due to consideration of repititive cycle is more prominent under negative displacement than that is observed under positive displacement. Nevertheless, analyzing the entire displacement history (3 repeated cycles at each displacement level), as used during the test, with adequately small increments of displacement in numerical analysis demanded enormous computational time and space. Therefore, for further analysis, only one cycle at each displacement level was adopted.

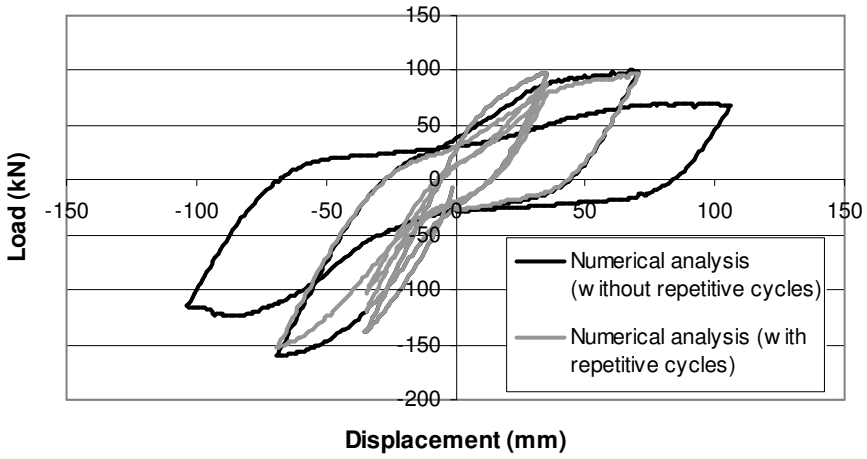

Fig. 6.15 Comparison of numerical response from repetitive and non-repetitive cyclic loading

As described earlier, a constant axial load of 300 kN was applied in the column before application of the cyclic loading. For each specimen, displacement history was adopted the same as that was used during the test. After a set of iterations by slowly adjusting the unknown material parameters (like plastic strain, width of crack opening, fracture energy, failure surface eccentricity, factor for tension stiffening etc.), finally obtained results from the numerical analysis and the test for 'GLD' and 'NonDuctile' specimens are shown in *Fig. 6.16* to *Fig. 6.18*.

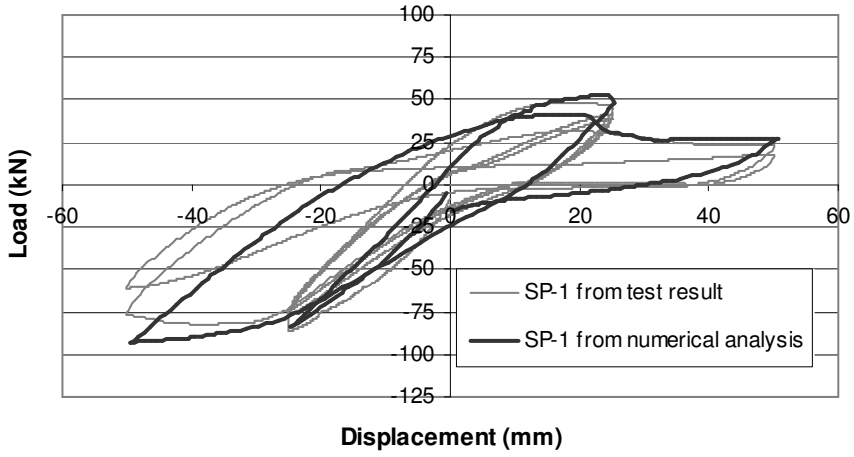

Fig. 6.16 Load-displacement hysteresis for SP-1 from test and numerical analysis

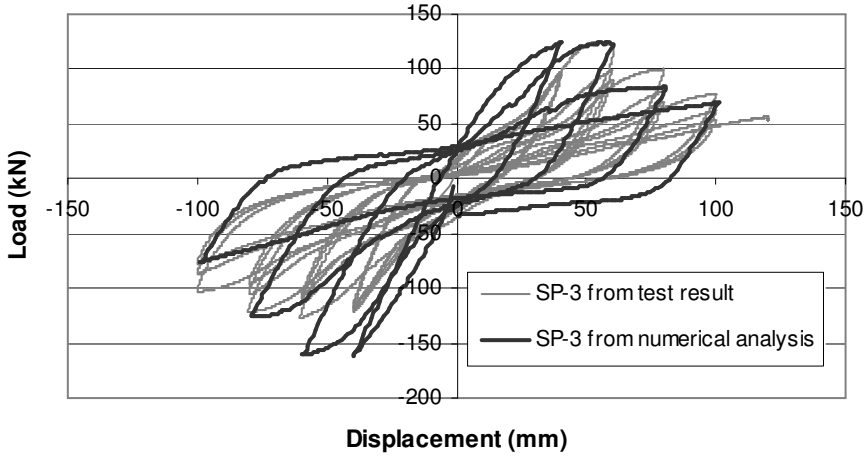

Fig. 6.17 Load-displacement hysteresis for SP-3 from test and numerical analysis

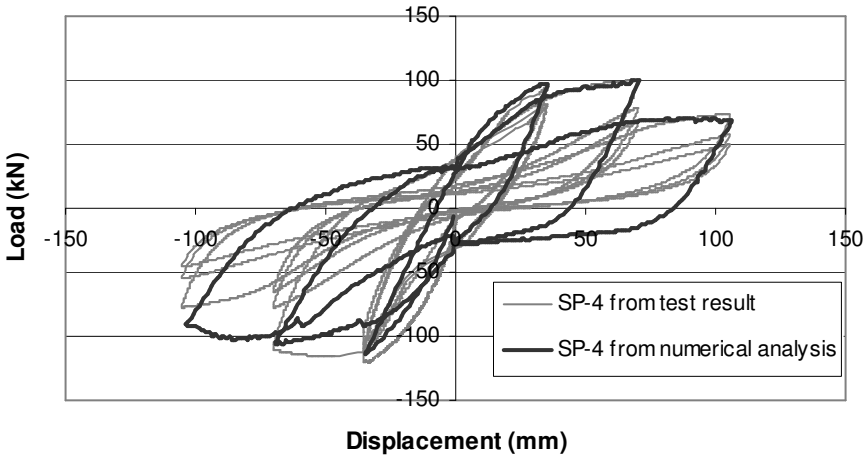

Fig. 6.18 Load-displacement hysteresis for SP-4 from test and numerical analysis

The figures (*Fig. 6.16* to *Fig. 6.18*) show that the results obtained from the numerical analysis are in good agreement with the experimental results. Further, development of cracks observed from numerical studies and experimental investigations are shown in *Fig. 6.19* to *Fig. 6.21*.

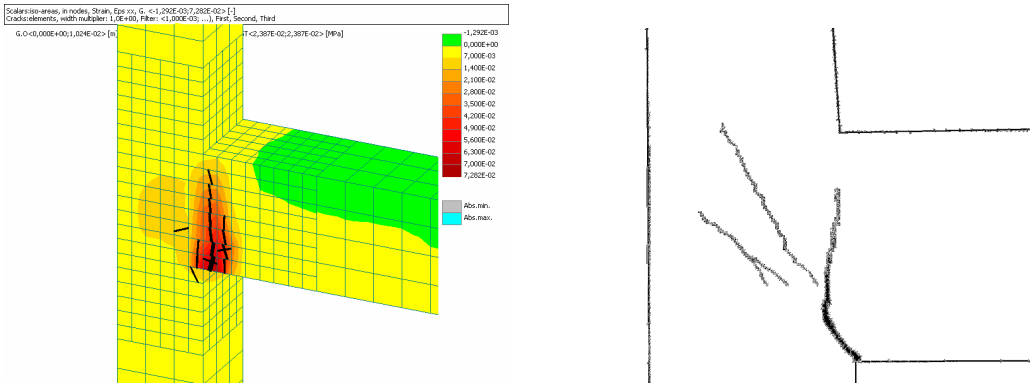

Fig. 6.19 Comparison of crack pattern for SP-1 from numerical analysis and test

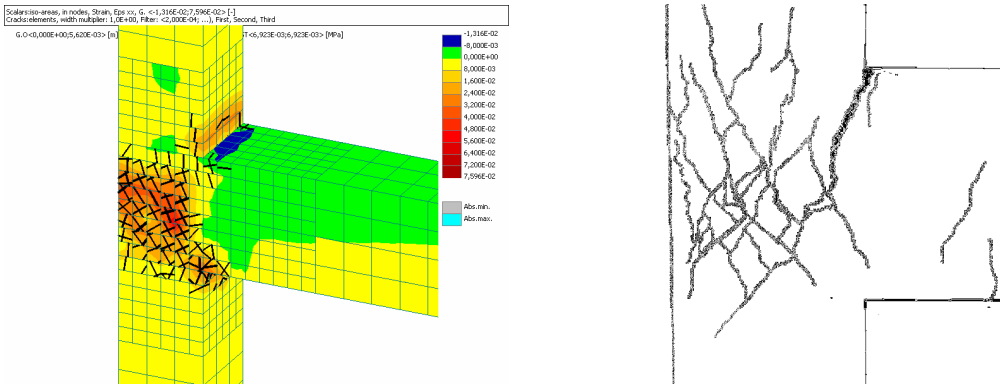

Fig. 6.20 Comparison of crack pattern for SP-3 from numerical analysis and test

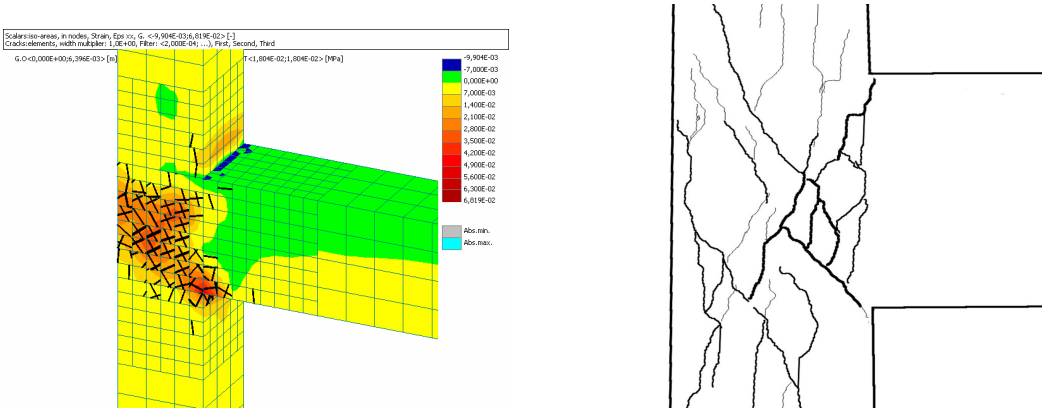

Fig. 6.21 Comparison of crack pattern for SP-4 from numerical analysis and test

For better representation and comparison, crack patterns obtained from the test were re-drawn in 2-D form. Crack patterns from the numerical analysis showed that the final damage in 'GLD' specimen was due to failure of bond in beam bottom reinforcement whereas in 'NonDuctile' specimens, almost all damages concentrated in the joint zone. It is evident from the figures that along with the load-displacement hysteresis, the numerical analysis can predict the crack pattern and final damage scenario quite accurately.

6.3.1 Parametric studies from numerical analysis on existing sub-assemblages

After obtaining the validated FE models for 'GLD' and 'NonDuctile' sub-assemblages, it was attempted to go for further studies.

6.3.1.1 Correlation of energy dissipation

Since in test three repeated cycles were applied at each displacement level whereas the numerical models were validated for single cycle at each displacement level, it is of great use to correlate the energy dissipations obtained from the test and numerical analysis so that the results obtained from the numerical analysis can reflect the extrapolated energy dissipation during real test. Towards this, all the experimented sub-assemblages were numerically analysed. Energy dissipation in first cycle from experiment (E1) and that of numerical analysis (N1) is shown in *Fig. 6.22*. Similarly, results obtained from all three cycles from experiment (E3) and single cycle from numerical analysis (N1) is shown in *Fig. 6.23*. Here, energy dissipation was calculated in kNm.

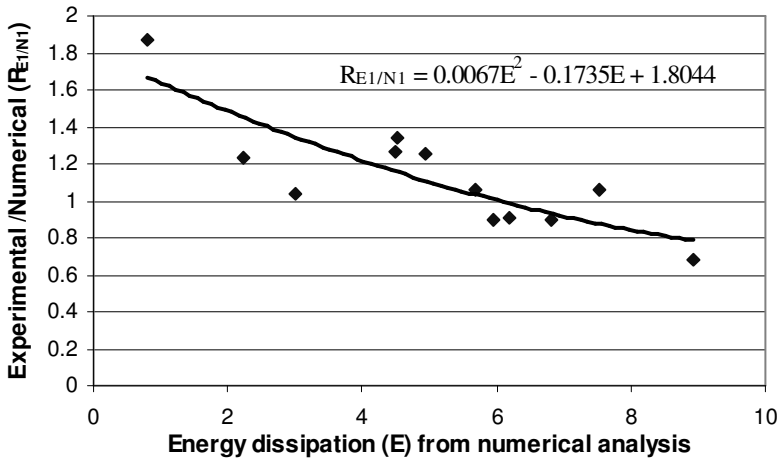

Fig. 6.22 Single cycle energy dissipation from experimental- and numerical- study

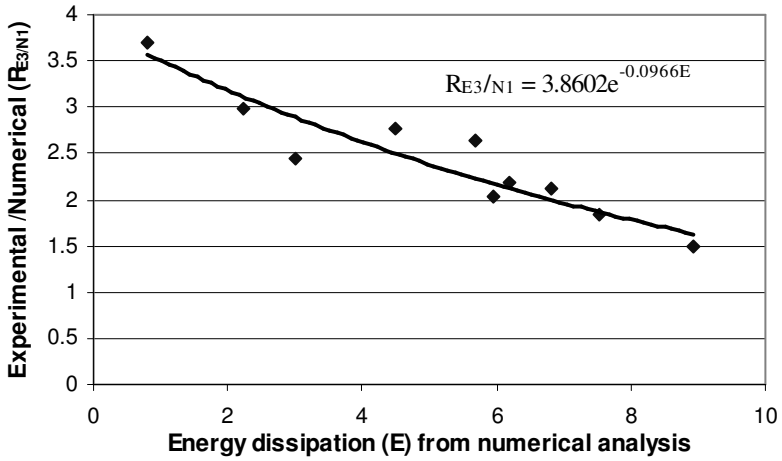

Fig. 6.23 Total energy dissipation from experimental- and numerical- study

The study and proposed relations between energy dissipation obtained from experimental- and numerical- investigation (shown in the figures) would help in practice to provide the guideline in evaluating the actual energy dissipation of any exterior sub-assemblage by obtaining that from numerical analysis. This would facilitate in improving the design and detailing of the sub-assemblage before adopting for a seismic resistant structure since the experimental investigations are not always possible, time consuming and costly as well.

6.3.1.2 Axial load effect

One of the most interesting issues still being discussed is the effect of axial load on seismic performance of RC sub-assemblages and structures as a whole. Several researchers have reported conflicted results and observations on the performance of RC structure where axial loading was a parameter. For example, Paulay et al. (1978) and Ghee et al. (1989) reported that increase in axial load in column would improve the shear strength of the section. Priestley and Park (1987) brought out the enhancement of moment carrying capacity at any section due to axial load effect. On the other hand, Lim and McLean (1991) suggested that higher axial load produced greater drop in strength whereas Mo and Nien (2002) observed that a greater axial load produced higher maximum load. But, it is almost agreed by most of the researchers that ductility of any section deteriorates as the level of axial load increases. In view of this, it is important to know the behaviour of sub-assemblages considered in this study under varying axial load. Using the validated FE models for 'GLD' and 'NonDuctile' specimens, parameters like rate of strength degradation and change in energy dissipation in every positive and negative cycle have been studied under a wide range of axial load ratios (defined as axial load in column divided by column axial capacity) and different drift ratios. Energy dissipation and the strength of the specimens (SP-1, SP-3 and SP-4) during cyclic

loading are shown in *Fig. 6.24* and *Fig. 6.25*, respectively, where drift ratio and axial load ratios are the parameters.

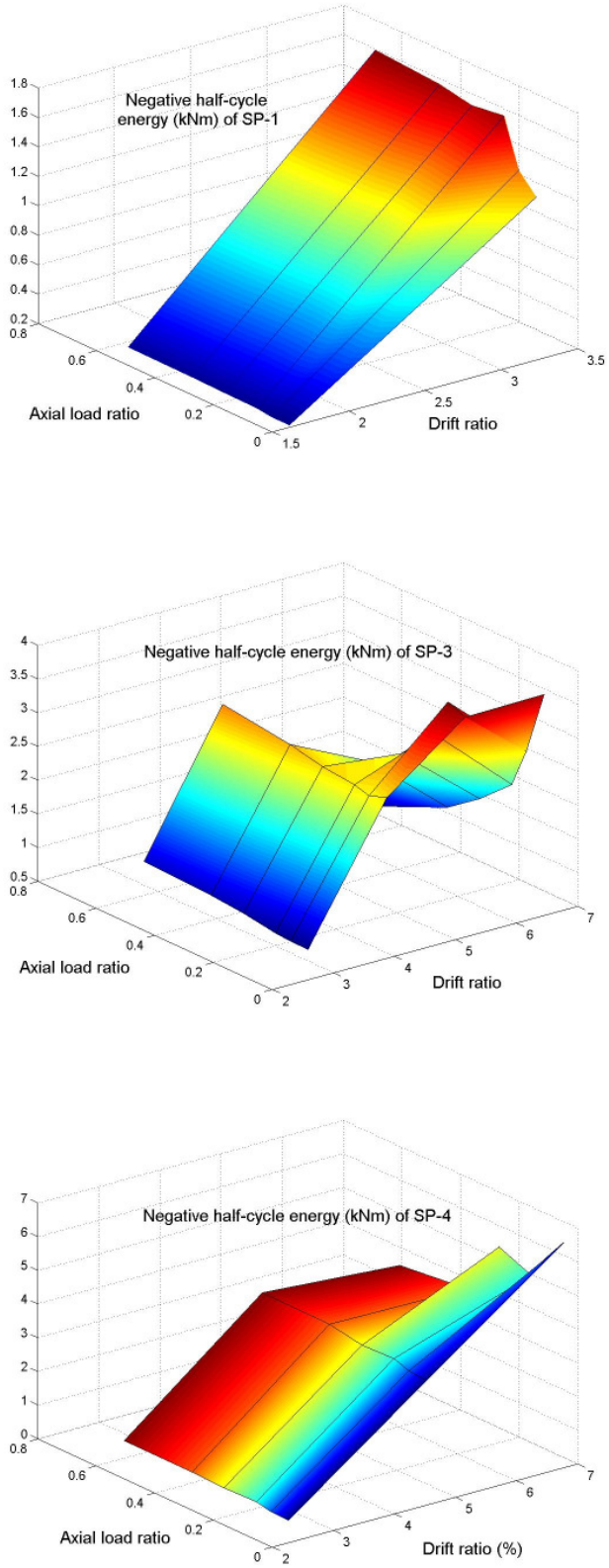

(a) Energy dissipation (kNm) of the specimens under negative half-cycle

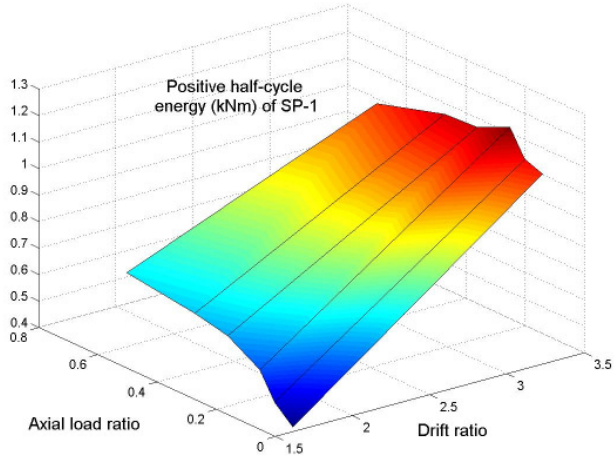

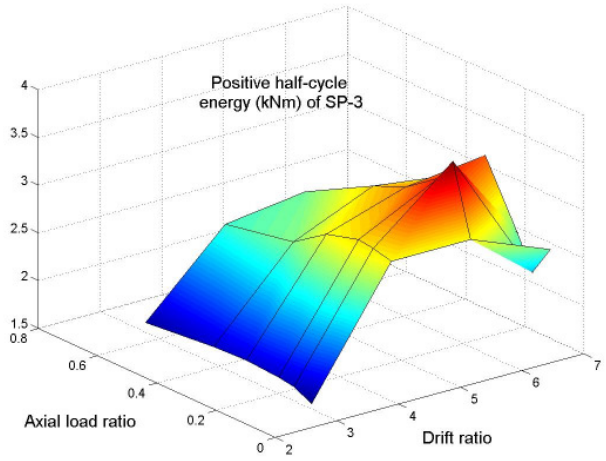

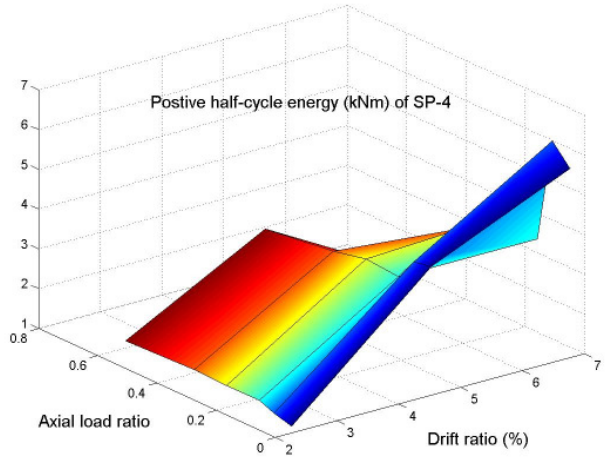

(b) Energy dissipation (kNm) of the specimens under positive half-cycle

Fig. 6.24 Energy dissipation (kNm) of the specimens with variation of axial load and drift ratio

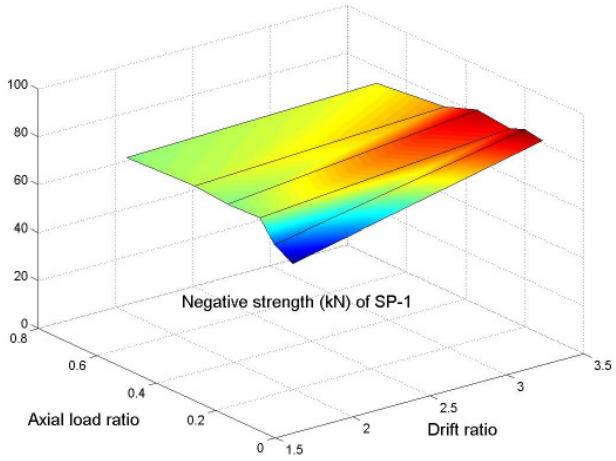

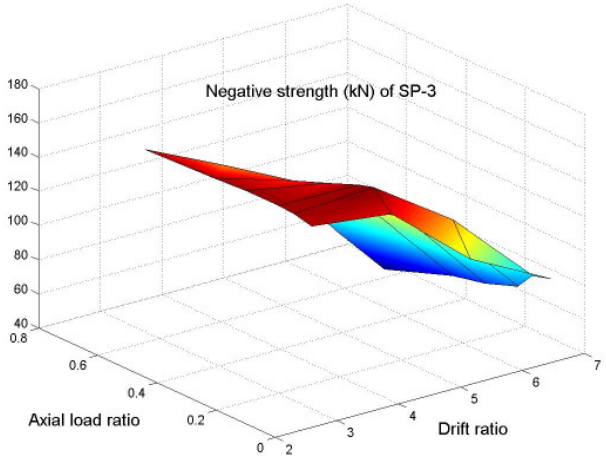

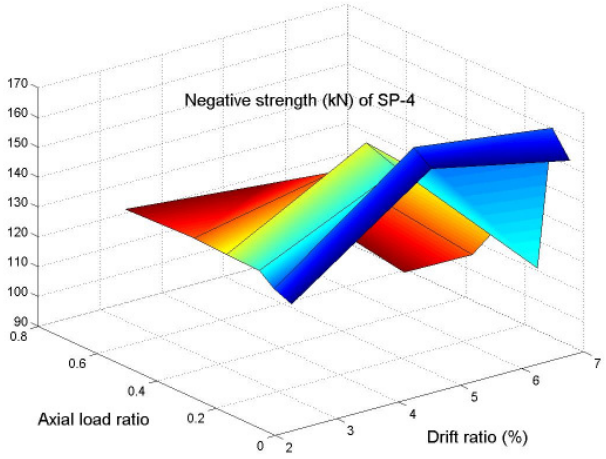

(a) Strength (kN) of the specimens under negative half-cycle

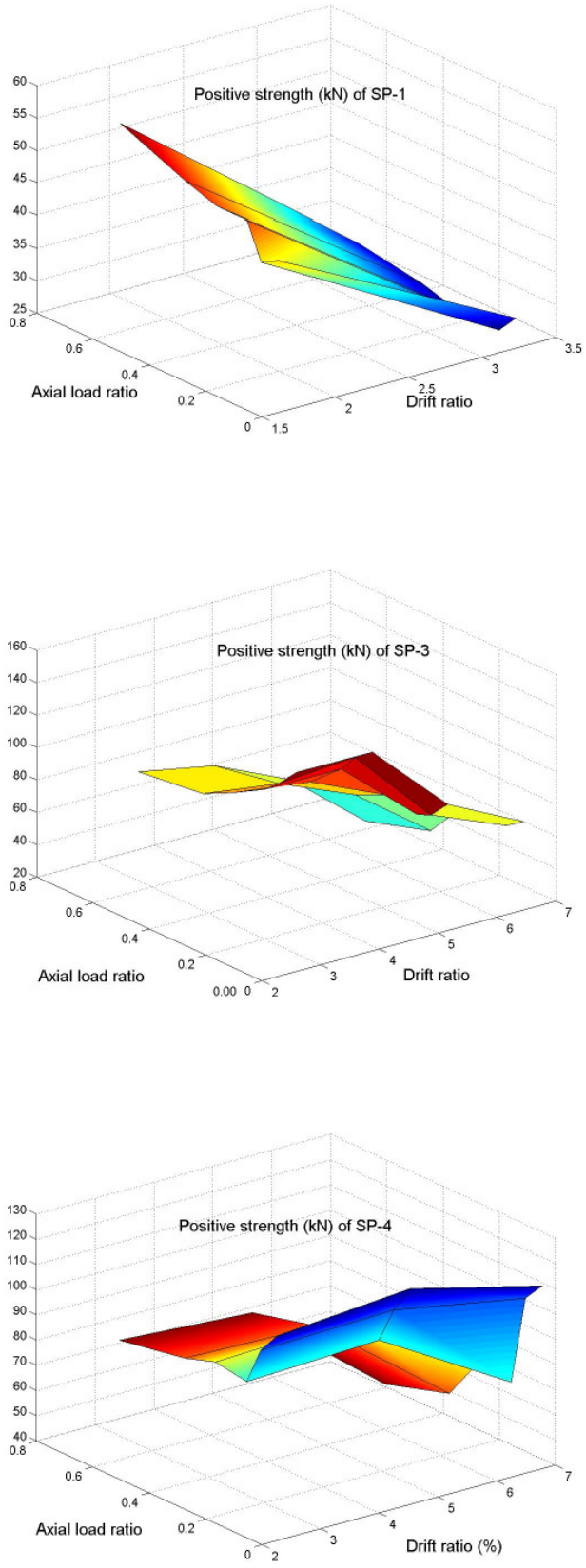

(b) Strength (kN) of the specimens under positive half-cycle

Fig. 6.25 Strength (kN) of the specimens with variation of axial load and drift ratio

From the study (as shown in *Fig. 6.24* and *Fig. 6.25*) on the axial load effect, a number of important observations have been made. (i) During negative loading (downward) with low drift ratio, axial load has negligible impact on energy dissipation of 'GLD' specimens whereas axial load provides a positive influence on negative energy dissipation under higher drift ratios. (ii) Unlike negative loading, during positive (upward) loading on 'GLD' specimen, axial load plays an important role in increasing energy dissipation under lower drift ratio and this effect reduces with increase in drift ratio. (iii) Both the 'NonDuctile' specimens show a clear behaviour that with increase in axial load, energy dissipation (positive and negative) increases. But, under a high drift ratio with high axial load, the specimens become so brittle that energy dissipation suddenly drops. Reduction in energy dissipation with higher axial load and higher drift ratio is more in Eurocode based 'NonDuctile' specimen in comparison to the Indian Standard based specimen. (iv) Strength corresponding to negative displacement in specimens increases with increase in axial load when drift ratio is not high. Under high drift ratio, though the decrease in negative strength in not so prominent in 'GLD' specimens, but in 'NonDuctile' specimens it is drastic. (v) Similar behaviour has been noted for change in strength corresponding to positive displacement, i.e., in low drift ratio axial load in column brings a favourable effect in change of positive strength of specimens though it does not hold good under high drifts. Moreover, presence of high axial load in column reduces its strength. From these observations on 'GLD' and 'NonDuctile' specimens, it can be stated that the contradictory results reported by previous researchers were valid in their range of experiments where a certain range of axial load and drift ratio on particular specimen(s) were considered. So, finally it is noteworthy to mention that an increase in axial load in column will provide a better seismic response for the structures under low seismic demand. Hence, any existing under-designed structure (both 'GLD' and 'NonDuctile') in low seismic zones may be improved or strengthened by simply increasing its column axial load using mechanical means such as external prestressing etc. On the other hand, in areas with high seismic demand, it will not only be invalid and insufficient, but could bring adverse effect due to increase in brittleness in the member with increase in axial load.

6.4 Numerical studies on the upgraded specimens

From the numerical simulations of the original specimens, it was found that the results and the damage pattern determined from the numerical analysis were in good agreement with the results obtained from the test. The validated numerical model of SP-1 ('GLD' specimen) was then taken for simulation of upgraded specimens. In numerical models for upgraded specimens, definition of solid concrete element, reinforcement, bond-slip relation for reinforcement and support conditions were considered as described previously.

Nevertheless, available material properties (concrete compressive and tensile strength) were suitably modified. Here, all the FRPs were modelled as 9-noded iso-parametric multi-layered shell elements. Shell element is a special case of 3D solid and has one dimension (thickness) very small compared to other two. Number of integration points depends on number of layers in shell element. Anisotropic behaviour of the bending and wrapping FRPs were simulated by adopting a single directional reinforcement embedded in epoxy matrix. Here, extra attention was paid in defining the local coordinate system of each shell element and '*master-slave*' definitions for non-conforming elements. All embedded reinforcements in matrix were oriented in local coordinate system. Further, it was observed that the common corner surfaces of shell elements were extremely important in defining the bent of FRPs. Hence, for best simulation, instead of orthogonal connection, 45^o diagonals were established in bent elements to provide the full contact wherever it was possible (as shown in *Fig. 6.26*).

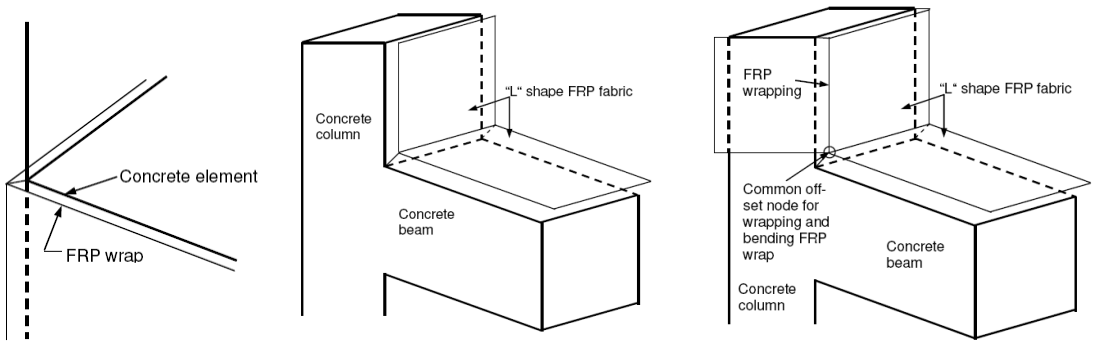

(a) "U" wrap at concrete joint, (b) "L" wrap on member face, (c) wrapping with "L" wrap

Fig. 6.26 Corner surface elements of bent FRP

Steel plate and bolts were modelled as isotropic shell and reinforcement bars, respectively. CFRP laminates were also modelled as reinforcements placed near surface. Bond-slip behaviour of CFRP laminate attached with concrete has been considered as that was reported by Mazzotti et al. (2005) as shown in *Fig. 6.27*. It can be seen from *Fig. 6.27* that descending part of the bond-slip behaviour, as found by Mazzotti et al. (2005), is very sharp and becomes negligible after a slip of 0.2 mm. But, for numerical stability (without much effect on global result), the residual bond stress was kept constant as 1 MPa.

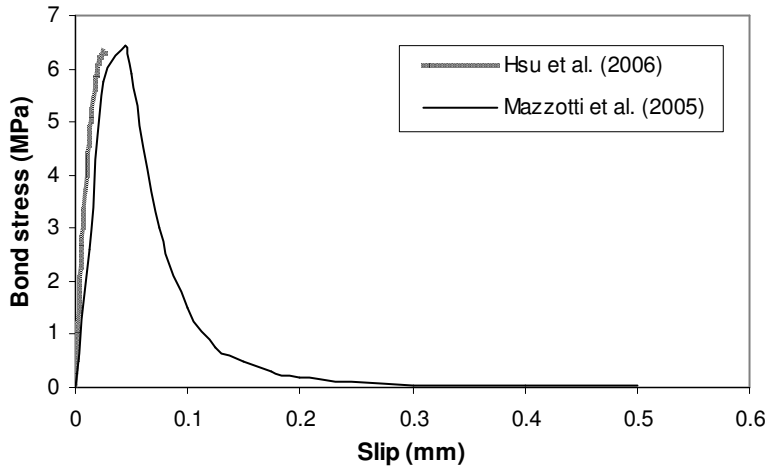

Fig. 6.27 Bond-slip relation of laminates attached to concrete

Interface behaviour of FRP fabric (both wrapping and bending) to concrete was simulated by defining the interface material as "contact element". In ATENA, the interface material is based on Mohr-Coulomb criterion with tension cut off. The bond between the concrete and FRP fabric is subjected to both peeling and shearing forces. It was found from the test that failure of the bond line was initiated as a tensile failure in the layer of concrete immediately below the composite bond layer. Therefore, the allowable bond stress perpendicular to the interface between the concrete and the FRP was taken to be equal to the tensile strength of the concrete, and the allowable bond stress parallel to the interface between the concrete and the FRP is taken as 4.8 MPa [Parvin and Granata (2000)]. Further for interface material, elastic normal and shear stiffnesses were assigned for initial and post-peak state. The post-peak stiffnesses are used only for numerical purposes after the failure of the element in order to preserve the positive definiteness of the global system of equations. Theoretically, after the interface failure the interface stiffness should be zero, which would mean that the global stiffness will become indefinite. To avoid this, minimal stiffnesses were assumed as 0.001 times of the initial ones.

6.4.1 Studies on the upgraded specimens experimentally investigated

During the numerical analysis, it was found that due to weak nature of anisotropic FRP in the direction perpendicular to embedded reinforcement, some of the shell elements representing FRPs were severely damaged (distorted) during higher displacement demand. Hence, zero or negative jacobians were formed due to distorted "inside-out" elements which caused a numerical instability to the computation procedure. To tackle this issue, further suitable refinement of mesh was carried out to avoid bad aspect ratio and to maintain the parity in neighbouring elements. Moreover, numerical analysis of the upgraded specimens was

performed under first three displacement cycles and last cycle of displacement (±100 mm) was not imposed. Load-displacement hysteresis of all the upgraded specimens (SP1-U1, SP1-U2 and SP1-U3) obtained from the numerical analysis and experimental investigation are shown in *Fig. 6.28* to *Fig. 6.30*, respectively. It can be stated from the figures that the load-displacement behaviour of the upgraded specimens obtained from numerical analysis and experimental investigation are well corroborated. It is also to mention that though the positive strength calculations are almost accurate, numerical analysis shows a higher negative strength than that obtained from experiment and this observation is similar for existing specimens also (*Fig. 6.16* to *Fig. 6.18*). Along with the load-displacement hysteresis, it is also important to know the damage pattern of the upgraded specimens determined from the numerical analysis. The final damage patterns of the upgraded specimens SP1-U1, SP1-U2 and SP1-U3 obtained from the numerical analysis and that observed during experiment are shown in *Fig. 6.31* to *Fig. 6.33*, respectively. The figures show that the joint-line failure of SP1-U1 and D-region failure of SP1-U2 and SP1-U3 were obtained from the numerical analyses which are identical as that were observed during experiment. Further, both experimental and numerical analysis confirmed that there was no damage in column region of any of the upgraded specimens.

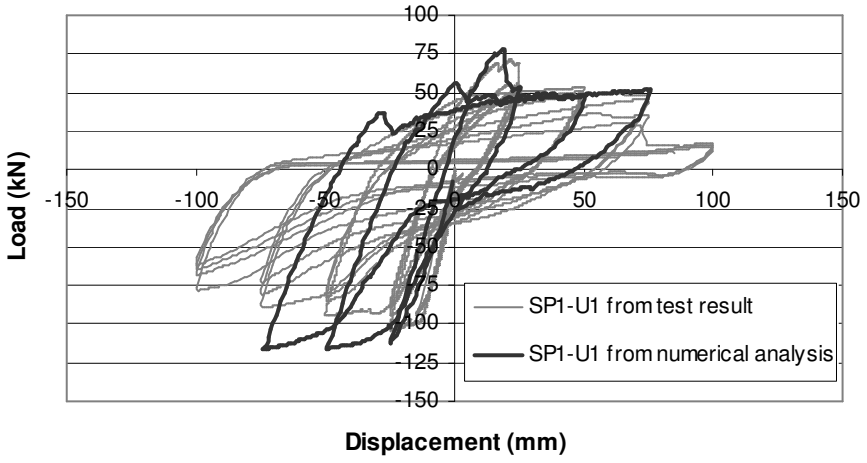

Fig. 6.28 Load-displacement hysteresis for SP1-U1 from test and numerical analysis

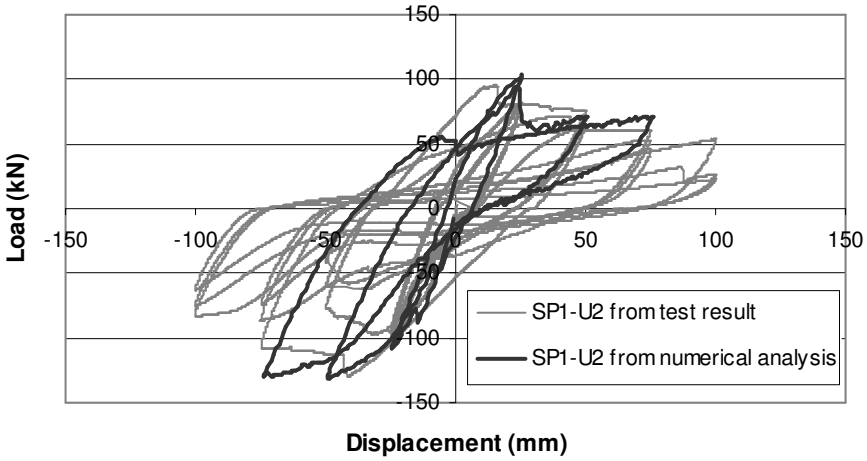

Fig. 6.29 Load-displacement hysteresis for SP1-U2 from test and numerical analysis

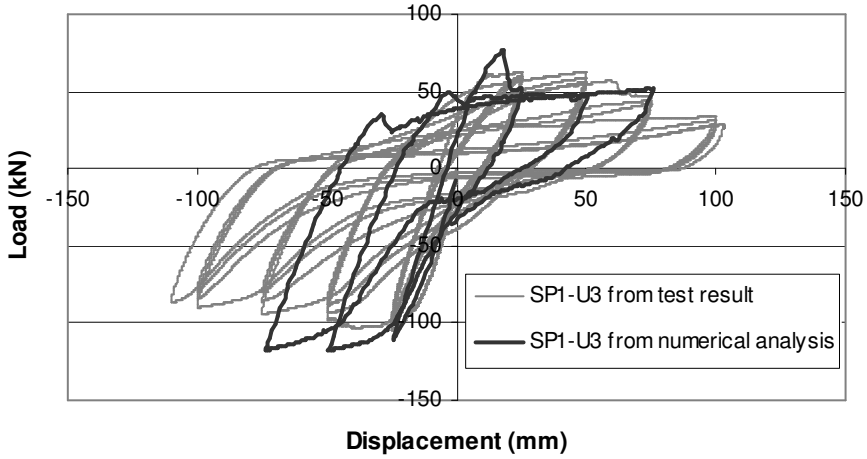

Fig. 6.30 Load-displacement hysteresis for SP1-U3 from test and numerical analysis

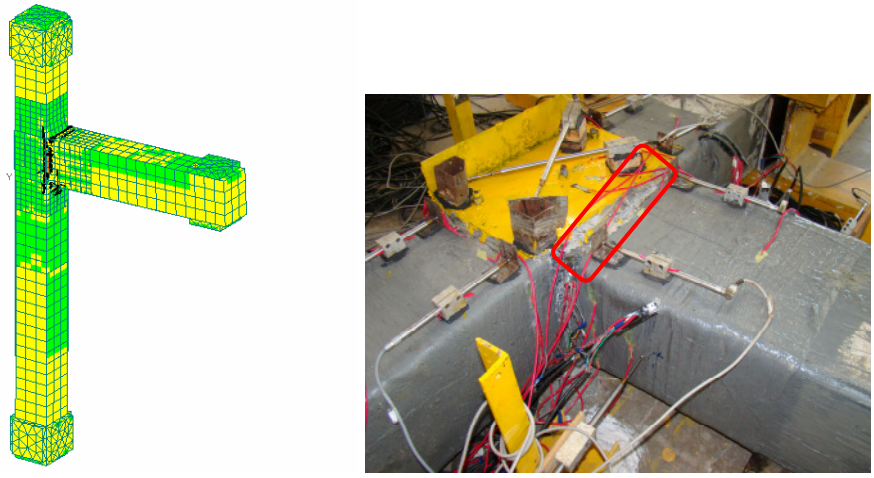

Fig. 6.31 Comparison of crack pattern for SP1-U1 from numerical analysis and test

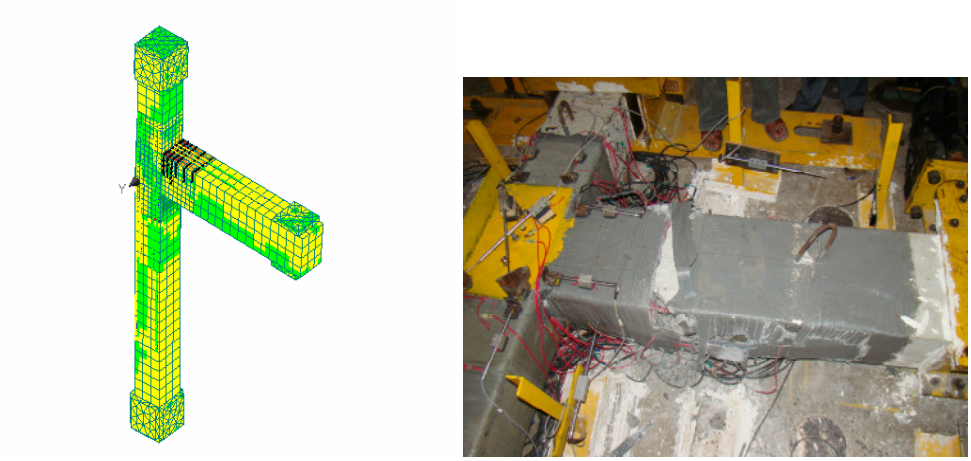

Fig. 6.32 Comparison of crack pattern for SP1-U2 from numerical analysis and test

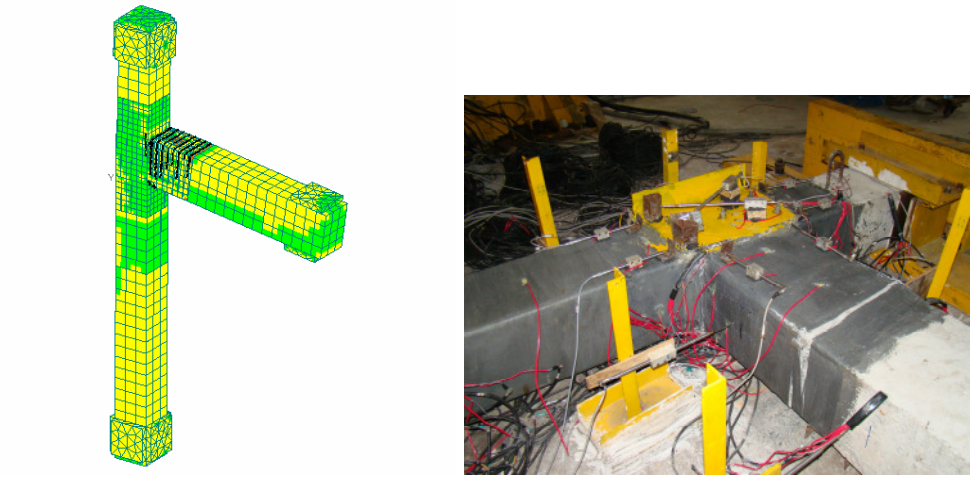

Fig. 6.33 Comparison of crack pattern for SP1-U3 from numerical analysis and test

Beside the study on strength of the specimens at each displacement cycle, it is also significant to evaluate and compare the dissipated energy obtained from both numerical analysis and experimental investigations. *Fig. 6.34* shows the ratio of energy dissipation from experiment and numerical analysis with respect to the energy dissipation calculated from numerical analysis.

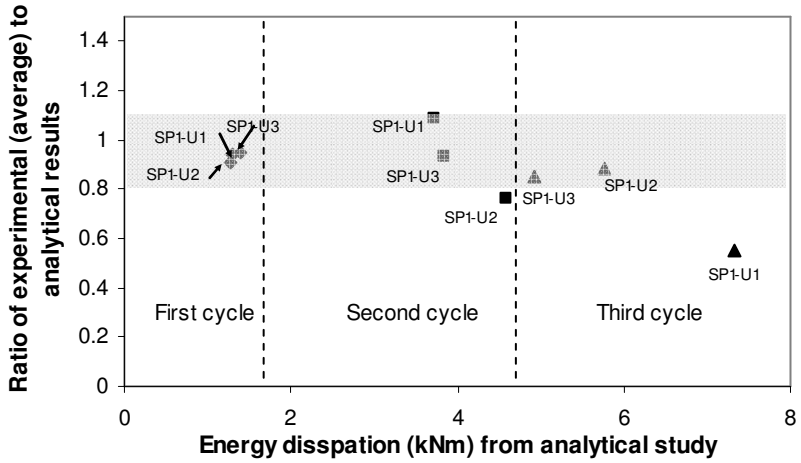

Fig. 6.34 Energy dissipation from numerical and experimental studies

As stated earlier, at each displacement level, no repetition of cyclic loading was carried out in numerical analysis whereas in experiment, 3 cycles were repeated at each displacement level. Here, *Fig. 6.34* brings out that ratio of energy dissipation from experiment (average from 3 repetitive cycles) and numerical analysis (one cycle at each displacement level) is varying between 0.77 to 1.1 for all the upgraded specimens except the last cycle of SP1-U1.

Before proceeding for further parametric studies on the upgraded specimens, it is important to underscore certain issues those were observed during the numerical analysis of the upgraded specimens. (i) Numerical simulation of the FRP based upgraded specimens is extremely computation intensive and space demanding. This aspect becomes more severe when a cyclic load analysis is carried out. (ii) Bond-slip relation of reinforcement-concrete or CFRP laminate-concrete plays a very critical role and needs to be carefully incorporated in the numerical model. (iii) Since FRP fabric can not be placed on concrete surface which can ensure fixed connectivity, interface contact elements are vital to bring out the near-practical behaviour of FRP based upgraded specimens. (iv) Incorporation of bond-slip behaviour and/or interface element in numerical models exponentially demands for computation time, so a judicious justification needs to be made on the assignment of those behaviours to fibers (at various locations) before any such analysis. (v) Unlike existing specimens (SP1-, SP-3 and SP-4), in case of upgraded specimens, number of iterations at each displacement step should be assigned much higher (80-100) for achieving target convergence towards better and consistent results. (iv) Reduction in ultimate strength and E-modulus of composite FRP fabric with the increase in number of layers was suitably incorporated. From the information available from reported studies, with introduction of second, third and fourth layer of CFRP and GFRP fabric composite, 10%, 9% and 8% reduction in strength was considered, respectively. Further a 3% reduction in E-modulus with introduction of each layer of

composite fiber was assumed. Though, a perfect linear rate of reduction with increase in number of layers may not hold always correct, but seems to be reasonably appropriate.

6.4.2 Studies on the parametric specimens derived from proposed schemes

The validated numerical models of upgraded specimens were then studied with different variables where amount and distribution of bending CFRP fabric and laminates, quantity of wrapping FRP and contact behaviour were the parameters. Since the first upgraded specimen (SP1-U1), though fully upgraded, could not show a significant improvement in comparison with the partly upgraded specimen SP1-U3, and both SP1-U2 and SP1-U3 showed significantly promising performance by forming damage away from the joint, all the parametric studies have been carried out for those two specimens. Description of the parameters derived from SP1-U2 and SP1-U3 and their identifications are given in *Table 6.2* and *Table 6.3* respectively.

Table 6.2 Parameter index for SP1-U2

Serial No	Specimen named in numerical analysis	Description				
		Numbers of bending laminate		Layers of wrapping		Contact property
		Top	Bottom	D- region	Beyond D-region	"U" wrap
1	SP1-U2*	3	3	4 GFRP	2 GFRP	Gap element
2	SP1-U2(2)	3 (up to D)	3	4 GFRP	2 GFRP	Gap element
3	SP1-U2(3)	2 (up to D)	3 (up to D)	4 GFRP	2 GFRP	Gap element
4	SP1-U2(4)	No	3 (up to D)	4 GFRP	2 GFRP	Gap element
5	SP1-U2(5)	No	1 (up to D)	4 GFRP	2 GFRP	Gap element
6	SP1-U2(6)	2 (up to D)	3 (up to D)	No	No	Gap element
7	SP1-U2(7)	2 (up to D)	3 (up to D)	2 GFRP	2 GFRP	Gap element
8	SP1-U2(8)	2 (up to D)	3 (up to D)	4 CFRP	4 CFRP	Gap element
9	SP1-U2(9)	No	No	4 CFRP	4 CFRP	Gap element
SP1-U2* is the numerical model corresponding to that experimentally investigated						

Table 6.3 Parameter index for SP1-U3

Serial No	Specimen named in numerical analysis	Description				
		Layers of bending CFRP		Layers of wrapping		Contact property
		Top	Bottom	D- region	Beyond D-region	"U" wrap/ laminate
1	SP1-U3*	4	4	2 CFRP	2 GFRP	Gap element
2	SP1-U3(2)	2	4	2 CFRP	2 GFRP	Gap element
3	SP1-U3(3)	No	4	2 CFRP	2 GFRP	Gap element
4	SP1-U3(4)	No	2	2 CFRP	2 GFRP	Gap element
SP1-U3* is the numerical model corresponding to that experimentally investigated						

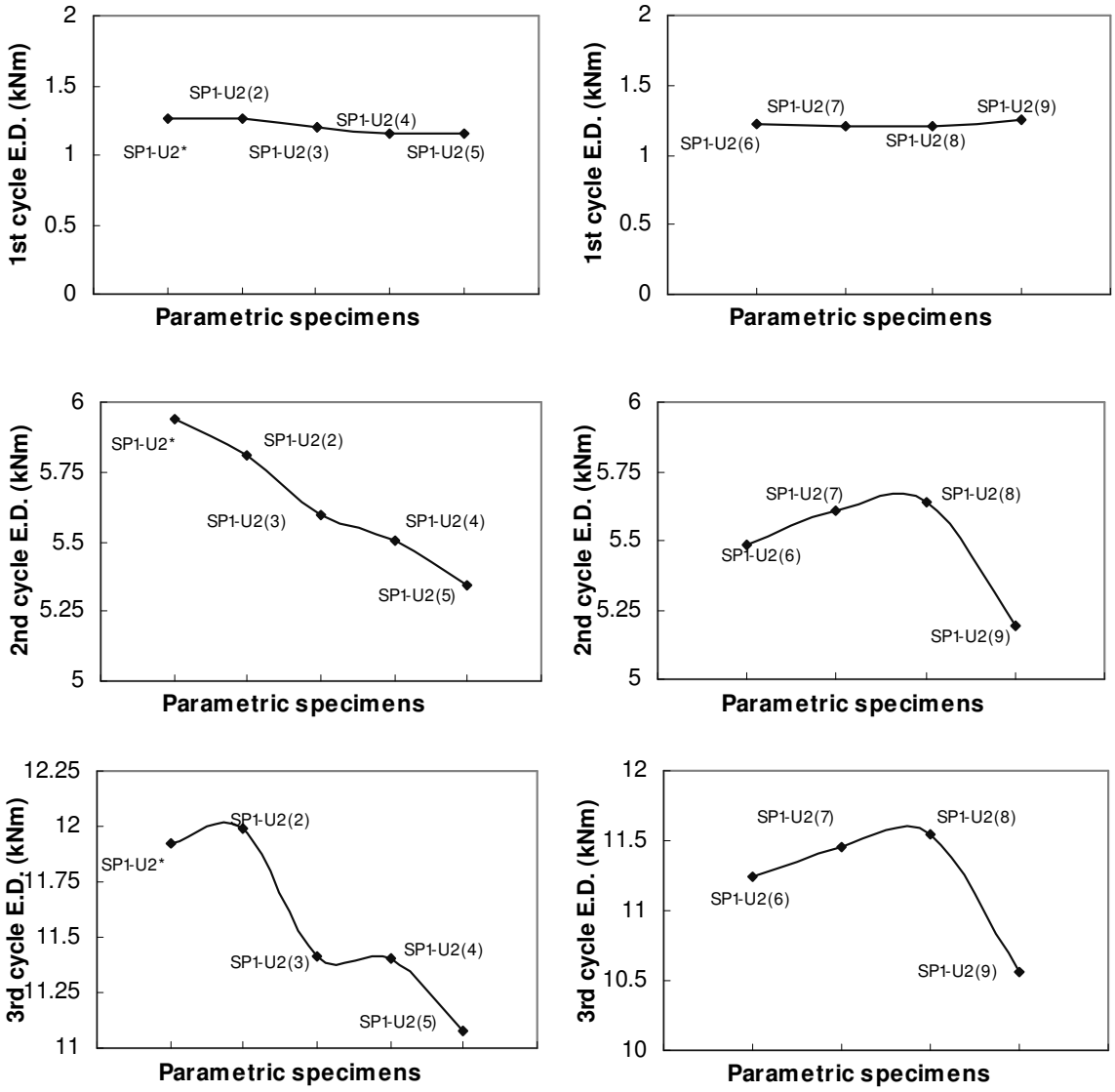

Fig. 6.35 Energy dissipation (E.D.) of the parametric specimens from SP1-U2

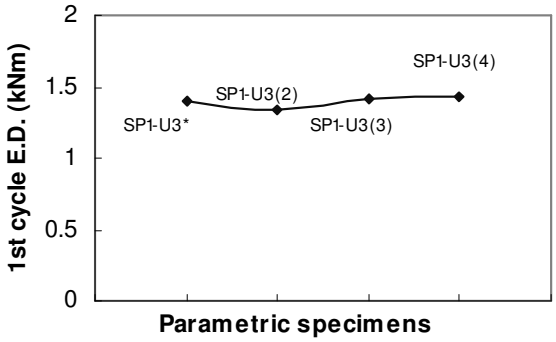

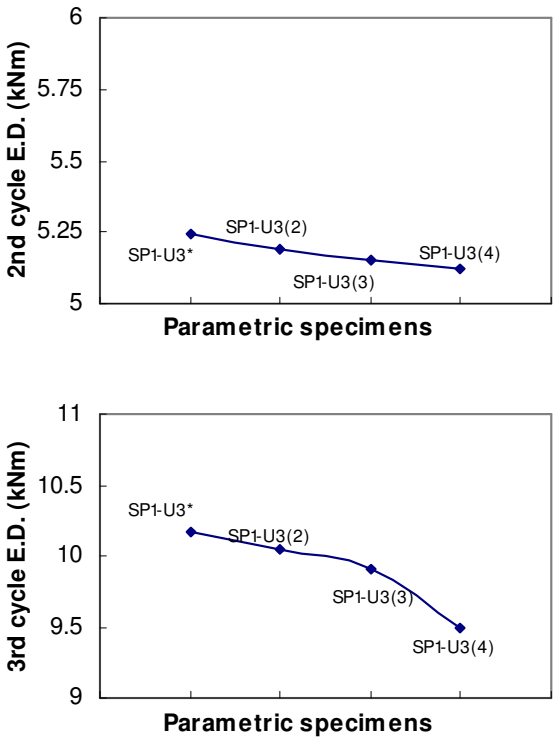

Fig. 6.36 Energy dissipation (E.D.) of the parametric specimens from SP1-U3

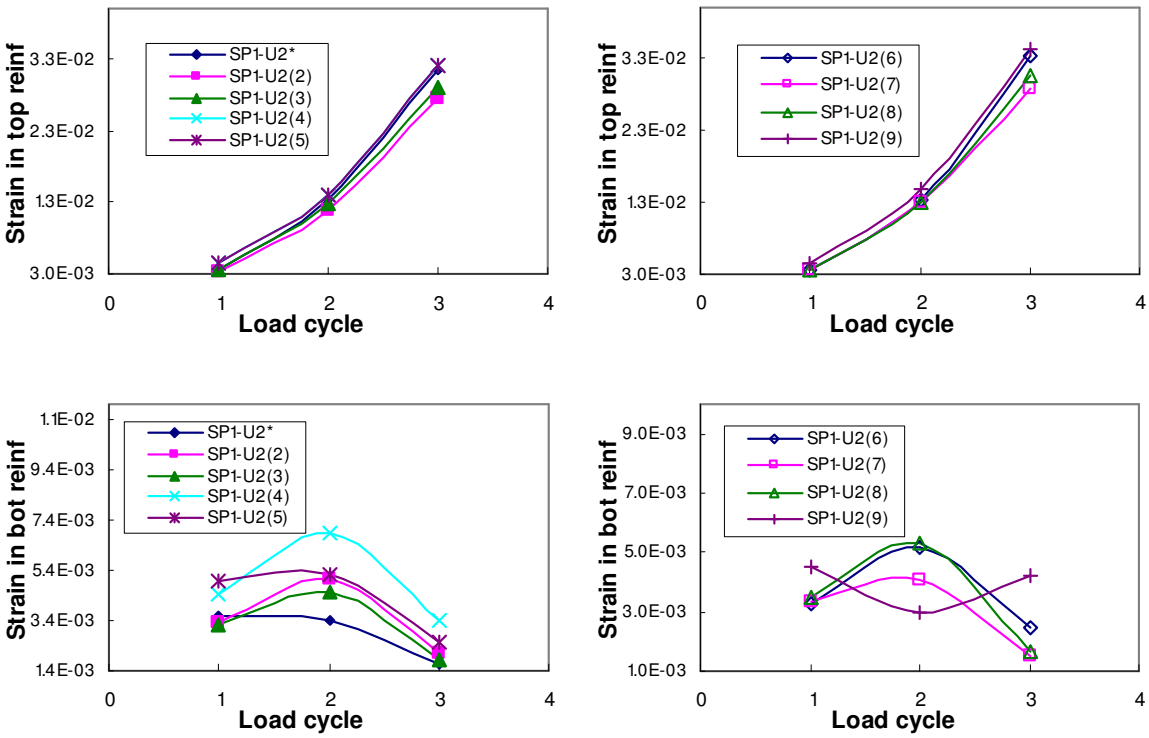

Fig. 6.37 Development of strain in parametric specimens from SP1-U2

Energy dissipation in each cycle of SP1-U2 with the variations of bending and wrapping parameters is shown in *Fig. 6.35*. This shows that reduction in energy dissipation (E.D.)

would take place with reduction in additional bending laminates. Efficiency of energy dissipation becomes more prominent in higher cycles. It is noteworthy that in third cycle SP1-U2(2) is able to dissipate more energy than SP1-U2* which was experimentally investigated. Since all the additional laminates on beam top in SP1-U2(2) are terminated at a distance D from the joint face (whereas in SP1-U2, out of three laminates only one was curtailed), it causes a better system for distinct damage location and is able to dissipate more energy. Among the specimens with wrapping parameter (bottom row of *Fig. 6.35*), it is clear that with better confinement (increase in number of layers and/or strength of FRP) would definitely help in enhancing energy dissipation capacity of the specimen and the rate of enhancement consistently increases in higher cycles. SP1-U2(8) and SP1-U2(9) show the inter-dependency between bending strengthening with wrapping in obtaining energy dissipation. In spite of extremely good wrapping (4 layers of CFRP), absence of proper number of bending laminates causes a drastic reduction in energy dissipation because the main damage occurs in- or near- the joint. *Fig. 6.36* shows that the variation of energy dissipation with different levels of bending strengthening of SP1-U3 is quite similar to the observations made from parametric studies derived from SP1-U2. But, decrease in energy dissipation with reduction in bending strengthening is slower than SP1-U2. It is due to the fact that contact elements between FRP in fabric form and concrete surface play more prominent role than laminates. Since the influence of variation of wrapping in SP1-U3 is found to be identical as that discussed for SP1-U2, the same has not been presented further. For all the parametric specimens, it is true that the energy dissipation from first cycle is almost unaltered by changing the bending or wrapping parameters and it increases consistently with increase in displacement (or load) cycles. So, the structures in moderate or high seismic zones, proper design of upgradation needs to be done where combination of bending strengthening and wrapping would ensure the maximum energy dissipation capacity.

Further, it was attempted to study the state of beam reinforcement during cyclic loading by changing the parameters. For that purpose, parametric specimens of SP1-U2 have been chosen. Maximum strain developed in both top and bottom reinforcement during each cycle is shown in *Fig. 6.37*. It is evident from the figures that maximum strain in beam top reinforcement does not undergo substantial changes whereas the beam bottom reinforcement does. With reduction in bending laminates, maximum strain increases significantly. It is to underline that though SP1-U2(5) possesses lesser reinforcement than SP1-U2(4) as given in *Table 6.2*, maximum strain in beam bottom reinforcement of SP1-U2(5) is lesser than SP1-U2(4). It is due to the fact that location of damage in SP1-U2(5) has been changed from D-distance along beam toward the joint line which reduces the effectiveness of the beam reinforcement itself. Further, amount of wrapping also plays an important role in development of strain in beam bottom reinforcement. Since the higher

amount of wrapping shifts the distribution of damage location from joint face towards the beam length, instead of amount of wrapping, place of damage caused from wrapping determines the maximum strain development in reinforcement. It is interesting to note that beam top reinforcement consistently gains its strain with increase in imposed displacement demand whereas strain in bottom reinforcement reduces after second cycle. It is due to the fact that the protections to the beam bottom reinforcement from slippage (due to absence in anchorage in original specimen) by providing laminate and/or wrapping would be gradually ineffective with increase in displacement. Hence, rate of decrease of strain in bottom reinforcement increases under higher cycles and with less amount of bending laminates. From the study, it is evident that development of strain in reinforcement and energy dissipation capacity in each displacement level would provide the vital information for optimisation of the materials for the upgradation.

6.4.3 Studies on the parametric specimens with intermediate upgradation

In the previous section, response from the upgradation schemes proposed in this study and their derived parametric specimens has been discussed to illustrate their behaviour. But, it is still not investigated the role of individual basic components like steel plate, "U" wrap and laminate in changing the behaviour of the original 'GLD' specimens. To bring the completeness in the study, finally, it is tried to bring out the level- and extent- of improvement by adopting those items individually. In this way, those elements will define their role in upgradation as well. The parameters considered here are presented in *Table 6.4*.

Table 6.4 Parameter index for SP-1 towards intermediate upgradation

Serial No	Specimen named in numerical analysis	Description	
			Contact/bond property
1	SP-1*	'GLD' sub-assemblage	
2	SP-1(2)	Only laminate on bottom side of beam of 'GLD'	Perfect
3	SP-1(3)	Only laminate on bottom side of beam of 'GLD'	With bond-slip
4	SP-1(4)	Only "U" wrap around the joint of 'GLD'	Perfect contact
5	SP-1(5)	Only "U" wrap around the joint of 'GLD'	Contact element
6	SP-1(6)	Only steel plate with bolt in joint of 'GLD'	
7	SP-1(7)	Steel plate with 2 laminates in top and bottom up to D of 'GLD'	
SP1* is the numerical model corresponding to that experimentally investigated 'GLD' specimen			

From the results obtained from the numerical study, it can be stated that laminates or "U" wrap though can change the behaviour of 'GLD' specimens under cyclic loading but it is very much dependent on quality of connection between them with concrete. If the interface is very

good then it can improve the response considerably. Role of each of the upgradation components is prominent during upward (positive) loading. From the numerical analysis, it is noted that during upward loading, "U" wrap provides a better behaviour than that with laminates at bottom of beam as reinforcement. But, most significant aspect is that after loosening of contact of "U" wrap or failure of bond of laminate, the specimen is merely left as a 'GLD' specimen. Hence, the efficiency of those components depends on delaying the loosening of contact or breaking of laminate. Among the alternatives of components, steel plate with laminates at both top and bottom [SP-1(7)] has been found to be most promising. It provides a much higher moment resistant capacity than others [47% more than SP-1*, 33% more than SP-1(3) and 25% more than SP-1(5)], but at higher displacement demand, rupture of laminates takes place and it results in sudden drop in strength. Energy dissipation capacities in each cycle of the parametric specimens are shown in *Fig. 6.38*. It is evident from the figure that the role of additional components for upgradation is almost insignificant in first cycle and it becomes active subsequently. As discussed earlier, loosening of contact or failure in bond in higher cycle could be prominently seen. It can also be identified that the specimen with steel plate on joint and extra laminates at top and bottom of beam behaves well until rupture takes place in third cycle (as seen from *Fig. 6.38*) whereas specimen with "U" wrapping but without any contact behaviour [SP-1(4)] is able to dissipate more energy until last. However, it is extremely difficult to achieve near-fixed contact behaviour of FRP with concrete. The specimen SP-1(5) where contact behaviour is incorporated shows a drastic reduction in energy dissipation capacity than that obtained from SP-1(4) and the reduction increases monotonically in higher cycles.

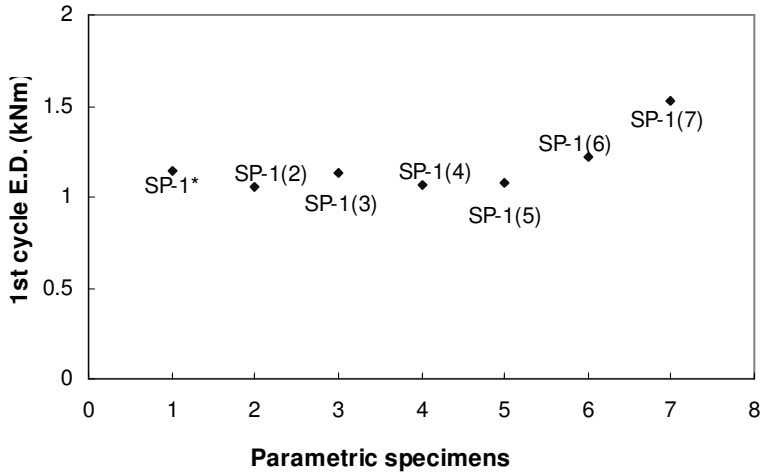

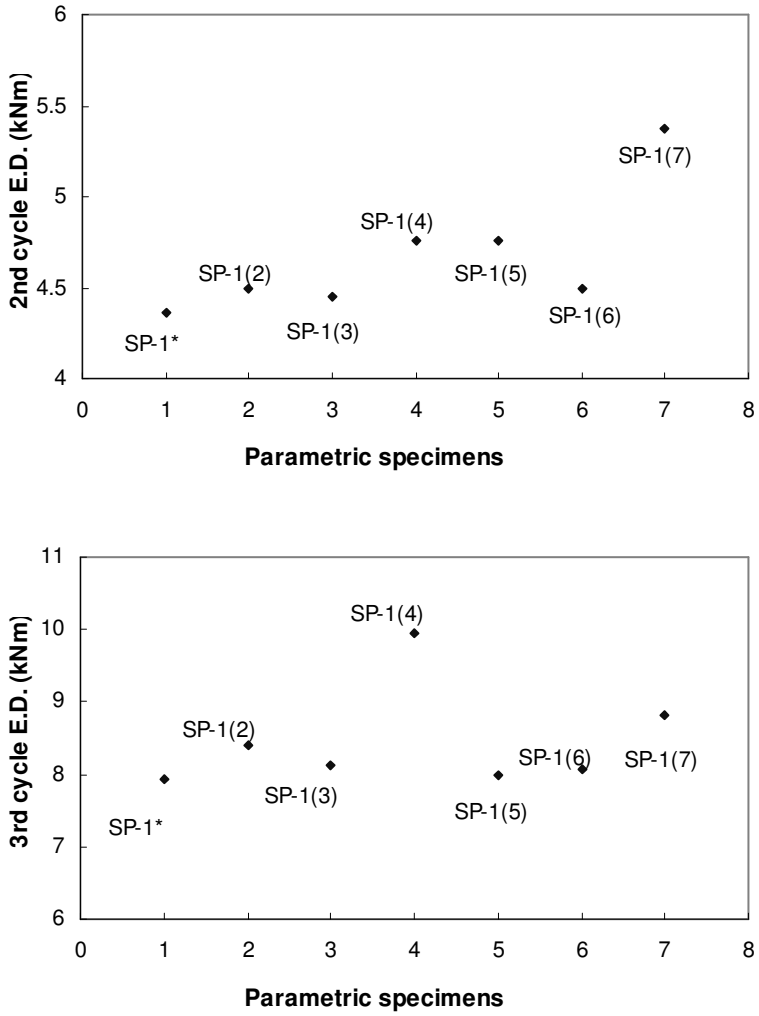

Fig. 6.38 Energy dissipation (E.D.) of the parametric specimens from SP-1 towards upgradation

During the numerical analysis, it has been found that along with the change in strength and energy dissipation of the parametric specimens, formation of cracks depends on the arrangement of the additional components with the original 'GLD' specimen. To describe the events, crack formation in last two cycles (50 mm and 75 mm) under negative (downward) and positive (upward) displacements for SP-1, SP-1(3), SP-1(5) and SP-1(7) are shown in *Fig. 6.39*. SP-1(2) and SP-1(4) are intentionally not presented here as those are the same cases as SP-1(3) and SP-1(5) without any bond or contact behaviour, respectively. Further SP-1(6) is the 'GLD' specimen with just joint confinement whereas additional laminates are used in SP-1(7). So, the results from SP-1(6) are also excluded for brevity.

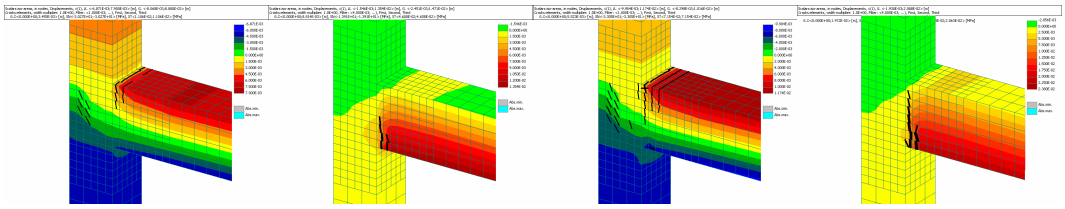

(a) Crack development in SP-1

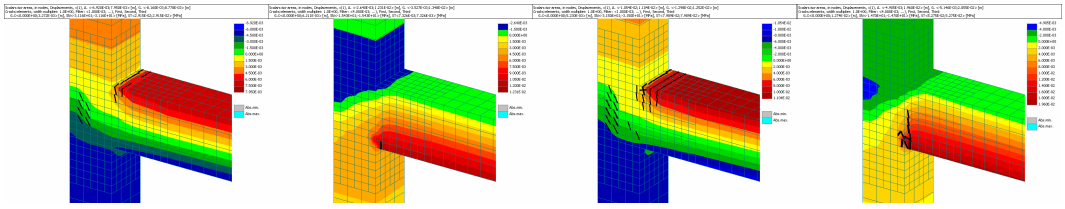

(b) Crack development in SP-1(3)

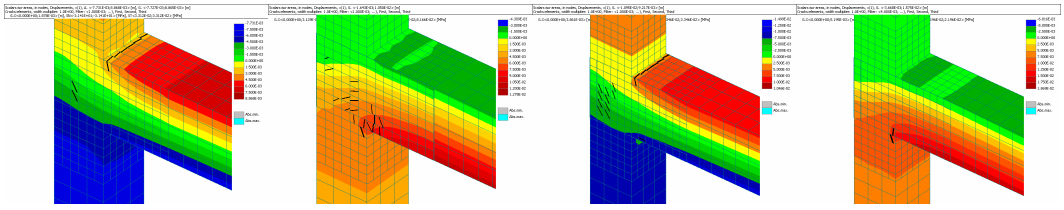

(c) Crack development in SP-1(5)

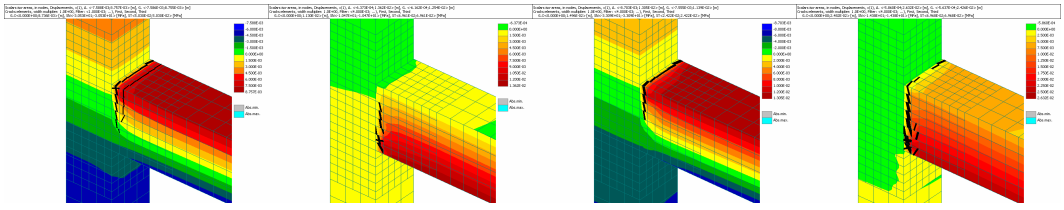

(d) Crack development in SP-1(7)

Fig. 6.39 Formation of crack during cyclic load in different parametric specimens

A few salient observations made from this study (as shown in *Fig. 6.39*) needs to be mentioned which would guide to the further attempt(s) for development of upgradation scheme or to optimize the usage of material. (i) Similar to the observation made from the capacity of energy dissipation (*Fig. 6.38*), mere application of laminates in beam bottom up to D region (to act as an anchorage) would not serve the purpose for shifting the plastic hinge. Though up to certain extent, it will arrest the development of crack at beam-column joint line during upward loading, this mechanism alone is seen to be insufficient in either strength enhancement, energy dissipation or development of plastic hinge at a safe distance. (ii) “U” wrap around the joint definitely helps in delaying the development of crack at vulnerable location, and application of “U” wrap and interface behaviour play a more important role than the strength of wrapping itself. (iii) When extra laminates are provided at both top and bottom of the beam along with the steel plate on joint [SP-1(7)], the figure shows that amount of laminates is not sufficient to shift the plastic hinge. Hence, major damage takes place along

the beam-column joint line. It is significant to mention that application of steel plate on joint provides the rigidity to the joint system and hence a sudden change in stiffness occurs along the beam. This causes a concentrated damage along beam-column joint line. It can be mentioned that unless adequate strengthening of beam (up to certain length) is done, intermediate upgradation of joint by application of plate is not optimum. (iv) For all the parametric specimens, efficiency in respect to energy dissipation and propagation of damage can be inter-related (*Fig. 6.38* and *Fig. 6.39*) which can help in deciding their performance. Further, similar to the observations made during experimental investigations, propagation of damage and location of plastic hinge formation demand more importance than other structural parameters in deciding their seismic performance. (v) The study though brings out the contribution of each of the upgradation components, however it shows that none of the intermediate upgradation schemes studied here [SP-1(2) to SP-1(7)] could alone provide the desirable behaviour (as shown in *Fig. 6.32* and *Fig. 6.33*). But, a combination of them would certainly be the feasible option (as discussed in section 6.4.2). It is worth mentioning that a proper upgradation can be achieved by strengthening the joint using steel plate, beam and column components using FRP, and a proper continuity between joint and beam by “U” wrap. In the same time, it needs to adequately confine the beam up to D-region by FRP wrapping to ensure the formation of the plastic hinge away from the joint and at a safe distance along the beam since incorporation of adequate flexural strengthening (for shifting plastic hinge) by providing extra reinforcement (in form of laminate, fiber or conventional reinforcement) may not always be practicable.

6.5 Summary on numerical studies

In the present study, the non-linear Finite Element (FE) program ATENA which is exclusively formulated for reinforced concrete structures has been employed for analysing the beam-column sub-assemblages of the existing structures which were considered for experimental investigations in the present study. It has been found that the results, in terms of load-displacement hysteresis and damage pattern, obtained from the numerical analysis are in close agreement with that obtained from the experimental investigations. Then, it was attempted to correlate the energy dissipation obtained from the numerical analysis with the experimental response. The proposed relations would certainly help the practicing engineers to obtain the guideline on the performance of any proposed beam-column sub-assemblage for seismic loading and can provide a scope for further improvement in the detailing of the sub-assemblage. Axial load effect on the seismic performance of the sub-assemblages was also numerically investigated. Further, the numerical analysis of the upgraded specimens was performed using the proper geometric- and material- modelling. During these studies,

computational aspects were suitably taken care of. The study shows that the appropriate and judicious use of the numerical analysis can be able to predict a considerably close response of the upgraded specimens as that was obtained from the experimental studies. Finally, a series of numerical studies have been carried out on the parametric specimens derived from the upgradation schemes proposed in this study. It is found that flexural strengthening up to a predefined length along the beam with adequate wrapping would provide the optimum seismic behaviour of the sub-assemblages. Hence, the laminates of the proposed upgradation scheme SP1-U2 can be terminated at a distance (≥ depth of the member) along the length of the beam without changing the amount of wrapping. Among the parametric specimens derived from SP1-U3, it is found that the upgradation scheme proposed in the study (SP1-U3) is showing the most impressive behaviour and hence, the same scheme may be attempted for further improvement using other materials. It is also observed that an inadequate wrapping would not only reduce energy dissipation, but formation of plastic hinge at specified area is not possible as well. The studies with various parameters would definitely enlighten the scopes for further improvement, alteration and optimisation. Further, an effort has been given to bring out the role and importance of individual components that have been proposed as the contributors of the proposed upgradation schemes. It is opined that their individual performance would pave the way for further development of upgradation schemes as well.

7 Conclusions and recommendations for further research

7.1 Summary and conclusions

In this study, it was attempted to explore the behaviour of critical regions of reinforced concrete (RC) structures under cyclic loading. For that, a commonly used 3-storied reinforced concrete building was considered and the most critical region was identified as the exterior beam-column joints (sub-assemblages). Primarily, the structure was analysed for dead-, live- and seismic- loadings and designed according to Eurocode and Indian Standard provisions. For obtaining the seismic forces, response spectrum analysis was carried out based on the spectra given in Eurocode 8. The main reason for choosing these two codes of practice (Eurocode and Indian Standard) is their enormous usage in seismic prone areas but lack of adequate attention in reported studies. Three different stages of design practice were considered, i.e., (i) gravity load designed ('GLD'), (ii) seismically designed but without any special ductile detailing ('NonDuctile'), and. (iii) seismically designed and detailed with proper ductile provisions ('Ductile'). Since the existing 'GLD' and 'NonDuctile' structures are vulnerable to any future earthquake, seismic performance of these structures is immensely important and studied in depth.

For evaluating the seismic performance, both experimental and analytical studies were carried out. The test set up was arranged on the test floor so that the beam-column sub-assemblage could be rest on the floor and the cyclic load was applied in the plane of the test floor. All the specimens were instrumented with LVDTs, strain gages and load cells, and an approximate axial load of 300 kN was applied in the column. In the cyclic load test, three complete cycles were performed at each displacement ductility level. From the test, it was found that 'GLD' specimen could hardly withstand any reverse loading due to insufficient reinforcement, inadequate bond capacity of bottom main reinforcement and poor detailing. Among the 'NonDuctile' specimens, failure pattern of both the specimens (based on Indian Standard and Eurocode) was qualitatively same and in either case, energy dissipation was mainly through the damage in joint region. Nevertheless, Indian Standard based specimen exhibited better performance (with a 33% more energy dissipation capacity, 12% less strength deterioration and 19% less stiffness degradation) over the Eurocode based specimen. It is also worth mentioning that the performance of both 'NonDuctile' specimens was well below the acceptable level for seismic design. Analytically, shear carrying capacity

of the joints using softening strut and tie model and moment carrying capacities of beam and column sections using moment-curvature relations were evaluated. Due to the non-uniformity among the provisions, for comparative studies, shear strength of the beam and column sections were calculated from different codes of practice [ACI 318-02, CSA-1994, NZS-3101, IS-456-2000 and Eurocode 2]. Finally, strength hierarchy of all the specimens was developed based on the results from analytical studies, and checked through experimental results, for identification of any need for further improvement and their quantification (if any).

It was then explored, in the present investigation, on how effectively retrofitting can be done for damaged structural components which can be re-used without compromising the safety issues. Towards this, an effective, simple and economical retrofitting scheme has been proposed for the damaged 'NonDuctile' and 'Ductile' specimens by judiciously using GFRP and steel plate. Well reported limitations and problems in using both the materials in RC joints were restricted since the joint concrete was confined by steel plate using through-through bolts and GFRP wrapping was applied beyond the joint zone. Surface treatment and epoxy injection were carried out to re-install concrete integrity and bond. After experimental studies on the retrofitted 'NonDuctile' specimen, though it performed well, a minor modification was made by using a horizontal "U" wrap of GFRP on the joint of damaged 'Ductile' specimen, for better continuity in components around the joint of the sub-assemblage. It was found from the experiments that, although both the specimens were severely destroyed, it could be retrofitted to its original stage and even better than original.

By this way, the short-comings of the 'NonDuctile' specimen were also improved for better performance. For example, strength degradation of the original and retrofitting 'NonDuctile' specimen was 55% (at drift ratio 7.7) and 15% (at drift ratio 11.2), respectively. Similarly, stiffness degradation of the original and retrofitting 'NonDuctile' specimen was 85% (at drift ratio 7.7) and 74% (at drift ratio 11.2), respectively. In 'Ductile' specimen, at the same drift ratio of 12.2, strength degradation of the original and retrofitting specimen was 48% and 7%, respectively. Similarly, stiffness degradation of original and retrofitting specimen was 91% and 81%, respectively. It is to mention that the cumulative energy dissipation of both the specimens was improved after retrofitting. To illustrate, due to retrofitting, enhancement in energy dissipations was observed to be 25% and 15% for 'NonDuctile' and 'Ductile' specimens. Further, energy dissipation in every cycle was monotonically increasing in both retrofitted specimens which was not observed in original specimens. This is also one of the most significant aspects for seismic energy dissipation. For 'NonDuctile' specimen, it is noted that ultimate deformation capacity of the specimen could be successfully increased due to retrofitting. Hence, it is to be stated that the retrofitting schemes as proposed in this study

can effectively be implemented for severely damaged 'Nonductile' or 'Ductile' structural components for their further usage.

The next focus was to upgrade the under-designed 'GLD' structures since extremely poor performance of those structures is witnessed from the previous earthquakes and has been quantitatively estimated in the present experimental study as well. In spite of increasing seismic risk, this type of structures is present throughout the world in massive quantity; so an upgradation scheme is utmost important which is reasonably practicable, considerably effective and economically viable as well. The expertise obtained from the proposed retrofitting schemes was utilised for upgradation with appropriate modifications. Demand strengths of the beam, column sections and joint were evaluated analytically and ductility requirements were decided from the common code of practice. Using the analytical formulation, a detailed study was carried out on improvement of strength and ductility due to application of external reinforcement and confinement (fixed and variable). Finally, three schemes were developed where in first two schemes CFRP fabric and CFRP laminate were respectively used for flexural strengthening, GFRP wrap was employed for confinement of beam and column sections, and steel plate-bolt system was adopted for confinement and shear strength enhancement in the joint. Finally, the third scheme was developed which was similar to that of first upgradation scheme but only the D-region was upgraded without any strength upgradation of beam and column section beyond the D-region. In first two schemes, all the members were upgraded based on their demand whereas the last scheme was intentionally kept unattended beyond the D-region. All three upgraded specimens were tested under identical cyclic load. Cyclic load history was used as same as that adopted for the previous test on performance evaluation of the 'GLD' specimen. At each level of displacement, three repeated cycles were used. The displacement levels for the 'GLD' specimen were ±25 mm and ±50 mm while for the upgradation schemes, two more displacement levels, i.e., ±75 mm and ±100 mm were considered.

It was observed that the responses of the upgraded specimens were way ahead of the existing 'GLD' specimen. It was evident that the upgraded specimens were able to provide a very good seismic performance. Main damage occurred in the first upgraded specimen at the joint line without much damage in joint as column was still active in carrying axial load. In second specimen, main damage took place at a distance D (equals to depth of the member) from the joint face along the beam. On the other hand, main damage in the third upgraded specimen was observed at a distance D from the joint face before imposition of final displacement. But, during final displacement, a second line of damage was found at beam-column joint line which showed a sign of spread plastic zone starting from the joint face up to a distance D along the beam length. It was noticed that the stiffness degradation and

strength deterioration were much slower and even, with almost same stiffness degradation and strength deterioration, double the displacement ductility could be achieved. Per cycle- and cumulative- energy dissipation were much higher and improved than the original 'GLD' specimen. It is to mention that the first upgraded specimen dissipated maximum energy during 50 mm displacement cycle whereas the second upgraded specimen dissipated maximum energy during 75 mm displacement cycle. It is also to note that the third upgraded specimen provided almost uniform energy dissipation in first cycles of 50 mm, 75 mm and 100 mm. Cumulative energy dissipation at each displacement level was almost same for all the upgraded specimens. At a displacement level of 50 mm and at final displacement level (100 mm), cumulative energy dissipation was 2- and 5- times, respectively, higher than original 'GLD' specimen. It was also evaluated that the cumulative energy dissipation was 20% more than Eurocode based 'NonDuctile' specimen and was similar to that obtained from Indian Standard based 'NonDuctile' specimen. Further, the cumulative energy dissipation from upgraded specimens was almost same as that reported for 'Ductile' specimen based on Eurocode. It is significant to note that in the upgraded specimens, formation of damage at a predefined location (away from the critical region) could successfully be achieved. Moreover, in the third upgraded specimen (only in D-region), spread plastic hinge in the beam region had been formed which guarantees a large and consistent dissipation of energy with increase in drift demand. Further, considerable reduction in the problem caused from inherent lack in anchorage of beam bottom reinforcements during reverse loading was observed. A step by step method for upgradation of deficient beam-column sub-assemblages is described in *Appendix (B)*.

Finally, in addition to experimental and analytical studies, non-linear Finite Element analysis using software ATENA was carried out on 'GLD', 'NonDuctile' and upgraded specimens. Concrete components were modelled using solid elements with special truss elements to present the reinforcement. For upgraded specimens, all fiber FRPs and steel plate were modelled with thin shell elements. Composite fibers were modelled using layered shell element with appropriate properties. The results obtained from numerical analyses of both existing and upgraded specimens were in good agreement with the experimental results. It is important to note that numerical simulation of the FRP based upgraded specimens is extremely computation intensive and space demanding. This aspect becomes more critical when a cyclic load analysis is carried out and the problem adds severity with the requirement for incorporation of bond-slip behaviour and/or interface contact element. Using the validated numerical models, it was proposed to correlate the energy dissipation from numerical analysis to that from experimental analysis. It would be helpful in practice to evaluate the seismic performance of the critical sub-assemblages before construction, using the numerical analysis itself. Further, it was found that the issues like effect of axial load in

changing strength and energy dissipation under cyclic load have attracted attention from a number of researchers but they have reported the inconsistent observations from their experimental investigations. Hence, in the numerical studies, this issue has been studied in details with the variation of axial load ratios (ratio is defined by applied axial load divided by axial strength). It is noted that increase in axial load in column will provide a better seismic response (in terms of strength and energy dissipation) for the structures under low drift demand. Under high drift demand, it has been found that higher axial load brings the brittleness in the sub-assemblages and results in sudden failure. It has also been found that reduction in energy dissipation with higher axial load and higher drift ratio is more in Eurocode based 'NonDuctile' specimen in comparison to the Indian Standard based specimen. It can be stated that, in low seismic zones, increase in axial load may be an option for strengthening the RC sub-assemblages, but in high seismic risk areas, it will not only be invalid and insufficient, but could bring adverse effect due to the increase in brittleness in the member with increase in axial load.

Further, the validated numerical models of upgraded specimens were used to conduct an investigation on the effects of amount of bending FRP, number of wrapping layers, effect of bond behaviour etc. The study points out that reduction in energy dissipation would take place with reduction in addition bending laminates, and efficiency among the parametric upgraded specimens becomes more prominent in higher cycles. It is noteworthy to mention that a proper detailing up to D-region by adopting flexural strengthening and wrapping, and adequate joint strengthening would provide the most promising result. It is evident from the study that better confinement would definitely help in enhancing energy dissipation capacity of the parametric specimens and the rate of enhancement consistently increases in higher cycles. Moreover, in spite of good wrapping, a lack in flexural strengthening would limit the improvement of the specimen. Among the intermediate strengthened specimens, it has been observed that "U" wrap is a promising component, provided the interaction between concrete and FRP is improved. A 'GLD' specimen with steel plate at joint and additional laminates at both top and bottom of beam would be a viable solution if the flexural strengthening is sufficient to shift the plastic hinge, otherwise a very stiff joint followed by an inadequately strengthened beam leads to a damage near the joint which is not optimal.

To conclude, the study as a whole brings out the seismic behaviour of one of the most critical components of existing RC structures designed based on two different codes of practice prior to ductility detailing. Further, the study proposes the strategies for retrofitting of severely damaged beam-column sub-assemblages for their further use. The study has later focused on the development of suitable upgradation schemes for poorly designed structural components for avoiding any catastrophic failure. Moreover, the numerical studies carried

out and the models proposed would provide the effective tools for performance evaluation and possible improvements of both existing and upgraded sub-assemblages.

7.2 Recommendations for further research

It is opined that the study would pave the way for further research on strengthening and rehabilitation of existing RC structures, in general, and steel plate-FRP based hybrid scheme, in particular. It is suggested that the following aspects need to be given adequate attention in future:

(1) Seismic performance of irregular and eccentric connections

Since most of the critical regions of RC structures are not regular and symmetric and with the demand from utility and architectural viewpoint, most of the beam-column joints are with irregularity and eccentricity. These connections need to be evaluated for their seismic performance. Force flow mechanism, damage pattern, shear strength criteria and design parameters require to be investigated.

(2) Rate dependent seismic response of beam-column joints

Most of the studies including the present one consider a slow rate of loading to investigate the change in structural behaviour parameters during cyclic loading. Since the seismic loading is truly random and extremely fast, it does have a considerable impact on the structural response. Thus, a vast range of rates of cyclic loading can be considered for further studies.

(3) Influence of nature of cyclic loading on seismic response of beam-column joints

It is understood from the review of literature that the influence of repetition in cyclic loading has a commendable effect on stiffness degradation, strength deterioration and energy dissipation. Hence, number of repeating cyclic loading at each level, direction of loading and level of increment in each stage should be exclusively studied.

(4) Dynamic analysis of beam-column joints

Dynamic analysis of beam-column joints is absolutely scarce and needs better attention. Behaviour of original, retrofitting or strengthened specimens under real time history loading or pseudo-dynamic loading would bring out much realistic behaviour of the structures exposed to seismic loading.

(5) Retrofitting of RC structures in global perspective

RC structures with fully or partly damaged components could be successfully retrofitted using steel plate-FRP hybrid system. But, the global response of damaged structure before and after retrofitting needs to be thoroughly evaluated since the locations of energy dissipation could be shifted to new places and in different forms. For that, shake table or performance based push-over test can be carried out on full scale or scaled structural model.

(6) Upgradation of poorly designed RC structures in global perspective

The study presented here is confined to the local structural components. Hence, the global response of upgraded structure needs to be assessed meticulously. For that, shake table or performance based push-over test on full scale or scaled original existing and upgraded structural model can be undertaken.

(7) Detailed parametric study on disposition of material in strengthened structure

From the present study, it is found that a hybrid steel plate-FRP system could make the retrofitting and upgradation of the structure/components very effective. In the next step, it is required to investigate (both experimentally and numerically) the effect of confinement on improvement in concrete constitutive model. Further, the disposition and quantity of material, properties of contact surface and bond behaviour could further be optimised by extended studies and using other types of fabrics available in market. There is also a great scope to include these schemes for retrofitting and upgradation in codes of practice after a rigorous study, evaluation and characterization.

References

1. Aboutaha, R.S., Engelhardt, M.D., Jirsa, J.O. and Kreger, M.E. (1999a), "Rehabilitation of shear critical concrete columns by use of rectangular steel jackets", ACI Structural J., 96(1), 68-78.
2. Aboutaha, R.S., Engelhardt, M.D., Jirsa, J.O. and Kreger, M.E. (1999b), "Experimental investigation of seismic repair of lap splice failures in damaged concrete columns", ACI Structural J., 96(2), 297-306.
3. ACI-ASCE Committee 352, "*Recommendations for Design of Beam-Column Joints in Monolithic Reinforced Concrete Structures*", American Concrete Institute, 1976.
4. ACI-ASCE Joint Committee 352, "*Recommendations for Design of Beam-Column Connections in Monolithic Reinforced Concrete Structures* (ACI 352R-02)," American Concrete Institute, Farmington Hills, Mich., 2002, 37 pp.
5. Adin, M.A., Yankelevsky, D.Z. and Farhey, D.N. (1993), "Cyclic behavior of epoxy-repaired reinforced concrete beam-column joints", ACI Structural J., 90(2), 170-179.
6. Ahmad, S.H. and Shah, S.P. (1985), "Behavior of hoop confined concrete under high strain rates", ACI J. Proc., 82(5), 634-647.
7. Aidoo, J., Harries, K.A. and Petrou, M.F. (2004), "Fatigue behavior of carbon fiber reinforced polymer-strengthened reinforced concrete bridge girders", J. of Composites for Construction, ASCE, 8(6), 501-509.
8. Aidoo, J., Harries, K.A. and Petrou, M.F. (2006), "Full-scale experimental investigation of repair of reinforced concrete interstate bridge using CFRP materials", J. of Bridge Engineering, 11(3), 350-358.
9. Alaee, F.J. and Karihaloo, B.L. (2003), "Retrofitting of reinforced concrete beams with CARDIFRC", J. of Composites for Construction, ASCE, 7(3), 174-186.
10. Alcocer, S.M. and Jirsa, J.O. (1993), "Strength of reinforced concrete frame connections rehabilitated by jacketing", ACI Structural J., 90(3), 249-261.
11. Al-Sulaimani, G.J., Sharif, A., Basunbul, I.A., Baluch, M.H. and Ghaleb, B.N. (1994), "Shear repair for reinforced concrete by fiberglass plate bonding", ACI Structural J., 91(4), 458-464.
12. American Concrete Institute Committee ACI 318-89, "*Building Code Requirements for Reinforced Concrete* (ACI 318-89)", American Concrete Institute, Detroit, 1989, 351 pp.
13. American Concrete Institute Committee ACI318-02 "*Building Code Requirements for Reinforced Concrete* (ACI 318-02)", ACI 318-95, 99, 02, Detroit, Michigan, 1995, 1999, 2002.
14. Antonopoulos, C.P. and Triantafillou, T.C. (2003), "Experimental investigation of FRP-strengthened RC beam-column joints", J. of Composites for Construction, ASCE, 7(1), 39-49.
15. ATENA theory manual (2006), "ATENA Program Documentation - Part 1: Theory", Revision 09/2006, Cervenka Consulting, Predvoje 22, Czech Republic, 207 pp.
16. Aycardi, L.E., Mander, J.B. and Reinhorn, A.M. (1994), "Seismic resistance of reinforced concrete frame structures designed only for gravity loads: Experimental performance of sub-assemblages, ACI Structural J., 91(5), 552-563.
17. Balsamo, A., Colombo, A., Manfredi, G., Negro, P. and Prota, A. (2005), "Seismic behavior of a full-scale RC frame repaired using CFRP laminates", Engineering Structures, 27(5), 769-780.
18. Bazant, Z.P. and Oh, B.H (1983), "Crack band theory for fracture of concrete", Materials and Structures, RILEM, 16(93), 155-177.
19. Beaufait, F. and Williams, R.R. (1968), "Experimental study of reinforced concrete frames subjected to alternating sway forces", ACI J. Proc., 65(11), 980-984.
20. Beres, A., El-Borgi, S., White, R.N. and Gergely, P. (1992), "Experimental results of repaired and retrofitted beam-column joint tests in lightly reinforced concrete frame buildings", NCEER Technical Rep. No. 92-25, State Univ. of New York, Buffalo, N.Y.
21. Bett, B.J., Klingner, R.E. and Jirsa, J.O. (1988), "Lateral load response of strengthened and repaired reinforced concrete columns", ACI Structural J., 85(5), 499-508.
22. Biddah, A., Ghobarah, A. and Aziz, T.S. (1997), "Upgrading of nonductile reinforced concrete frame connections", J. of Structural Engineering, ASCE, 123(8), 1001-1010.

23. Bizindavyi, L., Neale, K.W. and Erki, M.A. (2003), "Experimental investigation of bonded fiber reinforced polymer-concrete joints under cyclic loading", J. of Composites for Construction, ASCE, 7(2), 127-134.
24. Bligh, R.A., Fischer, S. and Ghosh, S.K. (2005), "Structural retrofit of special moment-resisting frames of concrete", Concrete International, 27(6), 47-53.
25. Bracci, J.M., Reinhorn, A.M. and Mander, J.B. (1995), "Seismic resistance of reinforced concrete buildings designed for gravity loads: performance of structural system", ACI Structural J., 92(5), 597-609.
26. BS 8110, "*Structural Use of Concrete- Code of Practice for Design and Construction*", London: British Standards Institution, 1985.
27. Calvi, G.M., Magenes, G. and Pampanin, S. (2002), "Relevance of beam-column joint damage and collapse in RC frame assessment", J. of Earthquake Engineering, 6(1), 75-100.
28. Canadian Standards Association (1994), "*Design of Concrete Structures* A23.3-94", Canadian Standards Association (CSA-1994), Rexdale, Ontario.
29. Carreira, D.J. and Chu, K. H. (1985), "Stress-strain relationship for plain concrete in compression", ACI Structural J., 83(6), 797-804.
30. Castellani, A., Negro, P., Colombo, A., Grandi, A., Ghisalberti, G. and Castellani, M. (1999), "Carbon fiber reinforced polymers (CFRP) for strengthening and repairing under seismic actions", Special Publication No. I.99.41, European Laboratory for Structural Assessment, Joint Research Center, Ispra, Italy.
31. CEN Technical Committee 250, "*Eurocode 2: Design of Concrete Structures-Part:1-1: General Rules and Rules for Buildings"* (EN 1992-1-1:2004), CEN, Berlin, Germany, 2005, 248 pp.
32. CEN Technical Committee 250/SC8, "*Eurocode 8: Design of Structures for Earthquake Resistance-Part: 1: General Rules, Seismic Actions and Rules for Buildings"* (ENV 1998-1:2004)," CEN, Berlin, Germany, 2006, 192 pp.
33. Chai, Y.H., Priestley, M.J.N. and Seible, F. (1991), "Seismic retrofit of circular bridge columns for enhanced flexural performance", ACI Structural J., 88(5), 572-584.
34. Chajes, M., Chou, T., Pan, Z. and Pan, D. (1998), "The retrofitting of reinforced concrete column-to-beam connections", Composites Science and Technology. 58, 1297-1305.
35. Chang, S.-Y., Li, Y.-F. and Loh, C.-H. (2004), "Experimental study of seismic behaviors of as-built and carbon fiber reinforced plastics repaired reinforced concrete bridge columns", J. of Bridge Engineering, ASCE, 9(4), 391-402.
36. Cheng, C. -T., Yeh, Y. -K. and Mo, Y. -L. (2004), "Flexural repair of hollow rectangular bridge columns failed due to earthquake-type loading", Materials and Structures, 37(274), 717-723.
37. Cheng, C.-T., Mo, Y.L. and Yeh, Y.-K. (2005), "Evaluation of as-built, retrofitted, and repaired shear-critical hollow bridge columns under earthquake-type loading", J. of Bridge Engineering, ASCE, 10(5), 520-529.
38. Comite Euro-International du Beton (CEB) (1990), "*CEB Model Code 90*", Bull. d'information, No. 203, Paris, France.
39. Corazao, M. and Durrani, A.J. (1989), "Repair and strengthening of beam-to-column connections subjected to earthquake loading", Tech. Rep., NCEER 89-0013, National Center for Earthquake Engineering Research, State University of New York at Buffalo, N.Y.
40. Corte, G.D., Barecchia, E. and Mazzolani, F.M. (2006), "Seismic upgrading of RC buildings by FRP: Full-scale tests of a real structure", J. of Materials in Civil Engineering, 18(5), 659-669.
41. Darwish, I.S., Saiidi, M. Saiid and Sanders, D.H. (1999), "Seismic retrofit of hinged and fixed reinforced concrete bridge columns with short bar anchorage in footings", ACI Structural J., 96(6), 988-996.
42. D'Ayala, D., Penford, A. and Valentini, S. (2003), "Use of FRP fabric for strengthening of reinforced concrete beam-column joints", In: 10th International conference on Structural faults and Repair, London.
43. Dhakal, R.P., Pan, T.-C., Irawan, P., Tsai, K.-C., Lin, K.-C. and Chen, C.-H. (2005), "Experimental study on the dynamic response of gravity-designed reinforced concrete connections", Engineering Structures, 27(1), 75-87.
44. Dogan, E. and Opara, N.K. (2003), "Seismic retrofit with continuous slurry-infiltrated mat concrete jackets", ACI Structural J., 100(6), 713-722.

45. Durrani, A.J. and Wight, J.K. (1985), "Behavior of interior beam-to-column connections under earthquake-type loading", ACI J. Proc., 82(3), 343-349.
46. Dutta, A. and Mander, B. (2001), "Energy based methodology for ductile design of concrete columns", J. of Structural Engineering, ASCE, 127(12), 1374-1381.
47. Ehsani, M.R. and Wight, J.K. (1985), "Exterior reinforced concrete beam-to-column connections subjected to earthquake-type loading", ACI J. Proc., 82(4), 492-499.
48. El-Amoury, T. and Ghobarah, A. (2002), "Seismic rehabilitation of beam–column joint using GFRP sheets", Engineering Structures, 24(11), 1397-1407.
49. El-Attar, A.G., White, R.N. and Gergely, P. (1997), "Behaviour of gravity load design reinforced concrete buildings subjected to earthquakes", ACI Structural J., 94(2), 133-145.
50. Elwood, K.J. and Moehle, J.P. (2002), "Shake table tests on the gravity load collapse of reinforced concrete frames", Seventh US National Conference on Earthquake Engineering, Boston, MA, Earthquake Engineering Research Institute.
51. ERC-1995, "*New Greek Earthquake Resistant Code*," Athens, Greece, 1995, 145 pp. (in Greek).
52. "Erdbebensicher Bauen", Planungshilfe für Bauherren, Architekten und Ingenieur, from Wirtschaftsministerium (Ministry of finance), Baden-Württemberg, 2001.
53. Estrada JI. (1990), "Use of steel elements to strengthen a reinforced concrete building", M.Sc. thesis, University of Texas at Austin.
54. FEMA 273 (1997), "*NEHRP Guidelines for the Seismic Rehabilitation of Buildings*", Report No. FEMA-273, Federal Emergency Management Agency, Washington D.C.
55. FIB Bulletin 14 (2001), "*Externally Bonded FRP Reinforcement for RC Structures*", Technical report on the Design and use of externally bonded fibre reinforced polymer reinforcement (FRP EBR) for reinforced concrete structures, 139 pp.
56. FIB Bulletin 24 (2003), "*Seismic Assessment and Retrofit of Reinforced Concrete Buildings*", State-of-art report prepared by Task Group 7.1, 306 pp.
57. Frangou, M., Pilakoutas, K. and Dritsos, S. (1995), "Structural repair/strengthening of RC columns", Construction and Building Materials, 9(5), 259-266.
58. Fuelong, R.W. (1967), "Strength of steel-encased concrete beam columns", J. of Structural Engineering, ASCE, 93, 113–24.
59. Geng, Z.-J., Chajes, M.J., Chou, T.-W. and Pan, D.Y.-C. (1998), "The retrofitting of reinforced concrete column-to-beam connections", Composite Science and Technology, 58(8), 1297-1305.
60. Gergely, J., Pantelides, C.P. and Reaveley, L.D. (2000), "Shear strengthening of RC T-joints using CFRP composites", J. of Composite for Construction, ASCE, 4(2), 56-64.
61. Ghee, A.B., Priestley, M.J.N. and Paulay, T. (1989), "Seismic shear strength of circular reinforced concrete columns", ACI Structural J., 86(1), 45-59.
62. Ghobarah, A., Aziz, T.S. and Biddah, A. (1997), "Rehabilitation of reinforced concrete frame connections using corrugated steel jacketing", ACI Structural J., 94(3), 282–294.
63. Ghosh, K.K. and Sheikh, S.A. (2007), "Seismic upgrade with carbon fiber reinforced polymer of columns containing lap-spliced reinforcing bars", ACI Structural J., 104(2), 227-236.
64. Grace, N.F., Abdel-Sayed, G. and Ragheb, W.F. (2002), "Strengthening of concrete beams using innovative ductile fiber reinforced polymer fabric", ACI Structural J., 99(5), 692-700.
65. Hakuto, S., Park, R. and Tanaka, H. (2000), "Seismic load tests on interior and exterior beam-column joints with substandard reinforcing details", ACI Structural J., 97(1), 11-25.
66. Hamilton, C.H., Pardoen, G.C., Navalpakkam, S. and Kanzanjy, R.P. (2004), "Reinforced concrete bridge column performance enhancement through shotcrete jacketing", ACI Structural J., 101(3), 332-340.
67. Han, S.W. and Jee, N.Y. (2005), "Seismic behaviours of columns in ordinary and intermediate moment resisting concrete frames", Engineering Structures, 27(6), 951–962.
68. Harajli, M.H. and Rteil, A. A. (2004), "Effect of confinement using fiber reinforced polymer or fiber reinforced concrete on seismic performance of gravity load-designed columns", ACI Structural J., 101(1), 47-56.
69. Harajli, M.H. (2007), "Cyclic response of concrete members with bond-damaged zones repaired using concrete confinement", Construction and Building Materials, 21(5), 937-951.
70. Harries, K., Ricles, J., Pissiki, S. and Sause, R. (2006), "Seismic retrofit of lap splices in nonductile columns using CFRP jackets", ACI Structural J., 103(6), 226-236.

71. Hoffschild, T.E., Prion, H.G.L. and Cherry, S. (1993), “Seismic retrofit of beam-to-column joints with grouted steel tubes”, Proc. Tom Paulay Symp. on Recent Development in Lateral Force Transfer in Buildings, 403-431.
72. Hognestad, E. (1951), “A study of combined bending and axial load in reinforced concrete members”, Bull, ser. No. 399, Univ. of Illinois Eng Experimental Station, Champaign, III.
73. Hoshikuma, J., Kawashima, K., Nagaya, K. and Taylor, A.W. (1997), “Stress-strain model for confined reinforced concrete in bridge piers”, J. of Structural Engineering, ASCE, 123(5), 624-633.
74. Hsu, T.T.C. (1993), “Unified Theory of Reinforced Concrete”, CRC Press, Boca Raton, Florida.
75. Hsu, T.T.C., Punurai, W., Jia, Y. and Bian, H. (2006), "Direct shear behaviour of CFRP laminates and concrete", J. of Testing and Evaluation, 34(3), 158-166.
76. Hwang, S.-J. and Lee, H.-J. (1999), “Analytical model for predicting shear strengths of exterior reinforced concrete beam-column joints for seismic resistance“, ACI Structural J., 96(5), 846-858.
77. Iacobucci, R.D., Sheikh, S.A. and Bayrak, O. (2003), “Retrofit of square concrete columns with carbon fiber reinforced polymer for seismic resistance”, ACI Structural J., 100(6), 785-794.
78. Indian Standard (IS 456-2000), “*Plain and Reinforced Concrete - Code of Practice*”, Bureau of Indian Standards, New Delhi, 2000.
79. Indian Standard (IS 13920-1993), “*Ductile Detailing of Reinforced Concrete Structures Subjected to Seismic Forces - Code of Practice*”, Bureau of Indian Standards, New Delhi, 2002.
80. Indian Standard (IS-1893-2002), “*Criteria for Earthquake Resistant Design of Structures. Part 1: General Provisions and Buildings*”, Bureau of Indian Standards, New Delhi. 2002.
81. Júlio, E.N.B.S., Branco, F.A.B. and Silva, V.D. (2005), “Reinforced concrete jacketing-interface influence on monotonic loading response”, ACI Structural J., 102(2), 252-257.
82. Karbhari, V.M. (1993), “Strengthening of concrete column stubs through resin infused composite wraps”, J. of Thermoplastic Composite Materials, 6, 93–107.
83. Knowles, R.B. and Park, R. (1969), “Strength of concrete filled steel tubular columns”, J. of Structural Engineering, ASCE, 95, 2565–2587.
84. Lim, K.Y. and McLean, D.I. (1991), “Scale model studies of moment-reducing hinge details in bridge columns”, ACI Structural J., 88(4), 465-474.
85. Lowes, L.N. and Moehle, J.P. (1999), “Evaluation of retrofit of beam-column T-joints in older reinforced concrete bridge structures”, ACI Structural J., 96(4), 519-532.
86. Ludovico, M. D., Nanni, A., Prota, A. and Cosenza, E. (2005), “Repair of bridge girders with composites: Experimental and analytical validation”, ACI Structural J., 102(5), 639-648.
87. Mander, J.B., Priestley, M.J.N. and Park, R. (1988), “Theoretical stress-strain model for confined concrete”, J. of Structural Engineering, ASCE, 114(8), 1804–1826.
88. Marsh, G. (1998), “Seismic retrofit provides opportunities for FRP”, Reinforced Plastics Magazine, 42(3), 38-43.
89. Mazzotti, C., Savoia, M. and Ferracuti, B. (2005), “A new set-up for FRP-concrete stable delamination test”, ACI special publication, 230, 165-180.
90. McLean, D.I. and Marsh, M.L. (1999), “Seismic retrofitting of bridge foundations”, ACI Structural J., 96(2), 174-182.
91. Menegotto, M. and Pinto, P.E. (1973), “Method of analysis of cyclically loaded R.C. plane frames including changes in geometry and non-elastic behaviour of elements under combined normal force and bending”, Proc. IABSE Symposium on Resistance and Ultimate Deformability of Structures Acted on by Well Defined Repeated Loads, 15-22.
92. Menétrey, P. and Willam, K.J. (1995), “Triaxial failure criterion for concrete and its generalization”, ACI Structural J., 92(3), 311-318.
93. Migliacci, A., Antonucci, R., Maio, N.A., Napoli, P., Feretti, A.S. and Via, G. (1983), “Repair techniques of reinforced concrete beam-column joints”, Final Rep., Proc. IABSE Symp. on Strengthening of Building Struct.-Diagnosis and Therapy, Int. Assn. of Bridge and Structure Engrg (IABSE), Switzerland, 355-362.
94. Mirmiran, A., Shahawy, M., Samaan, M., El-Echary, H., Mastrapa, J.C. and Pico, O. (1998), “Effect of column parameters on FRP-confined concrete”, J. of Composite for Construction, ASCE, 2(4), 175-185.

95. Mo, Y.L. and Nien, I.C. (2002), “Seismic performance of hollow high-strength concrete bridge columns”, J. Bridge Engineering, ASCE, 7(6), 338-349.
96. Moehle, J.P. (2000), “State of research on seismic retrofit of concrete building structures in the US”, US-Japan Symposium and Workshop on Seismic Retrofit of Concrete Structures-State of Research and Practice.
97. Mosallam, A. (1998), editor: “Advanced seismic repair and rehabilitation structural system”, In: Proceedings, CSUF State-of-the-Art Conference on Repair and Rehabilitation of Structures. Fullerton, CA. November 9. 201 pp.
98. Mosallam, A. (1999), “Seismic repair and upgrade of structural capacity of reinforced concrete connections: Another opportunity for polymer composites”, Proc., Int. Composites Expo ’99, Cincinnati, 1-8.
99. Mosallam, A.S. (2000), “Strength and ductility of reinforced concrete moment frame connections strengthened with quasi-isotropic laminates”, Composites Part B: Engineering, 31(6-7), 481-497.
100. Mosallam, A.S. and Banerjee, S. (2007), “Shear enhancement of reinforced concrete beams strengthened with FRP composite laminates”, Composites Part B: Engineering, 38(5-6), 781-793.
101. Nanni, A. and Norris, M.S. (1995), “FRP jacketed concrete under flexure and combined flexure-compression”, Construction and Building Materials, 9(5), 273-281.
102. Norris, T., Saadatmanesh, H. and Ehsani, M.R., (1997), “Shear and flexure strengthening of RC beams with carbon fiber sheets,” J. of Structural Engineering, ASCE, 123(7), 903-911.
103. Novák, B., Ramanjaneyulu, K., Roehm, C. and Sasmal, S. (2008), “Seismic performance of D-region of RC framed-structure designed according to different codal recommendations”, J. of Structural Engineering, 35(1), 46-51.
104. NZS 3101, “*The Design of Concrete Structures*“,1995, Standards New Zealand, Wellington, 1995.
105. Palermo, A., Pampanin, S. and Marriott, D. (2006), “Quasi-static tests of seismic resistant bridge piers with hybrid connections: comparison with monolithic solutions”, fib Proceedings of the 2nd International Congress, June 5-8, 2006, Naples, Italy.
106. Pampanin, S., Christopoulos, C. and Priestley, M.J.N. (2003), “Performance-based seismic response of frame structures including residual deformations. Part II: Multi-degree of freedom systems”, J. of Earthquake Engineering, 7(1), 119-147.
107. Pampanin, S., Christopoulos, C. and Chen, T.-H. (2006), “Development and validation of a metallic haunch seismic retrofit solution for existing under designed RC frame buildings”, Earthquake Engineering and Structural Dynamics, 35, 1739-1766.
108. Pantazopoulou, S.J. and Bonacci, J.F. (1994), “On earthquake resistant reinforced concrete frame connections”, Canadian J. of Civil Engineering, 21(2), 307-328.
109. Pantelides, C.P., Gergely, I., Reaveley, L.D. and Nuismer, R.J. (1997), “Rehabilitation of cap beam-column joints with carbon fiber jackets”, Proc., 3rd Int. Symposium on Non-Metallic (FRP) Reinforcement for Concrete Structures, Sapporo, Japan, Japan Concrete Institute, Tokyo, 1, 587–595.
110. Pantelides, C.P., Gergely, J., Reaveley, L.D. and Volnyy, V. (1999), “Retrofit of RC bridge pier with CFRP advanced composites”, J. of Structural engineering, ASCE, 125(10), 1094-1099.
111. Parra-Montesinos, G.J. and Wight, J.K. (2001), “Seismic repair of hybrid RCS beam-column connections”, ACI Structural J., 98(5), 762-770.
112. Parvin, A. and Granata, P. (2000), “Investigation on the effects of fiber composites at concrete joints”, Composites Part B: Engineering, 31(6), 499-509.
113. Paulay, T., Park, R. and Priestley, M.J.N. (1978), “Reinforced concrete beam-column joints under seismic actions”, ACI J. Proc., 75(11), 585-593.
114. Paulay, T. and Priestley, M.J.N. (1992), “Seismic Design of Reinforced Concrete and Masonry Buildings”, John Wiley & Sons, New York.
115. Popovics, S. (1973), “A numerical approach to the complete stress-strain curve of concrete”, Cement and Concrete Research, 3(5), 583-599.
116. Priestley, M.J.N., Seible, F., Xiao, Y. and Verma, R. (1994a), “Steel jacket retrofitting of reinforced concrete bridge columns for enhanced shear strength-Part 1: Theoretical considerations and test design”, ACI Structural J., 91(4), 394-405.

117. Priestley, M.J.N., Seible, F., Xiao, Y. and Verma, R. (1994b), “Steel jacket retrofitting of reinforced concrete bridge columns for enhanced shear strength-Part 2: Test results and comparison with theory”, ACI Structural J., 91(5), 537-551.
118. Priestley, M.J.N. (1997), “Displacement based seismic assessment of reinforced concrete buildings”, J. of Earthquake Engineering, 1(1), 157-192.
119. Priestley, M.J.N. and Park, R. (1987), “Strength and ductility of concrete bridge columns under seismic loading”, ACI Structural J., 84(1), 61-76.
120. Priestley, M.J.N., Seible, F. and Calvi, M. (1996), “Seismic Design and Retrofit of Bridges”, John Wiley & Sons, Inc., New York.
121. Prota, A., Nanni, A., Manfredi, G. and Cosenza, E. (2004), “Selective upgrade of underdesigned reinforced concrete beam-column joints using carbon fiber reinforced polymers”, ACI Structural J., 101(5), 699-707.
122. Pulido, C., Saiidi M. Saiid, Sanders, D., Itani, A. and El-Azazy, S. (2004a), “Seismic performance of two-column bents - Part I: Retrofit with carbon fiber reinforced polymer fabrics”, ACI Structural J., 101(4), 558-568.
123. Pulido, C., Saiidi M. Saiid, Sanders, D., Itani, A. and El-Azazy, S. (2004b), “Seismic performance of two-column bents -Part II: Retrofit with infill walls”, ACI Structural J., 101(5), 642-649.
124. Remmel, G. (1994), “Zum Zug- und Schubtragverhalten von Bauteilen aus hochfestem Beton“, Deutscher Ausschuss für Stahlbeton“, Beuth Verlag, Berlin, Germany, 1994, 77 pp.
125. Ritchie, P.A., Thomas, D.A., Lu, L. and Connelly, G.M., (1991), “External reinforcement of concrete beams using fiber reinforced plastics”, ACI Structural J., 88(4), 490-500.
126. Rodriguez, M. and Park, R. (1994), “Seismic load tests on reinforced concrete columns strengthened by jacketing”, ACI Structural J., 91(2), 150-159.
127. Rodriguez, M.E. and Santiago, S.A. (1998), “Simulated seismic load tests on two-story waffle-flat-plate structure rehabilitated”, ACI Structural J., 95(2), 129-141.
128. Saadatmanesh, H. and Ehsani, M. R., (1991), “RC beams strengthening with GFRP plates I: Experimental study”, J. of Structural Engineering, ASCE, 117(11), 3417-3433.
129. Saadatmanesh, H. (1997), “Extending service life of concrete and masonry structures with fiber composites”, Construction and Building Materials, 11(5-6), 327-335.
130. Said, A.M. and Nehdi, M.L. (2004a), “Use of FRP for RC frames in seismic zones: Part I. Evaluation of FRP beam-column joint rehabilitation techniques”, Applied Composite Materials, 11(4), 205-226.
131. Said, A.M. and Nehdi, M.L. (2004b), “Use of FRP for RC frames in seismic zones: Part II. Performance of steel-free GFRP-reinforced beam-column joints”, Applied Composite Materials, 11(4), 227-245.
132. Sause, R., Harries, K. A., Walkup, S. L., Pessiki, S. and Ricles, J. M. (2004), “Flexural behavior of concrete columns retrofitted with carbon fiber reinforced polymer jackets”, ACI Structural J., 101(5), 708-716.
133. Schofield, H.A., Ingham, J.M. and Pampanin, S. (2006), “Critical earthquake risk detailing in New Zealand’s multi-storey building stock: Understanding and improving the current perception”, New Zealand Society for Earthquake Engineering (NZSEE) Conference-2006, Paper Number 39.
134. Shama, A.A., Mander, J.B. and Aref, A.J. (2002), “Seismic performance and retrofit of steel pile to concrete cap connections”, ACI Structural J., 99(1), 51-61.
135. Shan, B., Xiao, Y. and Guo, Y. (2006), “Residual performance of FRP-retrofitted RC columns after being subjected to cyclic loading damage”, J. of Composites for Construction, ASCE, 10(4), 304-312.
136. Shannag, M.J., Barakat, S. and Abdul-Kareem, M. (2002), “Cyclic behavior of HPFRC-repaired reinforced concrete interior beam-column joints”, Materials and Structures, 35(6), 348-356.
137. Shannag, M.J. and Alhassan, M.A. (2005), “Seismic upgrade of interior beam-column sub-assemblages with high performance fiber reinforced concrete jackets”, ACI Structural J., 102(1), 131-138.
138. Shin, Y.-S. and Lee, C. (2003), “Flexural behavior of reinforced concrete beams strengthened with carbon fiber reinforced polymer laminates at different levels of sustaining load”, ACI Structural J., 100(2), 231-239.

139. Spoelstra, M.R. and Monti, G., (1999), “FRP-confined concrete model”, J. of Composites for Construction, ASCE, 3(3), 143-150.
140. Stark, A., Binici, B. and Bayrak, O. (2005), “Seismic upgrade of reinforced concrete slab-column connections using carbon fiber reinforced polymers”, ACI Structural J., 102(2), 324-333.
141. Stoppenhagen, D.R., Jirsa, J.O. and Wyllie, L.A. (1995), “Seismic repair and strengthening of a severely damaged concrete frame”, ACI Structural J., 92(2), 177-187.
142. Takiguchi, K. and Abdullah (2001), “Shear strengthening of reinforced concrete columns using Ferrocement jacket”, ACI Structural J., 98(5), 696-704.
143. Tsonos, A.G. (1999), “Lateral load response of strengthened reinforced concrete beam-to-column Joints”, ACI Structural J., 96(1), 46-56.
144. Tsonos, A.G. and Stylianidis, K.A. (1999). “Pre-seismic and post-seismic strengthening of reinforced concrete structural sub-assemblages using composite materials (FRP)”, Proc., 13th Hellenic Concrete Conf., Rethymno, Greece, 1, 455-466 (in Greek).
145. Tsonos, A.G. (2007), “Cyclic load behavior of reinforced concrete beam-column sub-assemblages of modern structures”, ACI Structural J., 104(4), 468-478.
146. Triantafillou, N.P. and N., Plevris (1992), “Strengthening of RC beams with epoxy-bonded fiber-composite materials”, Materials and Structures, 25(4), 201-211.
147. Van Mier, J.G.M. (1986), “Multi-axial strain-softening of concrete, Part I: fracture”, Materials and Structures, RILEM, 19(111), 179-190.
148. Vos, E. (1983), "Influence of loading rate and radial pressure on bond in reinforced concrete”, Dissertation, Delft University, 219-220.
149. Xiao, Y. and Ma, R. (1997), “Fiber reinforced polymer jacketed and shape-modified compression members: I-Experimental behavior”, J. of Structural Engineering, ASCE, 123(10), 1357-1364.
150. Yalcin, C., Kaya, O. and Sinangil, M. (2008), “Seismic retrofitting of R/C columns having plain rebars using CFRP sheets for improved strength and ductility”, Construction and Building Materials, 22(3), 295-307.
151. Zhang, J.W., Teng, J.G., Wong, Y.L. and Lu, Z.T. (2001), “Behavior of two-way RC slabs externally bonded with steel plate”, J. of Structural Engineering, ASCE, 127(4), 390-397.

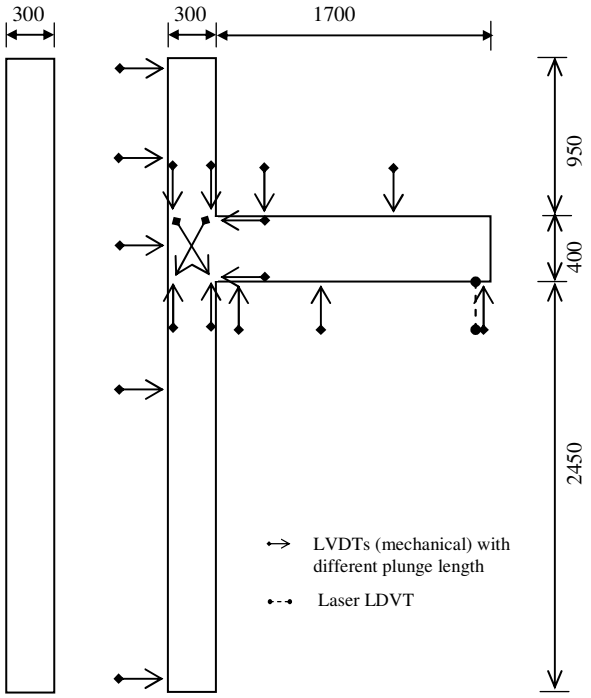

(a) Instrumentation plan for linear variable displacement transducers (LDVTs)

(continued..)

Column back elevation - long. reinforcement

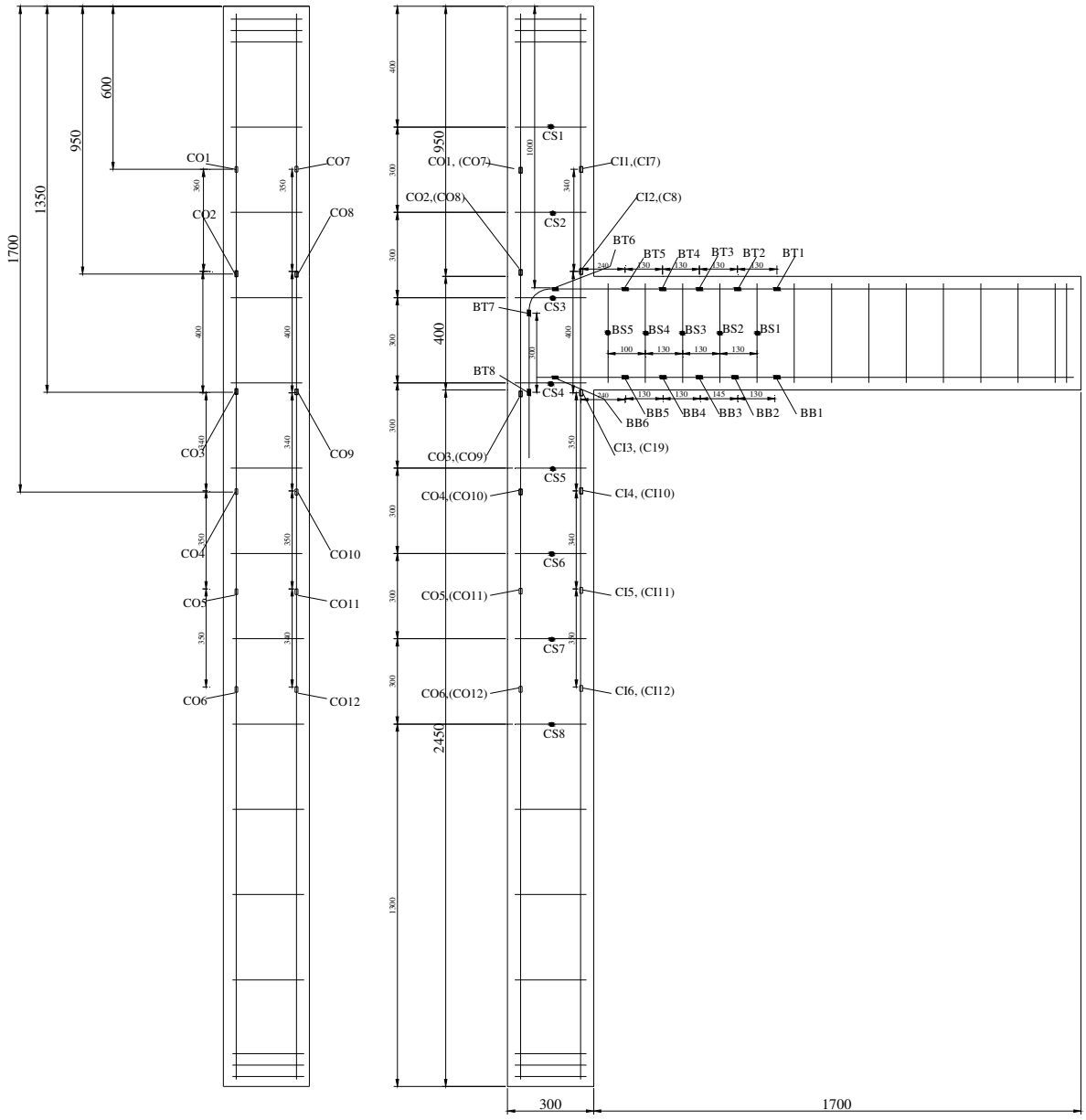

(b) Instrumentation plan for strain gages

Fig. A1 Typical instrumentation plan for LDVTs (top) and strain gages (bottom) on the specimens (exact locations were varied among the specimens based on requirement and suitability)

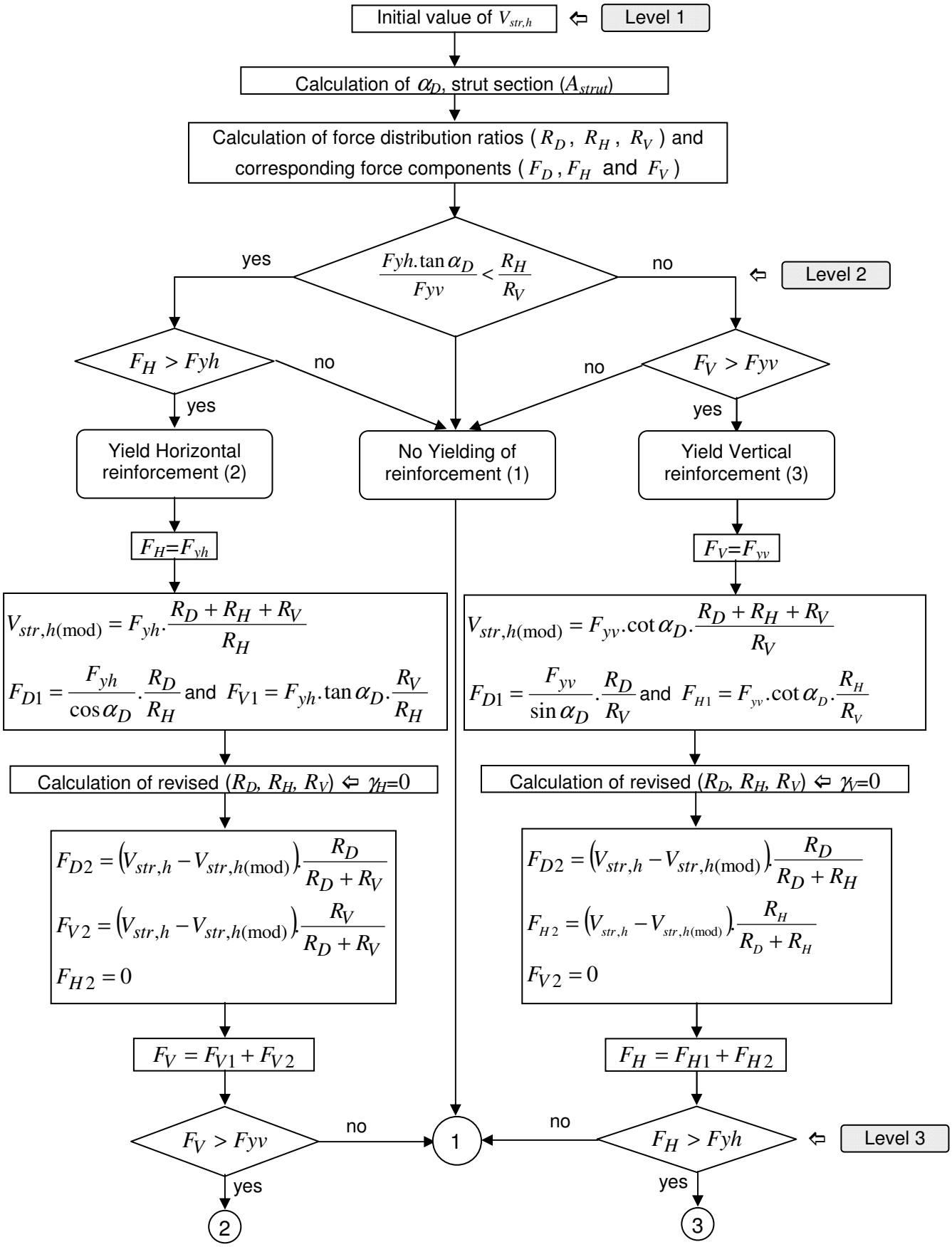
Initial value of $V_{str,h}$
Level 1
Calculation of α_D, strut section (A_{strut})
Calculation of force distribution ratios (R_D, R_H, R_V) and corresponding force components (F_D, F_H and F_V)
$\frac{Fyh.\tan\alpha_D}{Fyv} < \frac{R_H}{R_V}$
yes
no
Level 2
$F_H > Fyh$
$F_V > Fyv$
no
no
yes
yes
Yield Horizontal reinforcement (2)
No Yielding of reinforcement (1)
Yield Vertical reinforcement (3)
$F_H = F_{yh}$
$F_V = F_{yv}$
$V_{str,h(\mathrm{mod})} = F_{yh}.\frac{R_D + R_H + R_V}{R_H}$
$F_{D1} = \frac{F_{yh}}{\cos\alpha_D}.\frac{R_D}{R_H}$ and $F_{V1} = F_{yh}.\tan\alpha_D.\frac{R_V}{R_H}$
$V_{str,h(\mathrm{mod})} = F_{yv}.\cot\alpha_D.\frac{R_D + R_H + R_V}{R_V}$
$F_{D1} = \frac{F_{yv}}{\sin\alpha_D}.\frac{R_D}{R_V}$ and $F_{H1} = F_{yv}.\cot\alpha_D.\frac{R_H}{R_V}$
Calculation of revised (R_D, R_H, R_V) ⇦ γ_H=0
Calculation of revised (R_D, R_H, R_V) ⇦ γ_V=0
$F_{D2} = (V_{str,h} - V_{str,h(\mathrm{mod})}).\frac{R_D}{R_D + R_V}$
$F_{V2} = (V_{str,h} - V_{str,h(\mathrm{mod})}).\frac{R_V}{R_D + R_V}$
$F_{H2} = 0$
$F_{D2} = (V_{str,h} - V_{str,h(\mathrm{mod})}).\frac{R_D}{R_D + R_H}$
$F_{H2} = (V_{str,h} - V_{str,h(\mathrm{mod})}).\frac{R_H}{R_D + R_H}$
$F_{V2} = 0$
$F_V = F_{V1} + F_{V2}$
$F_H = F_{H1} + F_{H2}$
$F_V > Fyv$
$F_H > Fyh$
no
no
1
Level 3
yes
yes
2
3

Contd.…

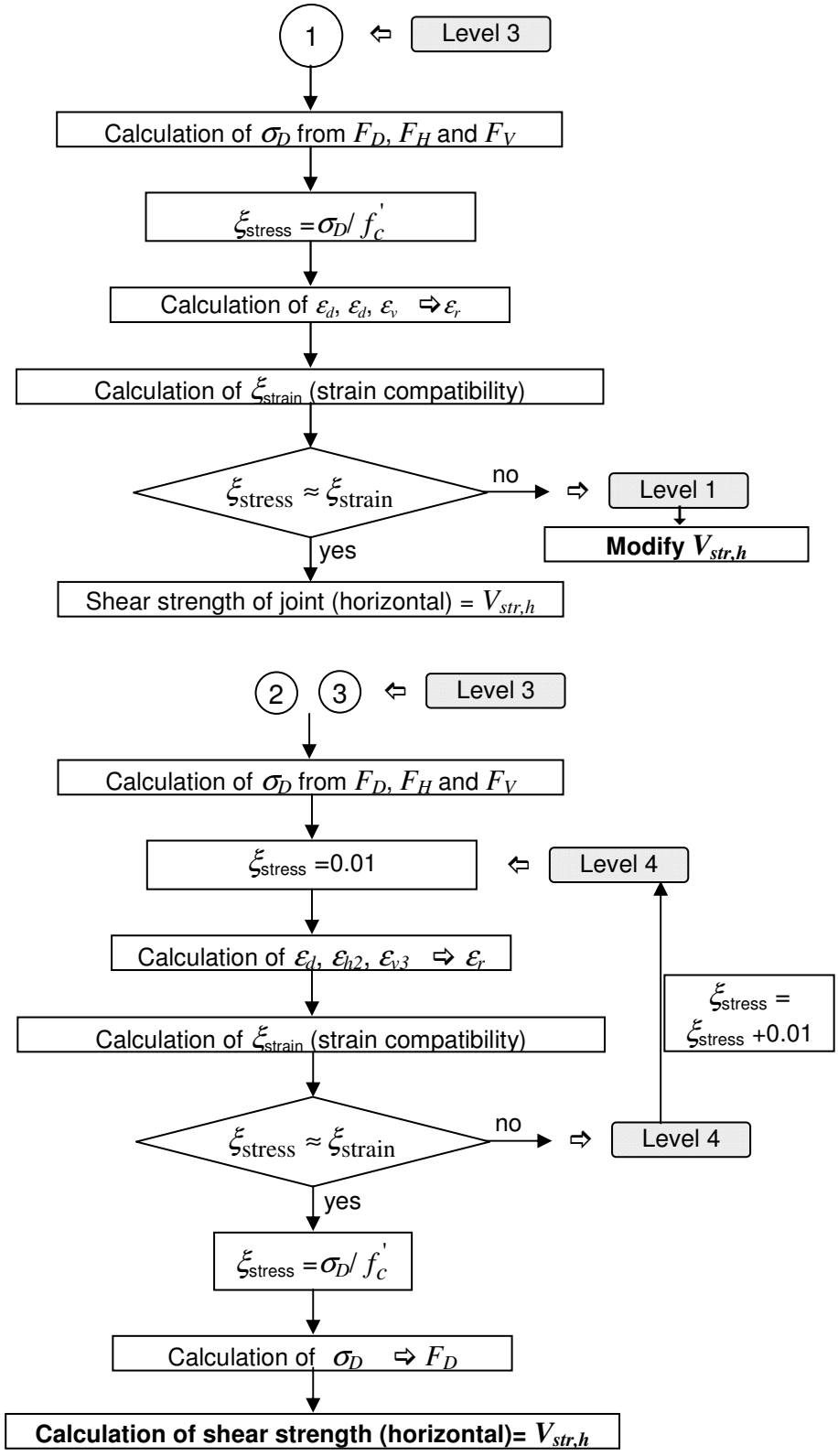

Fig. A2 Flow chart for determining the shear strength of a given joint [abbreviations are given in nomenclature, Hwang and Lee, 1999]

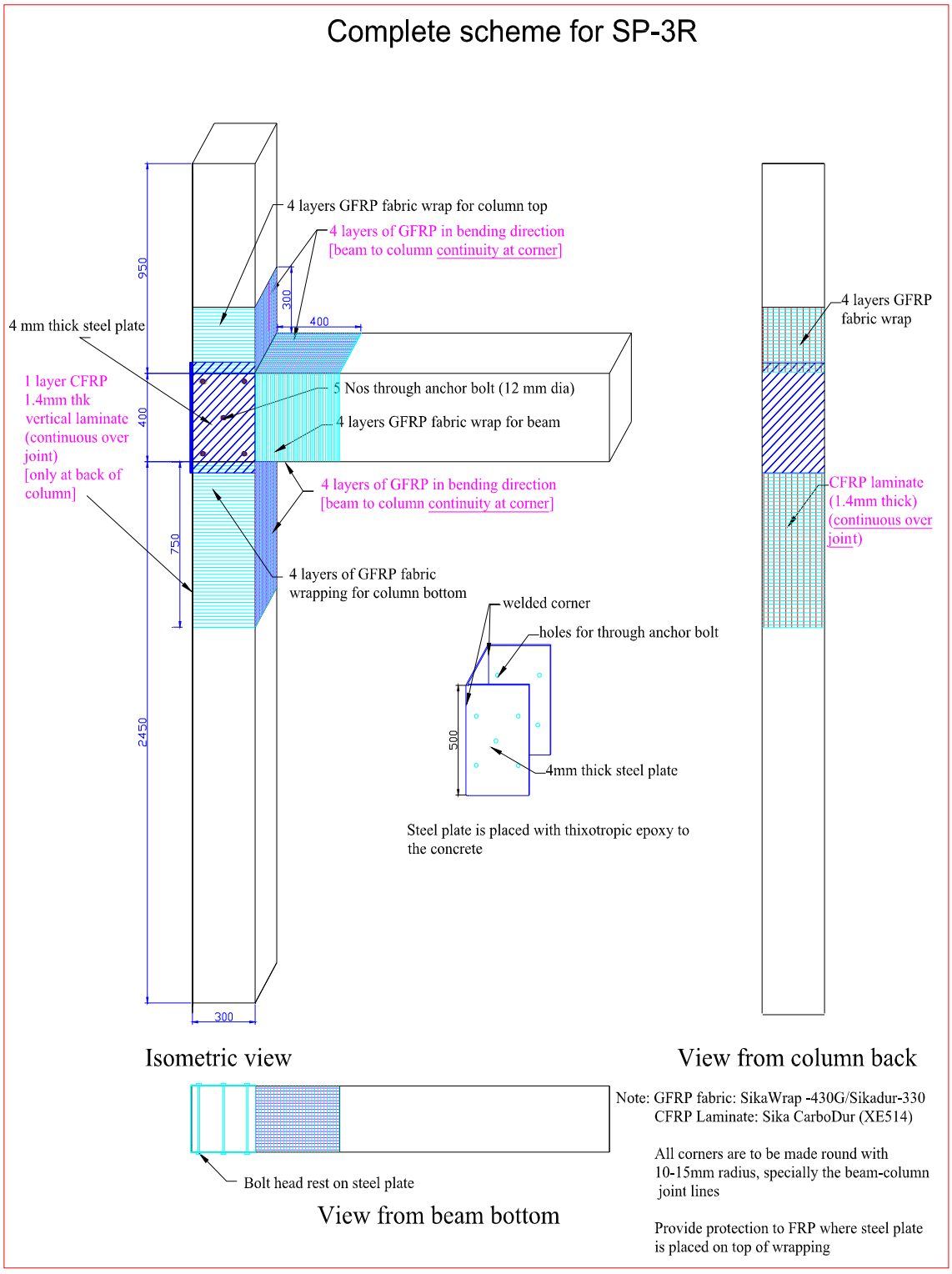

Fig. A3 Retrofitting scheme (SP-3R) used for damaged specimen SP-3

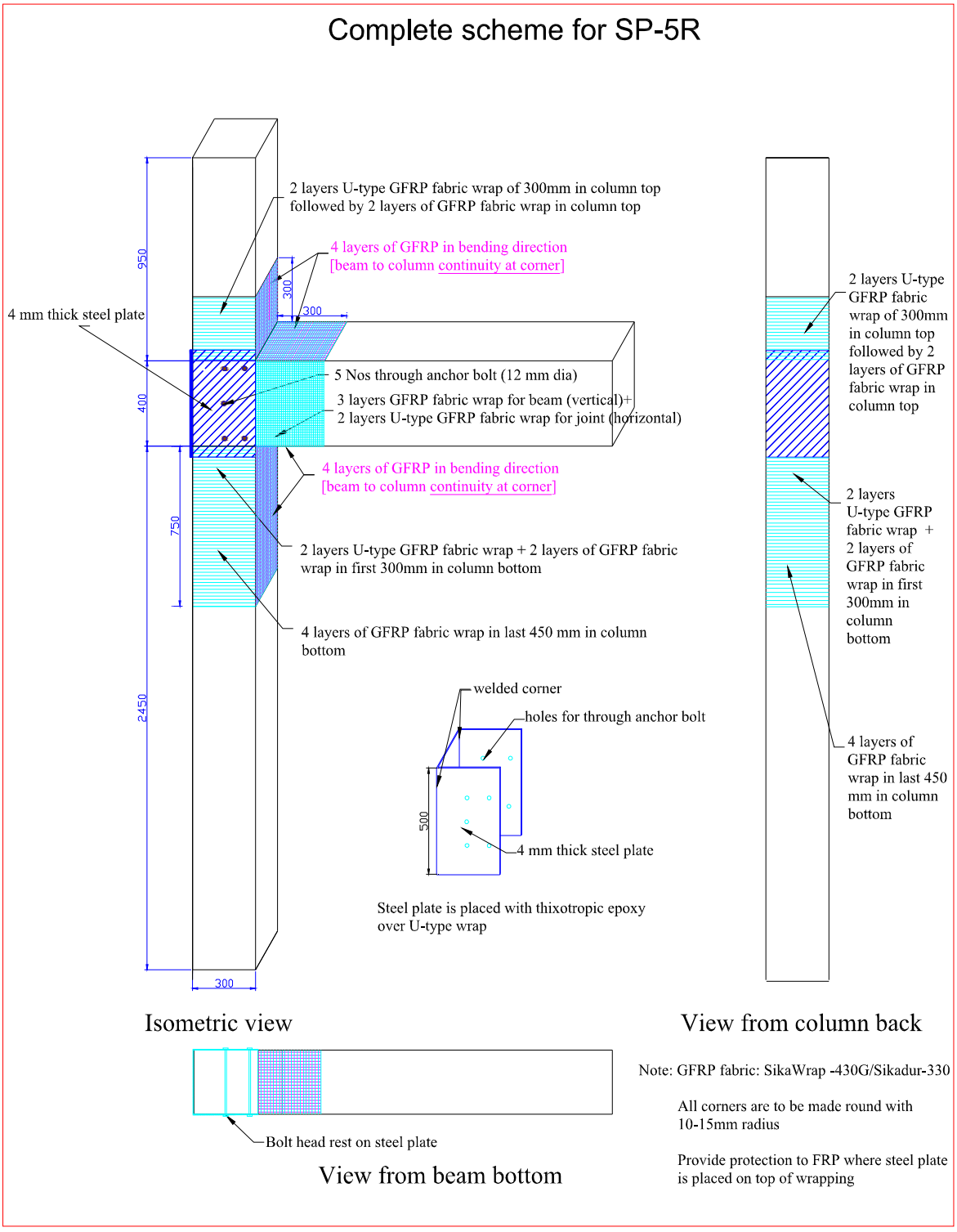

Fig. A4 Retrofitting scheme (SP-5R) used for damaged specimen SP-5

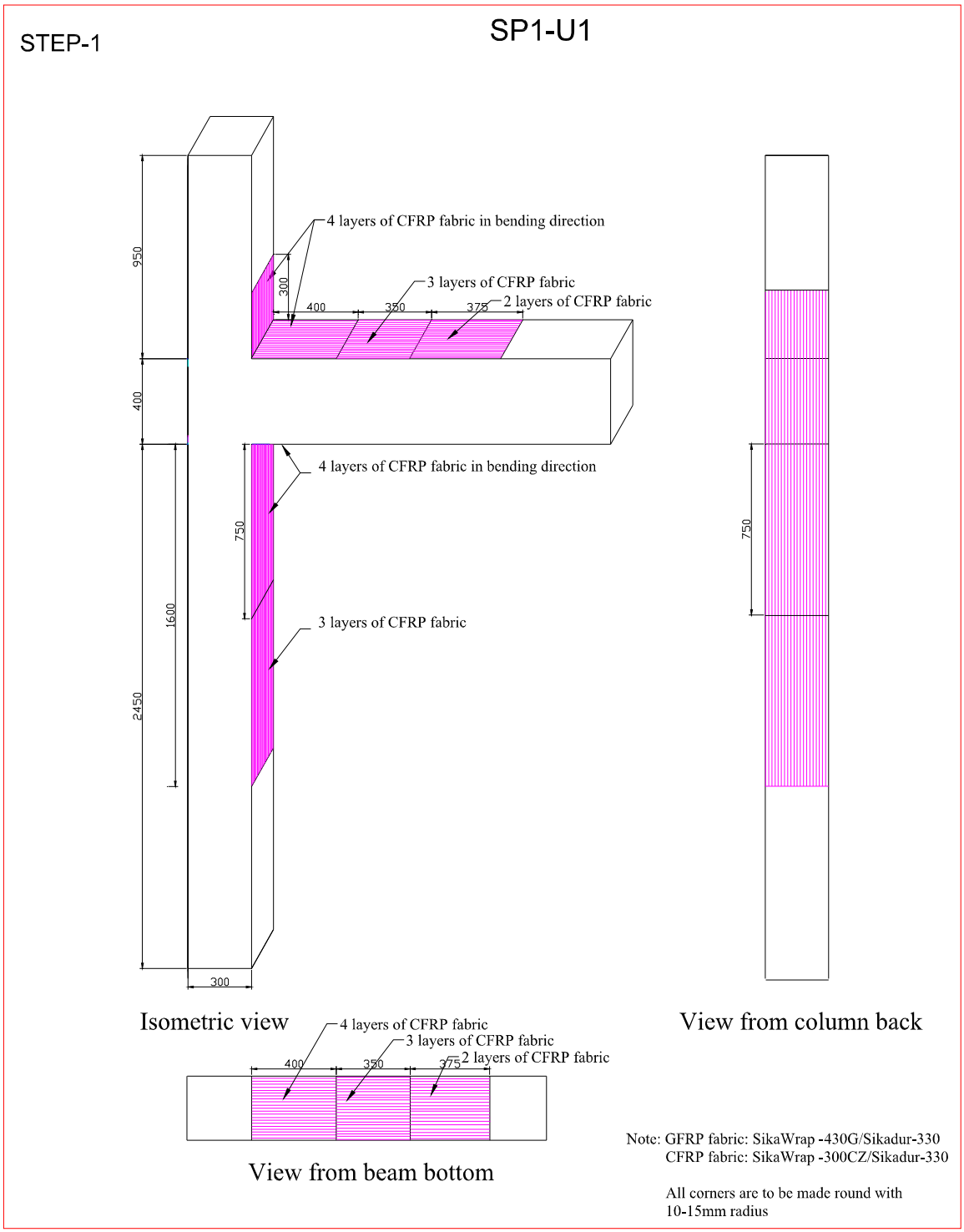

Fig. A5-1 First step of first scheme of upgradation for specimen SP-1 (SP1-U1)

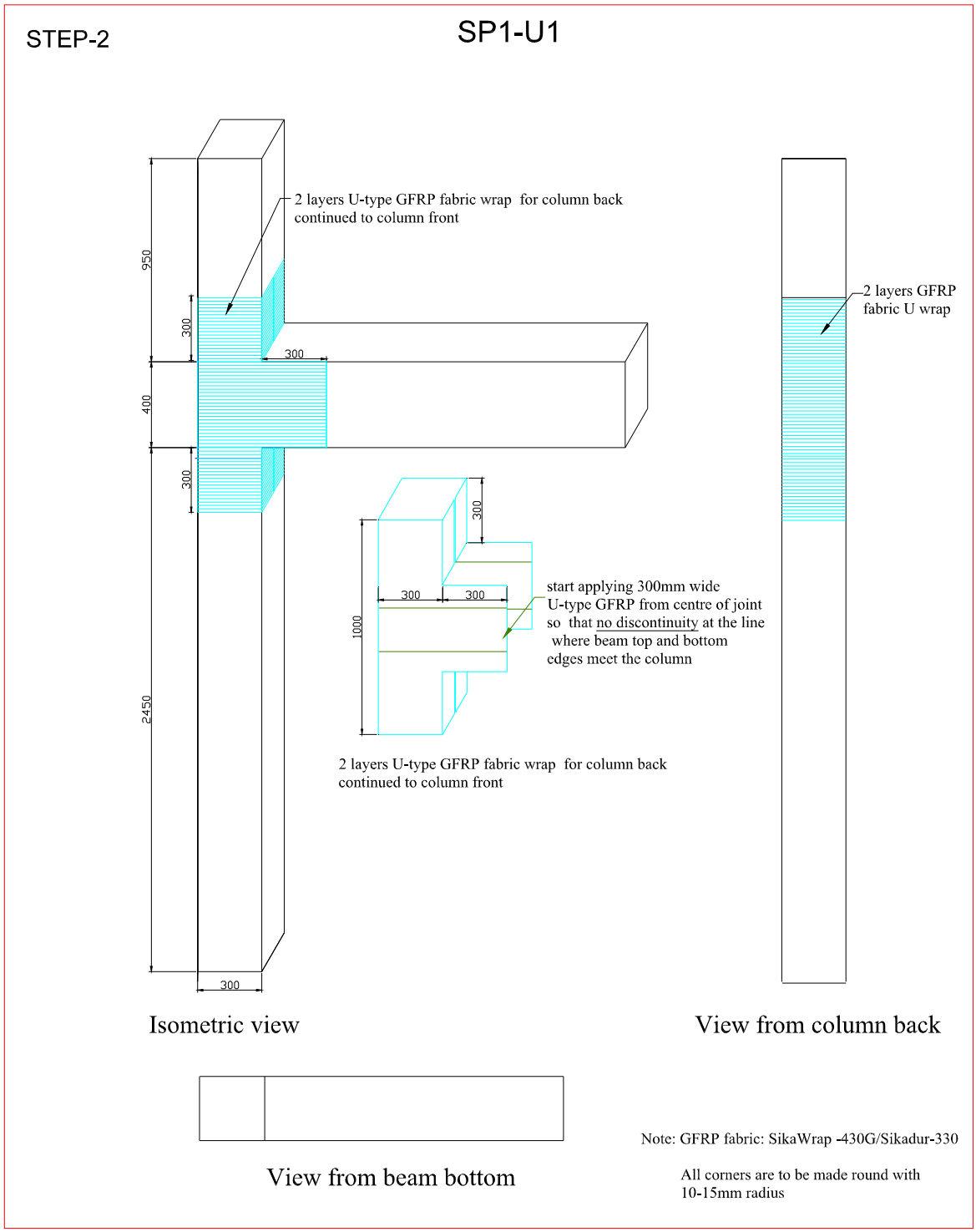

Fig. A5-2 Second step of first scheme of upgradation for specimen SP-1 (SP1-U1)

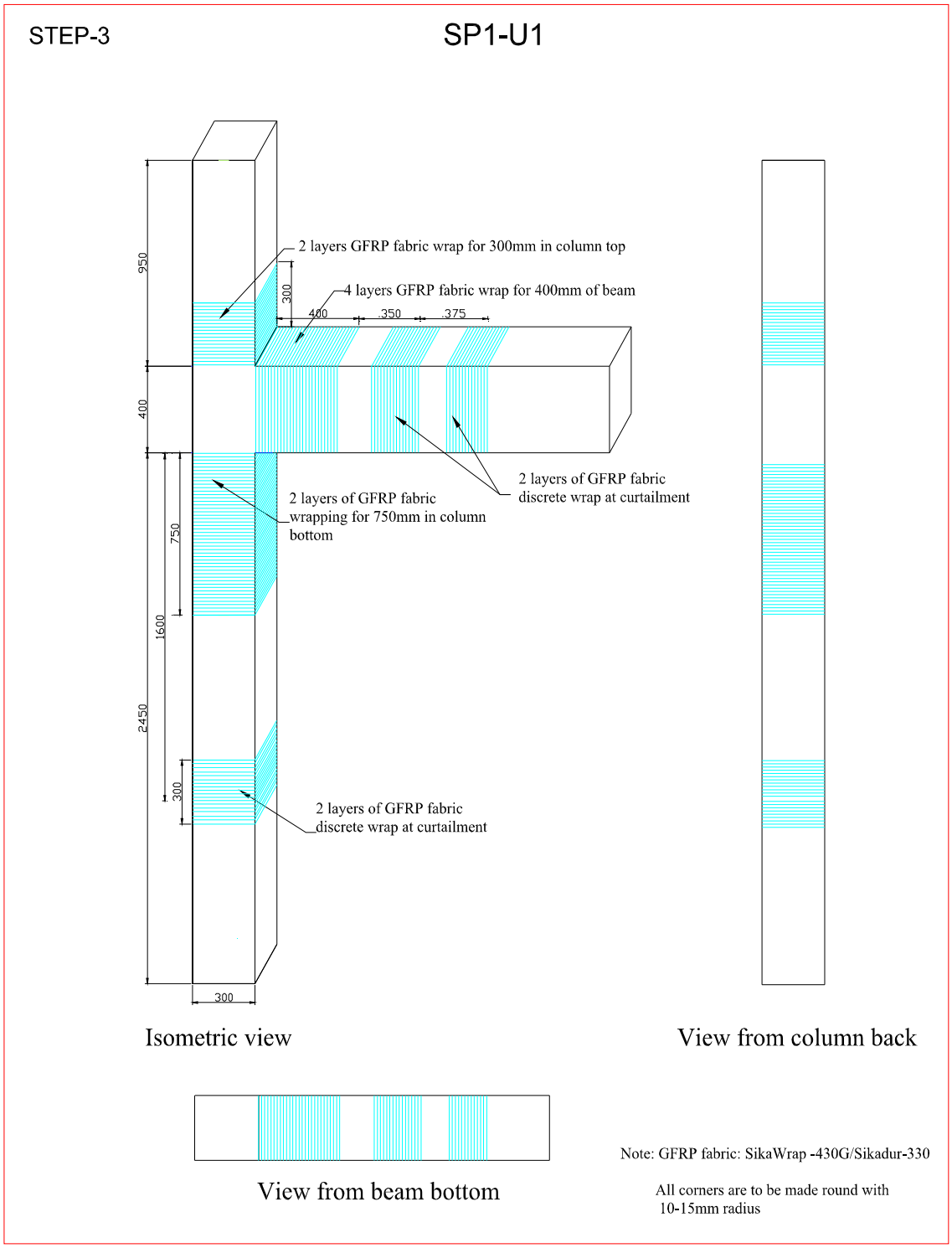

Fig. A5-3 Third step of first scheme of upgradation for specimen SP-1 (SP1-U1)

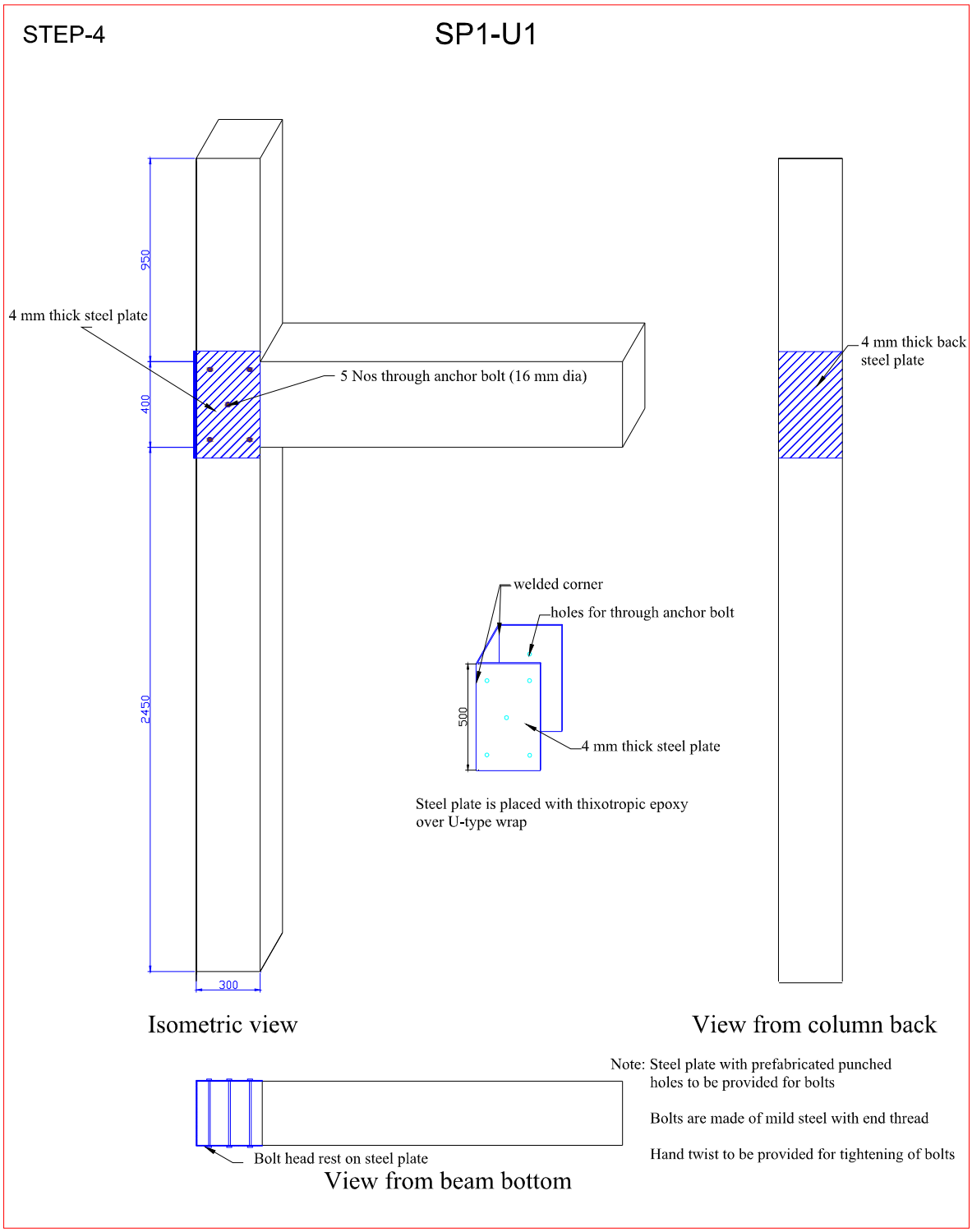

Fig. A5-4 Fourth step of first scheme of upgradation for specimen SP-1 (SP1-U1)

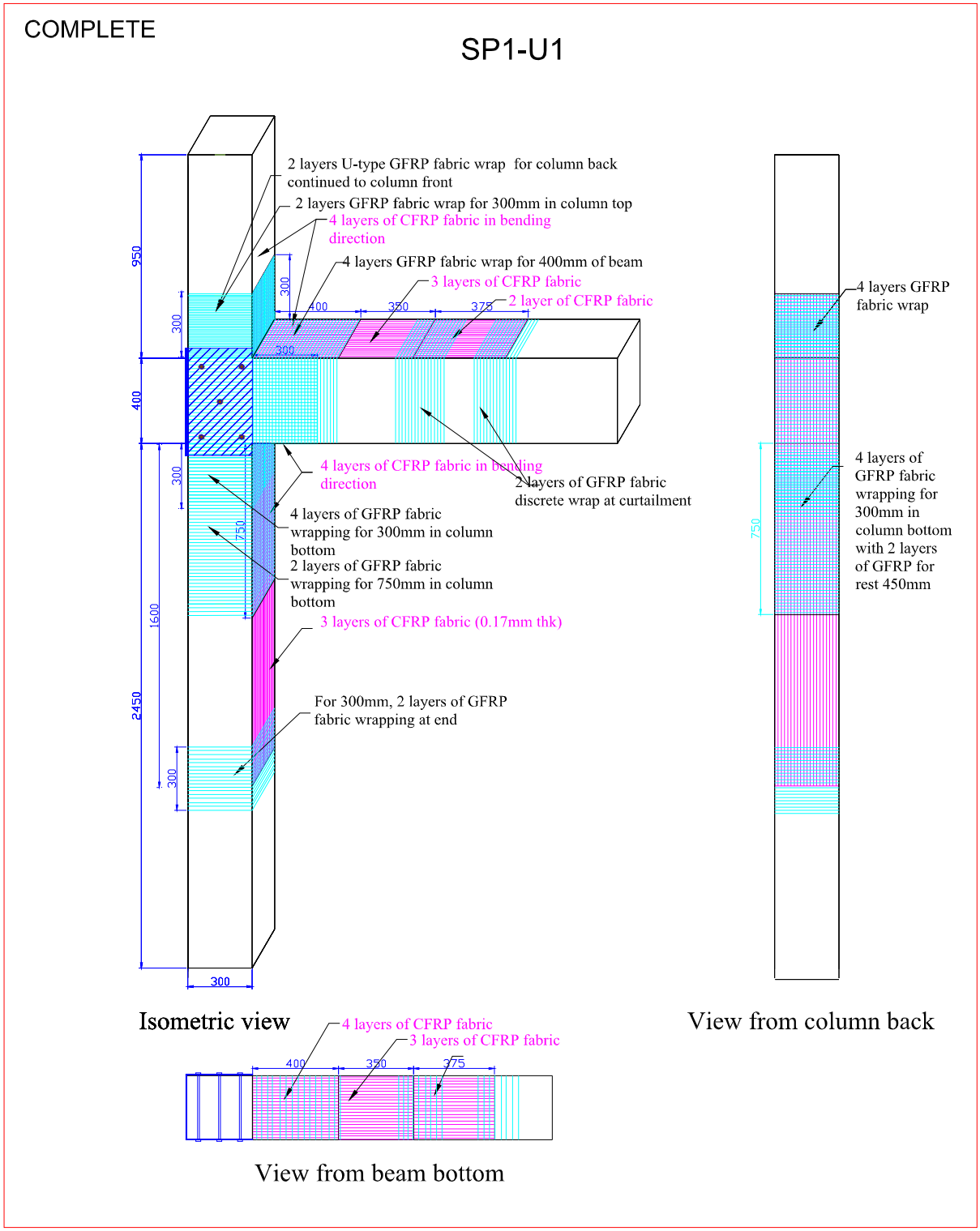

Fig. A5-5 First upgradation scheme (complete) for specimen SP-1

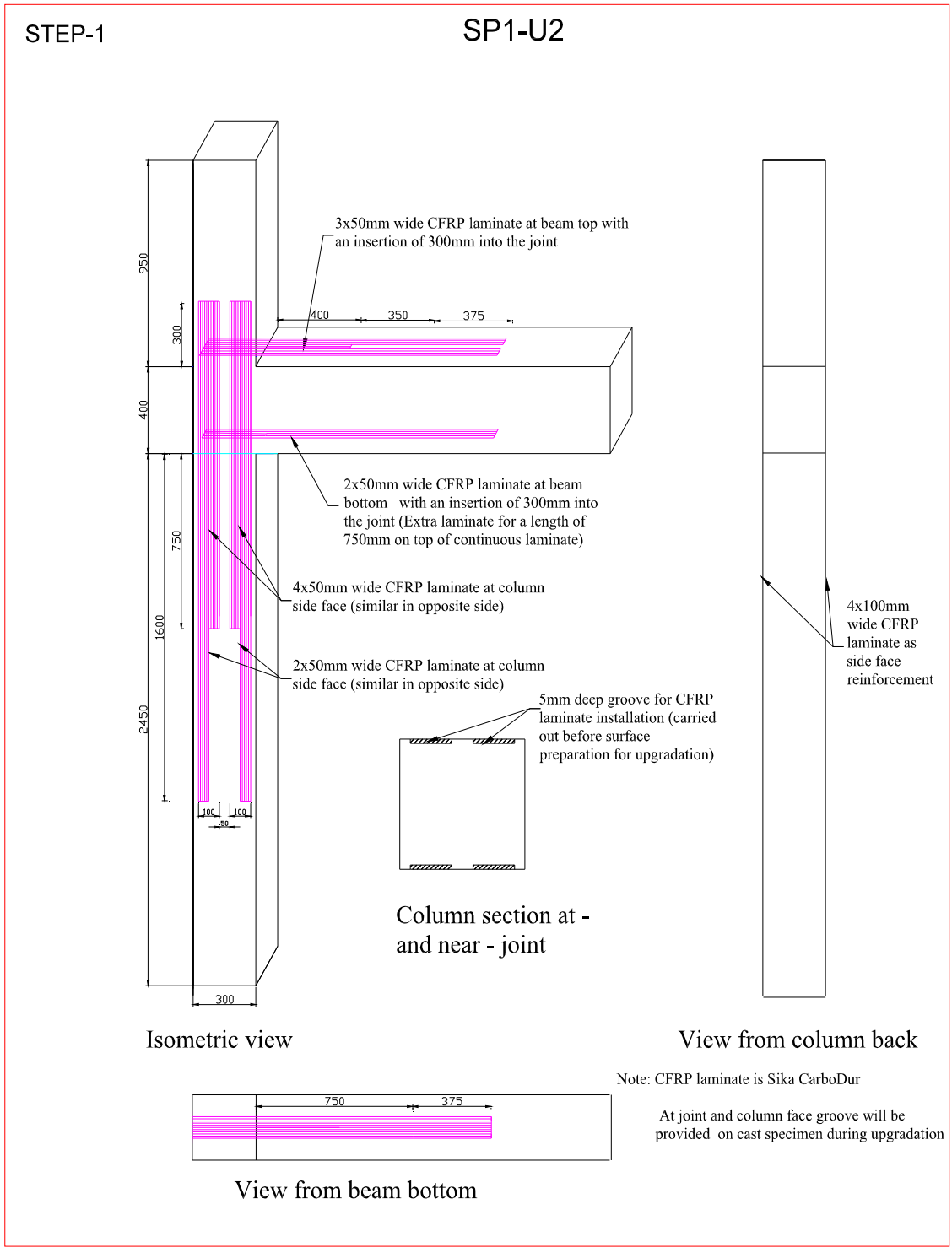

Fig. A6-1 First step of second scheme of upgradation for specimen SP-1 (SP1-U2)

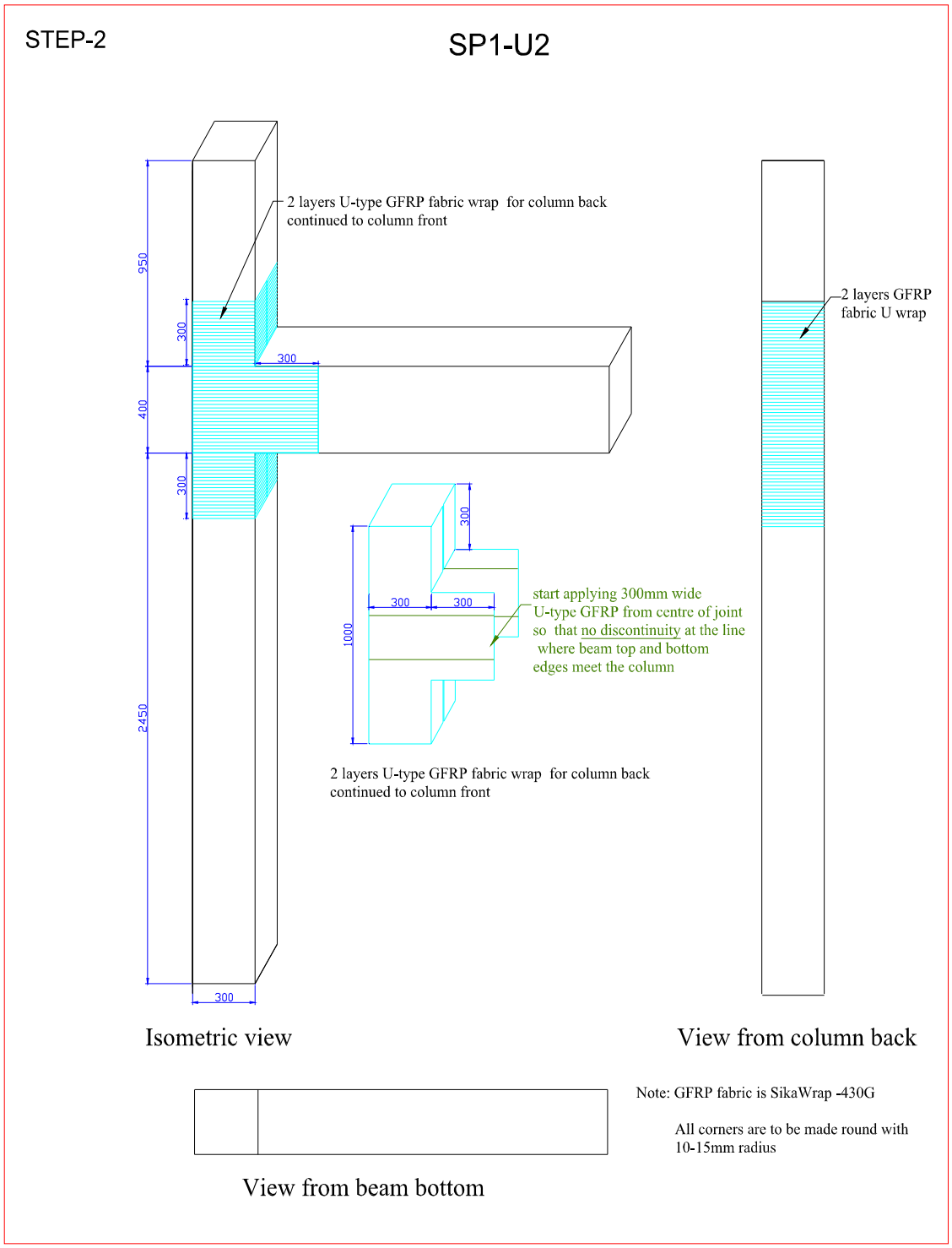

Fig. A6-2 Second step of second scheme of upgradation for specimen SP-1 (SP1-U2)

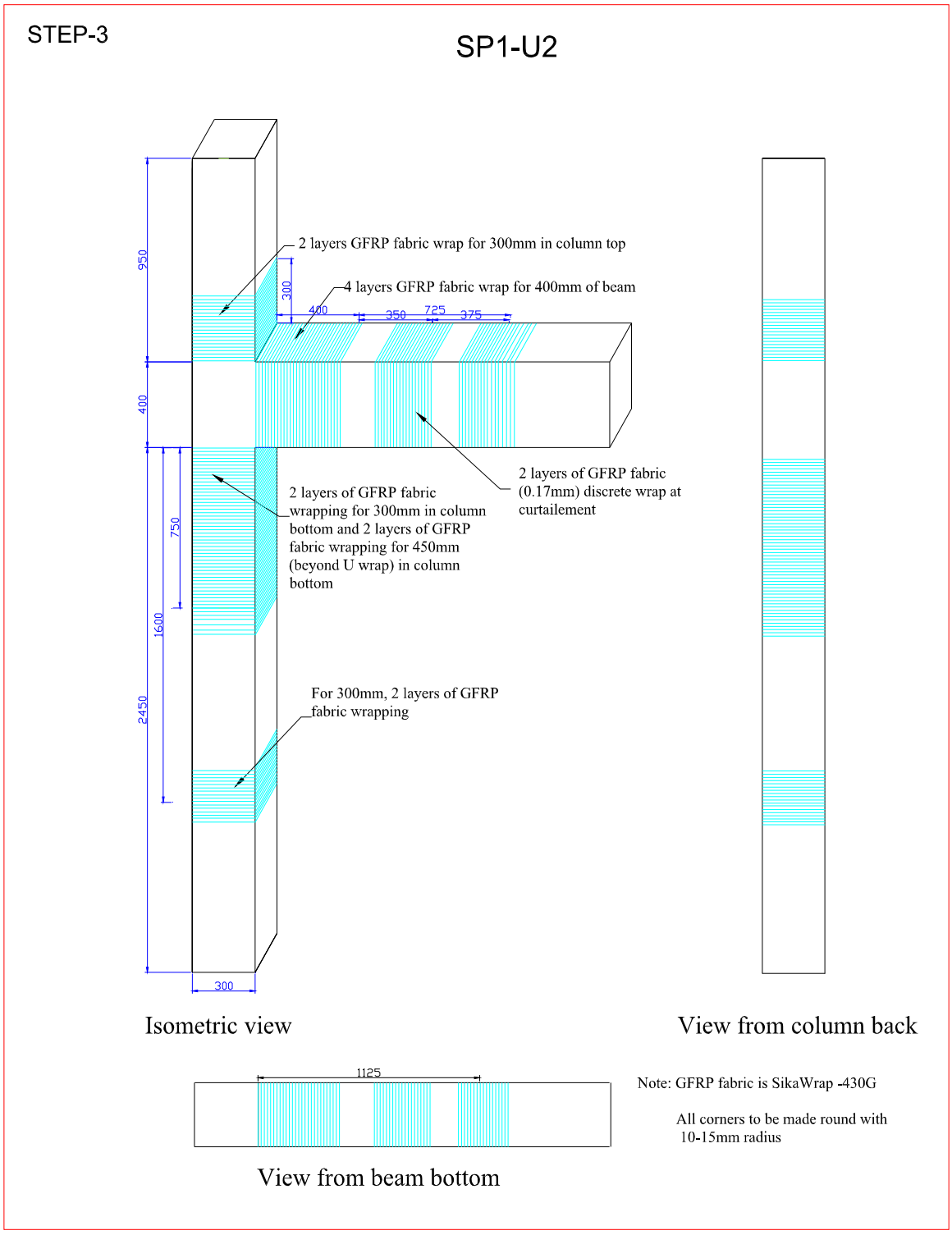

Fig. A6-3 Third step of second scheme of upgradation for specimen SP-1 (SP1-U2)

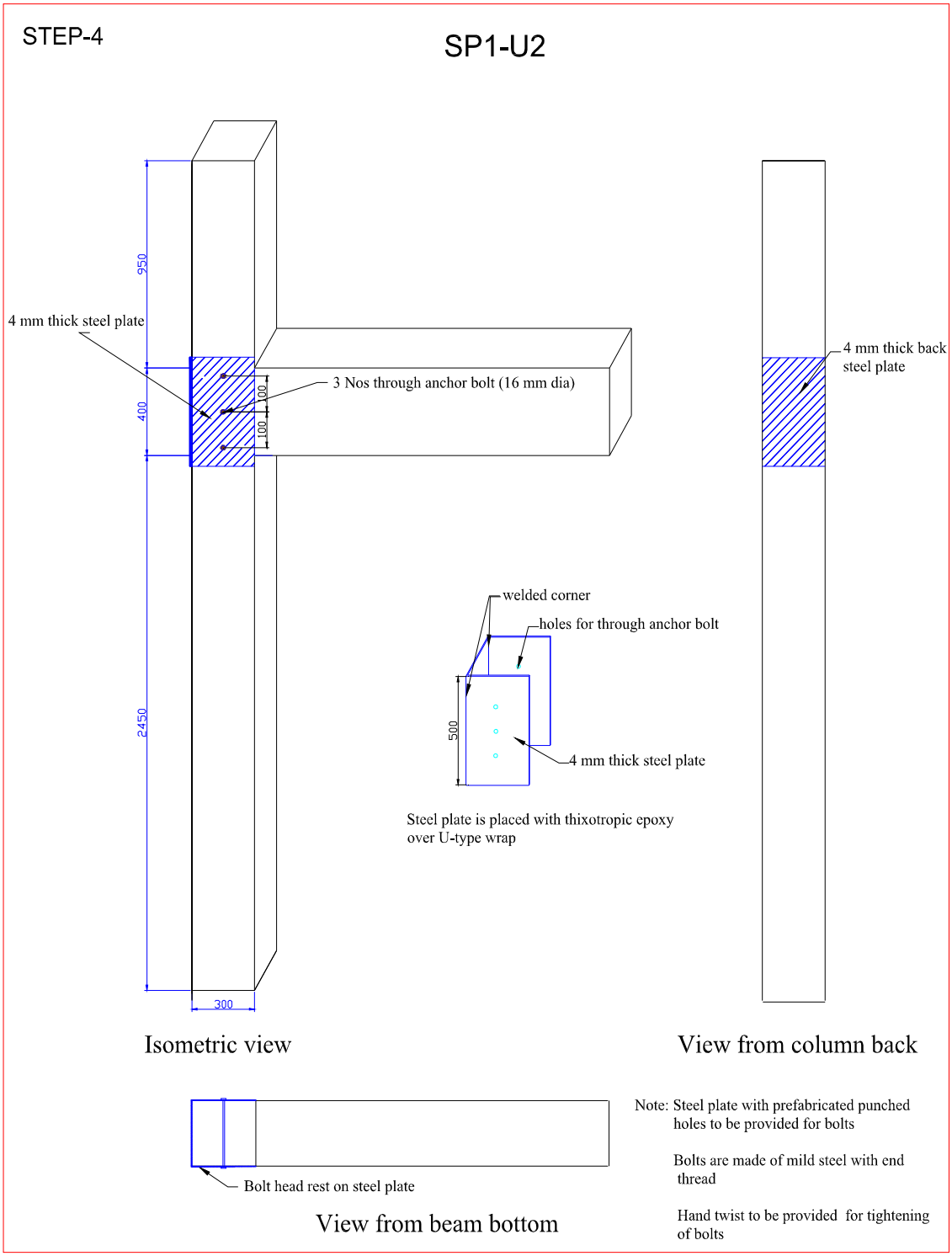

Fig. A6-4 Fourth step of second scheme of upgradation for specimen SP-1 (SP1-U2)

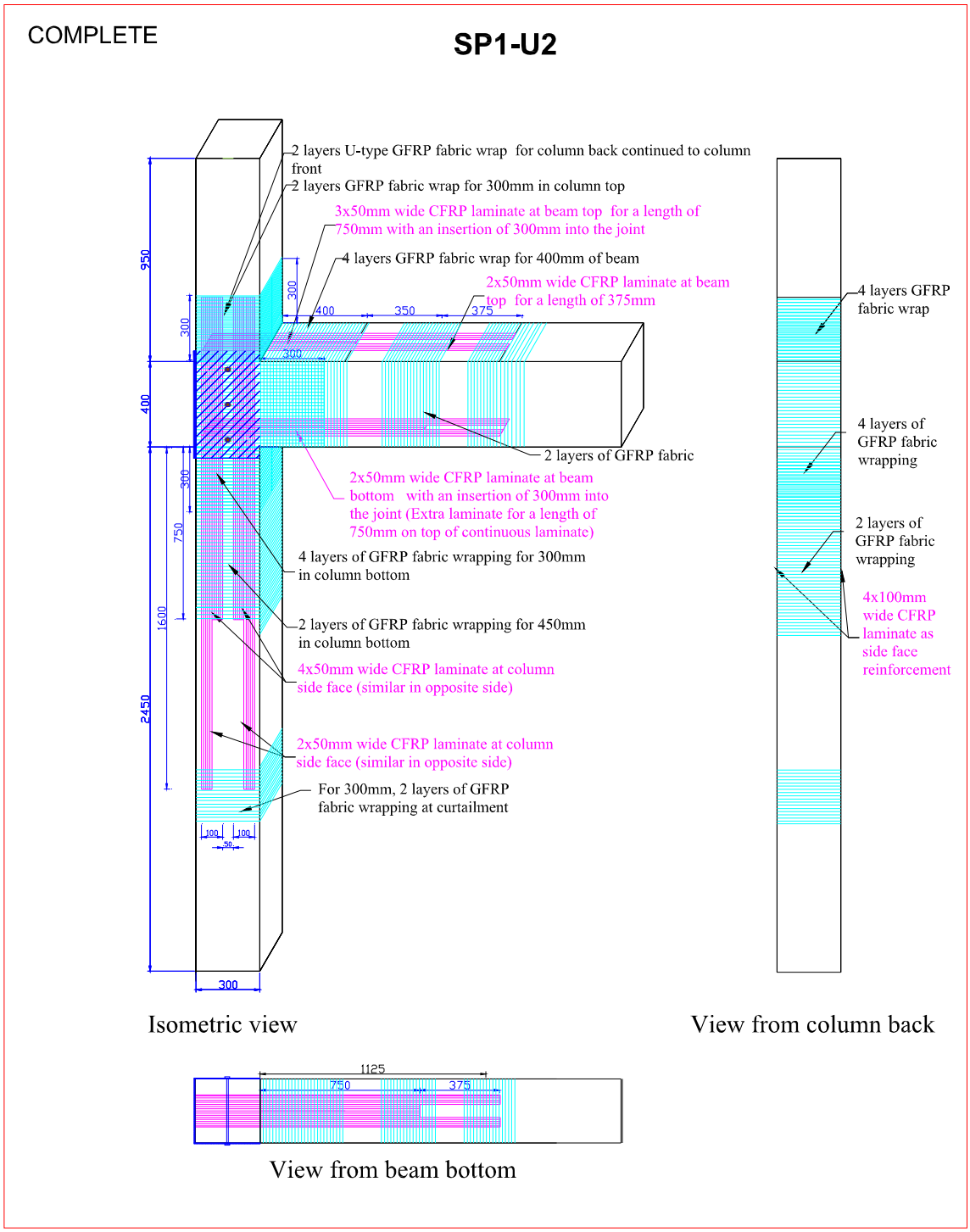

Fig. A6-5 Second upgradation scheme (complete) for specimen SP-1

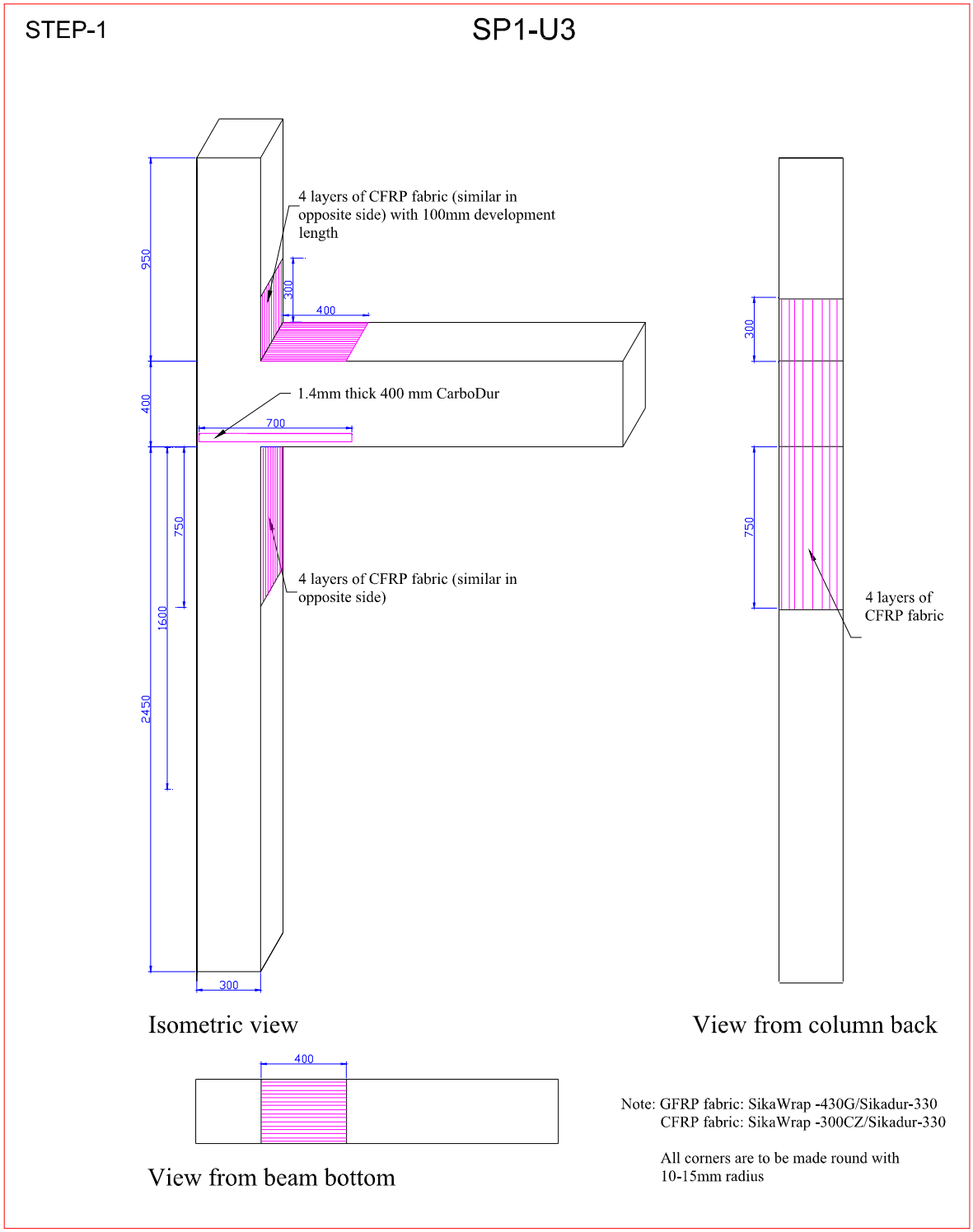

Fig. A7-1 First step of third scheme of upgradation for specimen SP-1 (SP1-U3)

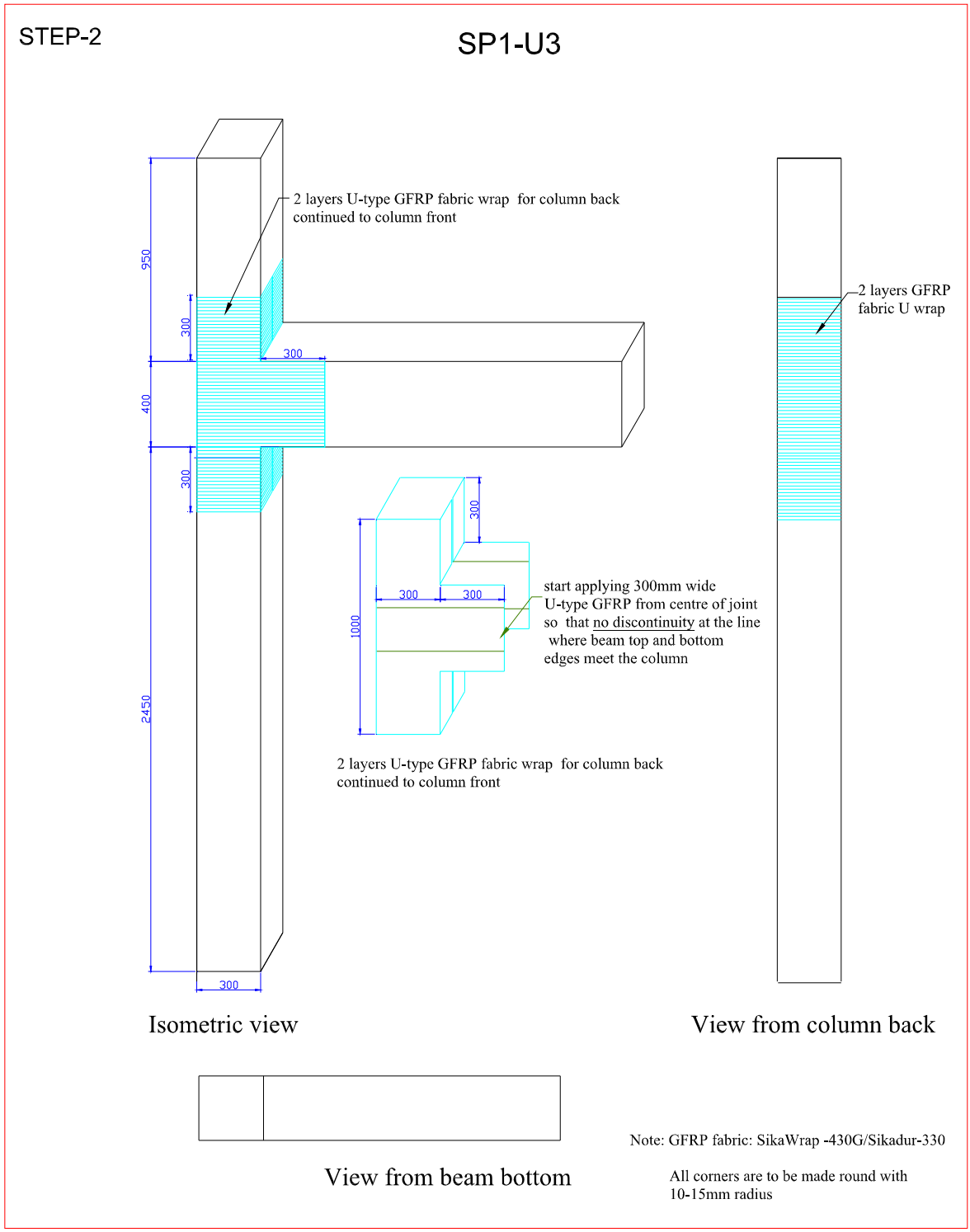

Fig. A7-2 Second step of third scheme of upgradation for specimen SP-1 (SP1-U3)

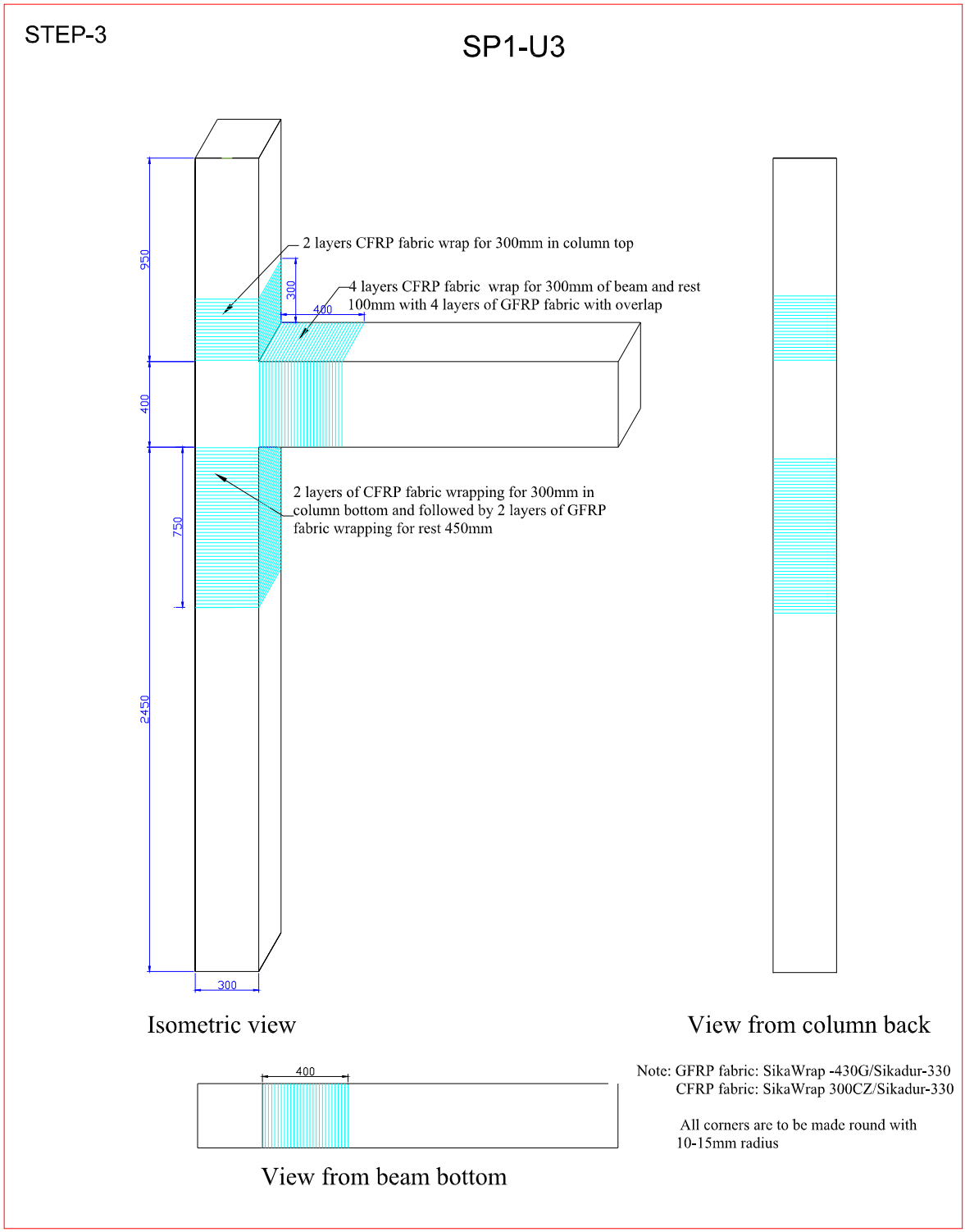

Fig. A7-3 Third step of third scheme of upgradation for specimen SP-1 (SP1-U3)

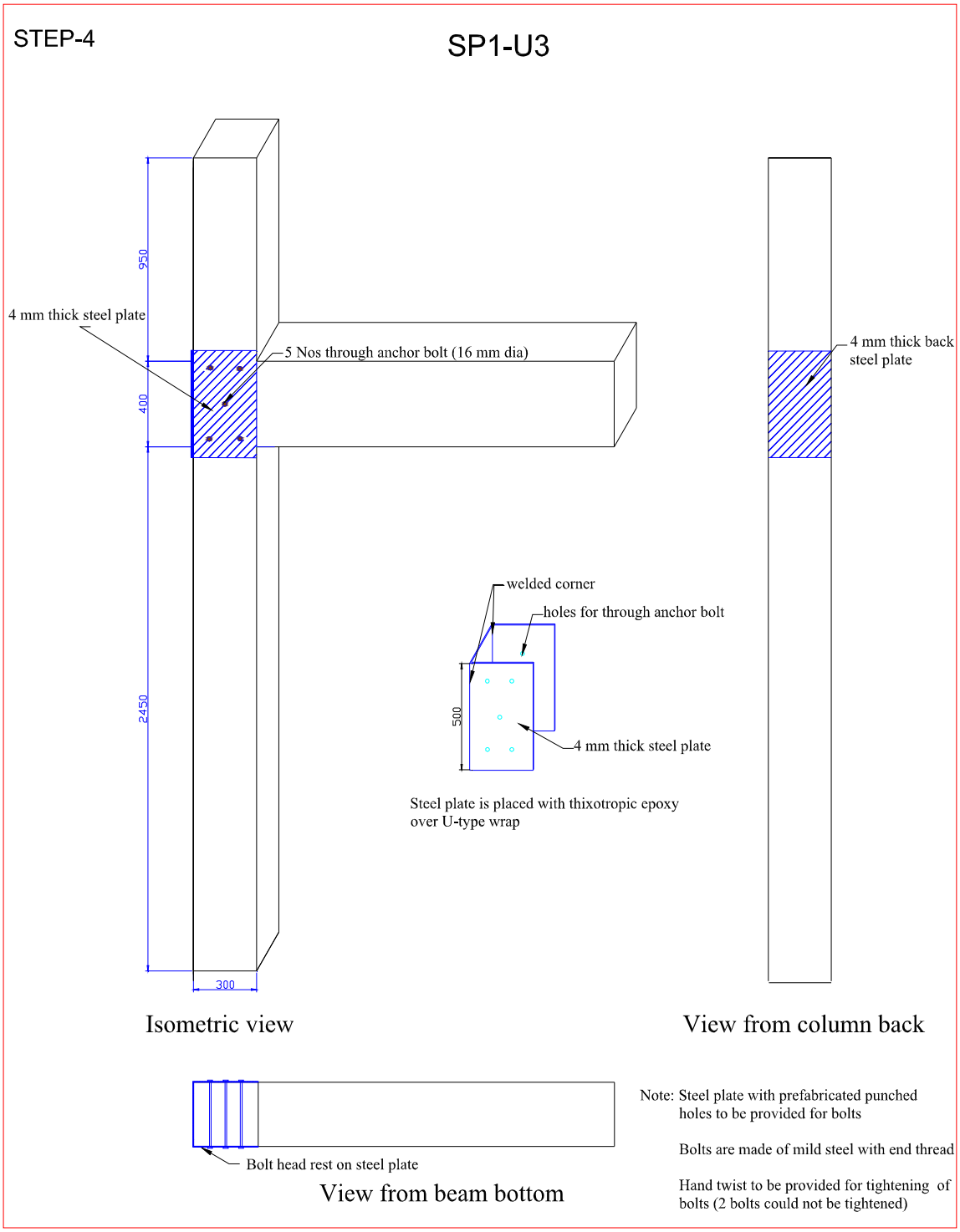

Fig. A7-4 Fourth step of third scheme of upgradation for specimen SP-1 (SP1-U3)

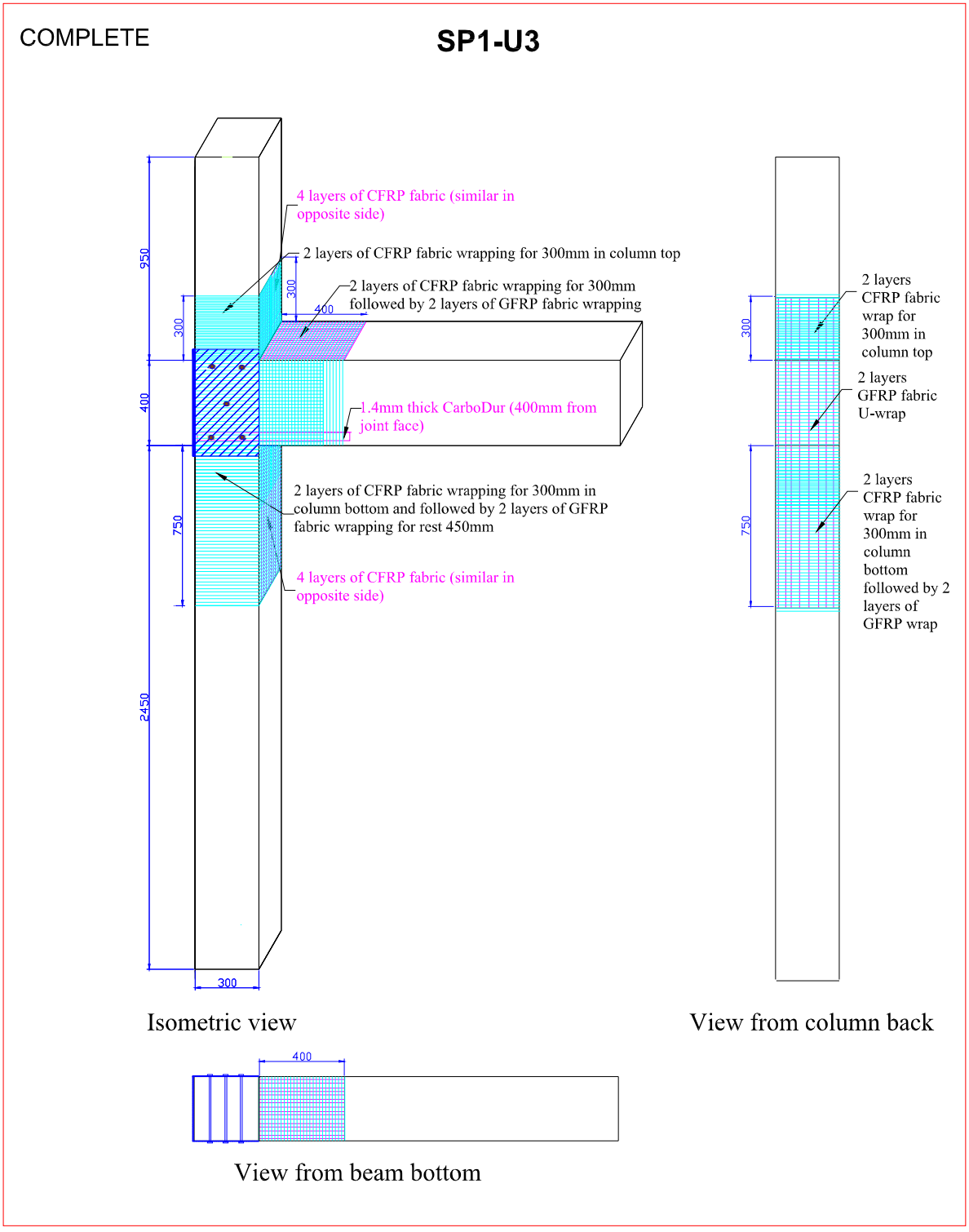

Fig. A7-5 Third upgradation scheme (complete) for specimen SP-1

(A1) Reported strengthening schemes using concrete jacketing

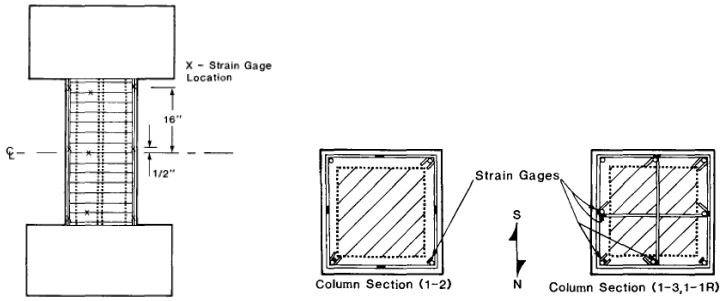

(a) Bett, B.J., Klingner, R.E. and Jirsa, J.O. (1988)

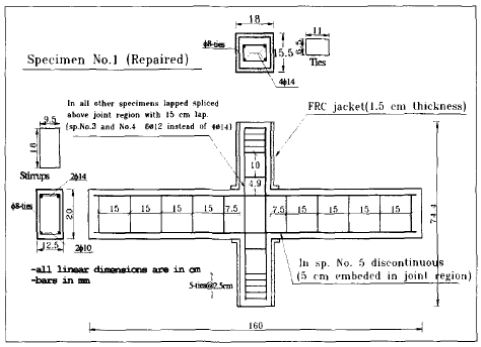

(b) Shannag, M.J., Barakat, S. and Abdul-Kareem, M. (2002)

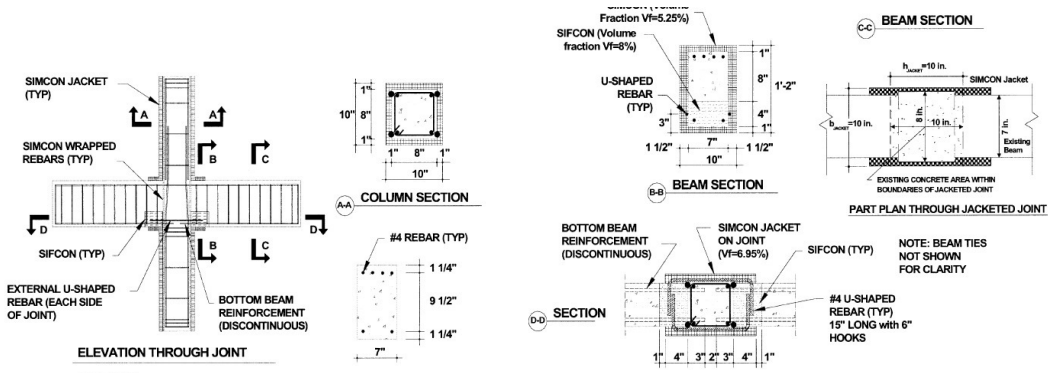

(c) Dogan, E. and Opara, N.K. (2003)

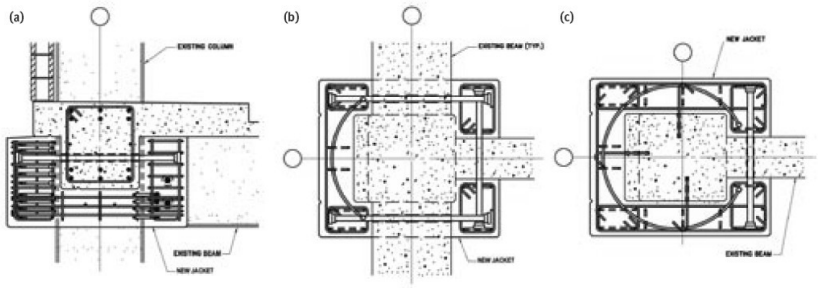

(d) Bligh, R.A., Fischer, S. and Ghosh, S.K. (2005)

(A2) Reported strengthening schemes using steel jacketing

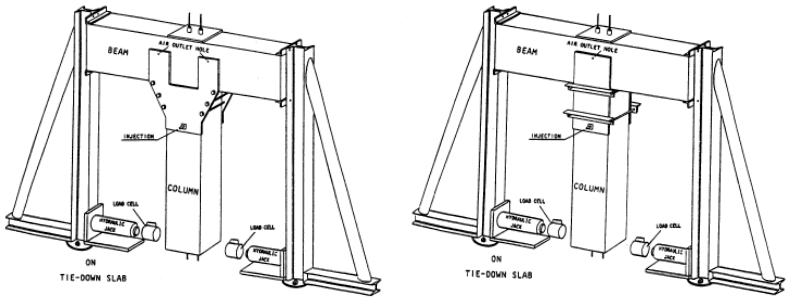

(a) Adin, M.A., Yankelevsky, D.Z. and Farhey, D.N. (1993),

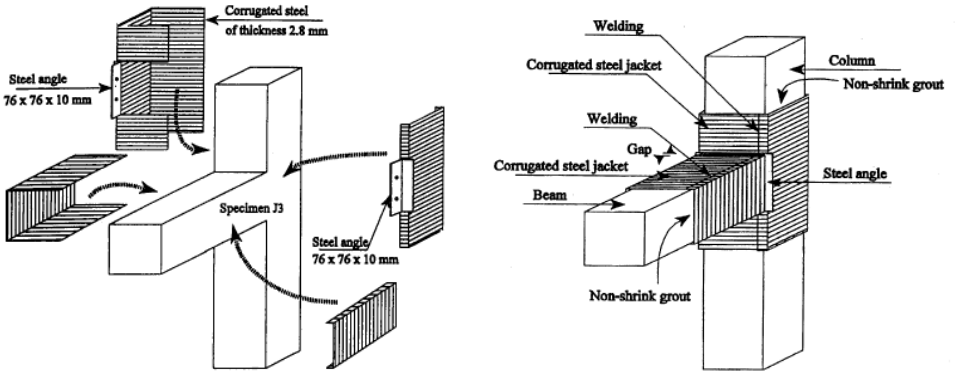

(b) Biddah, A., Ghobarah, A. and Aziz, T.S. (1997)

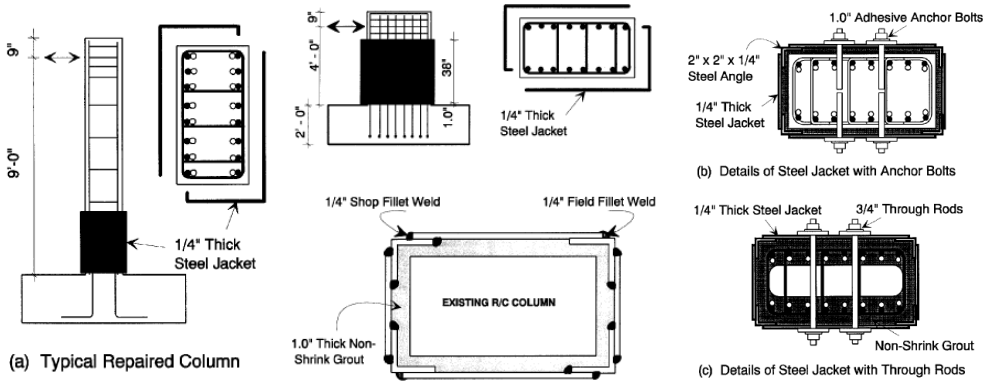

(c) Aboutaha, R.S., Engelhardt, M.D., Jirsa, J.O. and Kreger, M.E. (1999)

(A3) Reported strengthening schemes using FRP jacketing

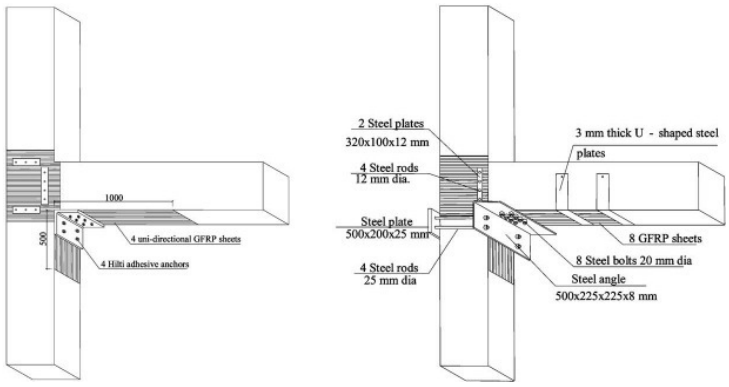

(a) El-Amoury, T. and Ghobarah, A. (2002)

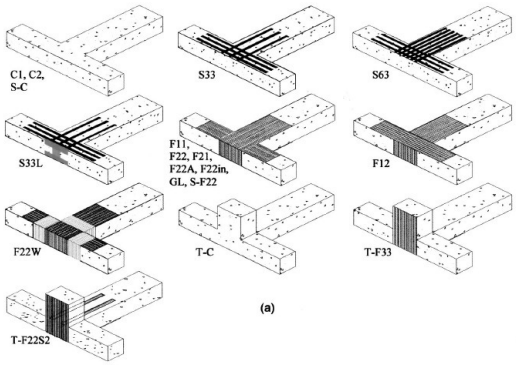

(b) Antonopoulos, C.P. and Triantafillou, T.C. (2003),

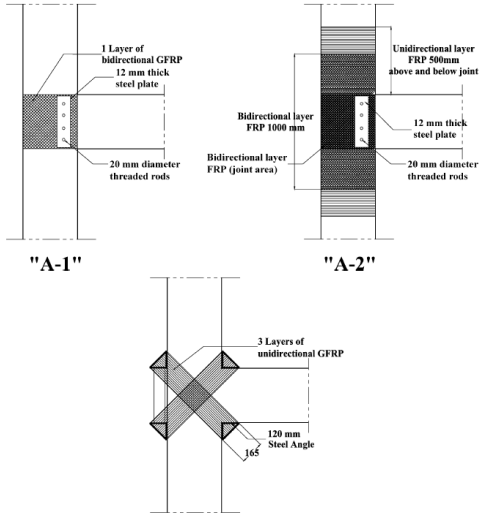

(c)Said, A.M. and Nehdi, M.L. (2004)

(A4) Reported strengthening schemes beyond jacketing

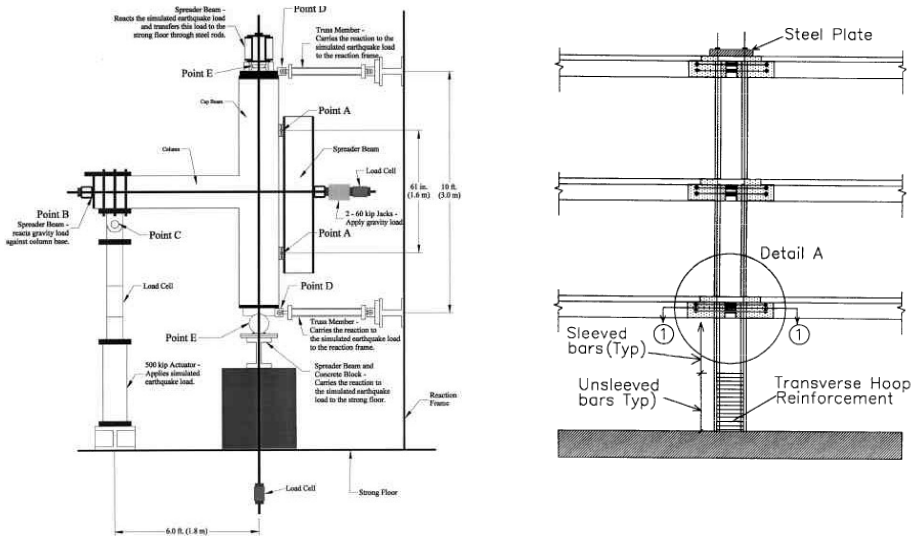

(a) Lowes, L.N. and Moehle, J.P. (1999) [left] and Bracci, J.M., Reinhorn, A.M. and Mander, J.B. (1995) [right]

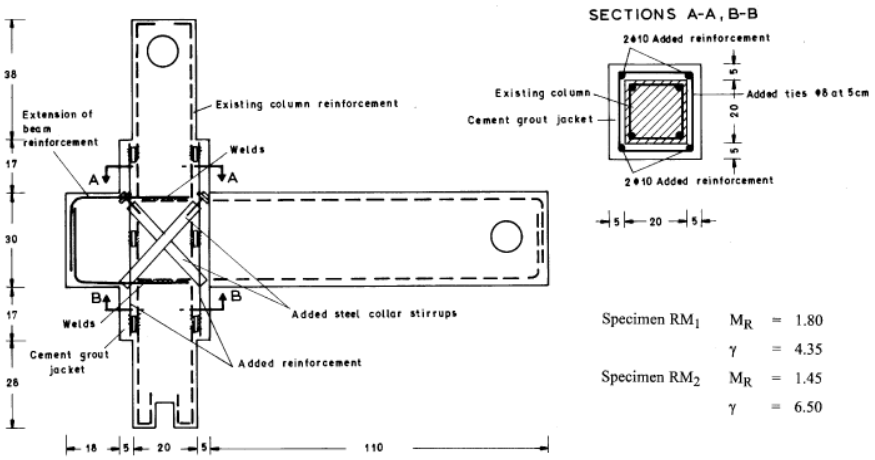

(b) Tsonos, A.G. (1999)

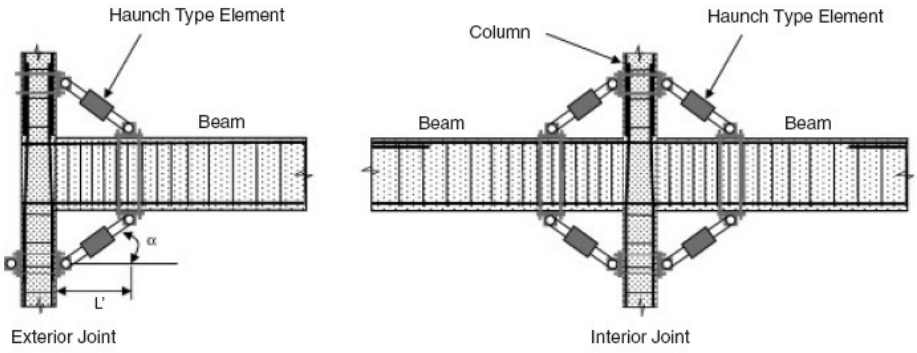

(c)Pampanin, S., Christopoulos, C. and Chen, T.-H. (2006)

(B) Step by step description on upgradation of deficient sub-assemblages of existing RC structures:

(1)P Analyse the existing global structure under general loads (dead load, live load etc.) along with the required response spectrum proposed by the respective code of practice for seismic load.

(2)P Identify the target sub-assemblages to be upgraded

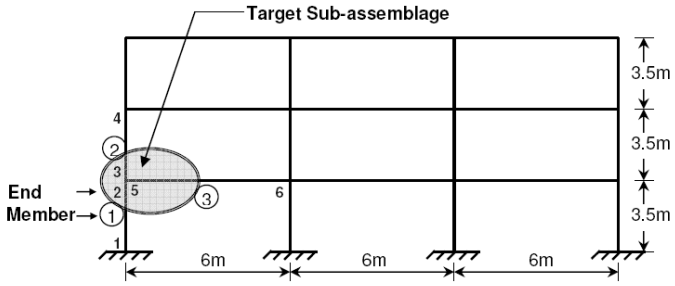

Fig. A8 Frame geometry and target sub-assembly

(3)P Calculate the demand forces against which the particular sub-assemblage should have been designed for (as described in *section 2.5*)

Based on the respective code of practice, all primary loads have to be considered in analysis and prescribed load combinations need to be carried out. In this example problem for demonstration, only Indian Standards have been considered and their provisions are followed.

Table A1 Forces obtained from the analysis (in kN, m unit)

Member and end number		DL (unfactored)			LL (unfactored)			SL (unfactored)		
		Axial	Shear	Bending	Axial	Shear	Bending	Axial	Shear	Bending
1	1	-165.2	6.23	7.31	-100	4.4	5.16	127.9	88.59	185.79
	2	-157.4	6.23	-14.51	-100	4.4	-10.24	127.9	88.59	124.28
2	3	-110.1	10.78	19.76	-66.6	7.61	13.95	60.8	60.52	95.12
	4	-102.2	10.78	-17.97	-66.6	7.61	-12.69	60.8	60.52	116.7
3	5	4.5	47.31	-34.27	3.2	33.39	-24.19	13.8	67.09	218.8
	6	4.5	-54.69	-56.43	3.2	-38.61	-39.83	13.8	67.09	183.71

Table A2 Forces considered for design (in kN, m unit)

Member and end number		1.5 DL +1.5 LL			1.5 DL +1.5 SL			1.2 DL + 1.2 LL + 1.2 SL		
		Axial	Shear	Bending	Axial	Shear	Bending	Axial	Shear	Bending
1	1	-397.8	15.945	18.705	-55.95	142.23	289.65	-164.76	119.064	237.912
	2	-386.1	15.945	-37.125	-44.25	142.23	208.185	-155.4	119.064	178.836
2	3	-265.05	27.585	50.565	-73.95	106.95	172.32	-139.08	94.692	154.596
	4	-253.2	27.585	-45.99	-62.1	106.95	202.005	-129.6	94.692	176.832
3	5	11.55	121.05	-87.69	27.45	171.6	379.605	25.8	177.348	332.712
	6	11.55	-139.95	-144.39	27.45	182.67	360.21	25.8	192.468	335.964

(4)P Calculate the length of the members of the target sub-assemblage to represent global force distribution (this step is also required for experimental investigation).

Table A3 Length of the members of the target sub-assemblage (in kN, m unit)								
Load combinations	Bot col moment	Top col moment	**Column length ratio**	Axial load in bot col	Axial load in top col	Shear in beam	Beam moment	**Beam length**
1.5 DL + 1.5 LL	37.125	50.565	1.36	386.1	265.05	121.05	87.69	0.724
1.5 DL + 1.5 SL	208.185	172.32	1.21	427.95	256.35	171.6	379.605	2.212
1.2DL+1.2LL+1.2SL	178.836	154.596	1.16	462.36	285	177.36	332.71	1.876

(5)P Collect the reinforcement details of the existing building and the sub-assemblage. In this demonstration, the sub-assemblage has been designed for dead load (DL) and live load (LL) and assumed as the prevailing reinforcement details of 'GLD' sub-assemblage of the existing RC structure. Further, based on the demand forces, re-design that particular sub-assemblage using demand forces as calculated in Step (3)P and according to special ductile provisions as proposed by the modern code of practice and called as 'Ductile' sub-assemblage

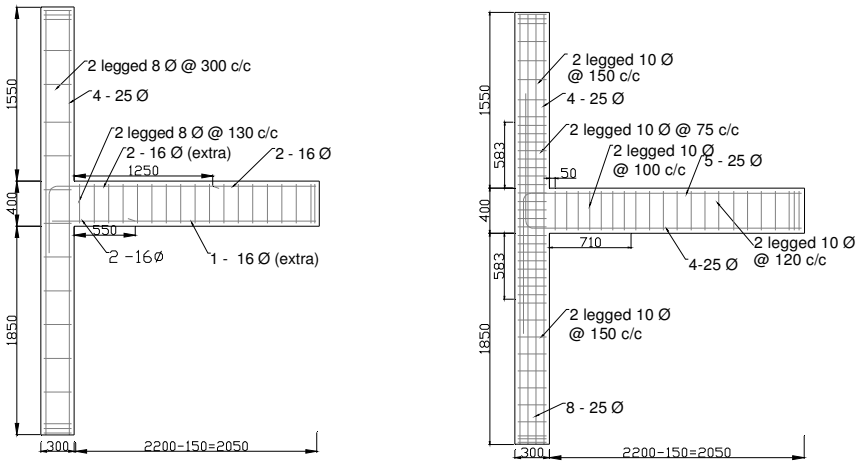

'GLD' sub-assemblage Seismically designed 'Ductile' sub-assemblage

Fig. A9 Details of the sub-assemblages to represent the existing and newly designed structure

(6)P Determine the available strength of the existing 'GLD' and designed 'Ductile' sub-assemblage [in terms of flexural strength of beam and column sections, shear strength of beam and column sections and joint shear strength (as described in *section 3.6.1, 3.6.2 and 3.6.3*, respectively)].

Table A4 Available strength of the sub-assemblages						
Sub-assemblages	Maximum moment capacity of beam (kNm) (+)ve	(-)ve	Maximum moment capacity of column (kNm)	Joint shear capacity (kN)	Maximum shear capacity of beam (kN)*	Maximum shear capacity of column (kN)*
'GLD'	64.78	125.67	103.83	338	188	93
'Ductile'	305.44	378.15	254.39	465	313	202
* Calculated only from Indian Standard						

(7)P Develop the strength hierarchy of both the existing- and ductile- sub-assemblage to find out the available and desirable mode of failure (as described in *section 3.6.4*)

Calculate the beam tip load (P) to produce the corresponding failure i.e., flexure or shear failure in beam, column and joint. For the given beam-column sub-assemblage (as shown in *Fig. A9*), beam tip load corresponding to sectional strength from different failure modes can be calculated from force equilibrium, and the same is given in Table A5.

Table A5 Towards identifying strength hierarchy

	Beam tip load (P) calculated					
	From moment resistance capacity			From joint shear strength	From shear strength of beam and column	
	Beam (+)ve	Beam (-)ve	Column		Beam	Column
'GLD'	31.99	62.06	97	60.06	188	160.71
'Ductile'	150.83	186.74	237.66	82.62	313	349.06

(8)U Calculate the magnitude of upgradation required (in terms of shear and flexural strength of beam and column sections and joint shear strength) by ensuring proper strength hierarchy as given in Eq. 5.1 and described in *section 5.1*.

Table A6 Required magnitude of upgradation from different modes of failure

Upgradation required for 'GLD' sub-assemblage	Increase in moment capacity of beam (kNm) (+)ve	(-)ve	Increase in moment capacity of column (kNm)	Increase in shear capacity of beam (kN)	Increase in shear capacity of column (kN)	Increase in joint shear capacity (kN)
	240.66	252.48	150.56	125	109	$844^{\$}$-338 = 506
$^{\$}$ Corresponding to strength of sub-assemblage > 150.83 kN = P from beam flexural strength in (7)P						

(9)U Carry out shear strengthening of existing sub-assemblage by using GFRP wrapping (as described in *section 5.3*)

Table A7 Amount of shear strengthening

	Beam	Column
Required strength from FRP wrapping	125 kN	109 kN
Thickness of FRP [using Eq. 5.3]	0.62 mm	0.56 mm
Hence, 4 layers of GFRP will be required for wrapping in beam and column		

(10)U Quantify the modified constitutive law of confined concrete produced from shear strengthening using wrapping. Both fixed and variable confinement can be considered during developing constitutive law for confined concrete (as described in *section 5.4*)

As described in (9)U, use of 4 layers of GFRP wrapping would lead to the maximum confinement pressure of 6.68 MPa (Eq. 5.11) and maximum confinement strain would be 0.03 (Eq. 5.9). Hence, compressive strength of confined concrete can be evaluated as 49.5 MPa (Eq. 5.7).

(11)U Level of joint strengthening would be carried out using steel plate with through-through bolt system. Thickness of steel plate and available shear strength of upgraded joint would be calculated as described in *section 5.6* in accordance with *section 3.5.3*.

Using the computer program based on soften strut and tie model (shown in *Fig. A2*), horizontal shear strength of the steel-plate confined reinforced concrete joint can be calculated. From a number of analyses, it is proposed to use 6 mm thick steel plate around the joint. In this case, the strength of concrete confined by steel plate is evaluated to be 57.6 MPa, and horizontal shear strength of the upgraded joint has been evaluated to be 811 kN.

(12)U Choose the proper material (CFRP laminate or fabric) for flexural strengthening and obtain the material requirement for flexural strengthening using the modified constitutive law of concrete (as described in *section 5.5*). Material properties have to be taken from concerned vendor as those are vendor- and country- specific.

Table A8 Amount of flexural strengthening

Upgradation required for 'GLD' sub-assemblage	Using CFRP fabric (*section 5.5.1*)			Using CFRP laminate (*section 5.5.2*)		
	Beam (+)ve	Beam(-)ve)	Column	Beam (+)ve	Beam(-)ve	Column
	4 layers	4 layers	4 layers	200mm wide	200mm wide	4x100mm wide
	To achieve the desired strength hierarchy, flexural upgradation of beam is suggested to be little lower than the demand since the strength of the specimen corresponding to flexural yielding of beam should be less than that obtained from joint shear failure. As shown in (11)U, steel confined joint with horizontal shear strength of 811 kN provides the strength of the specimens as 144.1 kN.					

From the experimental investigations as described in *section 5.7* and numerical studies presented in *section 6.4.2*, it is suggested to restrict the flexural upgradation of the beam to a distance equals to its depth. For fabric based upgradation, two laminates are to be provided at bottom of the beam for better anchorage.

(13)E Finally, execution of upgradation has to be carried out based on the chosen scheme as described in *section 5.7*. In brief, the executions steps are as follows: (i) provisions for bolts by through drilling, (ii) rounding of the sharp corners of concrete section followed by cleaning of all surfaces, (iii) application of flexural strengthening and "U" wrap around the joint, (iv) allow adequate time for curing of applied composite FRP before any further step, (v) application of GFRP wrapping for shear strengthening, (vi) placement of 3-parts steel plate at the joint with smooth bearing, (vii) tightening of bolts.

The schematic details of the upgradation schemes are presented in *Fig. A10* for CFRP laminate based- and *Fig. A11* for CFRP fabric based- upgradation.

Note: P*: Performance evaluation;* U*: Upgradation; and* E*: Execution*

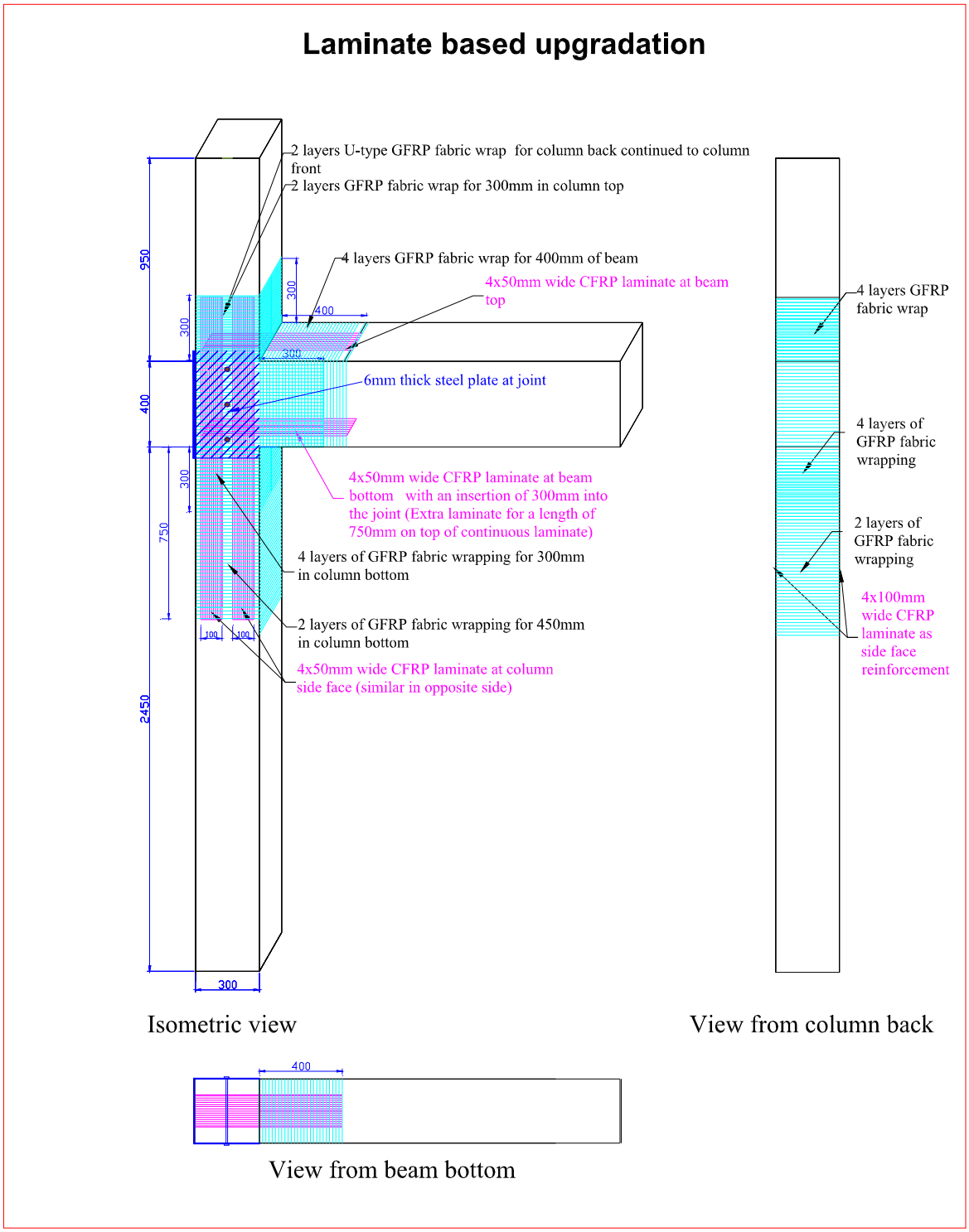

Fig. A10 Upgradation scheme using CFRP laminate

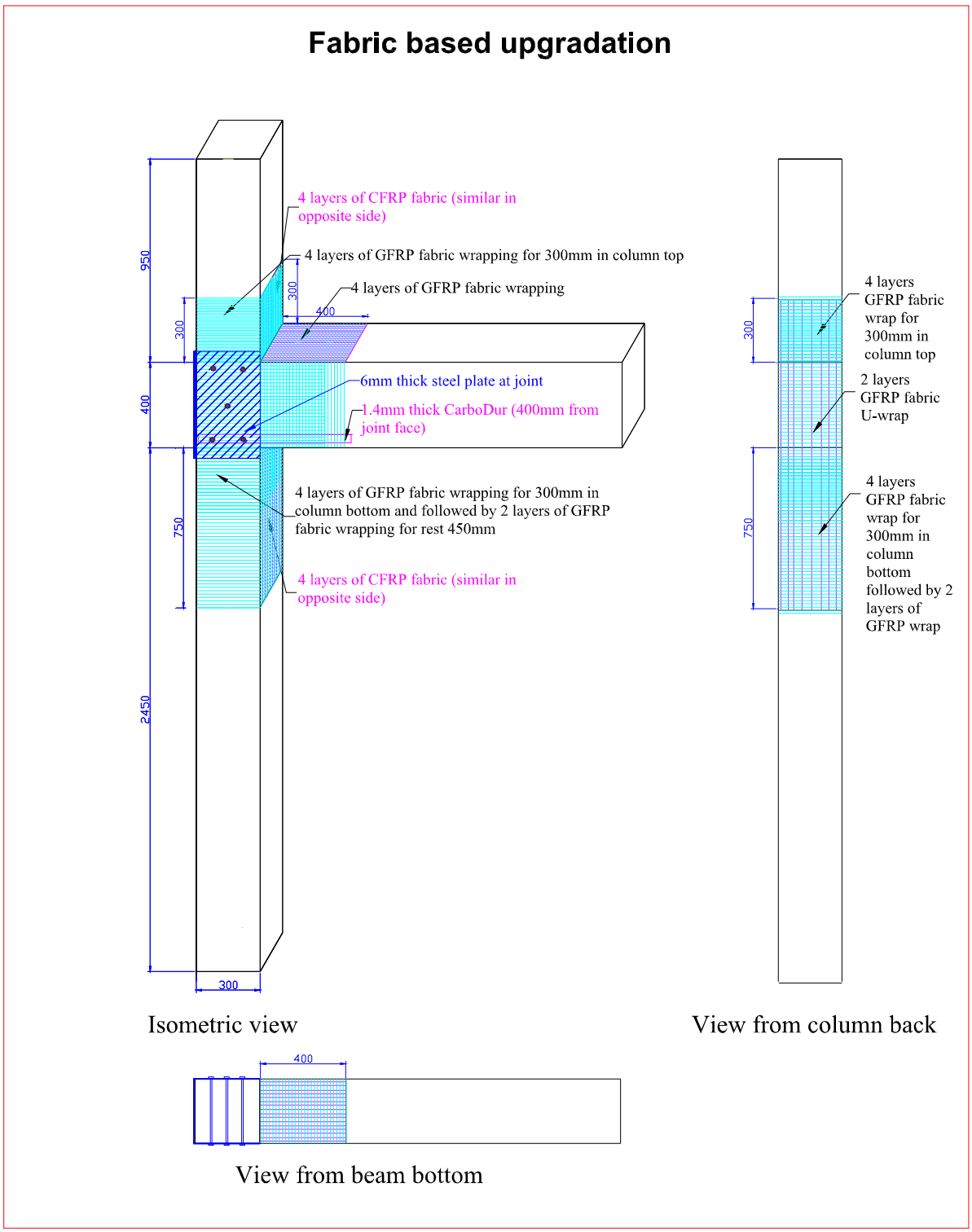

Fig. A11 Upgradation scheme using CFRP fabric

(C) Comparison of codes of practice

Here, a brief on the seismic criteria and detailing sprovisions stipulated in Indian Standard and Eurocode have been considered for comparison of their provisions toward design and detailing under seismic loading.

Basic seismic parameters

Design horizontal seismic coefficient

The design horizontal seismic force F_h for a structure, as described in Indian Standard can be determined by

$$F_h = [f(Z)]\left[\frac{I}{R}\right]\left[\frac{S_a}{g}\right]\cdot m \cdot g \qquad (A1)$$

where $f(Z)$ is zone factor, I is importance factor, R is response reduction factor, S_a / g is average response acceleration coefficient, m is mass of the structure and g is acceleration due to gravity. Similarly, Eurocode prescribes the design horizontal seismic F_h for a structure as

$$F_h = \left[\frac{I}{q}\right]\left[\frac{S_e}{a_g}\right]\cdot[S.\eta]\cdot m \qquad (A2)$$

where q is behaviour factor, S_e is elastic response spectra, a_g .is ground acceleration, S and η are soil- and damping- factors, respectively.

(i) Comparison of response spectra from Eurocode and Indian Standard (IS) can be seen in *Fig. A12*.

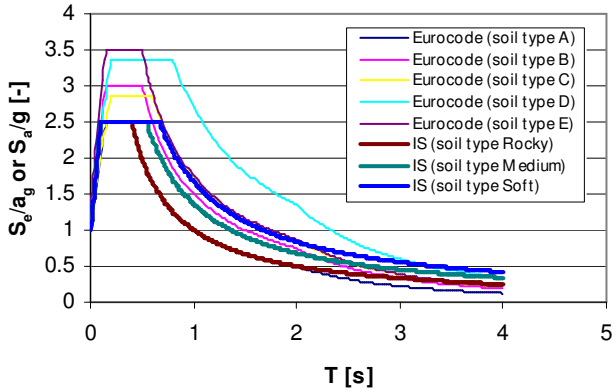

Fig. A12 Response spectra for different soil type

It is to mention here that Indian standard does not provide any additional soil factor whereas Eurocode suggests an increase in response by multiplying a soil factor (S) which varied from 1 to 1.4 for Type 1 spectra and 1 to 1.6 for Type 2 spectra depending on type of the soil. It can also be stated that both the codes of practice propose almost similar spectra for seismic analysis if the soil factor proposed by Eurocode is not considered.

(ii) Response reduction factor (R) in Indian Standard is proposed to be 3 for ordinary RC moment resisting frames and 5 for special RC moment resisting frames. On the other hand, EC8 distinguishes between three different ductility classes to account for different earthquake hazard and suitable earthquake measurements: DCL stands for low ductility, DCM for medium ductility and DCH for high ductility requirements which will be reached

through specific detailing rules for higher local and global ductility in critical regions and corresponding to different (response reduction factors) behavior factors *q*. For framed RC structures, Eurocode gives a behaviour factor (q) as 3 and 4.5 under DCM and DCH, respectively, which can further be increased by 10% for single storey and 20% for multi-storey buildings.

(iii) All the important structures like hospitals, schools, monumental structures, railway station fire station, etc. have been treated by Indian Standard with an importance factor (I) of 1.5 and the others have an importance factor of 1 whereas Eurocode divides the structures into 4 classes and the importance factor varies as 0.8, 1.0, 1.2 and 1.4 based on their importance and desired mode of failure.

Soft storey

In Indian Standard, a soft storey is defined by one in which the lateral stiffness is less than 70 percent of that in the storey above or less than 80 percent of the average lateral stiffness of the three storeys above. Instead of giving a specific quantification of soft storey behaviour, Eurocode describes the rules to avoid any soft storey effect, such as (a) All lateral load resisting systems, such as cores, structural walls, or frames, shall run without interruption from their foundations to the top of the building or, if setbacks at different heights are present, to the top of the relevant zone of the building, (b) Both the lateral stiffness and the mass of the individual storeys shall remain constant or reduce gradually, without abrupt changes, from the base to the top of a particular building, and (c) other restrictions for set back buildings

In defining the irregularities:

(i) Vertical irregularity: Indian Standard defines the vertical irregularity shall be considered to exist where the horizontal dimension of the lateral force resisting system in any storey is more than 150 % of that in its adjacent storey. In Eurocode, it is similar as described in Indian Standard if the irregularity is within 15% (from base) of the height of the building. Beyond that zone, it is called to be vertically irregular if horizontal dimension of the lateral force resisting system is differing by 120 % with respect to the adjacent floor.

(ii) Horizontal irregularity: If the set back in plan is more than 15-20% of the overall dimension of the structure, it is described by Indian Standard as a horizontally irregular structure. Eurocode defines as if in plan set-backs (re-entrant corners or edge recesses) exist, regularity in plan may still be considered as being satisfied, provided that these setbacks do not affect the floor in-plan stiffness and that, for each set-back, the area between the outline of the floor and a convex polygonal line enveloping the floor does not exceed 5 % of the floor area.

(iii) Torsional irregularity: It is one of the most important phenomenon when centre of mass and centre of stiffness do not match and this adds the enormous vulnerability of structures under seismic load. Indian Standard considers the existence of torsional irregularity when the maximum storey drift, computed with design eccentricity, at one end of the structures transverse to an axis is more than 1.2 times the average of the storey drifts at the two ends of the structure. In Eurocode, torsional irregularity is defined by the situation when the structural eccentricity is more than 30% of the torsional radius of the structure at a given level and /or radius of gyration of the floor mass is more than torsional radius (which is defined by the square root of the ratio of the torsional stiffness to the lateral stiffness).

Design eccentricity

Design eccentricity (e_{di}) at any floor *i* can be calculated according to Indian Standard as (i) $e_{di} = 1.5e_{si} + 0.05b_i$, and (ii) $e_{di} = 1.0e_{si} - 0.05b_i$ Where e_{si} is the static eccentricity of the floor i, defined as the distance between centre of mass to centre of rigidity, and b_i is plan dimension of *i*th floor perpendicular to the direction of force. Hence, the factor 1.5 represents the dynamic amplification factor and 0.05 is the extent of accidental eccentricity. Eurocode

also considers an accidental eccentricity of 5% to account uncertainties in the location of masses and in the spatial variation of the seismic motion. If the lateral stiffness and mass are symmetrically distributed in plan and unless the accidental eccentricity is taken into account by a more exact method, the accidental torsional effects may be accounted for by multiplying the action effects in the individual load resisting elements by a factor δ which is dependent on distance of the element under consideration from the centre of mass of the building in plan (x) and distance between the two outermost lateral load resisting elements (L_e) as $\delta = 1 + 0.6\frac{x}{L_e}$. Further, the factor 0.6 should be replaced by 1.2 in case on two planar structural frames.

Storey drift

The storey drift in any storey due to the minimum specified design lateral force with the partial safety factor of 1.0, has been defined in Indian Standard, as not exceeding 0.004 times the storey height. Whereas, Eurocode stipulates (a) 0.005 times the storey height for buildings having non-structural elements of brittle materials attached to the structure, (b) 0.0075 times the storey height for buildings having ductile non-structural elements, and (c) 0.01 times the storey height for buildings having non-structural elements fixed in a way so as not to interfere with structural deformations, or without non-structural elements:

Differences in detailing

Beam longitudinal reinforcement

The amount of reinforcement is designed as per IS 456 and EC2, but the minimum and maximum reinforcement ratios are adopted as shown in Table A9. It shows similar minimum reinforcement ratios for both codes, min ρ in EC2 depends on concrete and steel strength for standard and seismic design, in IS 456 it only depends on steel strength. The value for standard design is in general smaller than seismic design. The maximum reinforcement ratio is limited to 4% in standard design, for seismic design max ρ is reduced to 2.5% in IS 13920, whereas the value in EC8 is depending on ductility requirements and material characteristics. To account for higher ductility demand under seismic loading the value needs to be smaller.

Table A9: Minimum and maximum longitudinal reinforcement ratio (ρ) in beams

	Standard design		Seismic design	
	IS 456	EC2	IS 13920	EC8
Min ρ	$\frac{0.85}{f_y}$	$0.26 \cdot \frac{f_{ctm}}{f_{yk}} \geq 0.0013$	$0.24 \cdot \frac{\sqrt{f_{ck}}}{f_y}$	$0.5 \cdot \frac{f_{ctm}}{f_{yk}}$
Max ρ	0.04	0.04	0.025	$\rho' + \frac{0.0018}{\mu_0 \cdot \varepsilon_{yd}} \cdot \frac{f_{cd}}{f_{yd}}$

Beam shear reinforcement

To ensure ductile failure modes (e. g. flexural failure) with sufficient safety compared to brittle ones (e. g. shear failure), the development of overstrength moments in plastic hinges has to be taken into account during calculation of design shear forces. According to IS 13920 the shear force to be resisted by the vertical hoops shall be the maximum of: (a) calculated factored shear force as per analysis, and (b) shear force due to formation of plastic hinges at both ends of the beam plus the factored gravity load on the span (see *Fig. A13*). According to EC8 the design shear force shall be calculated based on the equilibrium of the beam under: a) the transverse load acting on it in the seismic design situation and b) end moments $M_{i,d}$

(with i=1,2 denoting the end sections of the beam), corresponding to plastic hinge formation for positive and negative directions of seismic loading. The end moments $M_{i,d}$ may be calculated as

$$M_{i,d} = \gamma_{Rd} M_{Rb,i} \min\left(1, \frac{\sum M_{Rc}}{\sum M_{Rb}}\right) \qquad (A3)$$

where γ_{Rd} is the factor accounting for possible overstrength due to steel strain hardening (1.0 for DCM and 1.2 for DCH), $M_{Rb,i}$ is the design value of the beam moment of resistance at end i in the sense of the seismic bending moment under the considered sense of the seismic action; ΣM_{Rc} and ΣM_{Rb} are the sum of the design values of the moments of resistance of the columns and the beams framing into the joint, respectively (see. *Fig. A13*). Hence, in both codes the design shear force is determined in accordance with the capacity design rule.

IS13920

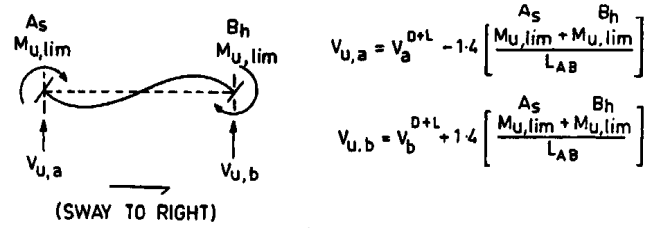

EC8

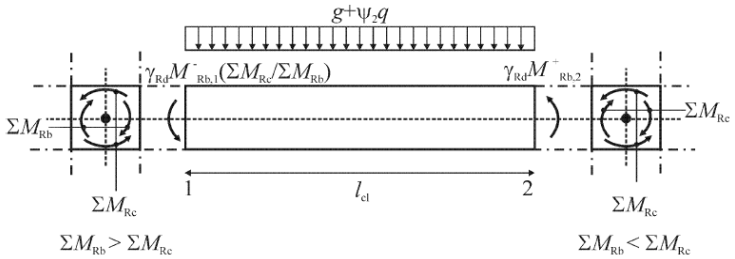

Fig. A13 Calculation of design shear force in beam

Beam ductile zone detailing

For the desired ductility of the structure the potential plastic hinge regions require a high plastic rotational capacity: additional confinement is required and local buckling of compression reinforcement needs to be avoided. Therefore special rules have to be followed for the detailing of plastic hinges (as presented in Table A10).

Table A10: Ductile zone detailing in seismic beams

	IS 13920	EC8 (DCM)
Critical length [mm]	2*d*	h_w
Diameter of hoops d_{bw}	≥ 6 mm	≥ 6 mm
Spacing of hoops [mm]	$s = \min\left\{\frac{d}{4}, 8d_s\right\}, \geq 100mm$	$s = \min\left\{\frac{h_w}{4}, 24d_{bw}, 225, 8d_{bl}\right\}$
Distance of first hoop from joint face	≤ 50 mm	≤ 50 mm
Spacing outside ductile zone	$s_{\max} = \frac{d}{2}$	$s_{\max} = 0.75 \cdot d(1 + \cot\alpha)$ (EC2)
Anchorage of hoops and hoop extension length (l)	135°-hook, $l \geq 10d_w$	135°-hook, $l \geq 10d_w$

To satisfy the local ductility requirement in the critical regions of primary seismic beams, the value of the curvature ductility factor μ_φ shall be at least equal to the value given as $\mu_\phi = 2q_o - 1$ if $T_1 \geq T_C$ and $\mu_\phi = 1 + 2(q_o - 1)T_C / T_1$ if $T_1 < T_C$. Hence, a stiffer structure (i.e. low time period) falls into the zone of higher spectral demand and requires higher ductility. When the compression zone reinforcement (in addition to any compression reinforcement needed for the ULS verification of the beam in the seismic design situation) is not less than half of the reinforcement provided at the tension zone, and when the reinforcement ratios in Table A9 are satisfied, then there is no need to check the curvature ductility factor.

Column shear reinforcement

According to EC8 the design shear force for seismic columns is determined following the same principle as described above for the beams, whereas

$$M_{i,d} = \gamma_{Rd} M_{Rd,i} \min\left(1, \frac{\sum M_{Rb}}{\sum M_{Rc}}\right) \qquad (A4)$$

where γ_{Rd} is equal to 1.1 for DCM structures and 1.3 for DCH structures, respectively. Further, in primary seismic columns the value of the normalised axial force v_d shall not exceed 0.65. At least one intermediate bar shall be provided between corner bars along each column side, to ensure the integrity of the beam-column joints. In IS 13920 there are no such rules. Further EC8 requires the total longitudinal reinforcement ratio ρ_l being not less than 0.01 and not more than 0.04. In symmetrical cross-sections symmetrical reinforcement should be provided ($\rho = \rho'$). Though the IS456 limits the longitudinal reinforcement ratio from 0.008 to 0.06, IS 13920 does not provide any limiting reinforcement ratios.

Column ductile zone detailing

According to both the codes, special confining reinforcement shall be provided in zones next to the joint where flexural yielding may occur under the effect of seismic loading to ensure minimum ductility and to prevent local buckling of longitudinal bars. The hoop pattern shall be such that the cross-section benefits from the tri-axial stress conditions produced by the hoops. Table A11 lists the requirements. According to IS 13920, the full column shall be treated as critical, if the point of contra-flexure is not within the middle half of the member clear height, and according to EC8 if the ratio of clear length of column l_c to largest cross-sectional dimension of column h_c is less than 3.

Table A11: Ductile zone detailing in seismic columns

	IS 13920	EC8 (DCM)
Critical length [mm]	$l_o = \max\left\{b_{\max}, \frac{1}{6}l_c, 450\right\}$	$l_o = \max\left\{h_c, \frac{1}{6}l_c, 450\right\}$
Diameter of hoops d_{bw}	≥ 6 mm	≥ 6 mm
Spacing of hoops	$s = \min\left\{\frac{b_{\min}}{4}, 75\right\}, \leq 100$ mm	$s = \min\left\{\frac{b}{2}, 175, 8d_{bl}\right\}$ mm
Anchorage of hoops and hoop extension length (l)	135°-hook, $l \geq 10d_w$	135°-hook, $l \geq 10d_w$
Spacing of long. reinforcement without cross-ties	s < 300 mm	s < 200 mm

In IS 13920 additional confining reinforcement is calculated as follows:

$$A_{sh} = 0.18 \cdot s \cdot h \cdot \frac{f_{ck}}{f_y}\left[\frac{A_g}{A_k} - 1.0\right] \qquad (A5)$$

where, s= spacing of hoops, h= longer dimension of the rectangular confining hoop measured to its outer face (should not exceed 300 mm), A_g = gross area of column cross section, and A_k = area of confined concrete core in the rectangular hoop measured to its outside dimensions.

In EC8 additional confining reinforcement is depending on the curvature ductility factor μ_ϕ, as discussed in beam ductile zone detailing. If for the specified value of μ_ϕ a concrete strain larger than ε_{cu2}=0,0035 is needed anywhere in the cross-section, compensation for the loss of resistance due to spalling of the concrete shall be achieved by means of adequate confinement of the concrete core, on the basis of the properties of confined concrete. These requirements are satisfied when

$$\alpha\omega_{wd} \geq 30\mu_\phi \nu_d \cdot \varepsilon_{sy,d} \cdot \frac{b_c}{b_o} - 0.035 \qquad (A6)$$

where ω_{wd} is the mechanical volumetric ratio of confining hoops within the critical regions as defined as $\omega_{wd} = \frac{volume\ of\ confining\ hoops}{volume\ of\ concrete\ core} \cdot \frac{f_{yd}}{f_{cd}}$, $\varepsilon_{sy,d}$ is the design value of tension steel strain at yield; h_c is the gross cross-sectional depth; h_o is the depth of confined core (to the centreline of the hoops); b_c is the gross cross-sectional width; b_o is the width of confined core (to the centreline of the hoops); α is the confinement effectiveness factor, equal to $\alpha = \alpha_n \cdot \alpha_s$, for rectangular cross-sections with

$$\alpha_n = 1 - \sum_n b_i^2 / 6 b_o h_o \text{ and } \alpha_s = (1 - s/2b_o)(1 - s/2h_o) \qquad (A7)$$

Detailing of beam-column joint

According to both IS 13920 and EC8 the horizontal confinement reinforcement in exterior joints of primary seismic beams with columns should be not less than that for the critical regions of columns. According to EC8 at least one intermediate (between column corner bars) vertical bar shall be provided at each side of a joint of primary seismic beams and columns.

Continuation of longitudinal reinforcement inside joint/ anchorage of beam reinforcement

(i) Anchorage of reinforcement according to EC8 is based on EC2 with some additional rules. Typical anchorage of reinforcement is shown in left of *Fig. A14* where typical mandrel diameters in the bend have to be satisfied. IS 13920 specifies that both the top and the bottom bars of the beam shall be provided with anchorage length, beyond the inner face of the column, equal to the development length in tension plus 10 times the bar diameter minus the allowance for 90 degree bend(s) in exterior joints (as shown in right of *Fig. A14*).

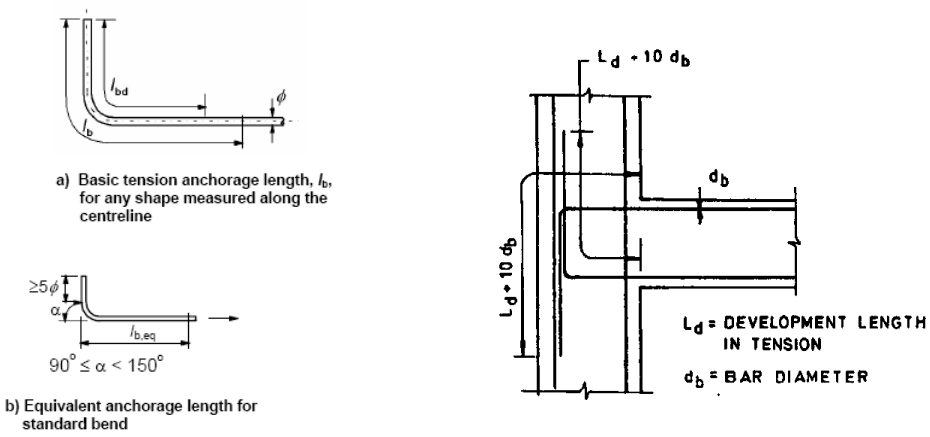

Fig. A 14 Anchorage of reinforcement (EC2) and implementation in exterior joint (IS 13920)

(ii) EC8 specifies that the part of beam longitudinal reinforcement bent in joints for anchorage shall always be placed inside the corresponding column hoops. To prevent bond failure the diameter of beam longitudinal bars passing through beam-column joints, d_{bL}, shall be limited in accordance with the following expressions:

$$\frac{d_{bL}}{h_c} \le \frac{7.5 \cdot f_{ctm}}{\gamma_{Rd} \cdot f_{yd}} \cdot (1 - 0.8 \cdot \nu_d) \qquad (A8)$$

Where, h_c is the width of the column parallel to the bars; f_{ctm} is the mean value of the tensile strength of concrete; f_{yd} is the design value of the yield strength of steel; ν_d is the normalised design axial force in the column, taken with its minimum value, for the seismic design situation ($\nu_d = N_{Ed}/f_{cd}A_c$); γ_{Rd} is the model uncertainty factor on the design value of resistances, taken as being equal to1.0 or 1.2 respectively for DCM or DCH (due to overstrength owing to strain-hardening of the longitudinal steel in the beam).

If the requirement specified cannot be satisfied in exterior beam-column joints because the depth, h_c, of the column parallel to the bars is too shallow, EC8 provides the the following additional measures to ensure anchorage of the longitudinal reinforcement of beams (as shown in *Fig. A15*). a) The beam or slab may be extended horizontally in the form of exterior stubs, b) Headed bars or anchorage plates welded to the end of the bars may be used, and c) Bends with a minimum length of $10d_{bL}$ and transverse reinforcement placed tightly inside the bend of a group of bars may be added.

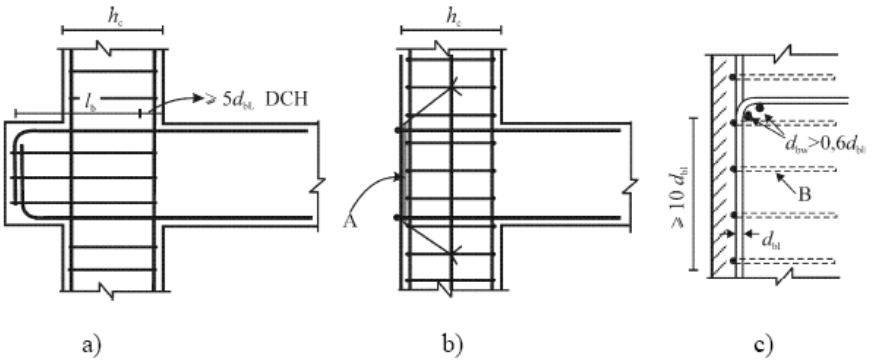

Fig. A15 Additional measures for anchorage in exterior beam-column joints (Note: A and B stand for anchor plate and hoops around column bar)

1. Personal Details

Name	**SAPTARSHI SASMAL**
Date of birth	19.08.1976
Place of birth	Midnapore, West Bengal, India
Schooling	Sarisha, 24 Parganas (south), India (1982-1994)
Bachelor of Engg	Jadavpur University, Calcutta, India (1994-1998)
Master of Engg	Jadavpur University, Calcutta, India (1998-2000)
Present designation	Scientist; Structural Engineering Research Centre (SERC), CSIR, India, since 2002
Work field	Central R&D area: numerical and experimental studies on structures; fuzzy applications, finite element analysis, seismic analysis, condition assessment, damage detection, strengthening of existing facilities

2. Awards and Achievements

- **National Scholarship** holder from Ministry of HR, Government of India (1992-1998)
- Awarded **Washington Chapter Annual Scholarship** in Bachelor of Engg Level in 1997
- Awarded **GATE scholarship** by University Grants Commission, Government of India during 1998-2000
- Received **Gold Medal** from Jadavpur University in Master of Engg Level for securing topmost position in 2000
- Received **Certificate of Merit** from Structural Engineering Research Centre in 2003-2004
- Awarded **DAAD Fellowship** (long term) for full doctoral studies in Germany in 2006
- The **George Oomen Memorial Award** for best paper in Civil Engineering section from Institute of Engineers (India) in 2006
- **Ramaiah Prize** for best technical paper by Structural Engineering Research Centre in 2007
- **Best technical paper award** from ING-IABSE (Indian national group of International Association for Bridge & Structural Engineering) in 2006, 2007
- **Paper** entitled "Fuzzy Logic Based Condition Rating of Existing Reinforced Concrete Bridges" was nominated for **Outstanding Paper Award** of J. Performance of Constructed Facilities, ASCE, 2007

3. List of publications in refereed journals (chronological order)

1) **Saptarshi Sasmal** and Dipankar Chakravorty, "*Response of Bridges Curved in Plan due to Dead and Live Loads Using Finite Element Method"*, Journal of Structural Engineering, Vol. 30, No. 1, 2003, pp 7-16.

2) K. Ramanjaneyulu, Ch. Lakshmi, V. Srinivas, K.K. Sukhesh, **Saptarshi Sasmal**, and S.Gopalakrishnan, "*Genetic Algorithm Based Optimal Design of Continuous Prestressed Concrete Bridge Box Girders*", Journal of Structural Engineering, Vol. 30, No. 1, 2003, pp 33-41.

3) V. Srinivas, K. Ramanjaneyulu, K.K. Sukhesh, **Saptarshi Sasmal**, and S. Gopalakrishnan, "*Automated Grillage Analysis of Continuous Span I- and T- Girder Bridges*", Journal of Structural Engineering, Vol. 31, No. 2, 2004, pp 101-110.

4) **Saptarshi Sasmal**, K. Ramanjaneyulu, V. Srinivas, S. Gopalakrishnan, "*Simplified Computational Methodology for Analysis and Studies on Behaviour of Incrementally Launched Continuous Bridges*", Structural Engineering and Mechanics, Vol. 17, No. 2, 2004, pp 245-266.

5) **Saptarshi Sasmal**, K. Ramanjaneyulu, S. Gopalakrishnan and N. Lakshmanan**,** "*Investigations on Free Vibration Characteristics of Bridges Curved in Plan*", Journal of the Institution of Engineers (India), Vol. 86, 2005, pp 72-78.

6) **Saptarshi Sasmal**, K. Ramanjaneyulu, S. Gopalakrishnan and N. Lakshmanan, "*Methodology for Construction Phase Analysis of Incrementally Launched Continuous Bridges*", Indian Group of International

Association of Bridge and Structural Engineers (ING-IABSE) Journal of The Bridge & Structural Engineer, Vol. 35, No. 3, 2005, pp 35-50.

7) **Saptarshi Sasmal**, Amarnath Santh and K. Ramanjaneyulu, *"Seismic Performance Evaluation of Reinforced Concrete Bridges Using Pushover Analysis",* Indian Group of International Association of Bridge and Structural Engineers (ING-IABSE) Journal of The Bridge & Structural Engineer, Vol. 36, No. 1, 2006, pp 39-50.

8) **Saptarshi Sasmal**, K. Ramanjaneyulu, S. Gopalakrishnan and N. Lakshmanan**,** "*Fuzzy Logic Based Condition Rating of Existing Reinforced Concrete Bridges*", Journal of Performance of Constructed Facilities-ASCE, Vol. 20, No. 3, 2006, pp 261-273.

9) **Saptarshi Sasmal** and K. Ramanjaneyulu**,** "*Transfer Matrix Method for Construction Phase Analysis of Incrementally Launched Prestressed Concrete Bridges*", Engineering Structures, Vol. 28, No. 13, 2006, pp 1897-1910.

10) **Saptarshi Sasmal**, K. Ramanjaneyulu and N. Lakshmanan**,** "*Condition Assessment of Existing Reinforced Concrete Bridges through Priority Ranking*", International Journal of "Structure & Infrastructure Engineering **-** Maintenance, Management, Life-Cycle Design & Performance", Vol. 3, No. 1, 2007, pp 75-89.

11) **Saptarshi Sasmal**, K. Ramanjaneyulu and N. Lakshmanan**,** *"Condition Ranking of Existing Bridges Using Analytic Hierarchy Approach*", Indian Group of International Association of Bridge and Structural Engineers (ING-IABSE) Journal of The Bridge & Structural Engineer, Vol. 37, No. 1, 2007, pp 23-36.

12) M.Prabhu, **Saptarshi Sasmal** and K. Ramanjaneyulu, "*Seismic Resistant Design of Bridges - A Comparison of Some Important Codes*", Indian Group of International Association of Bridge and Structural Engineers (ING-IABSE) Journal of The Bridge & Structural Engineer, Vol. 37, No.2, 2007, pp.9-20.

13) **Saptarshi Sasmal** and K. Ramanjaneyulu**,** "*Simplified Structural Response of Continuous Span Bridges Curved in Plan*", "Pollack Periodica, International Journal for Engineering and Information Sciences", Vol. 2, No.3, 2007, pp.57-72.

14) **Saptarshi Sasmal** and K. Ramanjaneyulu**,** *"Dynamic Behaviour of Bridge Decks Curved in Plan*", International Journal of Applied Mechanics and Engineering, Vol. 12, No.4, 2007, pp.1117-1134.

15) Balthasar Novák, K. Ramanjaneyulu, Constanze Roehm and **Saptarshi Sasmal**, *"Seismic Performance of D-region of RC Framed-structure Designed According to Different Codal Recommendations",* Journal of Structural Engineering, Vol. 35, No.1, April-May 2008, pp.46-51.

16) **Saptarshi Sasmal** and K. Ramanjaneyulu, "*Condition Evaluation of Existing Reinforced Concrete Bridges using Fuzzy Based Analytic Hierarchy Approach*", International journal of Expert Systems with Applications , Vol. 35, No. 3, October 2008, pp 1430-1443.

17) Balthsar Novák, **Saptarshi Sasmal**, Constanze Roehm, Thomas Schnabel and Reinhard Becker, „*um Nachträglichen Kürzen und Verankern von Glatten Spanngliedern im Verbund*", Beton und Stahlbetonbau, Wiley InterScience publication, Vol. 103, No. 8, 2008, pp. 522-529 (in German).

18) **Saptarshi Sasmal**, K. Ramanjaneyulu and N. Lakshmanan**,** *"Detection and Quantification of Structural Damage Using Transfer Matrix Technique* ", Engineering Structure (under review)

19) **Saptarshi Sasmal** and K. Ramanjaneyulu, "*Methodology for Structural Damage Detection Using Curvature of Rotational Flexibility*", International Journal of "Structure & Infrastructure Engineering **-** Maintenance, Management, Life-Cycle Design & Performance", (under review)

20) **Saptarshi Sasmal** and K. Ramanjaneyulu, "*State of Stress and Ultimate Strength of Multi-Layered Reinforced Concrete Sections Subjected to Combined Bending and Tension*", Indian Concrete Journal (under review)